Gabriel de Alemar Barberes

Unconventional Methods for Unconventional Plays
Surface Geochemical Prospecting For Hydrocarbon Exploration At South Portuguese Zone

Tese de doutoramento em Geologia, ramo em Recursos Geológicos e Ambiente, orientada por Dr. Rui Pena dos Reis, Dr. Paulo Emanuel Fonseca, Drª Teresa Barata e apresentada no Departamento de Ciências da Terra da Faculdade de Ciências e Tecnologia da Universidade de Coimbra

Maio de 2018

· U C ·

Universidade de Coimbra

FCTUC FACULDADE DE CIÊNCIAS
E TECNOLOGIA
UNIVERSIDADE DE COIMBRA

Gabriel de Alemar Barberes

UNCONVENTIONAL METHODS FOR UNCONVENTIONAL PLAYS

Surface Geochemical Prospecting for Hydrocarbon Exploration at South Portuguese Zone

Ph.D. program in Geology – Geological Resources and Environment

Advisors: Dr. Rui Pena dos Reis (University of Coimbra)
Dr. Paulo Emanuel Fonseca (Lisbon University)
Dr. Teresa Barata (University of Coimbra)

May, 2018

FCTUC FACULDADE DE CIÊNCIAS
E TECNOLOGIA
UNIVERSIDADE DE COIMBRA

Gabriel de Alemar Barberes

MÉTODOS NÃO-CONVENCIONAIS PARA *PLAYS* NÃO-CONVENCIONAIS

Prospecção Geoquímica de Superfície para a Exploração de Hidrocarbonetos na Zona Sul Portuguesa

Doutoramento em Geologia – Recursos Geológicos e Ambiente

Orientadores: Dr. Rui Pena dos Reis (Universidade de Coimbra)
Dr. Paulo Emanuel Fonseca (Universidade de Lisboa)
Drª. Teresa Barata (Universidade de Coimbra)

Maio, 2018

This PhD project was direct financed by Statoil Brazil through Sciences Without Borders program (CNPq Brazil) – process number 201943/2014-0, and by FCT resources, through Geosciences Centre (CGEO-University of Coimbra), Research Centre of Earth and Space (CITEUC-University of Coimbra) and Dom Luiz Institute (Lisbon University).

The project received important contributions from Partex Oil&Gas (Portugal), Repsol E&P (Spain), DigitalGlobe Foundation (USA), Polish Geological Institute (Poland), LNEG (Portugal), University of Lisbon (Portugal) and University of Barcelona (Spain).

PREFACE | I

All in all, the top 25 oil and gas companies on the Forbes Global 2000 (Forbes Magazine) generated €1.8 trillion in sales during 2016/2017 period and pocketed €60 billion in profit. That's down from €2.1 trillion in sales and €66 billion in profit in the previous year. Facing a market with such amount of currency circulation, how can an academic research project contribute to the deepen knowledge of hydrocarbon exploration? Well, Parke A. Dickey answered this question in 1958: "We usually find oil in new places with old ideas. Sometimes, also, we find oil in an old place with a new idea, but we seldom find much oil in an old place with an old idea. Several times in the past we have thought we were running out of oil whereas actually we were only running out of ideas".

In 2013, the first master thesis on shale gas was approved in Portugal, at the University of Coimbra, as a result of the first assessment project for unconventional hydrocarbons potential in this country. In the same year, the present doctoral project started, with direct and indirect funding of companies and institutions from Portugal, Spain, Norway, United States, Brazil and Poland.

In the following PhD thesis will be approached questions regarding the potential of the South Portuguese zone (Portugal) for the generation/accumulation of hydrocarbons in unconventional petroleum systems. Given the lack of seismic and petrophysical data the techniques used in this project, described in detail in the following chapters, are those that produced the most relevant data for hydrocarbon exploration in the region of southern Portugal, until today.

We hope that this project makes the Portuguese "critical mass" aware of the need to increase the research on the natural resources of the country. The ongoing discussion about the geoenergetic future of Portugal should not be guided by passion, but by rational communication between scientists, politics and the societal stakeholders.

ACKNOWLEDGMENTS | II

First of all I would like to thank the unconditional support of my advisors: Dr. Rui Pena dos Reis (University of Coimbra), Dr. Paulo Emanuel Fonseca (University of Lisbon) and Dr. Teresa Barata (University of Coimbra). Throughout these four years they have always been at my side, giving all the necessary support to carry out this work.

Thanks also to my friend, Dr. André Luiz Spigolon (Petrobras), for the countless discussions, debates and lessons he has given me over the last four years.

To Dr. Albert Permanyer (Universitat de Barcelona) for receiving me at his University and providing a pleasant PhD internship. Thanks also to Dr. Nuno Pimentel (University of Lisbon) for the important intellectual contribution to this project.

To the friend Dr Maria Helena Henriques (University of Coimbra) for all the support given during these almost 8 years of conviviality. To the other professors and researchers from the Universities of Coimbra, Lisbon and Barcelona who indirectly contributed to the success of this work, I offer my sincere thanks.

I would like to thank the companies and institutions that have contributed directly or indirectly to this thesis: Statoil ASA (Brazil-Norway), Partex Oil&Gas (Portugal), Repsol E&P (Spain), Petrobras (Brazil), DigitalGlobe (USA), Polish Geological Institute (Poland), LNEG (Portugal), FCT (Portugal), CNPq (Brazil), CGeo-UC (Portugal) and CITEUC-UC (Portugal).

I would like to thank my family: my wife Sílvia, my mother Maria Célia, my father Leonardo, my sisters Rafaela and Giuliana and my stepmother Mariana... I say this in the future of the past tense because honestly, I do not know how to do it. Without them, none of this would make sense, either academically or personally. They are all that I have most precious, they are the basis of my life. I love you, people!

To my eternal friends and housewives Michel and André, with whom I shared an important part of my life in Coimbra, thank you very much for the strength.

I will not mention here all those I would like because I have the fear of committing an injustice forgetting a name. I have made many friends these past eight years. People I'm going to carry for the rest of my life and who, somehow, were also part of it all.

ABSTRACT | III

The price and reliability of energy supplies, electricity in particular, are key elements in a country's energy supply strategy. Electricity prices are of particular importance for international competitiveness, as electricity usually represents a significant proportion of total energy costs for industrial and service-providing businesses.

In Portugal, the price of electricity and natural gas are among the highest in European Union. According to International Energy Agency, in 2016 20% of the electricity was generated by natural gas (52% of total electricity generation was made by fossil fuels) in this country.

This project aims to identify onshore hydrocarbon emanations by surface geochemical prospecting, rock-eval pyrolysis analysis and thorium normalization/hydrocarbon anomalies, in order to characterized an unconventional petroleum system in South Portuguese Zone (Portugal). This thesis also aims demonstrate a correlation between airborne gamma radiation data and high-resolution satellite images WorldView-2, in order to be an alternative way and facilitate the acquisition of radiometric data, in view of the high costs associated to an airborne gamma ray survey.

A total of 31 samples were collected for rock-eval pyrolysis performed by Weatherford Laboratories and Polish Geological Institute, financed by Repsol E&P (Spain), Partex Oil&Gas (Portugal) and Polish Geological Institute (Poland).

The collection of all samples for surface geochemical prospecting was performed using Isojars, with distilled water and a bactericide added to inhibit any bacterial activities. Twenty-seven soil samples were collected for this study, using a drilling machine, a metal tube and a hammer.

Thirty-one water samples were collected from artesian wells, boreholes and springs.

The remote sensing methodologies, used to define the sampling areas, proved to be very efficient to show possible hydrocarbon emanations. From the geological prospecting point of view the presence of hydrocarbon gases in South Portuguese Zone formation is clear and evident. They are present in soil and water, with significantly high levels.

Keywords: Geochemistry; Remote Sensing; Unconventional Hydrocarbons; Light Hydrocarbons; South Portuguese Zone

RESUMO | IV

O preço e a confiabilidade dos estoques de energia, eletricidade em particular, são elementos essenciais na estratégia de fornecimento de energia de um país. Os preços da eletricidade são de particular importância para a competitividade internacional, já que a eletricidade geralmente representa uma proporção significativa dos custos totais de energia para a industria e prestação de serviços.

Em Portugal o preço da eletricidade e do gás natural estão estre os mais caros da União Europa. De acordo com a Agência Internacional de Energia, em 2016 20% da eletricidade foi gerada por gás natural (52% do total da geração elétrica foi feita por combustíveis fósseis) neste país.

Este projeto tem como objetivo identificar emanações onshore de hidrocarbonetos através da prospecção geoquímica de superfície, análise de pirólise rock-eval e normalização de tório/anomalia de hidrocarbonetos, a fim de caracterizar um sistema petrolífero não-convencional da Zona Sul Portuguesa (Portugal). Esta tese também pretende demonstrar uma correlação entre dados de radiação gama e imagens de satélite de alta resolução WorldView-2, a fim de ser uma alternativa e facilitar a aquisição de dados radiométricos, tendo em vista os altos custos associados ao levantamento aéreo de radiação gama.

Um total de 31 amostras foram utlizadas para análises de pirólise rock-eval, tendo sido realizadas pelos laboratórios da Weatherford e do Insituto Polaco de Geologia, e sendo financiadas pela Repsol E&P (Espanha), Partex Oil&Gas (Portugal) e Instituto Polaco de Geologia (Polônia).

Toda a amostragem para a prospeção geoquímica de superfície foi feita utilizando frascos Isojars, com água destilada e adicionando bactericida,

para inibir qualquer atividade bacteriana. Vinte e sete amostras foram colhidas para este estudo, utilizando uma caroteadora, um tubo metálico e uma marreta. Trinta e uma amostras de água foram colhidas em poços artesianos, furos e nascentes.

As metodologias de detecção remota, utilizadas para definir as zonas de amostragem, mostraram-se bastante eficientes na indicação de zonas com possíveis ocorrências de emanações de hidrocarbonetos. Do ponto de vista da prospecção geológica a presença de hidrocarbonetos gasosos nas formações da Zona Sul Portuguesa é clara e evidente. Eles estão presentes no solo e na água, em quantidades significativas.

Palavras-chave: Geoquímica; Detecção Remota; Hidrocarbonetos Não-convencionais; Hidrocarbonetos Leves; Zona Sul Portuguesa

INDEX | V

LIST OF FIGURES | VI

LIST OF TABLES | VII

LIST OF GRAPHS | VIII

LIST OF MAPS | IX

LIST OF APPENDICES | X

LIST OF ABBREVIATIONS AND ACRONYMS | XI

AGSZ: Azores-Gibraltar Shear Zone

AOI: Area of Interest

atm: Atmosphere

B: Brangança

BAFG: Baixo Alentejo Flysch Group

BAOC: Beja-Acebuches Ophiolite Complex

BCSZ: Badajoz-Córdoba Shear Zone

CAZ: Central Armorican Zone

CIZ: Central Iberian Zone

CO: Cabo Ortegal

cps: Counts per Second

CZ: Cantabrian Zone

DRAD: Parameter defined by Saunders *et al.* (1993) to capitalise the relationships between KD and UD

ECD: Electron Capture Detector

ECN: Effective Carbon Number

ETM+: Enhanced Thematic Mapper Plus

EU: European Union

EUR/kWh: Euro per kilowatt hour

FID: Flame Ionization Detector

Fm(s): Formation(s)

FPD: Flame Photometric Detector

ft: Feet

g: Gram

GC: Gas Chromatography

GC-MS: Gas Chromatography and Mass Spectrometry

GMC: Galiza-Central Massif Ocean

GR: Gamma Radiation

HA: Hydrocarbon Anomaly

HI: Hydrogen Index

HS-GC: Headspace-Gas Chromatography

IPB: Iberian Pyrite Belt

IRMS: Isotope Ration Mass Spectrometry

IVB: Iberian Variscan Belt

K: Potassium

KD: Result of the equation $(K_s-K_i)/K_s$

kg: Kilogram

L: Litre

LB: Leon Block

LDB: Le Danois Bank

LEL: Lower Explosive Limit

m: Metre

M: Morais

MCL: Maximum Contaminant Level

µg: Microgram

µL: Microlitre

µm: Micrometre

mD: Millidarcy

mg: Milligram

ml: Millilitre

mm: Millimetre

min: Minute

MV(s): Mud Volcano(s)

NASZ: Norh American Shear Zone

NAZ: North Armorican Zone

n/d: not determined

nD: nanoDarcy

nL: Nanolitre

NPD: Nitrogen–Phosphorus Detector

O: Ordenes

OI: Oxygen Index

OMT: Ossa Morena Terrane

OMZ: Ossa Morena Zone

pA: Picoampere

PC: Pearson Correlation

PI: Production Index

PLA: Pulo do Lobo Antiform

ppb: Part per Billion

ppm: Part Per Million

ppmv: Part per Million by Volume

PQG: Phyllites-Quartzites Group

PSS: Petroleum Seepage System

PTSZ (PTFASZ): Porto-Tomar Ferreira do Alentejo Shear Zone

SASZ: South Armorican Shear Zone

SAZ: South Armorican Zone

SPME: Solid Phase Micro-Extraction

SPT: South Portuguese Terrane

SPZ: South Portuguese Zone

STZ: Saxo-Thuringian Zone

TBCSZ: Tomar-Badajoz-Córdoba Shear Zone

TC: Total Count

TCD: Thermal Conductivity Detector

Tg: Teragram

Th: Thorium

Tmax: Maximum temperature of hydrocarbon generation (sample)

TN: Thorium Normalization

TOC: Total Organic Carbon

TPES: Total Primary Energy Supply

TPS: Total Petroleum System

U: Uranium

UD: Result of the equation $(U_s-U_i)/U_s$

UPS: Unconventional Petroleum System

UTM: Universal Transverse Mercator coordinate system

VOC(s): Volatile Organic Compound(s)

vPDB: Vienna-PeeDee Belemnite

VR: Vitrinite Reflectance

VSC: Volcano-Sedimentary Complex

WALZ: West Asturian-Leonese Zone

WGS: World Geodetic System

wt%: Weight Percent

WV2: WorldView-2

LIST OF EQUATIONS AND EQUIVALENT UNITS | XII

1 ppm = 1 mg/L or mgL^{-1}

1 ppb = 1 µg/L

1 ppm = 1,000 ppb

1 mg/L = 1,000 µg/L

1 feet = 0.3048 metre

1 nanoDarcy = 0.000001 milliDarcy

INTRODUCTION AND OBJECTIVES | 1.0

Unconventional Hydrocarbons | 1.1

Organic-rich shale deposits with potential for hydrocarbon production are referred to as both unconventional reservoirs and resource plays (Boyer & Clark, 2011). Unconventional gas reservoirs contain low to ultra-low permeability and produced mainly dry gas (Boyer & Clark, 2011). Reservoirs with permeability greater than 0.1 mD (milliDarcy) are considered conventional, and those with permeability below 0.1 mD are called unconventional, although there is no scientific basis for this designation (Boyer & Clark, 2011). According to Sakhaee-Pour & Bryant (2011) the accurate measurement of the shales permeability is challenging because it is so small, in the order of 1 nD (nanoDarcy).

According to a more recent definition published by the US National Petroleum Council (NPC), unconventional gas reservoirs are those that can be operated and produced without a large fluid flow, neither in economically viable volumes, unless the well is stimulated by hydraulic fracturing or accessed by a horizontal, multilateral wellbore or some other technique that gives more flow from the reservoir to the well (US National Petroleum Council, 2007). This definition includes tight gas sands and carbonates, as well as resource plays as coal and shales (Ground Water Protection Council and All Consulting, 2009). The term resource plays refer to sediments that work as both reservoirs and source of hydrocarbons. Unlike conventional plays, unconventional plays cover a large area and are generally not restricted to geological structures (Law & Curtis, 2002; Boyer & Clark, 2011).

Hydrocarbons Seepage | 1.2

Natural hydrocarbon seepage has historically been important drivers of global petroleum exploration as a direct indicator of gas and/or oil subsurface accumulations (Link, 1952; Jones & Drozd, 1983; Etiope, 2004). They occur in all petroleum basins and form the basis for most geochemical, microbiological, and non-seismic geophysical hydrocarbon detection methods (Schumacher, 2012), and today it still drives the geochemical exploration for oil and gas (e.g., Schumacher & Abrams, 1996; Abrams, 2005). Seeps have driven petroleum exploration in many countries. They can assist hydrocarbon exploitation in the assessment of geochemical and pressure variations during fluid extraction, and are fundamental for the definition of the Petroleum Seepage System (Abrams, 2005).

There has been considerable scientific interest in extending geochemical methods to the acquisition of data that aid the search for petroleum

reservoirs. This involves studying the genesis and geochemical behaviour of elements and compounds that are naturally associated with these resources at depth and are able to migrate to the surface system (soil-water) (Hale, 2000). Gases exhibit a high degree of geochemical mobility and their dispersion is unconstrained by gravity (Hale, 2000). An active seep is a live indication of at least a partially functioning petroleum system (Berge, 2011). Petroleum system traps are rarely gas-tight and the more volatile hydrocarbons (indeed, in some cases, heavier hydrocarbons) may escape to the surface, producing microseeps (Hale, 2000). These emanation characteristics represent a potentially powerful combination (Hale, 2000), together with source presence, maturity, and migration risks could all be reasonably assigned a zero risk, eliminating an entire risk category. There is little in the explorationist's toolkit that can achieve that level of risk reduction (Berge, 2011).

Remote sensing for Petroleum exploration | 1.3

According to Yang *et al.* (2000) several authors (e.g. Almeida-Filho *et al.*, 1998; Zhang *et al.*, 2011) have attempted to use remote sensing imagery to detect the distinct spectral characteristics of surface manifestations of hydrocarbon microseepages resulting from oil and gas reservoirs at depth (assisting the characterization of the subsurface petroleum systems), as it can be related with some geotectonic structures like fractures and faults.

Almeida-Filho *et al.* (1998) mapped an anomaly in an area of hydrocarbon microseepage using a Landsat-Thematic Mapper false-colour in Tucano Basin, north-eastern Brazil. Zhang *et al.* (2011) also used Landsat-7 Enhanced Thematic Mapper Plus (ETM+) images to interpret hydrocarbon-induced alterations in the north-western part of the Songliao Basin, northeast China. According to these authors, the use of

remote sensing interpretation to define possible areas of hydrocarbon microseepage would be helpful in the primary stages of an exploration cycle.

Among radioactive nuclides in nature, potassium (^{40}K), uranium (^{238}U) and thorium (^{232}Th) have great importance for the petroleum industry since they are used for hydrocarbon prospection/exploration (Fertl, 1979). These three elements can be found, in different amounts, in rock formations and also in source and/or reservoir rocks (Fertl, 1979).

Saunders *et al.* (1993) developed a viable remote sensing prospection/exploration method for hydrocarbon exploration in stratigraphic and structural traps based on surface and aerial gamma-ray (GR) spectrometry data, named Thorium Normalization (TN).

Over the years, some researchers (e.g. Saunders *et al.*, 1993; El-Sadek, 2002; Al-Alfy *et al.*, 2013) have been applying TN as an auxiliary method for hydrocarbon exploration and also to minimize the risk of exploration, therefore increasing the success rate of potential areas. This method, based on TN, was applied in active exploration petroleum fields, matching positive anomalies in 70% to 80% of the actual producing fields.

The results obtained by Saunders *et al.* (1993) show that the TN for the spectral GR data detects hydrocarbons anomalies, at least, in 72,7% of the 706 gas and oil fields. This allows the measurement of detailed factors related to the hydrocarbon presence in depth.

Al-Alfy *et al.* (2013) applied the same method in several oil fields in Egypt in order to determine the hydrocarbon behaviour in sandy reservoirs. The results show that the calculated DRAD (definition in the chapter 4) curve can be used as an indicator of oil accumulations in different wells, with concordance ratios of 82%, 78% and 71%, respectively.

The application of these criteria, in the NE area of Wadi Araba Desert (Egypt), in the identification of an area with valid anomalies, indicated a potential accumulation of exploitable hydrocarbons (El-Sadek, 2002).

Tests were also done in two Australian basins, showing a correlation between the radiometricaly favourable areas and the known oil and gas producer regions (Saunders *et al.*, 1993).

The Aguarita and Dark Horse oil fields and Selden gas field, Texas, were actually discovered using GR spectral data in conjunction with soil gas sampling, magnetic susceptibility measurements, and subsurface geology (Prost, 2014). Barberes *et al.* (2014b) applied TN, using portable GR spectrometer in shales from the South Portuguese Zone (SW of Iberia) to determine areas with possible hydrocarbon emanations in order to characterise an unconventional petroleum system.

Relation between Gamma Radiation and Light Spectrum | 1.4

The relation between gamma radiation and light spectrums (including infra-red) is so far rarely been studied, being scarce the works that address this issue, such as Xie & Zhang (1997), Yonetoku *et al.* (2004) and Czaja *et al.* (2015). The combining of multi-component or multi-spectral images allows even greater ability to identify features with distinctive signatures, or population clusters. The recognition of patterns in the distribution of classes is an important outcome in remote sensing studies (Clark & Rilee, 2010).

Xie & Zhang (1997) collected 16 GR loud blazars (seven BL Lac objects and nine flat-spectrum radio quasars) with both observed near-infrared and GR flux densities and found that the near-IR luminosity correlates better with GR luminosity than with X-ray. According to the authors, a strong correlation between GR and near infrared radiation exists for all the 16 GR loud blazars with well-observed near-infrared and GR data. The authors suggest that this relation may be a common property of GR loud blazars (Xie & Zhang, 1997).

Another interesting work (Yonetoku *et al.*, 2004) estimated a GR burst formation rate based on the relation between the spectral peak energy and the peak luminosity. The authors found a high correlation between the peak energies and the peak luminosities. The work presented by Czaja *et al.* (2015) was based in multispectral data collected from the WorldView -2 (WV2) satellite and it was analyzed along with aerial GR spectra collected during the NNSA Aerial Measuring System response to the Fukushima Dai-ichi Nuclear Power Plant crisis. Using the non-linear dimension reduction method of diffusion maps, the authors had established the correlation of the a priori independent data sets of multispectral and aerial GR survey data collected over the area (Czaja *et al.*, 2015).

Another relevant work, based on other characteristics, was presented by Boyle (1982). As a general comment, the author argues that it seems like remote sensing methods using satellites and aircraft work better in desertic terrains where vegetation is sparse. Where vegetation is abundant the airborne spectral methods based on geochemically stressed that plant regimes resulting from the uptake of excess amounts of certain elements may be useful in the future as suggested by Hemphill *et al.* (1977) and Collins *et al.* (1978). The analysis of vegetation has been suggested as a method of locating uranium and thorium deposits. Enhanced satellite images show specific vegetation patterns which when combined with linear surface features look to be associated with concentrations of uranium and thorium (Boyle, 1982).

Gas Chromatography in Petroleum Industry | 1.5

The analysis of the constituents in petroleum started over 100 years ago, when in 1865 several aromatic hydrocarbons were identified as constituents of petroleum (Speight, 2001). Crude oil and light

hydrocarbons are characterized almost exclusively by GC. Since its introduction, GC has been widely used as principal analytical method for hydrocarbon gases, which have complex compositions. (McNair & Miller, 2009).

According to Rechsteiner Jr. *et al.* (2015), GC is a primary measurement tool for understanding petroleum composition throughout the value chain, from exploration through refining and fuel marketing.

According to Speight (2001), identification of individual constituents of petroleum continued, and the rapid advances in analytic techniques have allowed the identification of large numbers of petroleum constituents. GC is singularly capable to isolating components of interest from interferences demonstrating boiling range distribution, and establishing compositional properties of sample mixtures from air components up to virtually any hydrocarbon, that can be vaporized at <350°C (Rechsteiner Jr. *et al.*, 2015).

Gas analyses are critically important throughout the petroleum industry value chain. Beyond the implications inherent in the genesis of different hydrocarbons, the price of natural gas depends on the composition of the gas (Rechsteiner Jr. *et al.*, 2015).

Mass Spectrometry in Petroleum Industry | 1.6

Analysis of oil samples by mass spectrometry has been taking place for more than five decades with the application of GC-MS in the hydrocarbon analysis passed through an explosive period very much similar to mass spectrometry in the 1950's. This phenomenon was first applied in a petroleum laboratory by O.L. Roberts at the Atlantic Refining Company in October 1942. Several researchers also applied the technique to analyze light hydrocarbon samples and low boiling organic compounds (Mendez & Bruzual, 2003).

The application of mass spectrometry in the petroleum industry started with the analysis of gas and low boiling liquid samples. However, the composition analysis of hydrocarbons and aromatics compounds containing one or more of sulfur, nitrogen, and oxygen in distillates has become very important in refining of crude oils and in the storage and use of refined products. Moreover, sulfur- and nitrogen-containing species may poison catalysts and must be removed prior to certain oil refinery processes. The use of high-resolution mass spectrometry eliminates most of the interferences between saturate and aromatic hydrocarbons, and removes some of the interferences of sulfur compounds and overlapping hydrocarbons (Mendez & Bruzual, 2003).

The Isotope Ratio Mass Spectrometry (IRMS) required the complete combustion of individual hydrocarbons as they eluted from a GC column, separation of the product CO_2 from H_2O, and rapid determination of the $^{12}C/^{13}C$ ratio. To achieve complete combustion, eluting hydrocarbons flow through a ceramic capillary tube that contains strands of copper wire previous reacted with pure oxygen. At temperatures of ~900°C, all hydrocarbons, including methane, can be completely combusted before they exit the furnace (Walters *et al.*, 2003).

Toluene | 1.7

Toluene (also known as methylbenzene by International Union of Pure and Applied Chemistry) is a clear, colorless liquid with a sweet, pungent odor and is a natural component of coal and petroleum (Kirk *et al.,* 2004). It is a monocyclic aromatic compound with one hydrogen on the benzene ring by replacement of a hydrogen atom by a methyl group (molecular formula $C_6H_5CH_3$) (Government of Canada, 1992; McGraw-Hill, 2003; Oxford, 2005). Toluene is a volatile liquid (boils at 111°C; insoluble in water) that is flammable and explosive and has a relatively high vapor

pressure (3.7 kPa at 250°C) (Government of Canada, 1992; McGraw-Hill, 2003; Oxford, 2005). It is produced from two principal sources: catalytic conversion of petroleum and aromatization of aliphatic hydrocarbons, and is also produced by incomplete combustion of natural fuel materials, and as such is released during forest fires (Government of Canada, 1992; McGraw-Hill, 2003; Oxford, 2005; WHO, 2011). It may therefore be introduced into the environment through petroleum seepage and weathering of exposed coal containing strata and into groundwater from petroliferous rocks. The magnitude of such releases to the environment is unknown (US EPA, 1987). Industrial grade toluene is 98% pure and may contain up to 2% xylenes and benzene (Government of Canada, 1992; McGraw-Hill, 2003; Oxford, 2005).

Toluene can be released into water through chemical spills and spills of petroleum products and from discharges of industrial effluents, and also because of its solubility toluene may leach to groundwater (Government of Canada, 1992). According to Zogorski *et al.* (2006) the sources of most gasoline hydrocarbons (gasoline hydrocarbons are among the most intensively and widely used volatile organic compounds, including toluene) in aquifers probably are releases of gasoline or other finished fuel products. Estimates for the United States indicate that gasoline and oil spills account for about 90% of all toluene releases into water (Gilbert *et al.*, 1983). Aquifer conditions (aerobic and anaerobic) and microbial metabolism (respiration, fermentation, and co-metabolism) control the environmental degradation of volatile organic compounds (VOCs) in groundwater (Lawrence, 2006).

The soil-gas plumes of aromatic compounds like benzene or toluene are much more restricted to the vicinity of the source and somewhat retarded, toluene shows its maximum spreading around 120 days (Maier *et al.*, 2005).

Objectives | 1.8

Hydrocarbons seeps (emanations) occurs along a complex interconnected net of fences, joints, microfractures and also stratification planes (Saunders *et al.*, 1999). When the gas bubbles reach the phreatic level and soil, the gas inside the bubbles start entering the interstitial material, where it can be sampled, detected and characterized by sensitive gas chromatography/mass spectrometry (Saunders *et al.*, 1999).

According to Seneshen *et al.* (2010) a surface geochemical prospecting can be designed to assist the independent producers and explorers who have limited financial and personnel resources, reducing exploration costs and risk especially in environmentally sensitive areas, adding new discoveries and reserves.

This work aims to identify onshore hydrocarbon emanations by surface geochemical prospecting (Tedesco, 1995; Bandeira de Mello *et al.*, 2007; Seneshen *et al.*, 2010; Abrams, 2013) and thorium normalization/ hydrocarbon anomalies (Saunders *et al.*, 1993; Al-Alfy *et al.*, 2013; Barberes *et al.*, 2014b; Prost, 2014; Skupio & Barberes, 2017). Water and soil samples were collected in order to identify light hydrocarbons microseeps (Map 1.1).

New data from rock-eval pyrolysis analysis are also present in this thesis, in order to help the evaluation of the South Portuguese Zone (SPZ) potential for hydrocarbon generation. Rock-Eval pyrolysis is used for petroleum exploration to measure the quantity, quality, and thermal maturity of organic matter in rock samples (Peters & Cassa, 1994). Combined with total organic carbon (TOC) measurements, this is the most rapid and cost-effective screening method for large numbers of samples (Peters, 1999).

The remote sensing methodological techniques presented in this work have an exploratory character, and it were used to assist the surface

geochemical prospecting, in order to identify the best areas to evaluate the hydrocarbon occurrences in soils/groundwater and consequently the identification and characterization of unconventional petroleum system.

This thesis also aims to demonstrate a correlation between airborne GR data and high-resolution satellite images WorldView-2, in order to be an alternative way and facilitate the acquisition of radiometric data, in view of the high costs associated to an airborne GR survey.

The focus area is situated in a wide region along Beja and Faro districts, south of Portugal (Map 1.1), which include the Baixo Alentejo Flysch Group (BAFG) (Oliveira, 1983), composed by Mira and Brejeira Formations (Oliveira *et al.*, 2013). All these formations contain significant thicknesses of black shales mainly Brejeira, the southernmost formation. SPZ has several wide areas with significant average organic carbon content (TOC) and thermal maturation values within hydrocarbons generation zones (Abad, *et al.*, 2001; McCormack *et al.*, 2007; Fernandes *et al.*, 2012, Barberes *et al.*, 2014a). BAFG includes also one more formation, Mértola. However, for geological, geographical and logistical reasons, Mértola Fm. was not included in the surface geochemical sampling.

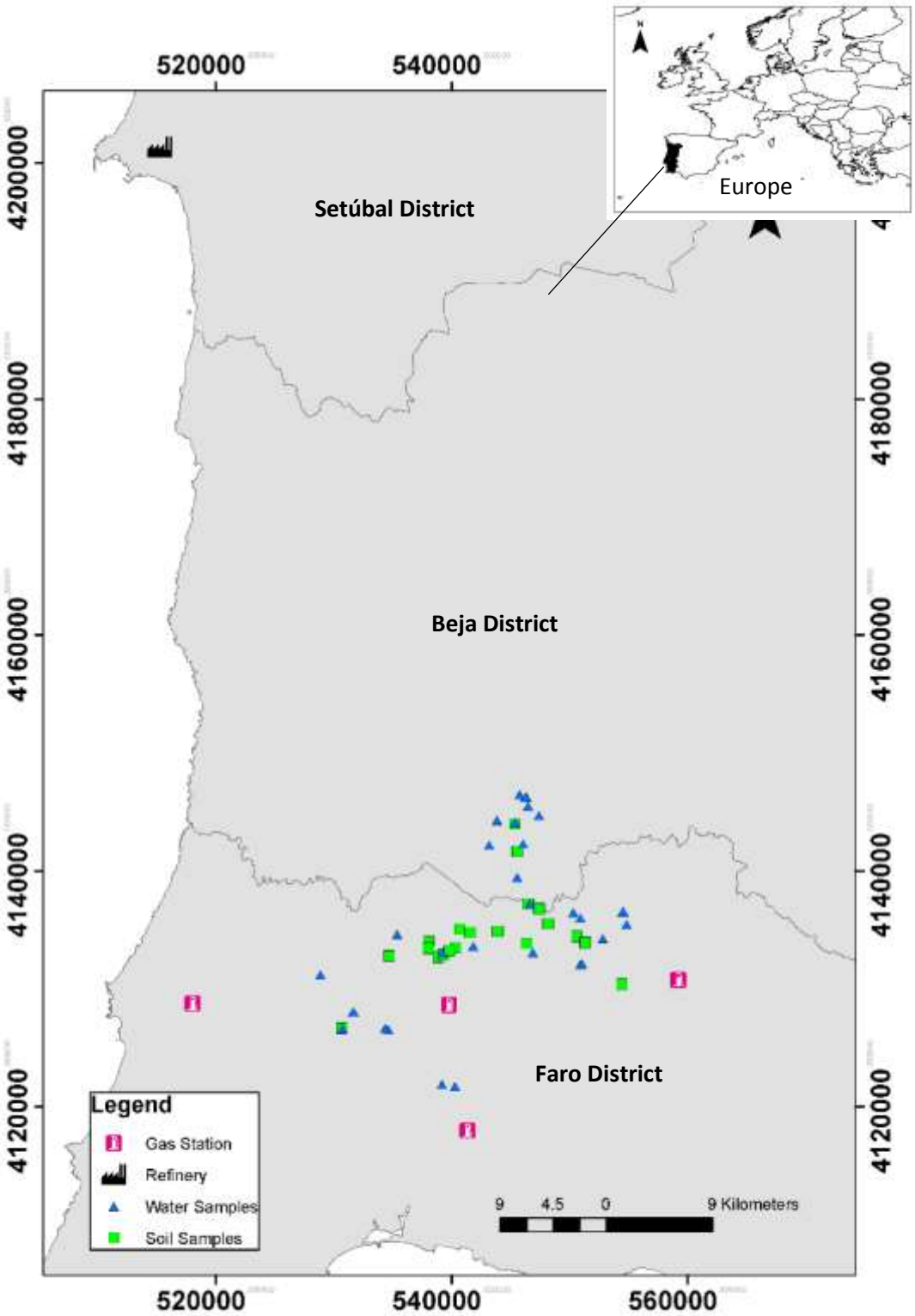

Map 1.1: Location of water and soil samples.

STATE OF ART | 2.0

Maturation Evaluation | 2.1

According to Fernandes *et al.* (2012), the thermal maturation of southwestern Portugal's Upper Palaeozoic rocks is too high, corresponding to the coal rank of high meta-anthracite (Figure 2.1). The same authors studied where there was no increase of the VR values until 1 km of depth, which is not compatible with the natural heat transfer. Therefore, it is interpreted as a result of sin- to post-orogenic heating.

Analysis of the VR made by McCormack *et al.* (2007) suggest that the Palaeozoic rocks of the SPZ (SW of Portugal) are strongly overmature with an average VR of 4.28%. The results from the thin levels of Carboniferous coal are very similar to the ones from the associated mudrocks. This means that the results from the regional mudrocks are not significantly influenced by the presence of reworked vitrinite. According to the author, this is a very important fact as the existence of reworked vitrinite could lead to an over-estimation of the vitrinite values, as the increase of tectonic stress during the coal formation could change its negative biaxial anisotrophy to positive, in case of high tectonic stress (Levine & Davis, 1989; Taylor *et al.*, 1998).

The integration of the stratigraphic evidences with the VR results of one oriented sample of Carboniferous coal shows that it reached the maximum temperature during the post-hercynian deformation, between Carboniferous and Upper Triassic (McCormack *et al.*, 2007). The results from the metamorphic aureoles associated to Mesozoic intrusions suggest that these igneous bodies did not influence the already high maturation levels of the Palaeozoic rocks, even along the dyke's margins (McCormack *et al.*, 2007).

According to the authors, any potential source rock, preserved in the Upper Paleozoic sequence, is now overmature and any potentially generated hydrocarbons would have been lost during the Hercynian deformation or the post-Hercinian uplift and erosion (Figure 2.2 [McCormack *et al.*, 2007]).

According to Abad *et al.* (2001), the diagenesis evolution of the SPZ shale's phyllosilicates until the green schist facies is characterized by several changes on the thickness of the crystal's domains and on the number of crystal imperfections. These changes were quantitative as there were no qualitative changes detected on levels below the epizone. This is in concordance with previous studies made on other low grade metamorphic sequences (Merriman & Peacor, 1999). On a sample scale, the chemical composition of the phyllosilicates is extremely heterogeneous. The increase of the metamorphic grade is the limited tendency towards the homogeneity. In the SPZ there is a general, but not gradual, increase of the metamorphic grade, due to the effect of tectonic compartmentalization associated to the fold-and-thrust system observed in the area of study, which produces a progressive overlapping of different tectonostratigraphic units – imbricated thrusts in overstep or piggy-back systems (Abad *et al.*, 2001).

According to Weatherford (2013) report, all samples of the "Shale Gas in Portugal" project (Partex Oil&Gas and Repsol E&P) have very little organic matter suitable for reflectance measurements. Therefore, the number of

measurements is small. Non-fluorescent granular amorphous organic matter (amorphinite) appears to be the dominant organic matter type in this samples (Table 2.1). There are also small particles that are difficult to identify; they could be solid bitumen, inertinite, or vitrinite. They are classified as pyrobitumen, by Weatherford. The average Ro of pyrobitumen are 1.63% (based on 10 measurements), 1.98% (based on 25 measurements), 2.26% (based on 7 measurements), 1.97% (based on 5 measurements) and 2.29% (based on 5 measurements). Using Schoenherr *et al.* (2007) equation, this translates into vitrinite reflectance equivalent of 1.78, 2.12, 2.38, 2.11, and 2.42% for five analyzed samples (Table 2.2). Brownish black pollen and spores were found in just one sample. In transmitted light, structureless organic matter is almost black with brown tint remaining, suggesting TAI 3.7 for all samples (Table 2.1). These reflectance values, TAI, and absence of fluorescence all suggest that the organic matter is post-mature and within the dry gas zone (Table 2.1) [Weatherford, 2013]).

Barberes *et al.* (2014a) projected the thermal maturation data from Weatherford Laboratories in a xy graph with the Th/K ratio for each value, based on the relation suggested by Fertl (1979), between Th/K ratio and the mean reflectance. The result was an apparent inverse relationship between such variables, allowing an estimation of the organic maturation values for the rest of the samples, based on the straight-line equation. This relation was used to estimate maturation in the other samples (Figure 2.2 [Barberes, *et al.*, 2014a]).

Kisch (1987) proposed a comparison table between the VR values, the low metamorphic grade zones (diagenesis, anquimetamorphism and epimetamorphism), the coal rank and the different windows of hydrocarbon generation (Figure 2.1).

The limits established by Abad *et al.* (2001) for the SPZ and for each of the low metamorphic grade zones were inserted on Kisch's table (1987), in order to compare the bibliographic organic maturation data, the illite's

crystallinity and the maturation values estimated for this work (Figure 2.1).

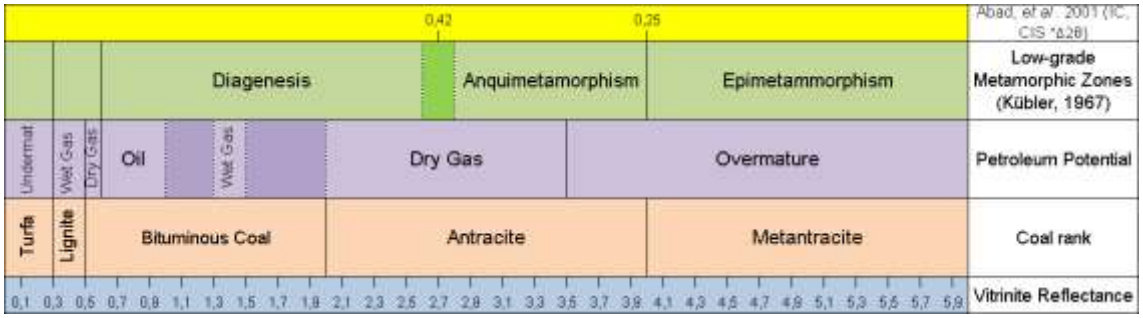

Figure 2.1: Comparison table between coal rank, VR, petroleum potential, low-grade metamorphic zones (Kübler, 1967) and the boundaries between zones of low grade, defined by Abad et al. (2001) for SPZ (adapted from Barberes et al., 2014a).

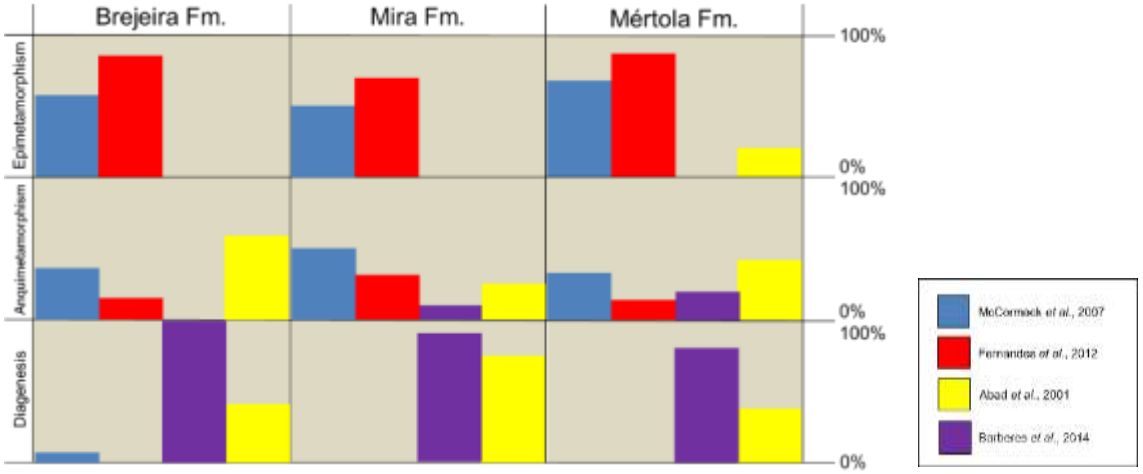

Figure 2.2: Compilation of VR values (Fernandes et al., 2012 and McCormack et al., 2007), illite crystallinity (Abad et al., 2001) and the estimated maturation for this work, from the relationship between Th/K ratio and VR values. The data is divided according to the percentage of occurrence values, each metamorphic area in the three formations (adapted from Barberes et al., 2014a).

Based on a table comparing the distribution, in percentage, of the data of each author on the different formations and for each metamorphic zone, it has been possible to distinguish two scenarios (Figure 2.2): (1) according to the Fernandes *et al.* (2012) and McCormack *et al.* (2007) data, the studied formations are mainly over mature in terms of hydrocarbon potential; (2) according to Abad *et al.* (2001) data and the

values estimated by Barberes *et al.* (2014a), the BAFG formations are mainly between wet and dry gas and the beginning of the overmature zone.

The difference between results from McCormack *et al.* (2007), Fernandes *et al.* (2012) and Barberes *et al.* (2014a) are not relevant from the point of view of hydrocarbon generation kinetics, all of them are inserted over dry gas window.

Formation	Liptinite (%)				Vitrinite (%)	Inertinite %	Solid Bitumen (%)	Liptinite Fluores. (%)	Oil prone (%)	Gas prone (%)	Pollen/ Spores	TAI (Staplin1969)
	Alginite (%)	AOM (%)		Other Liptinite (%)								
		Fluorescent	Non Fluorescent									
Brejeira_1	0	0	80	0	0	0	20	0	0	80	absent	3.7
Brejeira_2	0	0	75	0	trace	15	10	0	0	75	absent	3.7
Brejeira_3	0	0	70	0	trace	15	15	0	0	70	absent	3.7
Brejeira_4	0	0	80	0	trace	5	15	0	0	80	sporadic	3.7
Brejeira_5	0	0	75	0	0	10	15	0	0	75	absent	3.7

Table 2.1: Results of organic matter petrology from 5 samples (Brejeira 1, 2, 3, 4 and 5), analyzed by Weatherford Laboratories.

Formation	Brejeira_1	Brejeira_2	Brejeira_3	Brejeira_4	Brejeira_5
Minimum R_o (%)	1.5	1.5	1.89	1.78	2.07
Maximum R_o (%)	1.78	2.51	3	2.32	2.59
Number of points	10	25	7	5	5
Standard deviation	0.095	0.249	0.38	0.216	0.192
Mean R_o value of pyrobitumen (%)	**1.63**	**1.98**	**2.26**	**1.97**	**2.29**
VRE value (%) Schoenherr, 2007	**1.78**	**2.12**	**2.38**	**2.11**	**2.42**

Table 2.2: Results of organic matter maturation from 5 samples (Brejeira 1, 2, 3, 4 and 5), analyzed by Weatherford Laboratories.

Organic Matter Content | 2.2

The measured TOC values (Barberes, 2013) vary between 0.26 wt% and 1.84 wt%, with a mean value of 0.81 wt%, 0.91 wt% and 0.72 wt% for the Mértola, Mira and Brejeira formations, respectively. The majority of the

analysed samples had values between 0.5 wt% and 1.0 wt%, meaning that according to Peters & Cassa (1994) quality classification of rocks' petroleum potential they are classified as "reasonable",

Stratigraphically, the TOC values have a random distribution. However, the decrease of sampling (as explained above), from one unit to another, is responsible for some doubts about the conclusions associated to "vertical" behaviour of the TOC values. Therefore, future systematic analyses are required in order to prove these conclusions.

The mature source rock is usually characterized by lower TOC values than its immature equivalent before burial and hydrocarbon generation. This is due to the fact that some of its initial TOC was converted to oil and/or gas at the subsurface. Even if the gas is preserved in the subsurface, inside the source rock, it is expected a lower TOC value compared to the initial value, since the quantity converted to hydrocarbon cannot be measured as TOC anymore. For this reason, if the rock is mature, it will have a general lower TOC index, both in the surface and subsurface.

According to Verweij (1993), a plausible hypothesis for the remaining/measured TOC is that it represents around 40% of the initial TOC, in case of dry gas window. Even if the maturation is higher, there is always some TOC that remains as inert or pyrobitumen. As a consequence, if we want to compare the TOC of immature and mature areas, we have to make assumptions and then recalculate all the "initial TOC" values.

Considering the hypothesis of 60% loss (Verweij, 1993) of the initial TOC, all measured TOC values were recalculated in order to estimate its original values. The actual value represents the values before the hydrocarbon generation.

The recalculated values vary between 0.65 wt% and 4.59 wt%, having a mean of 2.02 wt%, 2.28 wt% and 1.80 wt% for the Mértola, the Mira and

the Brejeira formations, respectively. The majority of the recalculated values vary from 1.0 wt% to 4.0 wt%, which means that according to Peters & Cassa (1994) classification, they are improving from "Good" to "Very Good".

Offshore Thermogenic Hydrocarbon Occurrence | 2.3

Días-del-Río *et al.* (2003) reports the first discovery and sampling of vast fields of hydrocarbon-derived carbonate chimneys along the Gulf of Cadiz continental slope, at depths between 500 and 1200 m. A large variety of carbonate chimneys (more than 200 samples) were recovered from two different areas, named the DIASOM and TASYO fields (Map 2.1).

The chimneys are mainly composed of authigenic carbonates (ankerite, Fe-bearing dolomite and calcite) with abundance of iron oxides, forming agglomerates of pseudo-pyrite framboids, interpreted as formed from a mixture of deep thermogenic hydrocarbons and shallow biogenic methane (Figure 2.3 and 2.4 [Días-del-Río *et al.*, 2003]).

Overpressured compartments generated beneath salt/shale arched wedges have been suggested as a mechanism to provide avenues for hydrocarbon gases, brines and fluidized sediments to migrate upwards through contraction toe-thrust structures (Lowrie *et al.*, 1999).

The $\delta^{13}C$ values from the calcite chimney collected in the Hespérides mud volcano and associated with a mud diapir (Días-del-Río *et al.*, 2003) located in the TASYO field, also show values of -23.2‰, possibly related to a thermogenic gas source (Días-del-Río *et al.*, 2003). In contrast, on the Moroccan margin, in the ESF field, isotopic values of -37‰, corresponding to Fe-bearing dolomite chimneys with mushroom morphology, indicate their possible origin as mixing between thermogenic and biogenic sources (Días-del-Río *et al.*, 2003). Extremely depleted $\delta^{13}C$

values of -46‰ indicate their possible source as entirely from methane release (Figure 2.3 [Días-del-Río *et al.*, 2003]).

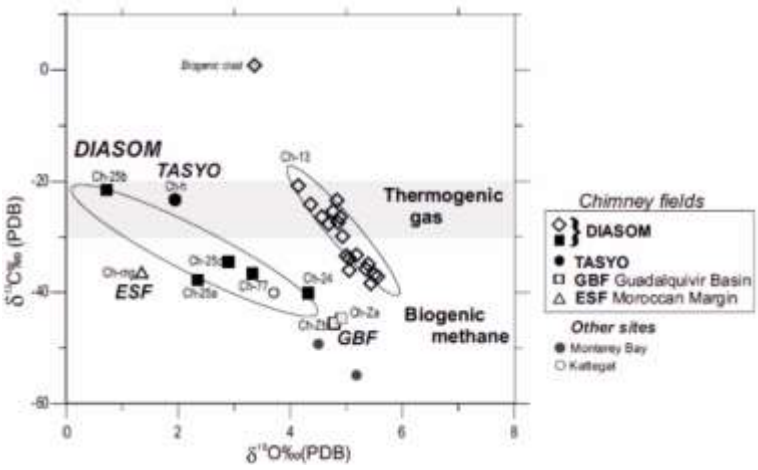

Figure 2.3: Plot of $\delta^{13}C$ and $\delta^{18}O$ values for carbonate chimney samples from the different fields of the Gulf of Cádiz. The boundary between thermogenically formed gas and biogenic gas is based on isotopic data of gas-charged sediments in mud volcanoes of the Gulf of Cádiz (Stadnitskaia et al., 2006). Adapted from Días-del-Río et al. (2003).

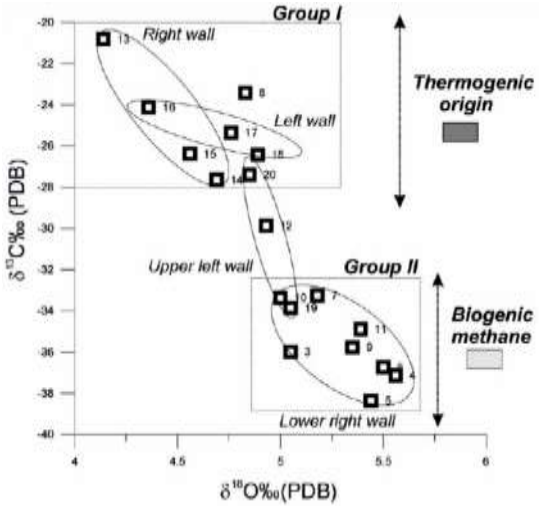

Figure 2.4: Plot of $\delta^{13}C$ and $\delta^{18}O$ values for the ankerite chimney ch13 from the Ibérico mound, Gulf of Cádiz: Group I shows low depleted $\delta^{13}C$ values (-20 to -26‰) and low $\delta^{18}O$ values interpreted as derived from thermogenic sources or high-order hydrocarbon. Group II shows more depleted $\delta^{13}C$ values from 333 to -38‰ that fit better within the isotopic window for biogenic gas in the Gulf of Cádiz (Stadnitskaia et al., 2006). Adapted from Días-del-Río et al. (2003).

In this sense, the $\delta^{13}C$ values from the ankerite chimneys of the DIASOM field, ranging from -20.81‰ to -35‰, fall almost entirely within the window of thermogenic gas formed (Figure 2.3). In contrast, only the mounded-type chimney shows extreme $\delta^{13}C$ depletion, with values of -40‰, indicating their probable origin from a biogenic methane source (Días-del-Río *et al.*, 2003). Furthermore, the dataset of $\delta^{13}C$ values within chimney ch13 (DIASOM) points to the existence of some types of variability in the hydrocarbon sources of the fluid venting, from

thermogenic to biogenic, during the formation of the chimneys in this field (Figure 2.4 [Días-del-Río *et al.*, 2003]).

Stadnitskaia *et al.* (2006) was the first detailed investigations of molecular and isotopic characteristics of hydrocarbon gas and organic matter in mud volcanoes (MVs) of the Gulf of Cádiz. They report the results on molecular and carbon isotopic characteristics of hydrocarbon gas collected in gas saturated pelagic sediments and mud volcano deposits (mud breccia) from six MVs in the Gulf of Cadiz (Map 2.1 and Table 2.3 – tree of these MVs are described here). One of the objectives was to determine the presence of thermogenic hydrocarbons that migrated from the deep subsurface (Stadnitskaia *et al.*, 2006).

Concentrations of methane and wet gas components in all studied locations of the Gulf of Cadiz are clearly anomalous (Stadnitskaia *et al.*, 2006). High concentrations of C_{2+} especially C_4 and C_5 hydrocarbons are expected if thermogenic gases are present (Cline & Holmes, 1977; Sandstrom *et al.*, 1983). This signifies that gases from both mud volcano provinces of the Gulf of Cadiz are characterized by input of thermogenic hydrocarbons from deeper sources. Besides, the down-core concentration profiles of C_1–C_4(C_5) hydrocarbons (despite their difference in concentration levels) show an absence of correlation with the TOC content, which also indicates an allochthonous nature of the gas to the hosting mud breccias (Stadnitskaia *et al.*, 2006).

The stable carbon isotope composition of methane is dependent on type and maturity of the initial source (Stahl, 1977, 1979). Migration and/or mixing may be a mechanism of carbon isotope fractionation, and is reflected in either enrichment or depletion with ^{12}C (Stadnitskaia *et al.*, 2006). Figure 2.5 shows that the composition characteristic of gas from the MVs of the Ginsburg and Jesus Baraza falls in the 'thermogenic gas field'. Besides, the source, from which the gas was derived, is indicated on the diagram as kerogen of type II for the Ginsburg MV and as a mixture

of kerogens II and III for the Jesus Baraza MV (Figure 2.5 [Stadnitskaia *et al.*, 2006]).

Mixing of gases of different origins is a common phenomenon (Whiticar, 1994), which indicates that gas components are not necessarily co-genetic. In a thermogenic co-genetic C_1–C_2 pair, methane is depleted in ^{13}C between 5 and 10‰ relatively to the ethane (Silverman, 1971; Deines, 1980). Nevertheless, it is difficult to recognize the source or sources for the methane from the Carlos Ribeiro MV (Figure 2.5). Mixing of early formed biogenic gas and later formed thermogenic gas results in a lack of abilities to differentiate the thermogenic gas due to compositional changes caused by mixing (Rice & Claypool, 1981). Besides, the earliest formed thermogenic methane is isotopically light, $\delta^{13}C$ values are -55‰ (Sackett, 1978; Stahl, 1979). The decrease in $\delta^{13}C$ difference between C_1 and C_2 is a result of an increase of the thermal maturity (James, 1983).

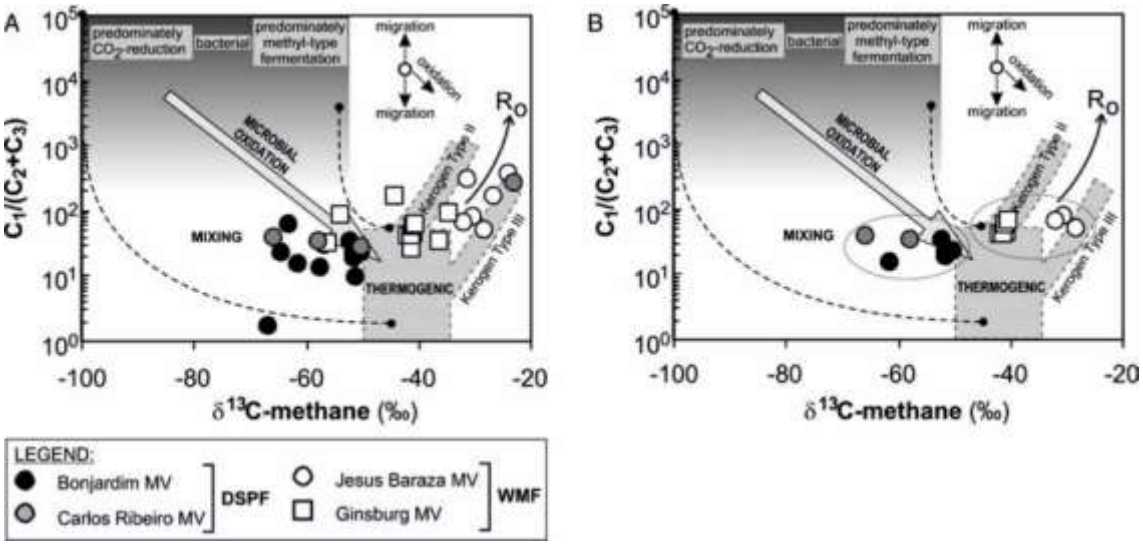

Figure 2.5: Bernard diagram to delineate gas types (after Whiticar, 1994). Two different groups of gases in the WMF and DSPF are recognized. The WMF gas represents mature gases, (Ro<1.2%), derived from kerogen type II and/or a mixture of kerogens of types II and III. The DSPF gas consists of a mixture of thermogenic and bacterial gases. (A) The complete suite of gas data; (B) the data from the intervals below 60 cm bsf. Adapted from Stadnitskaia et al. (2006).

Core No.	Interval (cm) bsf	Carbon Isotopes				
		C1	C2	C3	iC4	nC4
Western Moroccan field						
Jesus Baraza MV TTR10 AT-231G	10	-31	-27	-32	-25	-26
	30	-24	-31	-33	-27	-24
	50	-27	-30	-27	-29	-27
	63	-30	-16	-31	-34	-26
	79	-32	-25	-27	-27	-22
	89	-28	-19	n/d	n/d	n/d
	Average	-29	-25	-30	-28	-25
Ginsburg MV TTR10 AT-236G	10	-54	-16	n/d	n/d	n/d
	30	-36	-12	n/d	n/d	n/d
	88	-42	-23	-22	-25	-24
	135	-41	-24	-23	-26	-24
	Average	-43	-19	-23	-25	-24
Ginsburg MV TTR10 AT-238G	0	-35	-23	-22	n/d	n/d
	30	-44	-20	-22	-28	-30
	65	-41	-22	-22	-25	-24
	85	-56	-30	-21	-27	-19
	105	-42	-23	-22	-25	-24
	142	-41	-24	-23	-26	-24
	162	-41	-24	-24	-26	-25
	182	-40	-24	-23	-26	-25
	Average	-43	-24	-22	-26	-24
Deep South Portuguese field						
Bonjardim MV TTR10 AT-226G	20	-51	-29	-23	n/d	n/d
	50	-64	-23	-13	n/d	n/d
	90	-62	-31	-18	-27	n/d
	Average	-59	-28	-18	n/d	n/d
Bonjardim MV TTR10 AT-227G	24	-51	-34	-25	-30	-27
	36	-63	-26	-27	-28	-22
	46	-57	-28	-26	-27	-25
	75	-58	-24	-24	n/d	n/d
	141	-52	-28	-21	-28	-20
	161	-52	-29	-21	-28	-21
	195	-50	-28	-22	-28	-20
	Average	-55	-28	-24	-28	-22
Carlos Ribeiro MV TTR10 AT-243G	0	-23	n/d	n/d	n/d	n/d
	40	-50	-14	n/d	n/d	n/d
	60	-66	-20	-22	-26	-23
	136	-58	-25	-23	-27	-24
	Average	-49	-20	-22	-26	-23

Table 2.3: Stable carbon isotope compositions. Adapted from (Stadnitskaia et al., 2006).

The study of the Gulf of Cadiz on the basis of multichannel seismic profiles and wells illustrates the stratigraphy and tectonics (Map 2.1). The evolution of the southern Iberian margins was more complex than in most North Atlantic margins since it entailed several phases of rifting, convergence and strike-slip motions (Maldonado *et al.*, 1999). Fault-bounded blocks of flysch and Sub-betic units crops out over large areas of the southeastern Iberian shelf. The basement of the northwestern area, in contrast, is represented by the Paleozoic rocks of the Hercynian massif of Iberia (Figures 2.6, 2.7 and 2.8 [Maldonado *et al.*, 1999]).

The basement in the northwestern sector is restricted to a narrow zone close to the coastline, while the overlying Cenozoic deposits show significant seawards thickening (Maldonado *et al.*, 1999).

According to Maldonado *et al.* (1999) and Ramos *et al.* (2014) the same Paleozoic rocks of SPZ, are probably the basement under the offshore MVs (Map 2.1).

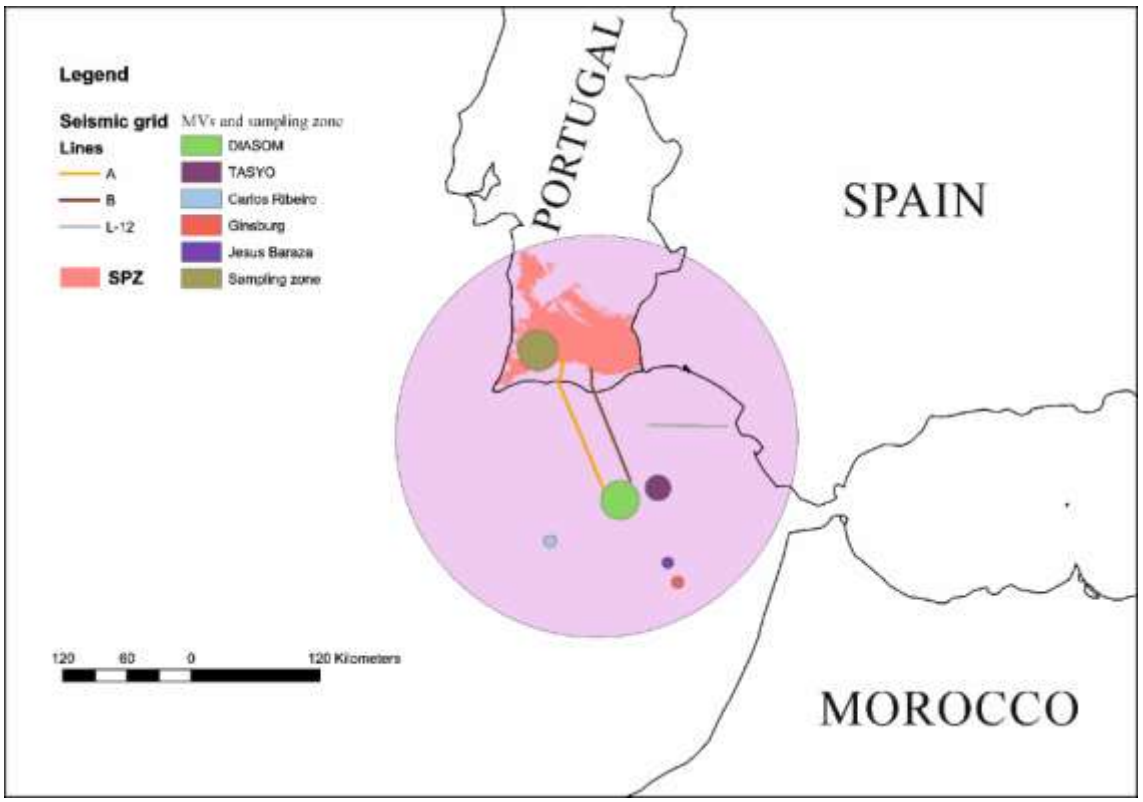

Map 2.1: Map with compiled information about thermogenic gas seeps/microseeps (from this project and offshore mud volcanos) and seismic lines (Maldonado et al., 1999; Días-del-Río et al., 2003; Stadnitskaia et al., 2006 and Ramos et al., 2014). The purple circle represents the possible carboniferous coverage are, onshore and offshore. This area was defined based on the onshore and off-shore occurrence of SPZPaleozoic formations.

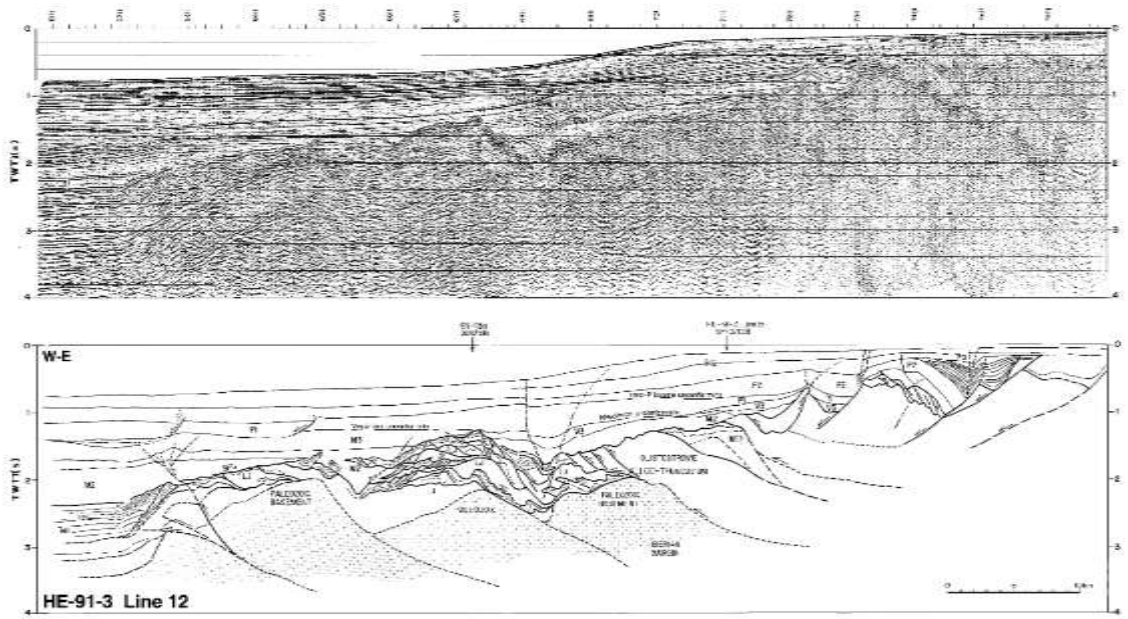

Figure 2.6: Seismic line 12 and representative cross-section of southern Gulf of Cádiz representing the offshore Paleozoic basement. For location please see the map 2.1. Adapted from Maldonado et al. (1999).

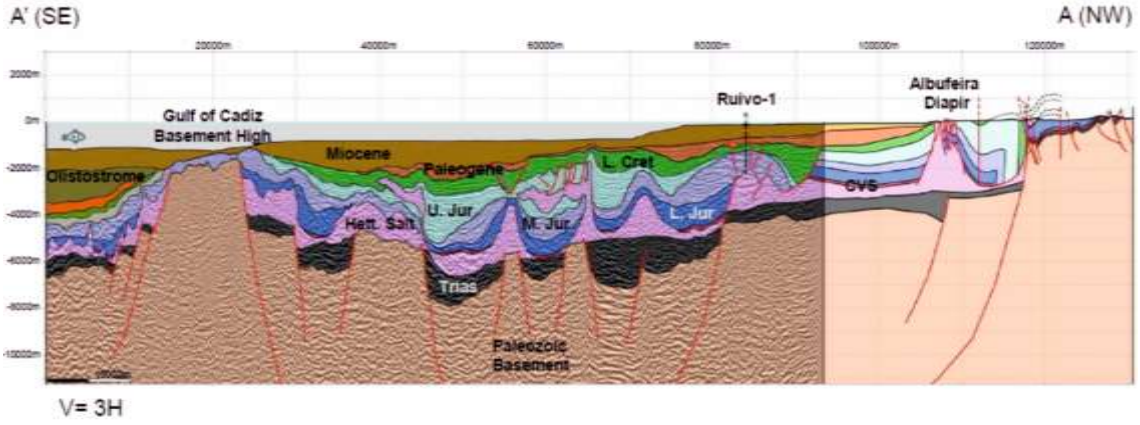

Figure 2.7: Seismic line A'-A representing the offshore Paleozoic basement. For location please see the map 2.1. Adapted from Ramos et al. (2014).

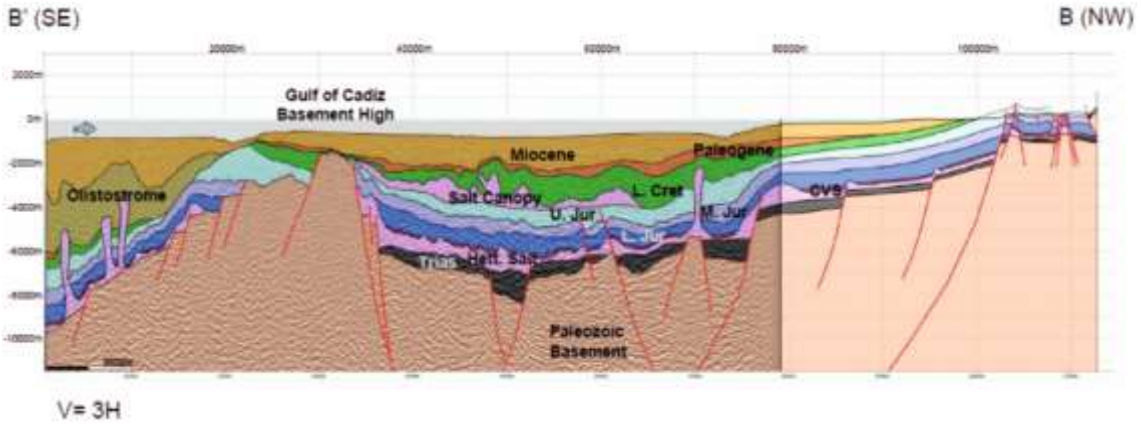

Figure 2.8: Seismic line B'-B representing the offshore Paleozoic basement. For location please see the map 2.1. Adapted from Ramos et al. (2014).

GEOLOGICAL FRAMEWORK | 3.0

Regional Tectonics | 3.1

According to Ribeiro *et al.* (2007), the Variscides tectonic style is clearly distinct from Alpinotype orogens, being possible to reconstruct a relatively continuous "Variscan Belt" extending from southern Iberia to northeastern Bohemia (Matte, 1986). The reason to relate the characteristics of ocean basins to the orogens generated by closure, according to Dias *et al.* (2016), depends on the lithosphere rheological evolution during the entire Wilson cycle. The authors say that the age of the first and main Variscan tectonic event is at least Middle Devonian in the inner domains of the Iberian Variscides and it propagates towards its external domains where it has an Upper Carboniferous age. In Early Carboniferous, the tectonic setting is similar, but previous plate convergence has evolved to continental collision

(Figure 3.1). In the Upper Carboniferous/Lower Permian a drastic change occurs (Brandon Weil *et al.*, 2013). The irregular shape of the southern margin of Laurentia/Baltica block has probably induced an anticlockwise rotation of Iberia during the intra-continental deformation (Dias & Ribeiro, 1995).

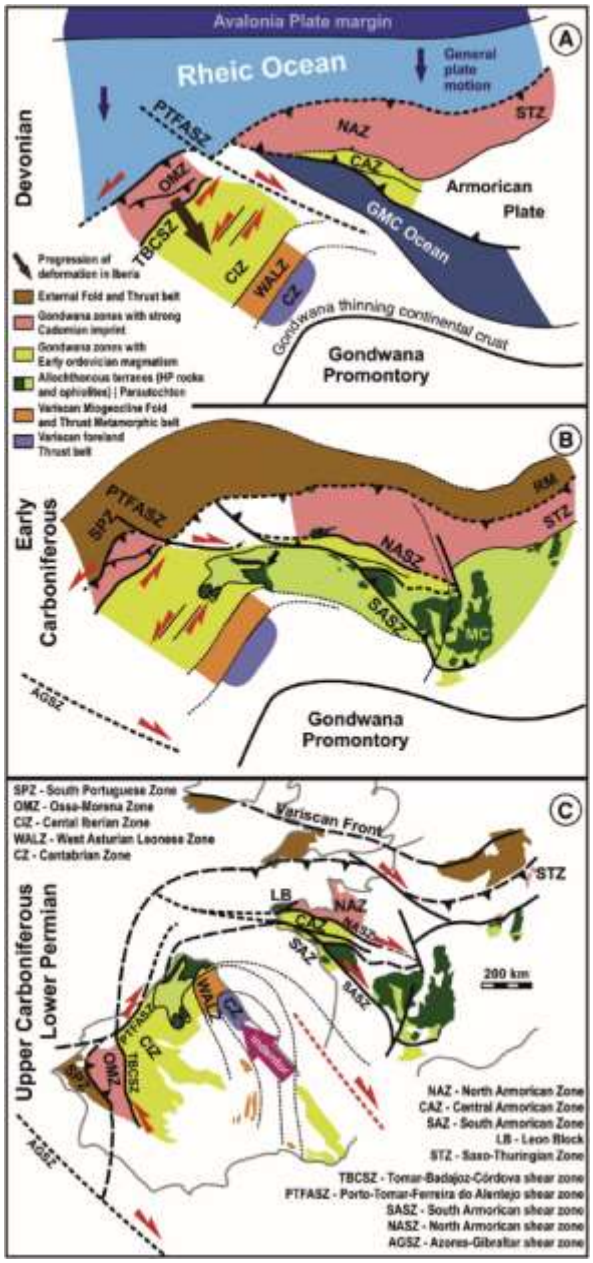

Figure 3.1: Schematic interaction between Avalonia/Armorica and northern Gondwana during Upper Paleozoic. A — Convergence between Iberia and Armorica during Middle Devonian; B — The collision stage with all the plates assembled; C — The westward indentation of the Cantabrian basement and the formation of major Iberian Arcs. GMC-Galiza-Central Massif Ocean. Adapted from Dias et al. (2016).

Iberian Variscan Belt | 3.2

The Iberian Variscan Belt (IVB) is part of the Variscan Iberian (or Hesperian) Massif, i.e. the pre-Alpine basement of the Iberian Peninsula, which crops out in the southwestern Iberian Peninsula (Tornos *et al.*, 2002). The IVB has long been subdivided into several zones, parallel to the belt axis, mainly based on the stratigraphic and palaeogeographic considerations (Tornos *et al.*, 2002). The SW IVB (southernmost segment of the Iberian Massif) comprises the Ossa Morena Zone (OMZ) and the South Portuguese Zone (SPZ) (Figure 3.2) (Tornos *et al.*, 2002; Onézime *et al.*, 2003; Pérez-Estaún *et al.*, 2004). The OMZ and SPZ are interpreted to represent continental fragments that collided during the Variscan orogeny and the border between them is marked by oceanic affinity units, which makes it to be recognized as a Variscan Orogen suture (now modified by strike-slip faults) recognized by detailed geological mapping and supported by petrofabric analysis, mineralogical and petrological/geochemical data (Fonseca & Ribeiro, 1993; Quesada *et al.*, 1994; Fonseca *et al.*, 1999; Mateus *et al.*, 1999; Tornos *et al.*, 2002; Figueiras *et al.*, 2002; Pérez-Estaún *et al.*, 2004), and this suture is defined by the Pulo de Lobo Antiform and the Beja-Acebuches ophiolite (Silva *et al.* 1990; Quesada *et al.* 1994; Fonseca *et al.*, 1999). The preservation of this ophiolite in the Variscan suture zone proves that some kind of plate tectonics model, involving a Wilson cycle and a type A collision (continent/continent collision) with opening and closure of the Palaeozoic Rheic ocean is necessary to explain the geotectonic evolution in the IVB (Fonseca & Ribeiro, 1993; Ribeiro *et al.*, 2007).

According Oliveira (1990a) within the SPZ, five main geological domains (Map 3.1) are recognized namely, Beja-Acebuches Ophiolite Complex (BAOC), Pulo do Lobo Antiform (PLA), Iberian Pyrite Belt (IPB), Baixo Alentejo Flysch Group (BAFG) and Southwest Portugal (Bordeira and Aljezur Antiforms). A clear geological relationship can be established

between the IPB, the BAFG and the SW Portugal domains (Oliveira, 1990a).

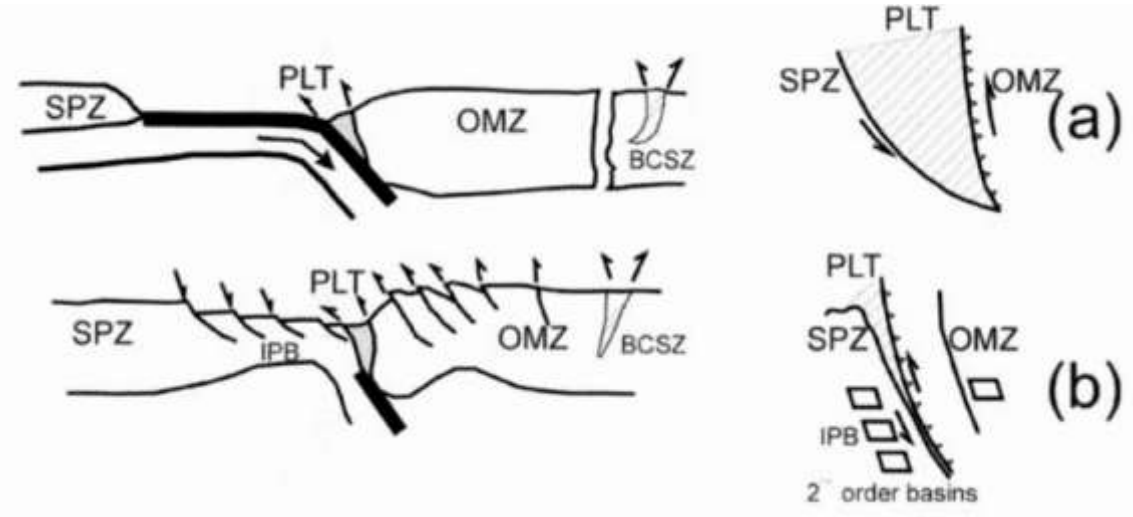

Figure 3.2: Interpretative cross section and map of the SW margin of the Variscan Belt of Iberia during Variscan times. Modified from Silva et al. (1990) and Quesada (1991). (a) Plate convergence, subduction and minor oblique collision and partial obduction during the late Devonian (pre-Fammenian); (b) Generalized oblique collision, lateral escape of the South Portuguese Zone and formation of second order pull-apart basins and volcanic alignments in the Iberian Pyrite Belt and Ossa Morena Zone during the late Devonian-Lower Carboniferous. Not to scale. SPZ, South Portuguese Zone; IPB, Iberian Pyrite Belt; OMZ, Ossa Morena Zone; BCSZ, Badajoz-Cordoba Shear Zone; PLT, Pulo de Lobo Terrane (including the Beja-Acebuches Ophiolite). Adapted from Tornos et al. (2002).

IPB (well-known metallogenic province) can be described as a succession of three Devonian to Dinantian formations: the Phyllites-Quartzites Group (PQG), the Volcano-Sedimentary Complex (VSC), and the Culm (Map 3.1) (e.g., Schermerhorn, 1970).

According to Onézime *et al.* (2003) the Devonian in the sense of the PQG corresponds to a passive margin detritic sequence and constitutes the oldest unit observed to the south of the PLA.

The uppermost unit of the IPB, the Culm, corresponds to a Visean flyschoid sequence commonly associated with the BAFG (Oliveira, 1983). However, Onézime *et al.* (2003) propose to consider the base of the BAFG,

the Culm formation, as part of the IPB, both sequences being closely associated. According to Moreno & González (2004), in the Portuguese part of IPB, the Culm is called BAFG.

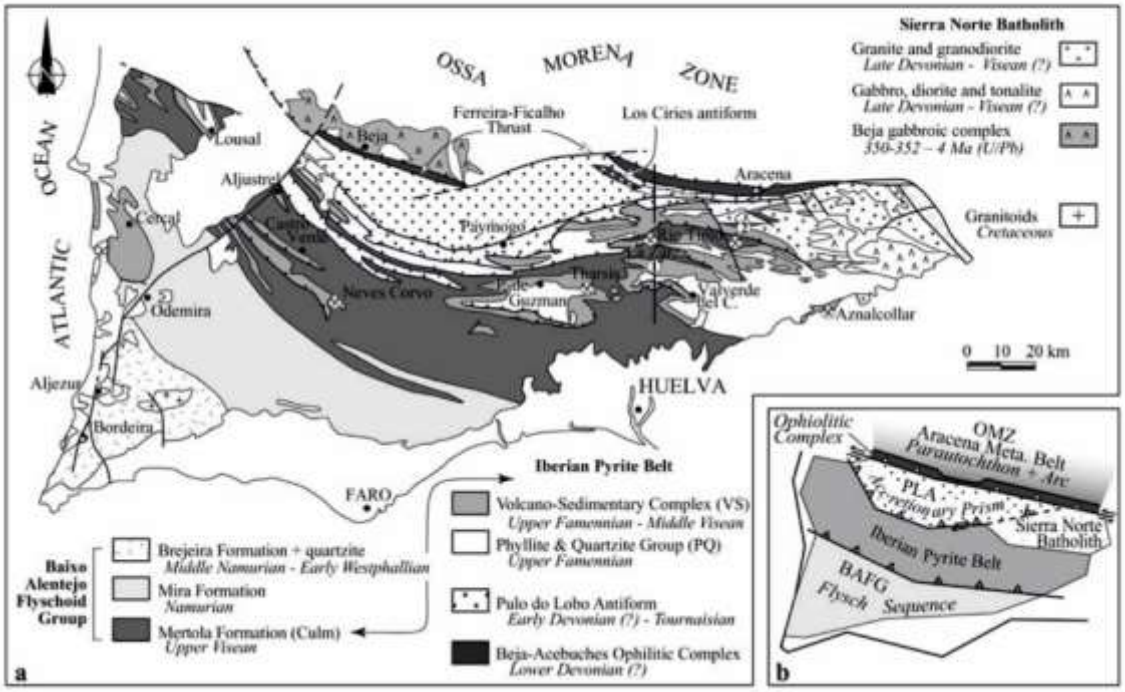

Map 3.1: (a) Geological map of the South Portuguese Zone [after Oliveira, 1990b]; (b) tectonic map of the South Portuguese Zone. Adapted from Onézime et al. (2003).

South Portuguese Zone | 3.3

The SPZ has been described for many works (e.g. Schermerhorn, 1970; Oliveira, 1983; Oliveira, 1990b) provides an interpretation synthesis of the geological environment based on sedimentary processes, volcanism and synsedimentary tectonism. According to Fonseca & Ribeiro (1993) and Pérez-Estaún *et al.* (2004) the SPZ includes Late Devonian - Late Carboniferous sediments and volcanics deposited in an intra-continental transtensional setting. The SPZ overstepped the contact with the Iberian terrane and was deformed in a transpressional regime during the Upper Carboniferous, with vergence towards the south-west, in a typical thin-

skinned thrust belt being constituted by Upper Palaeozoic low- to very low-grade metamorphic rocks (Munhá, 1990; Fonseca & Ribeiro, 1993; Abad *et al.*, 2001, 2002; Simancas, 2004). The SPZ shows the characteristic features of a foreland fold-and-thrust belt dominated by thin-skinned tectonics (Silva *et al.*, 1990; Simancas *et al.*, 2004).

The high-resolution crustal image given by the IBERSEIS seismic experiment (Figure 3.3) confirms a thrust pattern within the SPZ, which is characteristic of foreland thrust and fold belts (Simancas *et al.*, 2004). The thrusts dip to the northeast and merge in the middle crust, indicating a decoupling zone at this level (Simancas *et al.*, 2004). The figure 3.4 represents the hypothetical framework cross-section of the Aljustrel structure (SPZ) in the piggy-back system, according to Ribeiro *et al.* (2007).

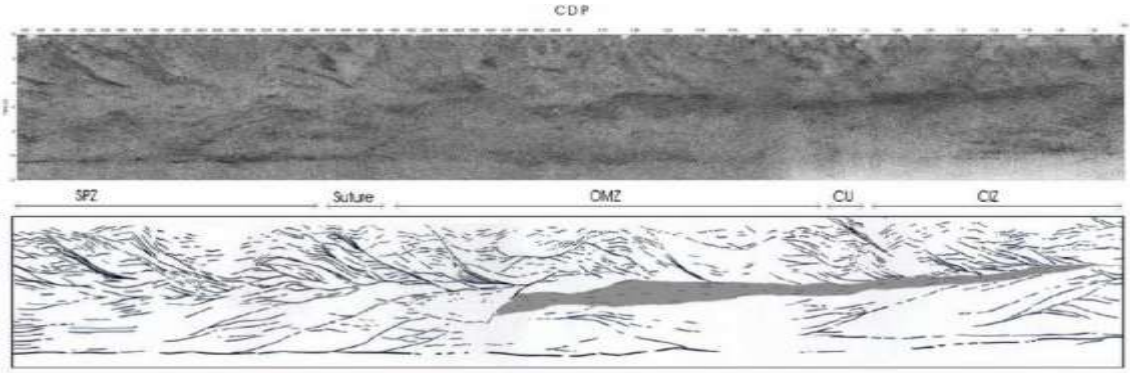

Figure 3.3: a) The IBERSEIS migrated crustal seismic image of SW Iberia; b) hand-drawing of reflectors in the IBERSEIS profile. Adapted from Simancas et al. (2004).

According to Mantero *et al.* (2011) foreland fold-and-thrust belts are typical features in the external zones of most orogenic belts. They generally involve only the sedimentary cover (i.e. thin-skinned style), although sometimes both the basement and the cover are deformed (i.e. thickskinned style).

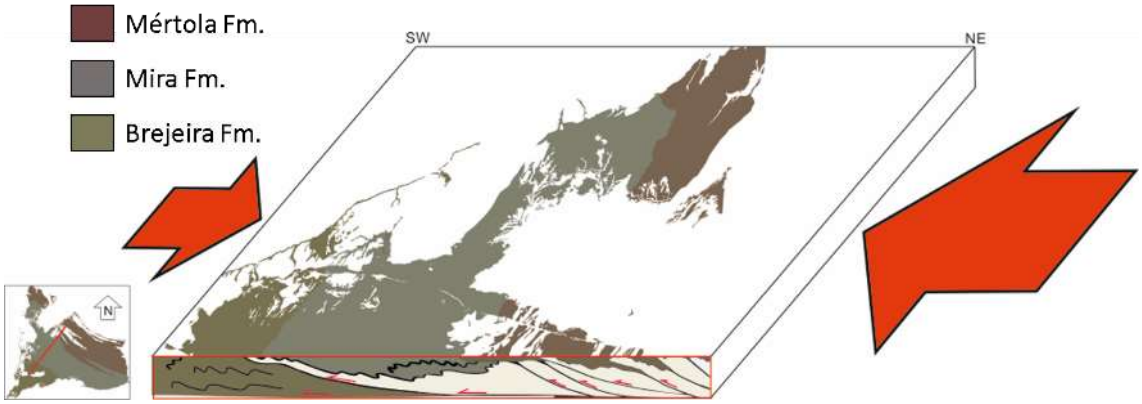

Figure 3.4: Hypothetical cross-section of Mértola, Mira and Brejeira Formations, emphasizing the piggy-back system. Adapted from Ribeiro et al. (2007).

According to Silva *et al.* (1990), the SPZ was in turn accreted to the OMZ during the Variscan orogeny, this accretion is also witnessed by the presence of various mélanges (Onézime *et al.*, 2003). This north directed subduction of the SPZ under the OMZ parautochthon, widely admitted nowadays, precludes some of the fore-mentioned models and is in agreement with the age and distribution of units composing the SPZ (Onézime *et al.*, 2003).

Structural analysis within the Spanish side of the SPZ supports continuous south propagating deformation, evolving from early synmetamorphic thrusting in the internal zone to thin-skinned tectonics in the southern external domain. Subsequent Visean continental collision is associated with the deposit of the south propagating flysch and the present geometry of the SPZ (Onézime *et al.*, 2003).

Also according to the authors, the formations are getting younger toward the south from the Early/Middle Devonian PLA, the late Devonian-Visean IBP (Map 3.1). A logical distribution of the main domains from north to south is also recognized, from the oceanic domain to the north (the BAOC) and the related PLA accretionary prism, to the foreland basin (i.e., the south propagating BAFG).

Baixo Alentejo Flysch Group | 3.4

The BAFG is mostly a turbidite sequence prograding to SW and with more than 3 km in thickness (some sectors reach more than 5 km, according to Fonseca *et al.*, 2015), being an important stratigraphic unit that covers, in some places by unconformity, more than half of the SPZ depositional area. The BAFG is composed by three main tectono-stratigraphic units (from the base to the top): Mértola, Mira and Brejeira Formations (Oliveira, 1983). These three formations generally trend to dip towards SW and sometimes, according to the structure, dip to the opposite side, NE, roughly parallel to the IPB and the OMZ-SPZ boundary. These formations are dated from Upper Visean, Upper Serpukhovian-Mid Bashkiriano and Mid Bashkirian-Upper Moscovian, respectively. Due to the general dip and vergence towards SW units tend to be younger towards the same direction (Oliveira, 1983).

Mértola Formation | 3.5

According to Oliveira (1990b), Mértola Fm. (Figure 3.5) is built up by sequences of thick- and thin-bedded sandstones, and alternating bands of shales and thin-bedded siltstones. The sandstone/shale ratio is high. The sandstones display many of the sedimentary features usually described for gravity flow sediments (Oliveira, 1990b). Massive and amalgamated sandstones, fluidized sandstones, slumps, conglomerates, sand dykes, mud flows and isolated sheeted sandstones are more common as far as the contact with the Pyrite Belt rocks are approached (Oliveira, 1990b). This facies distribution demonstrates the close relationship between the tectonostratigraphic evolution of the IPB and the flysch sedimentation (Oliveira, 1983). In the Mértola region, this unit has been divided into five members separated by five shaly horizons,

taken as markers beds (Oliveira & Silva, 1988). The members correspond to sedimentary lobes and the shaly horizons to interlobe sediments. The sedimentary lobes prograded to SSW. The Mértola Fm. was studied for palynomorphs in several regions: such as the Neves Corvo mine, Mértola town, Azenhas section in Guadiana River, Bens Farm, and are given a late Viséan age (Figure 3.8 [Oliveira *et al.*, 2007; Pereira *et al.*, 2007]).

Figure 3.5: Mértola Formation outcrop. According to Oliveira (1990b), this unit is built up by sequences of thick- and thin-bedded sandstones, and alternating bands of shales and thin-bedded siltstones.

Mira Formation | 3.6

According to Oliveira (1990b), the turbidites of this formation are commonly thin-bedded and show a sandstone/shale ratio < 1. An exception is the southeastern area where they have a sandstone/shale ratio similar to that of the Mértola Fm. (Figure 3.6). The contact with the Mértola Fm. is marked by a continuous shaly horizon, 50 to 100 m thick, which yielded goniatites of the *GoY* zone (Oliveira & Wagner Genthis, 1983; Oliveira, 1990b). The age of this formation is late Viséan to early

Bashkirian (Figure 3.8), based on the ammonoids *Dombarites*, *Lyrogoniatites* and *Cravenoceras* (Korn, 1997). Palynostratigraphic data are scarce at the present time and are only restricted to black shale samples obtained in the Castro Marim region.

Figure 3.6: Mira Formation outcrop. According to Oliveira (1990b), the turbidites of this unit are commonly thin-bedded and show a sandstone/shale ratio < 1.

Brejeira Formation | 3.7

According to Oliveira (1990b), this unit is broadly divided into two distinct sedimentological belts: one, 5 to 10 km wide, is composed of packets of relatively mature sandstones, several meters thick, and alternating shales; the other, to the southwest, crops out over a large area and is mostly made up of dark immature greywackes and shales. In the Aljezur and Bordeira Antiforms, the lower part of the Brejeira Fm. (Figure 3.7) is locally composed of thick-bedded and coarse-grained greywackes (Oliveira, 1990a). Quartzwackes and impures quartzites are also locally

present. In this case, an erosional contact with the underlying rocks of the Carrapateira Group is discernible. In the Brejeira Fm. turbidites (the younger unit of the BAFG) palynostratigraphic study revealed 6 miospore biozones, ranging from the Bashkirian to late Moscovian (Figure 3.8 [Pereira *et al.*, 2007]). These miospore ages are consistent with the local ammonoid biozonation (Korn, 1997), which mark the local deepening of the basin floor, probably as a response to the southward moving orogenic wave (Oliveira *et al.*, 2007).

According to Pereira *et al.* (2007), the distribution of the palynological assemblages, supports the southwestward progradation of the turbidites. The Variscan tectonic deformation in this sector is Kasimovian in age (Pereira *et al.*, 2007).

According to Oliveira & Wagner Genthis (1983) this formation exhibits flow directions mainly to the SE and E, with some paleocurrent measurements indicating flow towards the SW and N.

Figure 3.7: Brejeira Formation outcrop. According to Oliveira (1990b), the southwest of this unit, crops out over a large area and is mostly made up of dark immature greywackes and shales.

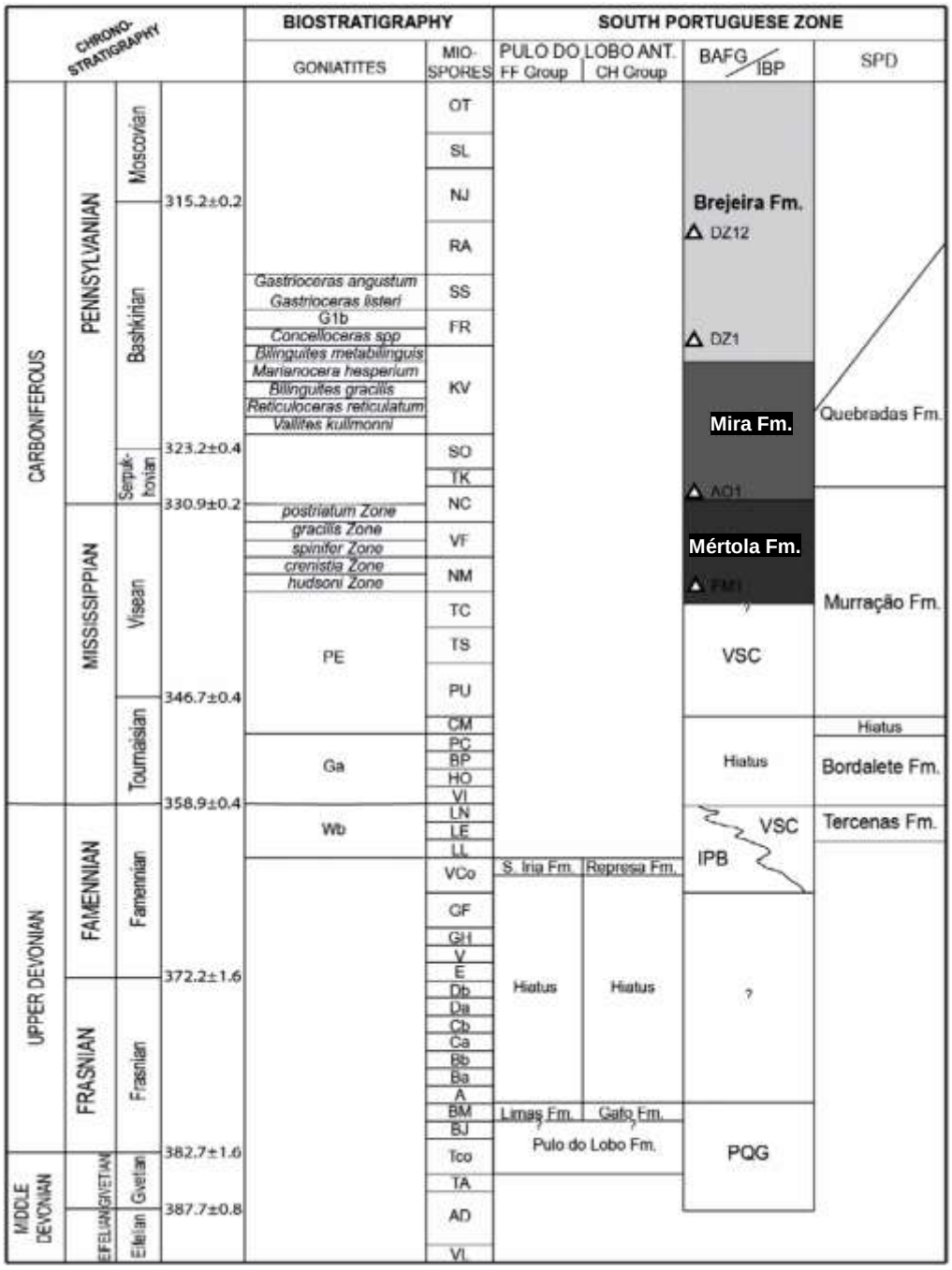

Figure 3.8: Stratigraphy of the South Portuguese Zone showing the position of the samples studied. Adapted from Pereira et al. (2008). FF Group, Ferreira-Ficalho Group; CH Group, Chanca Group; BAFG, Baixo Alentejo Flysch Group; IPB, Iberian Pyrite Belt; SPD, SW Portugal Domain; VSC, Volcano- Sedimentary Complex; PQG, Phyllite Quartzite Group. Adapted from Rodrigues et al. (2015).

Provenance | 3.8

Jorge *et al.* (2013) suggest that the greywackes from the Mértola and Mira Fms. show similar modal compositions, while Brejeira greywackes are more enriched in quartz and have lithoclasts composed mostly by sedimentary and metasedimentary grains. The source area of Mértola greywackes is heterogeneous, dominated by rocks with granitoid composition and minor mafic input (Jorge *et al.* 2013). The mafic component becomes residual in greywackes of Mira Fm., where granitoid source predominates. Greywackes from the Brejeira Fm. exhibit a clear felsic signature with significant increase in recycled components. All analyzed shales show geochemical features compatible with provenance areas of mostly granodioritic composition (Jorge *et al.* 2013).

Jorge *et al.* (2013) suggest that Mértola and Mira Fms. underwent moderate weathering in the source areas, where reduced variation of both palaeoweathering indices indicates steady-state weathering conditions. The authors say that the youngest Brejeira Fm. show moderate to intense weathering as a consequence of a non-steady-state conditions. Shales from Mértola, Mira and Brejeira Fms., have a more complex history of chemical weathering associated with multiple cycles of sedimentary recycling. Pereira *et al.* (2013) suggest that the sedimentation in the SPZ from the Visean to the Moscovian is marked by variability in sedimentary sources, involving the denudation of different crustal blocks and a break in synorogenic volcanism and Jorge *et al.* (2013) comment that the weathering conditions of BAFG sediments source area(s) changed from moderate to intense probably as a consequence of tectonic instability in the area (Figure 3.9).

U–Pb detrital zircon spectra from the BAFG show significant differences between the Mertola–Mira Fms. and the Brejeira Fm. (Rodrigues *et al.*, 2015). The main peaks in the detrital zircon spectra of the Mértola and

Mira Fms. are at 330 Ma, in contrast to the Brejeira Fm., for which the main peaks are at 615 Ma. Moreover, U–Pb detrital zircon ages of 900–1100 Ma are encountered in the Brejeira Fm. but are absent in the Mértola and Mira Fms (Rodrigues *et al.*, 2015).

According to Jorge *et al.* (2013), petrographic analyses, geochemical signatures of major and trace elements and multi-element tectonic discriminant diagrams suggest a continental arc/active margin as the most prominent origin for BAFG sediments (Figure 3.9). These data also indicate that an old upper continental crust contributed to the sediments of the Mira and Brejeira Fm., more pronouncedly to the latter (Figure 3.9). Still according to the author, collectively, geochemical signatures of three BAFG formations are compatible with provenance from the SW border of OMZ mostly, with possible contribution of an external (Avalonian) source (Figure 3.9). Rodrigues *et al.* (2015) suggest that the abundance of detrital zircon in the 500–750 and 900–1100 Ma age range intervals in the Brejeira Fm. suggests a source region in the Avalon–Meguma terranes with minor recycling from the SW Portugal Domain (Tercenas Fm.). The existence of late Ordovician and Silurian zircons in Brejeira turbidites which have no correspondence in the Gondwana basement of SW Iberia indicates Laurentia as their most probable source (Figure 3.9 [Pereira *et al.*, 2013]). The process of formation of Pangea by collision between Laurentia and Gondwana caused denudation of the two continental blocks, and the resulting debris were deposited in the SPZ (Figure 3.9 [Pereira *et al.*, 2013]).

The different provenance areas for the units of the BAFG are attributed to the presence of a physical barrier that was formed during the development of the foreland basin. This barrier was active from mid-Visean times and separated the sub-basins where the formations sediments accumulated (Rodrigues *et al.*, 2015).

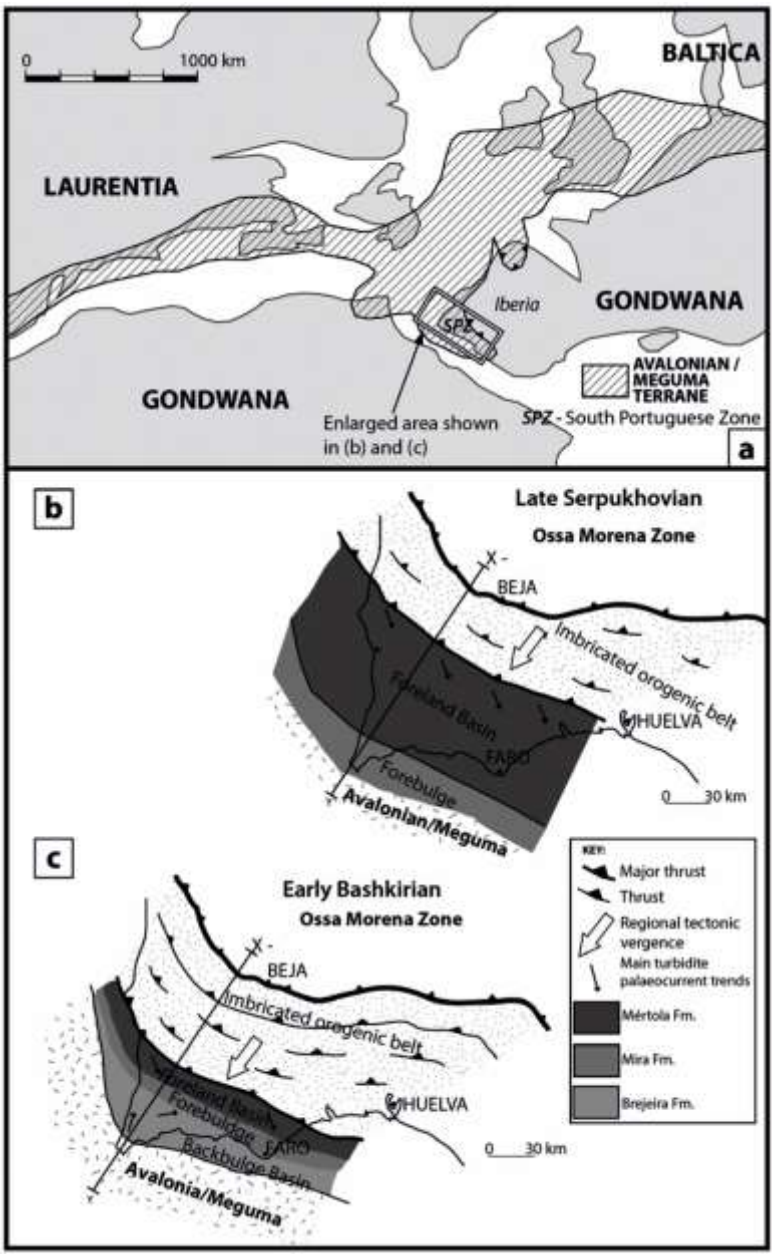

Figure 3.9: (a) Schematic palaeogeographical reconstruction for Pennsylvanian times showing the position of the South Portuguese Zone in relation to adjacent terranes (after Simancas, 2004). (b, c) Geodynamic evolution of the SPZ during the deposition of the Baixo Alentejo Flysch Group in (b) the Late Serpukhovian and (c) the Early Bashkirian (adapted from Oliveira et al. 2013). Adapted from Rodrigues et al. (2015).

MATERIALS AND METHODS|4.0

Rock-Eval Pyrolysis|4.1

A total of 31 samples were collected for rock-eval pyrolysis (22 in Brejeira Formation, 3 in Mira Formation and 1 in Mértola Formation [Appendix 10.65]). The laboratorial analyses (using Rock-Eval 6) were performed by Weatherford Laboratories and Polish Geological Institute and were financed by Repsol E&P, Partex Oil&Gas and Polish Geological Institute. All the samples performed by Polish Geological Institute were selected for rock-eval pyrolysis, however the Weatherford Laboratories just analyzed samples with TOC higher than 1.0 wt%.

Rock is crushed to fine sand particle size (0.125-0.25 mm) and 100 mg samples are loaded into pyrolysis crucibles (Peters, 1999). The samples are pyrolyzed under helium at 300°C for 3-4 min, followed by heating at 25°C/min to 550°C. Hydrocarbons (HC; compounds containing only hydrogen and carbon) and carbon dioxide evolved from organic matter during heating are measured over time. Each analysis requires about 20 min.

WorldView-2 Satellite Images and Airborne Gamma Radiation | 4.2

According to the DigitalGlobe data sheet (DigitalGlobe, 2016), the WV2 was launched in 2009, and is the first high-resolution 8-band multispectral commercial satellite. The satellite operates at an altitude of 770 km with 46 cm spatial resolution in panchromatic band and 185 cm for multispectral bands (Table 4.1).

Three images (satellite images courtesy of the DigitalGlobe Foundation), described in the table 4.1, were used to construct a mosaic (WGS 1984 UTM 29N zone) that covered the all AOI (Figure 4.1 and Table 4.2). From this mosaic 8 image bands were extracted to be used for the correlation with gamma radiation (Table 4.1).

The airborne radiometric survey data, used in this work, was operated by Rio Tinto Zinc Co. (RTZ) in 1991 and was generously donated by the National Laboratory of Energy and Geology (Geological Survey) from Portugal. The data were provided with the file format ".grid" and the unit of measurement is counts per second (cps). In order to convert the cps values to part per million-ppm (^{238}U and ^{232}Th), percent (^{40}K) and nanoGray per hour-nGy/h (total count) the standard conversion rate, suggested by Geosoft (2005), were used (Table 4.3). The distance between the measurement points was 75 meters and the Mértola and Mira Formations were entirely covered by the flights. However, the Brejeira Fm.

wasn't completely covered, and thus the most southern area of the formation was not analyzed. So, based on kriging method, the thematic maps were interpolated.

The sample points from airborne gamma survey (with 75m of distance) were used as references for the pixel value extraction from all the 8 mosaic bands. Therefore, there are 204,972 points with 13 different data: 8 WV2 bands, TC, Th, U and K.

Satellite	Band	Pixel range	nm	Resolution (cm)
WorldView-2	1-Coastal	0-255	400 - 450	185
	2-Blue	0-255	450 - 510	185
	3-Green	0-255	510 - 580	185
	4-Yellow	0-255	585 - 625	185
	5-Red	0-255	630 -690	185
	6-Red edge	0-255	705 - 745	185
	7-Near-IR1	0-255	770 - 895	185
	8-Near-IR2	0-255	860 - 1040	185
	Panchomatic	0-2047	450 - 800	46

Table 4.1: Worldview-2 imagery bands information (DigitalGlobe, 2016).

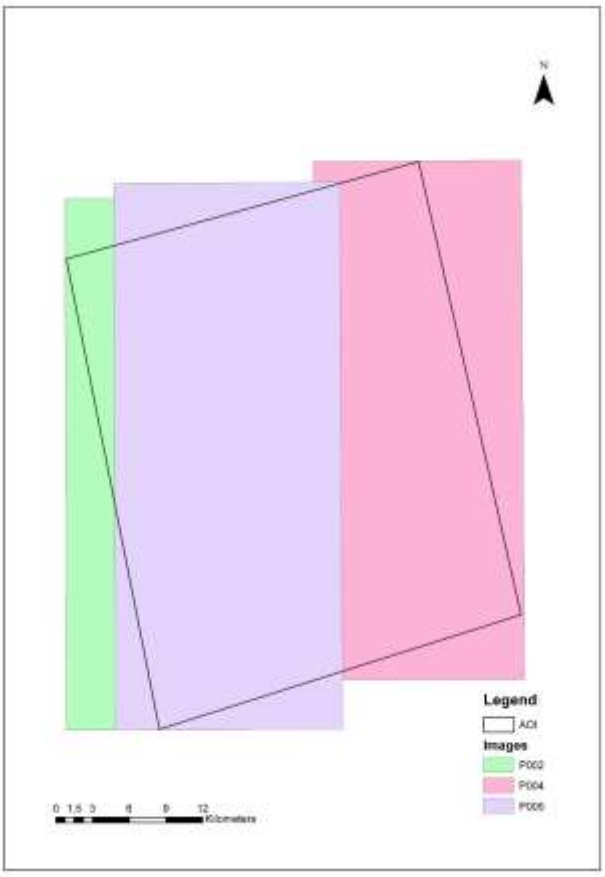

Figure 4.1: Contours of the images used for the mosaic design of the area of interest (AOI).

For each pixel value from bands (from 0 to 255) it was calculated the average GR value (TC, Th, U and K). The simple xy graphing would not be sufficient to determine which bands could present the best correlation for each radiometric variable.

Image	DigitalGlobe reference
P002	15JUL26112846
P004	15JUL23113907
P006	14MAR06114313

Table 4.2: References of the images used for the mosaic design.

	Units	Conversion rate
Total Count	cps/nGy/h	23
Thorium	cps/ppm	4,5
Uranium	cps/ppm	7,5
Potassium	cps/%	75

Table 4.3: Values of standard conversion rate suggested by Geosoft (2005).

Thus, it was used the Pearson's correlation coefficient (PC), one of the most used statistical quantitative method in geosciences, which measures the degree of (linear) interrelation between two sampled (data size n) variables, x and y (Mudelsee, 2003). For this thesis, the PC was calculated using IBM SPSS software.

Thorium-Normalization and Hydrocarbon Anomaly | 4.3

As said before, one of most successful models for identifying radiometric anomalies related to hydrocarbon occurrence was developed by Saunders *et al.* (1993). A basic assumption is that whatever changes the concentration of a radioactive isotope it also changes the concentration of the other two isotopes, in the case of hydrocarbon presence. According to the author, if hydrocarbons are not present, ^{238}U, ^{40}K and ^{232}Th should be present in natural and constant proportions. Lithological and environmental variables that once were problematic are now suppressed by the correction of ^{40}K and ^{238}U readings using the TN process (Saunders *et al.*, 1993).

Based on detailed studies of radiometric measurements in oilfields, Saunders *et al.* (1993) developed a relationship between the ^{238}U, ^{40}K and ^{232}Th data in order to help identify the hydrocarbon anomalies (HA). ^{40}K concentrations appear to be significantly lower over oil and gas fields, and ^{238}U was found to be slightly concentrated in profiles over Alabama Ferry, Leona, O.S.R., and Lonesome Dove fields, Texas (Saunders *et al.*, 1993; Prost, 2014). ^{232}Th is considered to be highly "retained" in rocks and local soils, not being affected by the hydrocarbon ascension. Based on these assumptions, Saunders *et al.* (1993) defined the "ideal" ^{40}K and ^{238}U as:

$$K_i = (K_{av}/Th_{av})\ X\ Th_s \quad \text{(Equation 1)}$$

$$U_i = (U_{av}/Th_{av})\ X\ Th_s \quad \text{(Equation 2)}$$

where the subscript "s" refers to the measured or sampled value, "i" is the ideal value and "av" is the mean value of the studied area, generally at least 5 times greater than the predicted anomaly. This can result if the area to be investigated is of several km^2. The difference between the measured values and the ideal values is then calculated (Saunders *et al.*, 1993):

$$KD = (K_s - K_i)/K_s \quad \text{(Equation 3)}$$

$$UD = (U_s - U_i)/U_s \quad \text{(Equation 4)}$$

In hydrocarbon presence, KD should decrease and UD generally increases. To capitalise upon these 2 relationships, the same authors defined a new parameter, known as DRAD:

$$DRAD = UD - KD \quad \text{(Equation 5)}$$

Therefore, HA is normally characterised by positive values of DRAD and negative values of KD and UD (sometimes positive values) (Saunders *et al.*, 1993).

Surface Geochemical Prospecting | 4.4

The presence of near-surface migrated hydrocarbons can provide strong evidence an active petroleum system is present as well as critical information on source, maturity and migration pathways (Abrams *et al.*, 2001; Abrams, 2013). When applied to hydrocarbon exploration, soils, sediments, air, water and rock samples can be sampled and tested through various analytical methods (Bandeira de Mello *et al.*, 2007).

The procedures for surface geochemical sampling campaign begin with preliminary planning actions, such as area selection (target), geological base maps, satellite imagery, etc., as well as choose the most suitable months for field operations (Bandeira de Mello *et al.*, 2007). Once the research area has been established, the efforts are focused on potential

hydrocarbon systems (conventional or unconventional), thus defining the positioning of the sampling points. After these adjustments, the most appropriate sampling methodologies and respective standard procedures are defined (Figure 4.2 [Bandeira de Mello *et al.*, 2007]).

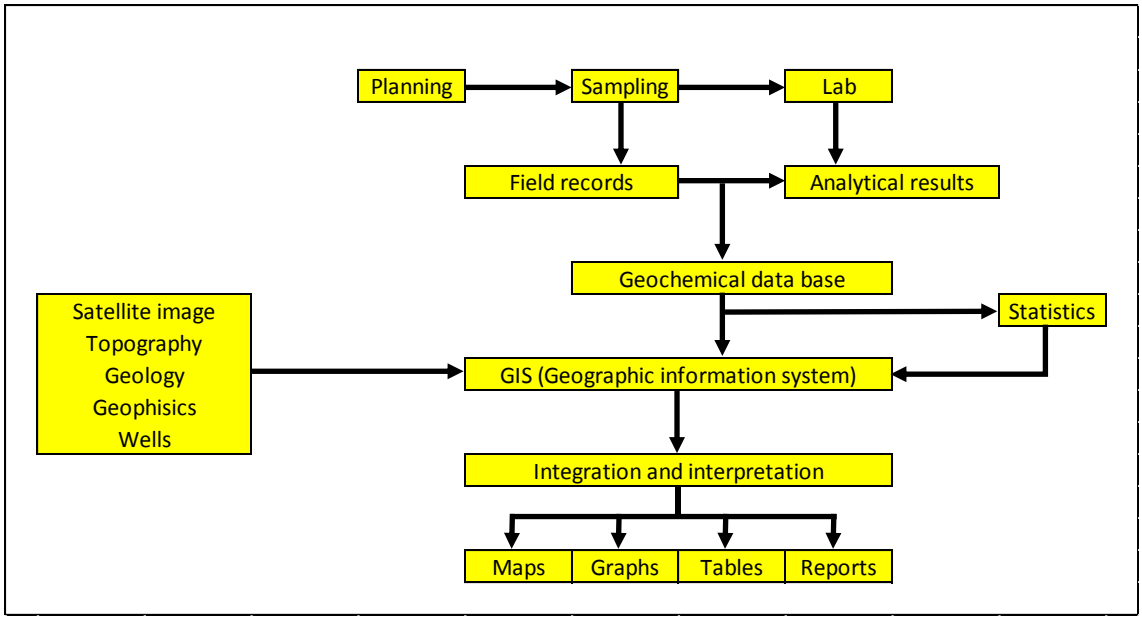

Figure 4.2: General scheme of the activities relates to surface geochemical prospection of hydrocarbons. Adapted from Bandeira de Mello et al. (2007).

According to Abrams (2013) the light hydrocarbons require special handling and containers to limit volatile loss and prevent post sampling microbial alteration. Several methods are used for direct hydrocarbon sampling such as probe and headspace for free gases, blender and disrupter for occluded gases, acid extraction for adsorved gases and sorbing fibers (Bandeira de Mello *et al.*, 2007).

In general, the research methodologies in surface geochemistry aims to quantify hydrocarbons movement in a medium, on a time scale (Tedesco, 1995). Under standard conditions for temperature and pressure (25°C and 1 atm) light hydrocarbons (methane [CH_4], ethane [C_2H_6], propane [C_3H_8], isobutane [i-C_4H_{10}] and n-butane [n-C_4H_{10}]) are present, on the surface, in the gas format. Hydrocarbons of slightly larger molecular

weights such as n-pentane (nC$_5$) and n-hexane (nC$_6$) are present, on the surface, in the liquid format. However, they can be found as gas (vapor) just with a small increase of the temperature. In the soil, light hydrocarbon can "stay" in three formats: (1) as a free gas in the effective porosity; (2) as interstitial hydrocarbon, or occlusion in the pore space between the grains; (3) adsorved in the sediment particles or in the carbonate cement (Schumacher & Abrams 1996).

The sampled volume goes on to review research investigations and case history studies of every gas that might act as an indicator or pathfinder and to elaborate the models developed to explain the resulting observations (Hale, 2000). Gas composition by itself will not provide sufficient information to fully evaluate anomalous sediment gas origin. Compound specific isotopic analysis from IR GC-MS analysis is critical to determine gas maturity and source facies as well as potential mixing with in-situ derived gases and secondary alterations (Abrams, 2005; Abrams & Dahdah, 2011; Abrams, 2013). Only where these are overcome effectively can the detection of trace quantify of gases derived from mineral deposits and petroleum accumulations at depth (Hale, 2000).

The collection of all samples was performed using Isojars (Figure 4.3B), with distilled water and a bactericide added to inhibit any bacterial activities. Twenty-seven soil samples were collected for this study, using a drilling machine (*F* and *P* samples [Figure 4.3D and Appendix 10.64]), a metal tube and a hammer (*SPZ* samples [Figure 4.3A, C and Appendix 10.64]). Thirty-one water samples (*W* samples) were collected from artesian wells, boreholes and springs (Appendix 10.64).

Figure 4.3: A) Hammer; B) Isojar, by Isotech (Weatherford); C) Tubes used for soil sampling; D) Drilling machine used for deeper sampling.

Methods and analysis conditions for headspace-gas chromatography (HS-GC) and mass-spectrometry by Isotech Laboratories Inc. and Isolab b.v. |4.5

In order to achieve the best performance when using HS-GC, careful attention should be used in sample preparation and instrument setup. Key issues to address when setting up HS-GC systems include minimizing system dead volume, maintaining inert sample flow paths, and achieving efficient sample transfer (Restek, 2000).

According to Isotech (2014), the procedure for taking cuttings samples in IsoJars are:

1. Put the sample in jar (approximately 1 cup);

2. Only add water to reach the line on the label;

3. Do not fill the jar with water as the headspace gap is needed to allow gas to desorb into the gap;

4. Leave about a 1-inch gap between the water and top of the jar;

5. Add 10 drops of the dilute bactericide, Benzalkonium Chloride, to the jar;

6. Screw the lid on as tight as possible;

7. Tape the lid to keep it tight and from vibrating loose during shipment. Tape in same direction (clockwise) that the lid is screwed on.

According to Abrams (2013), the bactericide is used to prevent in-situ microbial activity. The amount of bactericide required to prevent microbial activity has not been rigorously examined. To the best of the author's knowledge, no comprehensive studies have been conducted to evaluate the effectiveness of these anti-bacterial agents, how much is required, or if the anti-bacterial agents impact the geochemistry results.

Molofsky *et al.* (2016) suggests that an open-system collection technique is prone to loss of exsolving gases as methane, resulting in low-biased concentrations associated with the water samples. According to Parker & Britt (2012), the VOC most susceptible to loss is dichlorodifluoromethane, with 76% loss (Henry's constant 3.0 atm m3/mol). Methane is significantly more volatile than the VOCs evaluated by Parker & Britt (2012), according to Molofsky *et al.* (2016).

Composition analysis of mudgas samples (including CO_2 concentration) (by Isolab b.v.):

For composition analysis of samples with low gas concentration like mudgas samples in isotubes or isojars, an Agilent 7890B GC (Agilent Technologies, Santa Clara, US) equipped with a 30m 0.32mm Gaspro column and a 50m 0.32mm Porabond Q column (both from Agilent) is used. The Gaspro column is coupled to a flame ionization detector and used for analysis of hydrocarbons. The Porabond Q column is coupled to a TCD detector and used for the analysis of the CO_2 concentration. Samples are injected into a heated injection valve on the GC using a gastight syringe. The detector responses are calibrated against a reference gas (Scott Specialty Gases Netherlands BV, Breda, The Netherlands) several times a day.

Minimum concentrations: ca. 1 ppm for methane to 0.1 ppm for pentane and ca. 50 ppm for CO_2.

Analysis of carbon isotopes of methane (by Isolab b.v.)

Carbon isotopes of methane are analyzed with an Agilent 6890N GC (Agilent Technologies, Santa Clara, US) interfaced to a Finigan Delta S IRMS (Finigan is now part of Thermo Scientific, Bremen, Germany) using a Finigan GC-C II interface. The GC is equipped with a 12m, 0.32mm molsieve column (Agilent) and an injection valve. Samples are calibrated regularly against a calibration standard and results are reported in promille vs. vPDB.

Minimum concentration: ca. 25-50 ppm.

Gas Chromatography (GC) | 4.6

All collected samples were analyzed by GC (58 water and soil samples), for molar composition purpose (CO_2, C1, C2, C3, *n*C4, *i*C4, *n*C5 and *i*C5), being 40 from Brejeira Fm. and 18 from Mira Fm.

Gas chromatography is a chromatographic analytical technique for separating the volatile compounds of various mixtures. Basically, according to Sparkman *et al.* (2011), the operating principle of GC involves volatilization of the sample in a heated inlet or injector of a gas chromatograph, followed by separation of the components of the mixture in a specially prepared column (Figure 4.4).

The liquid or gas mixture is injected into a capillary silica column (typical dimensions: 30 m long, 0.32 mm ID). This Column is coated by a stationary phase which consist of a liquid or solid film from about 0.25 up to 30 µm thick (Figure 4.4). The temperature of injector and detector can be adapted according nature of the analyzed sample and is usually set to about 25 degrees above the boiling point of the highest boiling component of interest. To transport the analytes (i.e. “the sample being analyzed", according to McGraw-Hill, 2003, p.23) through the column, a

mobile phase, usually consisting of helium or hydrogen is used. This mobile phase has a typical flow of about 1-4 ml/min depending on the application and column dimensions (Figure 4.4).

Temperature control can be either isothermal or programmed to increase with analysis time continuously or in stages. Proper choice of column and operating conditions (flow rate and temperature) results in separations to enable interference-free measurement of the desired components of the mixture (Peters *et al.*, 2005; Rechsteiner Jr. *et al.*, 2015).

As the analysis cycle progresses the separated components elute from the column and emerge at the end of the column at different times and can be detected (progress into the detector.). The time (retention time) that has passed between sample introduction and the emergence of the individual analyte bands-the peaks-is, under given conditions, characteristic of the individual analytes, while the size—height or area—of the individual peaks is proportional to their amount (Kolb & Ettre, 2006; Rechsteiner Jr. *et al.*, 2015). The retention time of the component is qualitative, while the area under the curve is quantitative. Calibration samples are used to relate known component area to the concentration of the same component in unknown samples (Rechsteiner Jr. *et al.*, 2015).

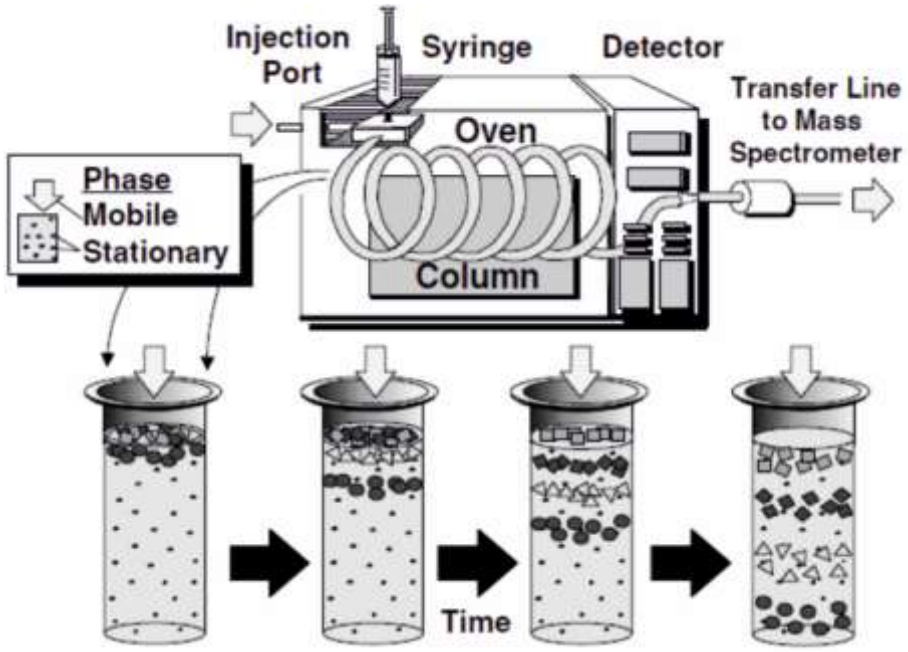

Figure 4.4: Detailed view of a typical gas chromatograph used to separate mixtures of compounds. The blow-up (bottom) shows the separation of compounds during movement down the chromatographic column, which results from their repeated partitioning between the mobile and stationary phases. Adapted from Peters et al. (2005).

According to Grob (2004), the separation depends on the ability of each component in the mixture to become a sorbate (i.e. "substance that has been either adsorved or absorbed", according to McGraw-Hill, 2003, p.352 [Figure 4.5]). Once the column packing has been saturated (i.e., when it is no longer able to sorb more components), the mixture then flows through with its original composition (Figure 4.6 [Grob, 2004]).

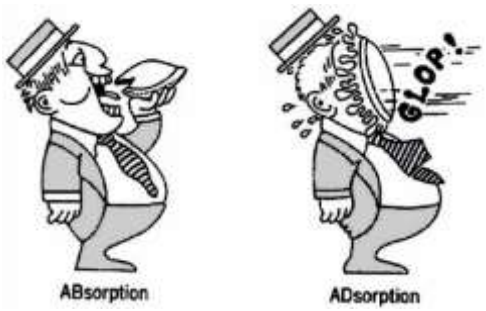

Figure 4.5: Difference between absorption and adsorption. Adapted from Miller (2005).

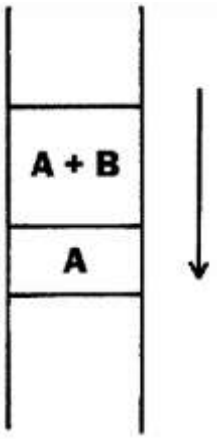

Figure 4.6: Frontal analysis. Component B is more sorbed than component A. Adapted from Grob (2004).

Isotope Ratio Mass Spectrometry | 4.7

Five samples (1 water sample and 4 soil samples) were analyzed by IRMS, generating 5 results for $\delta^{13}C1$ and 1 result for $\delta^{13}C2$, $\delta^{13}C3$, $\delta^{13}nC4$, $\delta^{13}iC4$, $\delta^{13}nC5$ and $\delta^{13}iC5$.

The isotopic composition of light elements can be changed as a result of isotope fractionation during natural chemical, biological and physical processes at different speeds and therefore the isotopic composition of the element, which is part of the given compound, depends on the history and origin of the sample. These changes are proportional to the mass difference between isotopes (Sevastyanov, 2015).

Isotope fractionation occurs in various natural processes, including photosynthesis and isotope exchange reactions between compounds of carbon. Photosynthesis leads to the enrichment of synthesized organic compounds with the isotope ^{12}C. On the other hand, the isotopic exchange reaction between gaseous CO_2 and the carbonates dissolved in water leads to the enrichment of the carbonates with ^{13}C. As a result, the prevalence of the ^{13}C isotope in carbon on Earth's surface varies within 100‰ vs. vPDB (Sevastyanov, 2015).

The isotope ratio mass spectrometry (IRMS) of light elements is an important method of analytical geochemistry having an extremely high

sensitivity and accuracy of measurement of isotope ratios. It can be divided into three fundamental parts, namely the ionization source, the analyser, and the detector (Figure 4.7). The main function of the mass analyser is to separate, or resolve, the ions formed in the ionization source by their mass to charge ratios (*m/z*) furnishes the molecular weight and chemical formula of compounds and their relative amounts and offers nondestructive examination of the sample (Ashcroft, 1997; Speight, 2001; Sevastyanov, 2015).

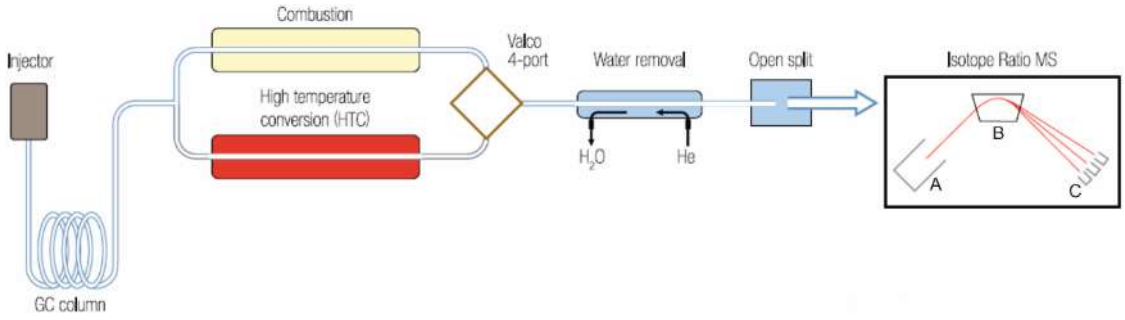

Figure 4.7: Schematic overview of the GC-IRMS solution. The isotope ratio mass spectrometry can be divided into three fundamental parts, namely the ionization source (A), the analyser (B), and the detector (C). Adapted from Thermo SCIENTIFIC (2014).

Since the relative isotopic composition can be measured with greater accuracy than the absolute isotopic composition, to represent the relative isotopic composition of light elements the quantity δ (delta), which is calculated by the following formula (Sevastyanov, 2015):

$$\delta = (R_x - R_{std})/R_{std)\ x\ 1000} \quad \text{(Equation 6)}$$

where "R" is the ratio of the abundance of the heavy isotope to the light isotope, "x" is an index, indicating the measured sample, "std" is an index denoting the standard sample. The value of R for the stable isotopes of hydrogen can be written as D/H, for the carbon isotopes $^{13}C/^{12}C$, for the nitrogen isotopes $^{15}N/^{14}N$, for the oxygen isotopes $^{18}O/^{16}O$, etc. The value of δ is expressed in thousandths (per mil), which are indicated by ‰. A

positive value of δ means that the ratio of the heavy isotope to the light one in the analyzed sample is greater than in the standard sample (Sevastyanov, 2015).

The value of δ is calculated by measuring the intensity of ion signals in the isotope mass spectrometer and recorded, for example for carbon, as $\delta^{13}C$ vs. vPDB. Usually, for pure gases the reproducibility of the results of isotopic analysis is ±0.1‰ or better (Sevastyanov, 2015).

The resolution ® of a mass analyzer, or its ability to separate two peaks, is defined as the ratio of the mass of a peak (M1) to the difference in mass between this peak and the adjacent peak of higher mass (M2) (Ashcroft, 1997).

$$R = M_1/(M_2-M_1) \text{ (Equation 7)}$$

According to Bandeira de Mello *et al* (2007) for the determination of light hydrocarbon origin, thermogenic or biogenic, the sample with higher gas concentration, often methane, is used for stable carbon isotope analysis ($\delta^{13}C$).

Static Headspace Gas Chromatography Sampling (Isojar) | 4.8

Some samples need to be modified for the specific requirement of a particular analytical technique (Kolb & Ettre, 2006). Most consumer products and geological samples (as hydrocarbons) are composed of a wide variety of compounds that differ in molecular weight, polarity, and volatility (Restek, 2000).

Most of these cleanup techniques use some type of initial extraction procedure such as solvent extraction, solid-phase extraction, or supercritical-fluid extraction. A number of solvent-less procedures to collect the analytes from the samples were developed for the analysis of volatile organic compounds (Moldoveanu & David, 2002). However, if the

interesting is in highly volatile compounds, it can use an inert gas for this purpose; gas is an ideal "solvent" for volatile compounds, since it is easy to handle and is available in a much higher purity than most organic solvents. This is an aspect that is particularly important for traces analysis. A gas extract is ideally suited for analysis by GC, and this combination is called "headspace–gas chromatography" (HS-GC sampling), the fastest and cleanest method for analyzing volatile organic compounds. A headspace sample is normally prepared in a vial containing the sample, the dilution solvent, a matrix modifier like a bactericide, and the headspace (Restek, 2000; Kolb & Ettre, 2006).

Volatile components from complex sample mixtures can be extracted from non-volatile sample components and isolated in the headspace or vapor portion of a sample vial. An aliquot of the vapor in the headspace is delivered to a GC system for separation of all of the volatile components (Restek, 2000).

These gas sampling techniques can be classified into two general groups, "static headspace" and "dynamic headspace" (Figure 4.8). Static headspace techniques are those that collect the analytes (and possibly part of the matrix) from a closed vessel where the sample is assumed to be in equilibrium with its vapors at a specific temperature and pressure, in a single step or by stepwise repeating of the extraction (multiple headspace extraction) (Figure 4.8 [Moldoveanu & David, 2002; Kolb & Ettre, 2006]).

Dynamic headspace techniques remove analytes (and possibly part of the matrix) from the sample in a stream of gas flowing over or through the sample and processes them further for analysis, also by stripping the volatiles (dynamic headspace) by a continuous flow of an inert purge gas (Figure 4.8 [Moldoveanu & David, 2002; Kolb & Ettre, 2006]). Headspace type separations of the analytes from the sample significantly simplify the matrix and are common cleanup procedures selected for the analysis of volatile compounds (Moldoveanu & David, 2002; Kolb & Ettre, 2006).

According to Kolb & Ettre (2006) the simplicity of static HS-GC is unsurpassed by any other cleanup techniques: the sample is filled into the headspace vial (IsoJar), which is closed immediately and remains closed until an aliquot has been withdrawn from the vial and transferred directly to the gas chromatograph device with the IsoJar preferably upside down, thus guaranteeing sample integrity and is followed by injection (using a gas-tight syringe [Figure 4.10]) in a GC instrument for analysis (Moldoveanu & David, 2002). This vial is then thermos tatted at a constant temperature until equilibrium is reached between the two phases, soil or rock, and gases (Figure 4.9 [Kolb & Ettre, 2006]). This simplicity enabled the early automation of the whole procedure.

According to Moldoveanu & David (2002) a number of parameters influence the transfer of analytes from the sample into the headspace, and for a compound "i" in the sample (index "s") and in headspace (index "h"), the following equilibrium occurs:

$$i_S \overset{K_{hs}}{\rightleftharpoons} i_h$$

This equilibrium is described by the liquid-to-gas partition coefficient given by the expression:

$$K_{hs} = C_{i,h} / C_{i,s} \quad \text{(Equation 8)}$$

Where $C_{i,s}$ is the concentration of the analyte in the sample, and $C_{i,h}$ the concentration in the headspace. According to Tipler (2013), compounds with a high value for partition coefficients (>1) will favor the liquid phase, whereas compounds with low coefficients (<1) will favor the headspace phase.

In resume, static HS-GC is a technique used for the concentration and analysis of volatile organic compounds. This technique is not new, has been practiced since the early days of gas chromatography, is relatively simple and can provide sensitivity similar to dynamic purge and trap analysis (Kolb & Ettre, 2006). The popularity of this technique has grown

and has gained worldwide acceptance for analyses of alcohols in blood and residual solvents in pharmaceutical products. Other common applications include industrial analyses of monomers in polymers and plastic, flavor compounds in beverages and food products, petroleum hydrocarbons, and fragrances in perfumes and cosmetics (Restek, 2000).

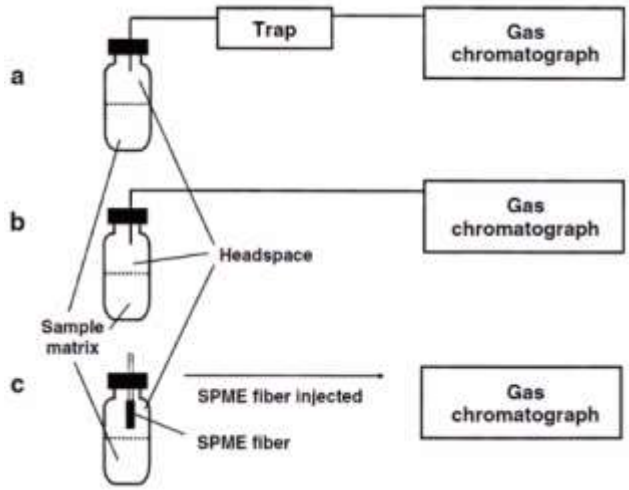

Figure 4.8: Comparison of dynamic, static, and SPME (Solid Phase Micro-Extraction) headspace sampling. (a) Dynamic headspace sampling uses a sorbent or cold trap to concentrate volatile analytes before analysis by the GC. (b) Static headspace sampling uses direct transfer of a volume of gas from the headspace above the heated sample vial directly to the GC for analysis. Injection designs are illustrated in Figure 4.10. (c) SPME headspace sampling uses a fiber support with solidphase coating. The fiber is placed in the headspace and reaches equilibrium with the headspace volatile analytes. The SPME fiber is transferred by means of a syringe and thermally desorbed in the injector of the GC for analysis. Adapted from B'Hymer (2010).

Figure 4.9: An example of the label on the Isojar–complete the label with all information available. Adapted from Isotech (2014).

Figure 4.10: The designs of static headspace injection systems used for the analyzes. The gas-tight syringe system uses a syringe to collect and transfer a headspace aliquot to the GC. Adapted from B'Hymer (2010).

THEORY OF HYDROCARBON SEEPS | 5.0

Total Petroleum System and Petroleum Seepage System | 5.1

An important concept, for hydrocarbon seeps research, is the "Petroleum Seepage System" (PSS), defined by Abrams (2005) as "the interrelationships among total sediment fill, tectonics (migration pathway), hydrocarbon generation (source and maturation), regional fluid flow (pressure regime and hydrodynamics), and near surface processes (zone of maximum disturbance)". The PSS is part of the Total Petroleum System (TPS), that according to Magoon & Schmoker (2000) describe the entire hydrocarbon-fluid system in the lithosphere (that can be mapped), including the essential elements and processes required for oil and gas accumulations, migrations, and seeps. The concept presumes that migration pathways must exist, either now or in the past, connecting the provenance with accumulations (Etiope, 2015). Seeps are not an exception, but a common, integral component of a TPS. The PSS would then be the connection between the TPS and Earth's

surface. Abrams (2005) also indicated that "Understanding the PSS, hence petroleum dynamics of a basin, is key to understanding and using nearsurface geochemical methods for basin assessment and prospect evaluation." TPS and PSS concepts call attention to the fact that petroleum accumulations are not totally closed, isolated, and sealed compartments accumulations (Etiope, 2015). Gas (and oil) frequently leak from reservoirs through cap rocks, even in large and productive fields, implying that perfect sealing is not necessary for having a commercial reservoir. Seeps are not a problem, but an opportunity (Etiope, 2015).

Seeps Classification | 5.2

Natural gas seepage is the steady or episodic, slow or rapid, visible or invisible flow of gaseous hydrocarbons from subsurface sources to Earth's surface (Etiope, 2015).

The rate and volume of hydrocarbon seepage to near-surface sediments controls the surface geological, geophysical, biological, and geochemical expression (Figure 5.1 [Roberts *et al.*, 1990]) which can range from macroseepage to microseepage (Abrams, 2013). The surface expressions of natural gas seepage can be classified on the basis of spatial dimension, visibility, and fluid typology, as summarized in the following scheme (Etiope, 2015):

- Macro-seeps
  - Focused flow
    - Gas seeps (*gas only*)
    - Oil seeps (*gas and oil*)
    - Gas-bearing springs (*dissolved gas*)
    - Mud volcanoes (*gas, water and sediments*)
  - Diffuse flow — Miniseepage (invisible)
- Microseepage {Diffuse flow — (invisible, independent from macro-seeps)

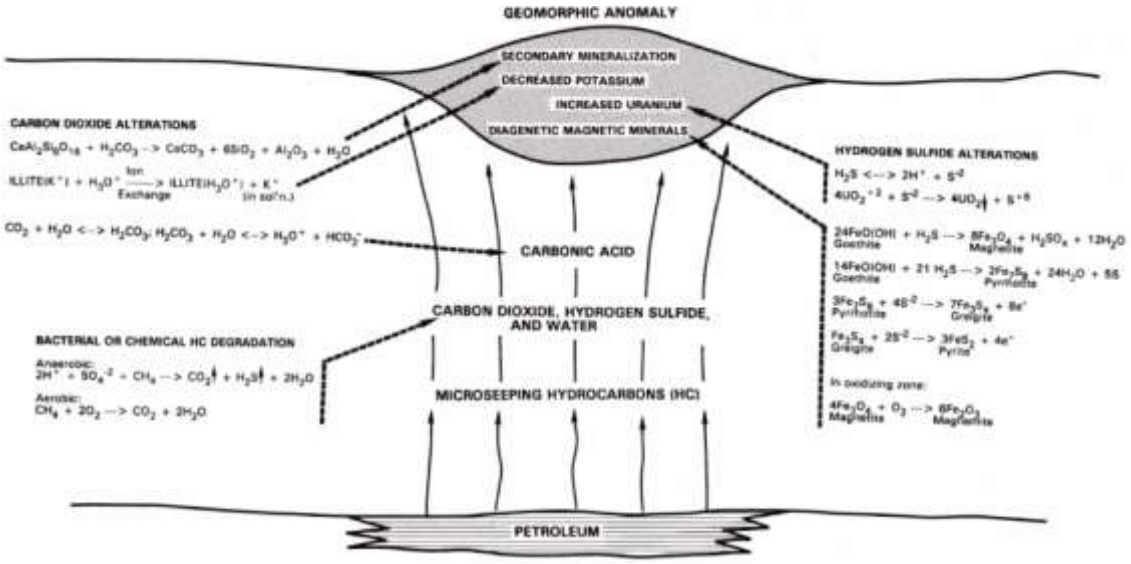

Figure 5.1: Possible model of hydrocarbon microseepage-related alteration over petroleum deposits. Adapted from Saunders et al. (1999).

Macroseeps (or seeps) are "channelled" flows of gas, typically related to fault systems. Gas flux is expressed in terms of mass/time (e.g., kg/day or tons/year). This surface macroseeps (visible gas vents or oil leaks from the soil or rock outcrops) are generally an indication of a fault in an active PSS (Abrams, 2005) belonging to a TPS (Magoon & Schmoker, 2000; Etiope, 2009a).

Microseepage is the slow, continual loss or episodic loss of methane and light alkanes from gas-oil-prone sedimentary basins where thermal degradation of indigenous organic matter is occurring (Figure 5.2 [Etiope & Klusman, 2002; Etiope, 2009c; Etiope, 2015]). Is basically the pervasive, diffuse exhalation of gas from soil, independent of the presence of macroseeps (Etiope, 2015).

Microseepage is assumed to be a general phenomenon driven by buoyancy of the gas phase relative to connate water (Klusman & Saeed, 1996; Matthews, 1996; Etiope, 2015). The migration is vertical, with frequent lateral displacement by faulting and flow through carrier beds toward basin margins (Figure 5.3 [Thrasher *et al.*, 1996; Rostron & Toth, 1996]). Field measurements have indicated that microseepage is

enhanced along faults and fractures that also serve as significant migration pathway (channels) for increased rate of flow by microbubbles, especially those produced by neotectonics, and can have strong seasonal variations (Figure 5.3 [Varhegyi *et al.*, 1992; Etiope & Lombardi, 1996; Etiope, 1998; Kostakis & Harrison, 1999; Brown, 2000, Klusman, 2003; Etiope & Klusman 2010, Etiope, 2015]).

Sometimes the term "microseeps" is used in the scientific literature, especially in the marine environment (e.g., Hovland *et al.*, 2012) to define relatively smaller seeps, not observable, for example, by hydroacoustic methods. However, the term can be misleading as it may be confused with microseepage. The classification in the above scheme is, in theory, valid for either subaerial (landbased) or underwater (marine and lake) environments (Etiope, 2015).

According to Etiope (2004), potentially areas of microseeps comprise all sedimentary basins with hydrocarbon generation processes at depth: this area is estimated to be around 43,366,000 km^2 leading to a global emission of CH_4.

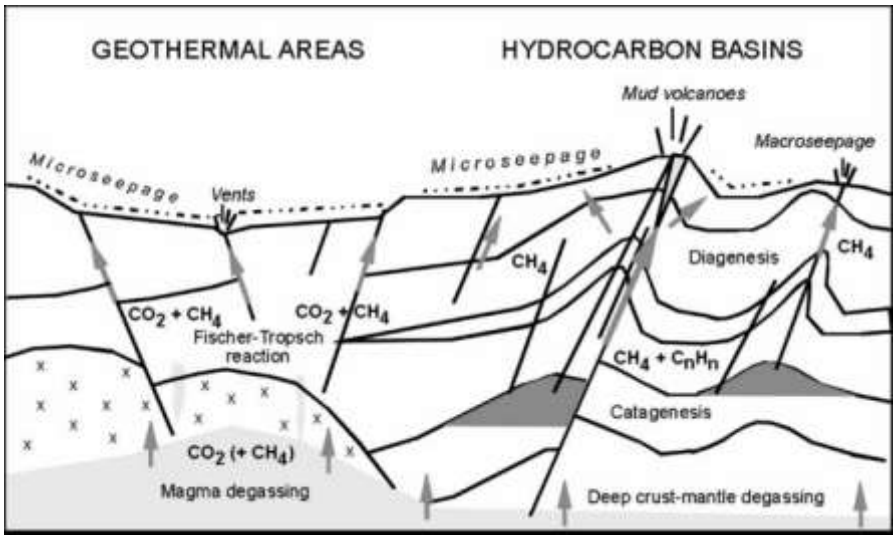

Figure 5.2: Sketch of geological methane production and release. Adapted from Etiope & Klusman (2002).

Migration Mechanism | 5.3

Gas seepage implies the long-distance movement of gas that can be on the order of several kilometers. However, according to Hale (2000) the relatively slow gas diffusion rates in rocks of low porosity at depth have brought the contribution of diffusion to long-distance gas migration into question. The half-life of Rn is so short that its persistence and detection after transport by diffusion over tens or hundreds of meters is extremely unlikely (Hale, 2000).

The release of hydrocarbon gases from reservoirs creates the potential for it to move into near-surface environments through natural and human-made pathways (Figures 5.2 and 5.3 [Stolp *et al.*, 2006]). Natural pathways include fractures through the rock layers and voids between the grains of rock. Human-made pathways can be created when different types of wells are drilled (Stolp *et al.*, 2006). Regional structural and stratigraphic features influence the storage of gases, being lighter than air tends to vertical migration from subsurface accumulations of hydrocarbons, whether or not they are commercially significant (Figures 5.2 and 5.3 [Eltschlager *et al.*, 2001; Etiope, 2015]). Seepage along faults can be more an effusive process, rather than microseepage (Etiope & Klusman, 2002). However, pressure gradients cause gases to migrate to areas of lower pressure. These migrations may be in directions other than vertical. Natural overburden pressure is a mechanism that force gas to the surface (Eltschlager *et al.*, 2001).

The existence of this vertical or near-vertical migration has been controversial for many years. Arguments against it have included the following. (1) If reservoirs leaked enough to be detected, they would have long ago been depleted. (2) If seepage did occur, it would be deflected by groundwater movements, and anomalies would be displaced laterally for relatively long distances (Saunders *et al.*, 1999). The ways in which gases

experience dispersion in the subsurface natural environment are more diverse and less well characterized than mechanisms of dispersion in the solid and liquid phases. (Hale, 2000). Two main categories of fluid migration mechanisms exist: (1) diffusion, ruled by Fick's Law, where gas moves by concentration gradients; and (2) advection, ruled by Darcy's Law, where movement is determined by pressure gradients (Etiope, 2015). Advection is the leading mechanism for seeps and microseepage (Etiope, 2015). However, Hale (2000) argues that for migration in the gas phase, diffusion and mass flow are both well-established mechanisms and each has a role to play in gas transport in the crust. Their relative contributions to gas migration at different positions in the crust is less certain. A more controversial mechanism, applicable to gas transport through groundwater, is gas streaming (Hale, 2000).

Buoyant hydrocarbon microbubbles rising through the water-filled network of fractures, joints, and bedding planes provide a logical mechanism for vertical migration of light hydrocarbons from reservoirs to the surface and commonly occupy the pore voids in rocks, overburden and soil (Figure 5.3 [Saunders *et al.*, 1999; Hale, 2000]). Kristiansson & Malmqvist (1982) and Malmqvist & Kristiansson (1984, 1985) hypothesize that, in the zone of saturation, pressure gradients and pressure shocks cause over-saturation, leading to the formation of gas bubbles. These streams upward at a comparatively rapid rate until they reach the water table (any gas that dissolves in groundwater could, given the appropriate conditions, migrate by streaming) and mix with the soil air. The resulting mixture is then driven slowly further upward by the pressure gradient caused by the bubble stream (Hale, 2000).

Geochemistry of Gases | 5.4

Attempts to detect light hydrocarbon microseeps in the 1930s mark the origins of gas geochemistry (Hale, 2000). In the past, microseepage was investigated for hydrocarbon exploration with alternate outcomes and opinions (Philp & Crisp 1982; Tedesco, 1995). Progressive sophistication has yielded techniques to characterize effectively microseeps both onshore and offshore. Regional surveys involving the determination of light hydrocarbons adsorved into soil have contributed to successful petroleum prospecting (Hale, 2000).

A compilation of papers edited by Aminzadeh *et al.* (2013) focused on the use of new technologies designed to image seeps for exploration and field development applications. Such invisible seepage can easily be detected using soil-gas analyses, revealing anomalous concentrations of gaseous hydrocarbons in the soil (Figure 5.3), and using a closed-chamber technique that allows determinations of gas flux to the atmosphere (Etiope, 2015).

In particular, the assessment of the origin of seeping gas is a key task for understanding, without drilling, the subsurface hydrocarbon potential, genesis and quality, e.g. the presence of shallow microbial gas, deeper thermogenic accumulations, the presence of oil and non-hydrocarbon undesirable gases (CO_2, N_2, H_2S). Low quality, biodegraded petroleum can also be recognized, before drilling, through specific geochemical features of the seeping gas (Etiope, 2004). The geochemical analysis of seeping gas, in particular, can be effective to understand the potential and nature of subsurface accumulations (Etiope, 2009a, 2009b).

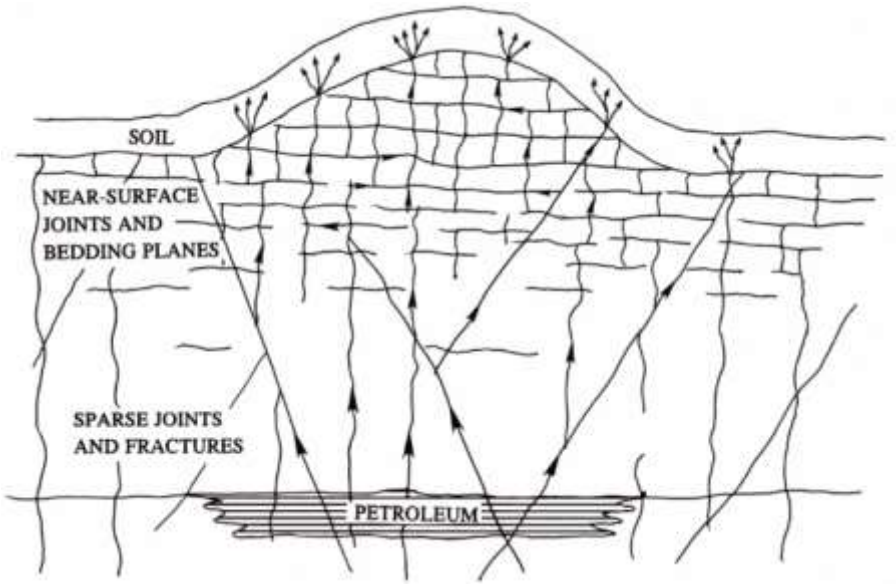

Figure 5.3: Possible microseepage paths up through the network of fractures, joints, and bedding planes. Adapted from Saunders et al. (1999).

Why is important to know the seeps? | 5.5

Saunders *et al.* (1999) reports that since 1976 have used various combinations of surface hydrocarbon microseepage and related alteration methods of petroleum exploration, resulting in the discovery of 38 oil and gas fields, mostly in regions where seismic has had limited effectiveness.

Many large oil and gas fields in North America, Europe, the Caspian Basin, Asia, and the Caribbean were, in fact, discovered after drilling in the vicinity of seeps (Link, 1952; Macgregor, 1993; Abrams, 2005). More generally, gas and oil seeps are important for four main reasons (Etiope, 2009a, 2009b):

- Seeps can be indicators of petroleum or natural gas reservoirs;

- Seeps indicate the occurrence of a fault (according to Etiope [2015], gas in fact, follows preferential pathways of movement [less resistance paths], as determined by fractures and faults);

- Seeps can represent a geo-hazard for societal community and industry;

- Seeps are natural sources of greenhouse gas.

According to Schumacher (2012), the surface manifestations of hydrocarbon microseepage can take many forms, including:

- anomalous hydrocarbon concentrations in soils, sediments, waters, and atmosphere (Figures 5.3 and 5.1);

- microbiological anomalies;

- mineralogic changes such as formation of calcite, pyrite, uranium, elemental sulfur, and magnetic iron oxides and sulfides (Figure 5.1);

- bleaching of redbeds;

- clay-mineral changes (Figure 5.1);

- acoustic anomalies;

- radiation anomalies;

- electrochemical changes;

- biogeochemical changes and geobotanical anomalies.

According to Hale (2000), if a mineral deposits or petroleum accumulations are judged or can be shown to liberate a gas into a porous medium such as overlying rock, overburden or soil then, in the simplest case, the gas will form a broad spherical halo.

Chemical alterations of near-surface sediments by carbon dioxide and hydrogen sulfide, produced by microbial degradation of microseeping hydrocarbons, and a reduction chimney in an otherwise aerated and oxidising environment provide reasonable explanations for observed geomorphic, seismic, magnetic, and radiometric anomalies over petroleum deposits and prospects (Figure 5.1 [Saunders *et al.*, 1999; Hale, 2000]). The effects induced in soil, rocks and vegetation can sometimes be detected from satellites (Hale, 2000).

Applications of hydrocarbon microseepage to petroleum exploration and production include (Schumacher, 2012):

- documenting that oil/gas has been generated in frontier basins;

- high-grading leads and prospects on basis of likely hydrocarbon charge;

- identifying presence of by-passed pay in old or abandoned fields;

- monitoring hydrocarbon drainage due to production in producing fields or waterfloods

For this reason, seepage has historically been an important driver of global petroleum exploration.

Directly detecting microseeping hydrocarbons and their alterations can provide the ability to carefully focus seismic exploration efforts where the chance of success is greatest for either structural or stratigraphic accumulations, therefore, reflects the permeability of the subsurface and may provide considerable information for structural geology (Saunders *et al.*, 1999; Etiope, 2015). However, Saunders *et al.* (1999) argument that no method dependent only on hydrocarbon microseepage can distinguish depth to reservoirs. A surface anomaly may be sourced from any depth between the surface and the basement.

According to Hale (2000), there are no gases uniquely associated with mineral deposits or petroleum accumulations. Even those that are perhaps the most obvious indicator gases (sulphur gases and volatile hydrocarbons) can sometimes be generated by biogenic reactions in the soil.

Worldwide Seeps | 5.6

Seeps have been polluting the environment for a long time. Many seeps around the globe have been prolific and more continuously active (Map 5.1). Overall, natural seepage never stops. (Berge, 2011) So, what is the

volume of seepage worldwide? It is extremely difficult to estimate seep rates and the global coverage of seepage is unknown. According to Clarke & Cleverly (1991), the global number of terrestrial seeps seem to exceed 10,000 (but only a small number has been directly investigated). However, as shown by innumerable surveys performed for petroleum exploration (e.g. Schumacher & Abrams 1996; Saunders *et al.*, 1999; Wagner *et al.*, 2002; Etiope, 2005; Khan & Jacobson 2008; Tang *et al.*, 2010; Sechman, 2012) all petroleum basins contain microseepage.

Etiope & Klusman (2002) work documents that significant amounts of "old" methane, produced within the Earth crust, can be released naturally into the atmosphere through gas permeable faults and fractured rocks. A global analysis of more than 200 onshore seeps worldwide (including 143 mud volcanoes) revealed that methane is thermogenic in about 80% of the cases, microbial gas is in only 4 % of seeps, mixed gas in the remaining cases (Map 5.1 [Etiope, 2009a]).

Submarine seeps, mud volcanoes and microseepage in sedimentary basins represent the major geologic methane source (biogenic and thermogenic methane) and, subordinately, to inorganic reactions (Fischer-Tropsch type) in geothermal systems. Geologic CH_4 emissions include diffuse fluxes over wide areas, or microseepage (Etiope & Klusman, 2002). Areas of potential emission represent about 1/3 of the land surface. Microseeping areas include all of the sedimentary basins contained in dry climates, generally considered a major CH_4 sink, with petroleum and gas generation processes at depth, estimated to be 43,366,000 km2 (Klusman & Saeed, 1996; Etiope & Klusman, 2002).

Etiope & Klusman (2010) assumed that microseepage occurs within the TPS. On Earth, 42 countries produce 98 % of total petroleum and 70 countries produce 2 % (the remaining 90 countries produce 0 %). So, the TPS and, consequently, the potential for microseepage, occur in 112 countries (Etiope, 2015).

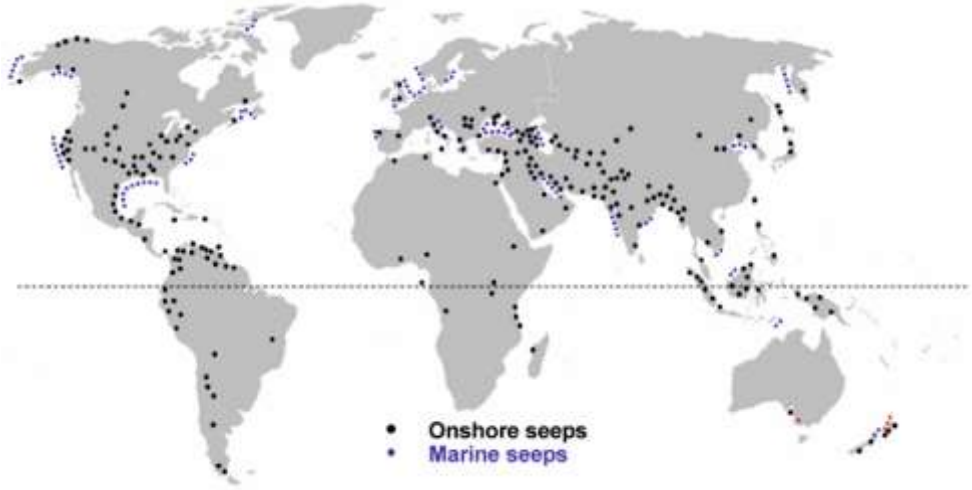

Map 5.1: Global distribution of petroleum seeps. Adapted from Etiope (2009a).

Hydrocarbon-prone areas in Europe which host oil and/or natural gas reservoirs, potentially or actually producing thermogenic methane emissions, occur in 25 countries (26 including Azerbaijan). (Map 5.2 [Etiope, 2009c]).

Map 5.2: Map of potential microseepage areas related to oil e gas field distribution (points: petroleum and natural gas fields; redrawn from digital maps of USGS [2000]) and location of the main, known active hydrocarbon macro-seepage zones in Europe (triangles: macro-seep sites; black: onshore; white: offshore). Adapted from Etiope (2009c).

THEORY OF METHANE|6.0

CH_4 and Bacterial Activity|6.1

The generation of bacterial gas is regulated by several key factors (Rice, 1992). One of these factors is: Methanogenic bacteria are obligate anaerobes that are widely distributed in anaerobic environments (like organic-rich environments), therefore cannot tolerate any oxygen (Wolfe, 1971). A succession of metabolic processes leads to the generation of bacterial gas. Although fermentation is the pathway for generation in some modern environments, CO_2 reduction is the most important pathway for ancient bacterial gas accumulations (Rice, 1992). Soil biochemical reactions may also produce low-oxygen levels and occasionally methane (Eltschlager *et al.*, 2001). According to Freitas *et al.* (2010), biodegradation of organic compounds in groundwater can be a significant source of methane in contaminated sites.

On the opposite side, the only known group of bacteria able to grow on CH_4 are the aerobic methylotrophic bacteria which oxidize CH_4 with O_2 to CO_2 (Conrad, 1996). The methanotrophs are subdivided into two major groups, type I and type II. Type I methanotrophs (the genera *Methylobacter* and *Methylomonas*) belong to the g-subdivision of the

Proteobacteria and use the ribulose monophosphate pathway for formaldehyde assimilation. Type II methanotrophs (the genera *Methylosinus* and *Methylocystis*) belong to the a-subdivision and use the serine pathway (Conrad, 1996). A third group, type X, is often proposed for *Methylococcus capsulatus* (g-subdivision), because this bacterium has characteristics of both of the other groups (Conrad, 1996). According to Etiope (2015), during the summer, methanotrophic activity increases and microseepage flux decreases. The opposite is true in the winter.

Thermogenic CH_4 | 6.2

The thermogenesis of methane may operate for substantial periods of geologic time, then gradually decline as the organic matter matures, losing its ability to generate hydrocarbons (Figure 6.1 [Hunt, 1996]). Continued thermal degradation of hydrocarbons in reservoirs and dispersed through the sedimentary column contributes to an upward, buoyant flux of CH_4 and light alkanes (devolatilization). Thermogenic methane forms as organic matter is buried deep under sediments, commonly termed the process of maturation (diagenesis, catagenesis, and metagenesis are three consecutive alteration stages, that collectively make up thermal process, within the carbon cycle that irreversibly effect progressive changes in the composition of sedimentary organic matter - Figure 6.1 [Horsfield & Rullkotter, 1994]). As sedimentary layers build, progressively higher temperature (>165°C) and pressure regimes develop, and the thermal decomposition (cracking) of the organic matter begins (diagenesis [Friedman & Sanders, 1978]). Substantial transformation of oil into wet gas occurs later in catagenesis. Metagenesis falls between catagenesis and rock metamorphism (inorganic maturation) and is characterized by dry gas generation (Figure 6.1 [Horsfield & Rullkotter, 1994]).

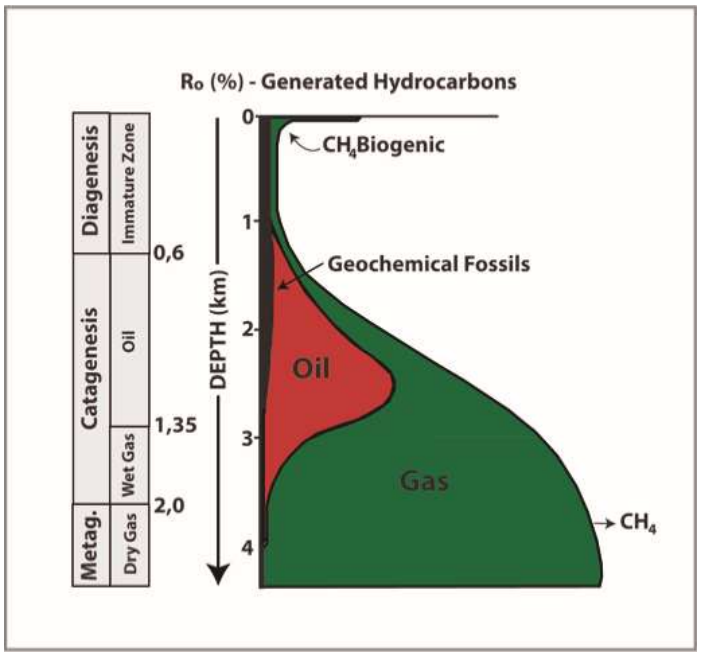

Figure 6.1: Schematic diagram showing the relative abundance of liquid and gas hydrocarbons as a function of the thermal evolution of kerogen. Adapted from Tissot & Welte (1978).

Hydrocarbon gases, primarily methane, are generated and stored in sedimentary rocks (including metasedimentary and volcano sedimentary rocks) associated with conventional or unconventional petroleum systems (Eltschlager *et al.*, 2001). Ethane and the heavier alkanes (ethane, propane, butane, etc.) are also found in soils at low levels (also variable, but more typically less than 1 ppm), especially in petroleum producing basins (Fontana, 2000), however, the presence of methane, or any hydrocarbon, does not necessarily indicate that a large petroleum reservoir underlies an area (Eltschlager *et al.*, 2001). Methane in appreciable amounts can exist over a large area and be widely disseminated in a variety of rocks (Eltschlager *et al.*, 2001). Other hydrocarbon gases such as ethane and propane often occur naturally with methane.

Methane is found everywhere in the atmosphere and in soils typically between at 1 to 4 ppm (Fontana, 2000). It can also be found at much higher concentrations (percent levels) where degradation of organic material is present, such as buried plant material, a natural swamp, wetland or stuary, or in a landfill (Fontana, 2000). Ethylene (or ethene) and propylene (or propene), are light hydrocarbons typically found in soils and these two compounds are typically from biodegradation of man-made or naturally occurring hydrocarbons (Fontana, 2000).

According to Quay *et al.* (1999), the global methane cycle includes both terrestrial (formed as a result of microbial [biogenic] or thermal [thermogenic or petrogenic] alteration of organic matter [Eltschlager *et al.*, 2001]) and atmospheric processes, and may contribute to feedback regulation of the climate. Most oxic soils are a net sink for methane, and these soils consume approximately 20 to 60 Tg of methane per year (Holmes *et al.*, 1999).

Methane gas can be transported by groundwater in dissolved or pure gaseous states and does not react with silica, carbonates, iron, or any other substances commonly found in groundwater. It does not impair the odor, taste or color of the water, nor does it in any way affect the potability of the water (Eltschlager *et al.*, 2001). As water is agitated or reduced in pressure, small bubbles may form and appear to make the water milky or translucent. The water will quickly clear as the gas escapes into the atmosphere (Eltschlager *et al.*, 2001). Methane in groundwater is not explosive; but when water containing dissolved methane comes into contact with air, the methane quickly escapes from the groundwater into the atmosphere. If this process occurs in a confined space, then the methane could ignite; or if it is allowed to accumulate, it could explode (USGS, 2006).

According to Fontana (2000), the USEPA (US Environmental Protection Agency) or OSHA (Occupational Safety and Health Administration) only regulates methane as a simple asphyxiant (dilution of oxygen in air) and

flammable gas. Methane, and the other light hydrocarbons are not known to be toxic (Fontana, 2000).

The US Department of the Interior, Office of Surface Mining, suggests that when the level of methane gas in the water is less than 10 ppm it is safe, but monitoring is required at 10 to 28 ppm, and immediate action is needed above 28 ppm (Table 6.1). At a level of 28 ppm, the water is fully saturated with methane (because the solubility of CH_4 in water is between 28 and 30 ppm [standard temperature and pressure]) and it is likely that any air space in the well is at or approaching the LEL (lower explosive limit) (B.F. Environmental Consultants Inc., 2012). The air and outgassing methane (not the water) is now flammable (as a combustible gas can catch on fire if airborne concentrations exceed 5% [Eltschlager *et al.*, 2001]). Occasionally, the subterranean migration of methane presents a hazard at the ground surface, primarily in structures (buildings). Entry into a structure can occur through cracks in the floor, along buried utilities, or as a dissolved component of water. When allowed to accumulate in a structure, an explosion may result.

Action Level	Atmospheric (Percent Volume)		Dissolved in Water (mg/litre)	Soil Gas (percent volume)
	Occupiable Scape (homes)	Un-Occupiable Spaces		
Immediate Action	>1.0%	>3.0%	>28 mg/L	>5.0%
Warning, Investigate	>0.5% but <1.0%	>1.0% but <3.0%	>10 mg/L but <28 mg/L	>3.0% but <5.0%
Monitor to Determine Concentration Trends	>0.25% but <0.5%			<3.0% but >1.0%
No Immediate Action	<0.25%	<1.0%	<10 mg/L	

Table 6.1: Recommended action levels for methane. Adapted from Eltschlager et al. (2001).

The typical $\delta^{13}C$ of thermogenic methane range between -25‰ and -50‰, according to Santos Neto (2004) (Figure 6.2). Still according to the author, the typical $\delta^{13}C$ of biogenic methane is lower than -60‰ (Figure 6.2). However, methane can be obtained from anaerobic biodegradation of toluene and had a $\delta^{13}C$ value of -55.3 ± 1.8‰ (Freitas *et al.*, 2010)

Quay *et al.* (1999) suggest that the global atmospheric CH_4 has a $\delta^{13}C$ of -53.4 to -57.1‰ depending on the magnitude of the fractionation effect during OH reaction. The southern hemisphere was more enriched than the northern hemisphere in $\delta^{13}C$ by -0.23‰ (Quay *et al.*, 1999).

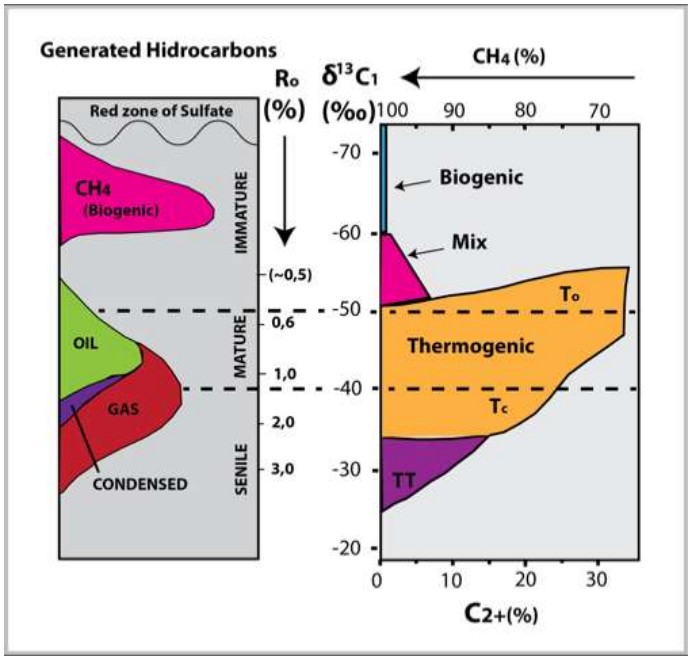

Figure 6.2: Genetic classification of methane given by its $\delta^{13}C_1$ value and the relative gas wetness, through thermal maturity evolution. T – Gas associated to oil (o) and condensed (c); TT – Dry gas. Adapted from Schoell (1983) and Santos Neto (2004).

Stahl *et al.* (1981) show that the isotopic composition of the methane adsorved in near-surface sediments above deep hydrocarbon accumulations is similar to the isotope ratios of the methane from the deep reservoir (Figure 6.3). According to the authors, this similarity is evidence that migration occurs from deep hydrocarbon reservoirs and

source rocks to the surface. Using carbon isotopes to identify the origin of methane adsorved in near-surface sediments will considerably improve the results of geochemical surface exploration (Stahl *et al.*, 1981).

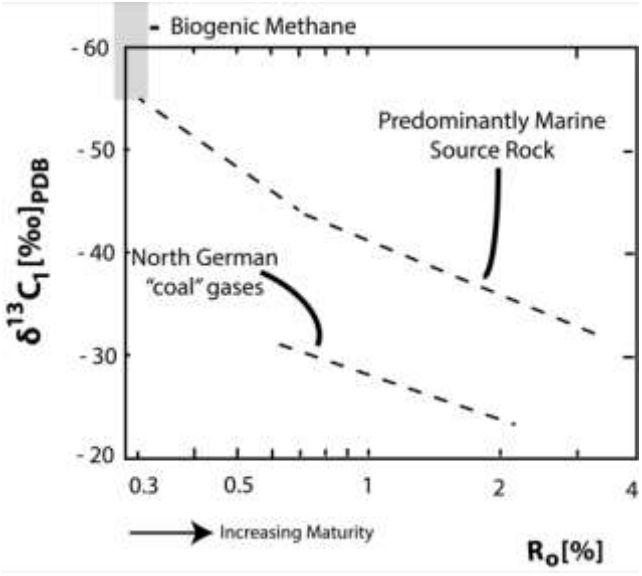

Figure 6.3: Relation between carbon isotopic composition of methane natural gas reservoirs and maturity (vitrinite reflectance R_o) of their source rocks. Adapted from Stahl et al. (1981).

RESULTS AND DISCUSSION | 7.0

SPZ Unconventional Petroleum System | 7.1

The petroleum system is a unifying concept that encompasses all the disparate elements and processes of petroleum geology, that form the functional unit that creates hydrocarbon accumulations. Practical application of petroleum systems can be used in exploration, resource evaluation, and research (Magoon & Dow, 1994).

Globally, there are different perceptions of the unconventional petroleum system (UPS) definition. Unconventional gas accumulations include deep gas, shale gas, tight-sandstone gas, coalbed methane, shallow biogenetic gas, and natural gas hydrates (Zou *et al.*, 2013).

In addition to the characteristics mentioned in the introduction of this thesis (subchapter "unconventional hydrocarbons"), according to Law & Curtis (2002)there is a fundamentally important geoeconomic distinction between conventional and unconventional systems: conventional hydrocarbon resources are buoyancy-driven deposits, occurring as discrete accumulations in structural and/or stratigraphic traps, whereas unconventional hydrocarbon resources are generally not buoyancy-driven accumulations. They are regionally pervasive accumulations, most commonly independent of structural and stratigraphic traps.

There are obvious differences between unconventional petroleum geology and conventional petroleum geology, including geological characteristics, classification systems, studied content, and evaluation methods (Zou *et al.*, 2013). The key content for UPS are not formation parameters (i.e., source rocks, reservoirs, caprocks, migration, trap, and preservation), which are the main concerns in conventional petroleum systems (Zou *et al.*, 2013). Unlike conventional petroleum systems, dominated by elements, the unconventional petroleum system is dominated by processes.

The regionally pervasive characteristic of the UPS implies that these processes may vary according to the geotectonic characteristics of in the region. Barberes *et al.* (2015) proposed and designed a model for unconventional petroleum system in the study area (Figure 7.1).

The tectonic processes affect important variables of the system such as maturation/hydrocarbon generation, by compression and folding; fluid leaks/losses (oil and/or gas), by thrusts, uplifts and erosion; and preservation, by post-orogenic overburden, uplifts and erosion.

As said before, the SPZ was largely affected by the Variscan orogeny and as such its tectonic-structural products were considered as processes of this model.

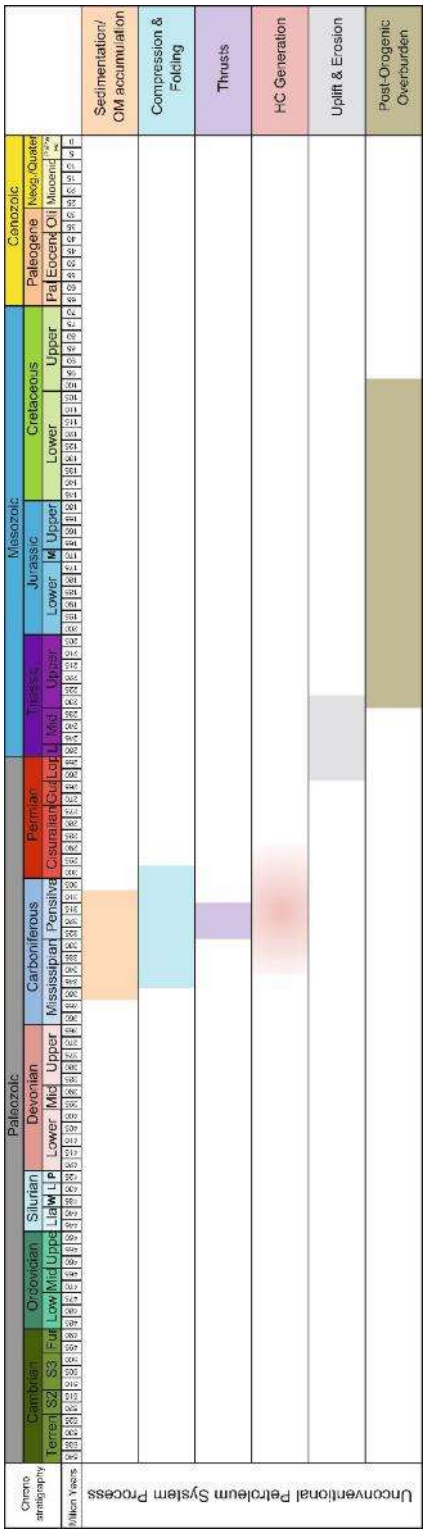

Figure 7.1: Unconventional Petroleum System of South Portuguese Zone.

Thus, the proposal unconventional petroleum system model, for SPZ, is composed by:

- Sedimentation and organic matter accumulation
- Compression and folding
- Thrusts
- Hydrocarbon generation
- Uplift and erosion
- Post-orogenic overburden

The information contained in McCormack *et al.* (2007) and Fernandes *et al.* (2012) were used in establishing the processes of "sedimentation and organic matter accumulation" and "hydrocarbon generation" limits. Fernandes *et al.* (2012) refers that the peak temperatures were attained at the Pennsylvanian, thus the inferior and superior limits of "hydrocarbon generation" were extended and represented in a colour gradient.

The "post-orogenic overburden" (Mesozoic cover) information was extract from Pena dos Reis *et al.* (2011). "Compression and folding", "Thrusts" and "Uplift and

erosion" were established according to Fonseca *et al.* (2015).

Thorium-Normalization and Hydrocarbon Anomalies | 7.2

As mentioned before, the Brejeira Formation wasn't completely covered by aerial spectrometry and the intrusion of the igneous Monchique Massif complex further limits the study area, because the data corresponding to this Massif were not used to calculate TN and HA values.

It is also important to highlight that the relation between hydrocarbons emanations and mineralogical alteration, is pointed by several authors (*e.g.*, Saunders *et al.*, 1999; Van der Meer *et al.*, 2002), which can include the formation of calcite, pyrite, uranite, elemental sulphur, iron sulphides, magnetic iron oxides and/or clay mineral alteration (Van der Meer *et al.*, 2002).

According to Weatherford (2013) in all the analysed samples of the Brejeira Formation, the pyrite is abundant and common (Figure 7.2), and it may result (at least partially) from hydrocarbon emanations associated to these samples.

In order to help data interpretation, 5 thematic maps were designed. Map 7.1 shows the DRAD values (hydrocarbon anomalies), positives and negatives, covering all the SPZ, and the surface of Mértola and Mira Formations appear as the most affected by the HA, from a simple quantitative point of view. However, when considered the highest values as the most significant, as suggested by Skupio & Barberes (2017), covering the same area, it could be noted that Brejeira Formation, seems to be the most promising area for hydrocarbons emanations (Map 7.2).

Most of the works on remote sensing applied to petroleum geology using the TN and HA methods were based in aerial GR spectrometry in order to cover large areas. Despite of that, the measurements were made in active

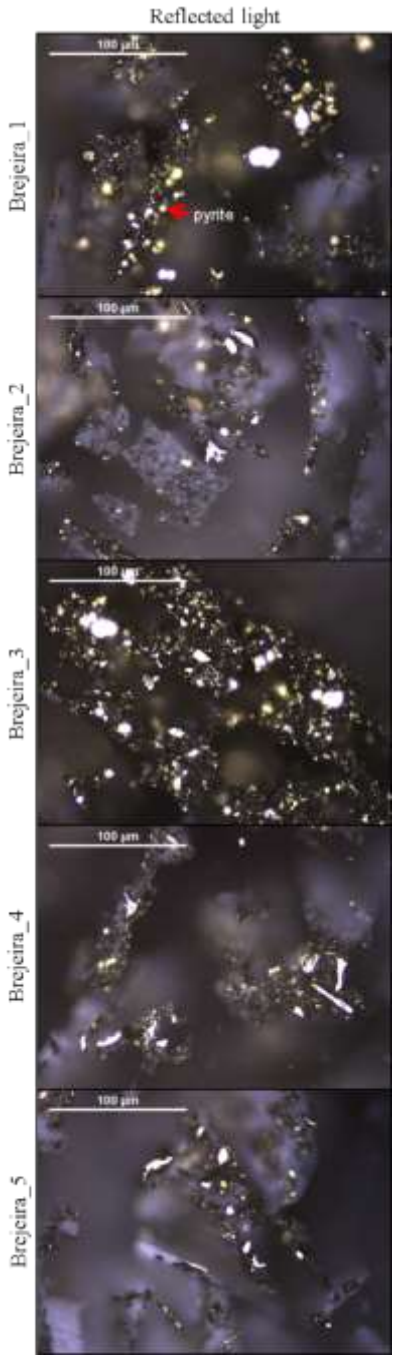

Figure 7.2: Pyrite under reflected light from five samples of SPZ (Weatherford, 2013).

oil and gas fields to analyse the viability of the DRAD values for hydrocarbon exploration. Some authors also applied this method on wells in order to check if the DRAD values match the hydrocarbon source and reservoir levels (saturation).

As said before, Portugal does not have active hydrocarbon production and most of the onshore wells do not include or have GR data. Therefore, comparison of aerial GR data with active oil/gas fields is not possible, so far. But previous data (before the surface geochemical prospecting) as organic carbon, thermal maturation and surface mineralogical alterations suggest a presence of unconventional petroleum system bellow SPZ.

The HA results point to a higher probability of hydrocarbon microseeps in the Brejeira Formation, when compared with the Mértola and Mira Formations area (Map 7.2). However, it is important to remember that the network of fractures, joints and bedding planes, characteristic of these formations, can help the migration of fluids, creating pathways to other areas, far from the source.

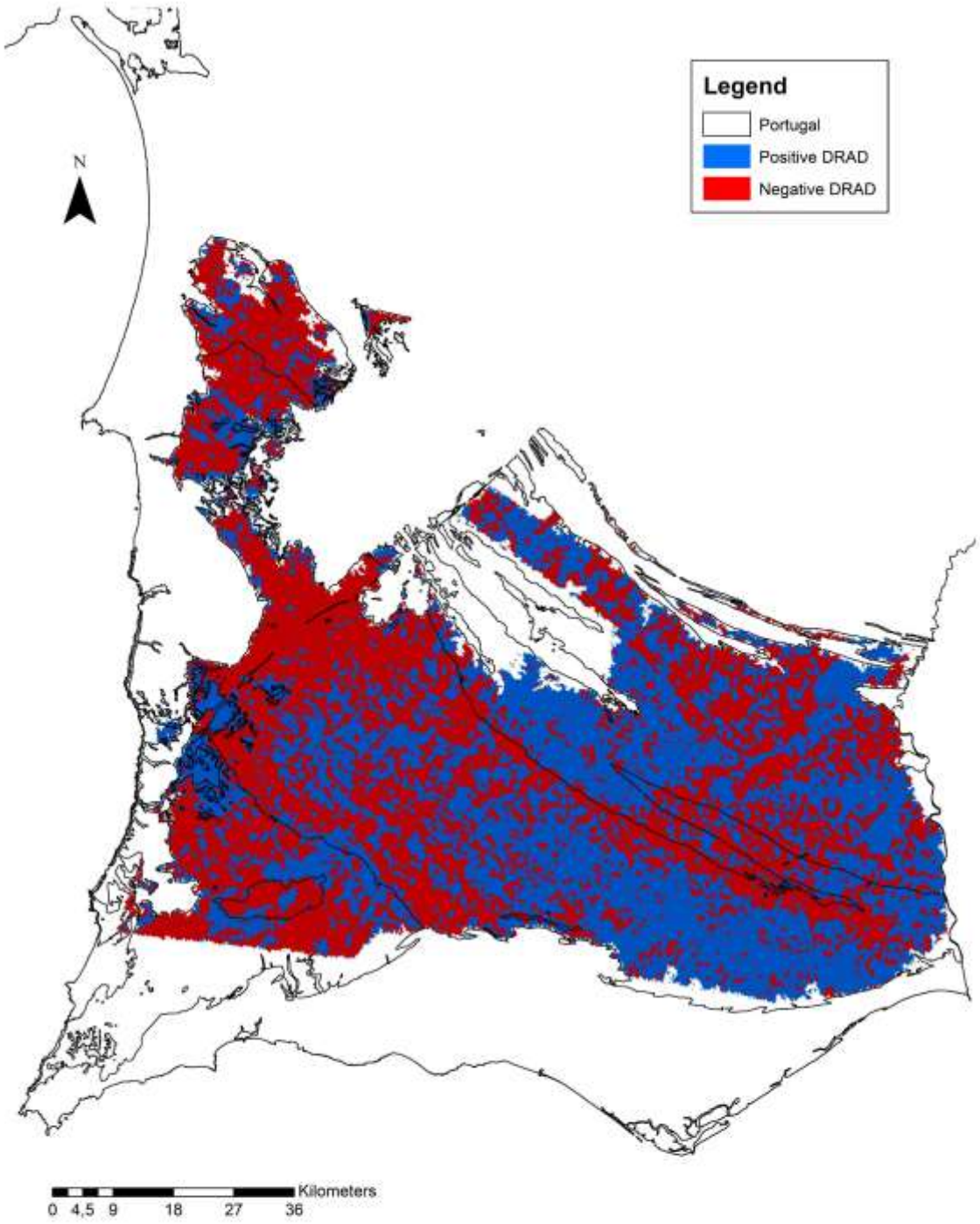

Map 7.1: Positives (blue) and negatives (red) values of DRAD for the studied area. Airborne gamma radiation courtesy of the LNEG.

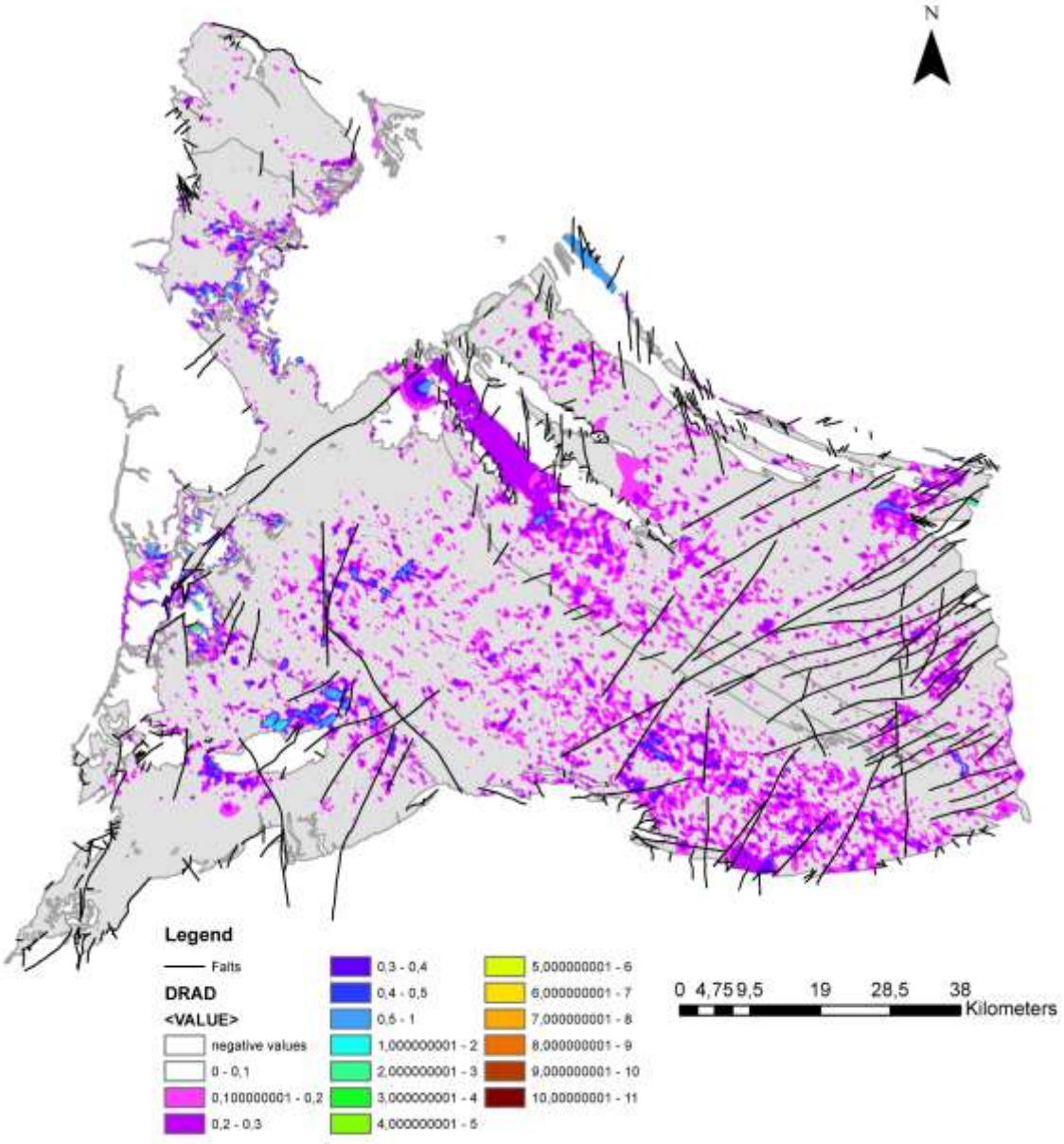

Map 7.2: Values of DRAD higher than 0.1 for the studied area. Airborne gamma radiation courtesy of the LNEG.

The figure 7.3 show a possible pathway system, taken by light hydrocarbons to surface, the Porto-Tomar Ferreira do Alentejo Shear Zone. Dias & Ribeiro (1993) reported that the Porto-Tomar Shear Zone was active throughout much of the Devonian as well as the Hercynian. Thus, the shear zone is not simply a late feature cutting earlier sinistral shears. This places a major constraint on the magnitude of movement along the sinistral shears of Iberia during the Hercynian, but it allows the possibility of very large-scale movement along the dextral Porto- Tomar Ferreira do Alentejo Shear Zone (Shelley & Bossière, 2000).

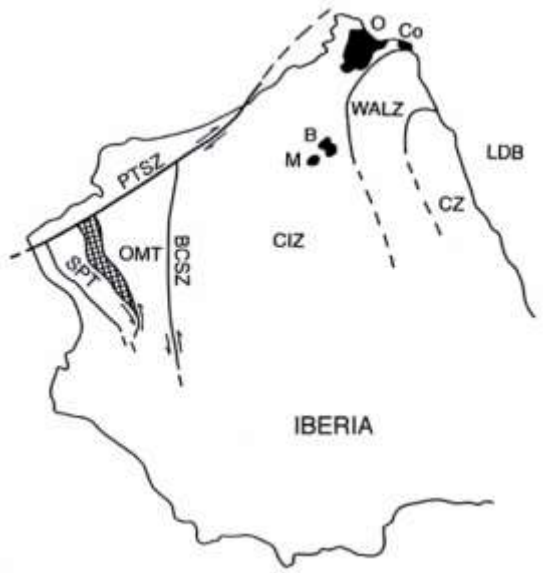

Figure 7.3: Tectonostratigraphic terranes of Gondwanan Iberia. The relative positions of Iberia after Lefort (1989). Iberia: CO = Cabo Ortegal, O = Ordenes, B = Brangança, M = Morais, all representing klippe with ophiolite and other complexes; LDB = Le Danois Bank; CIZ (Central Iberian Zone), WALZ (West Asturian-Leonese Zone) and CZ (Cantabrian Zone) represent Paleozoic sedimentary zones within the Iberian Terrane; PTSZ = Porto-Tomar Ferreira do Alentejo Shear Zone; BCSZ = Badajoz-Córdoba Shear Zone; OMT = Ossa Morena Terrane; Cross-hatched area = Pulo do Lobo Oceanic Terrane; SPT = South Portuguese Terrane. The eastern part of Iberia is mainly covered with post-Hercynian deposits, though inliers of Proterozoic and Paleozoic material with uncertain affinities occur throughout. The area west of PTSZ exposes post-Hercynian basinal sediments. Adapted from Shelley & Bossière (2000).

Relation between Airborne Gamma Radiation and WorldView-2 | 7.3

The statistical analysis results represented in the table 7.1 show high levels of correlation, direct or inverse, between the GR and WV2 image bands. The table also highlights two qualities of PC values: the higher values of each bands and each of GR variables. In the case of Th, U, and K, these two values match, but in case of TC they refer to two different bands (1 and 8). Therefore, the band 8 was chosen as TC correlative because the band 1 is more correlative with K.

Graph 7.1 represents all xy graphs between the 8 bands and 4 radiometric variables. The 4 most significant correlations, shown in the table 7.1, are highlighted in order to make clearer the level of correlations among the variables described above.

	K	TC	Th	U
Band 1	**-,723**	**-,705**	-,719	-,356
Band 2	-,718	-,687	-,681	-,388
Band 3	-,362	-,279	-,360	,393
Band 4	-,642	-,646	-,676	-,003
Band 5	-,664	-,694	**-,742**	-,152
Band 6	,625	,646	,538	**,746**
Band 7	,660	,637	,587	,611
Band 8	,632	,648	,615	,629

Table 7.1: Pearson correlation statistical analysis results. Yellow boxes represent the values used for gamma ray correlation. Red numbers represent the highest values for each radiometric element.

The use of the above described statistical methods confirms the correlation trends suggested by the maps (Figures 7.4, 7.5, 7.6 and 7.7). The spectra in question have an obvious link between them, since the geological/geomorphological aspect highlight the same lithology, structures, components, etc. The results presented in this thesis show that it is possible, at least partially, to extract radiometric information from WV2 images.

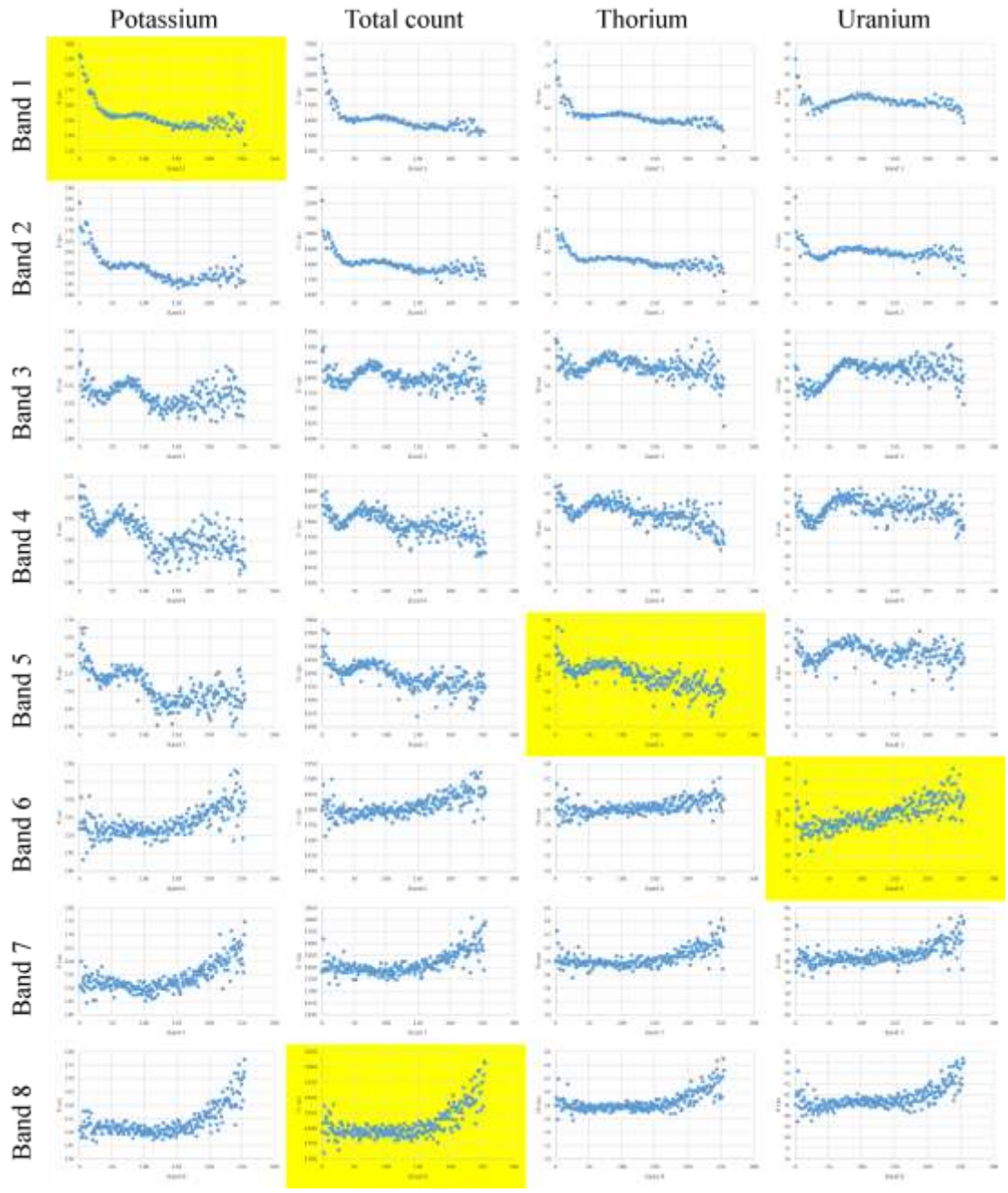

Graph 7.1: XY graphs between WV2 bands (1-8) and radiometric elements (K, TC, Th and U). The yellow graphs represent the best relation used for this work, based on Pearson´s correlation statistical analysis.

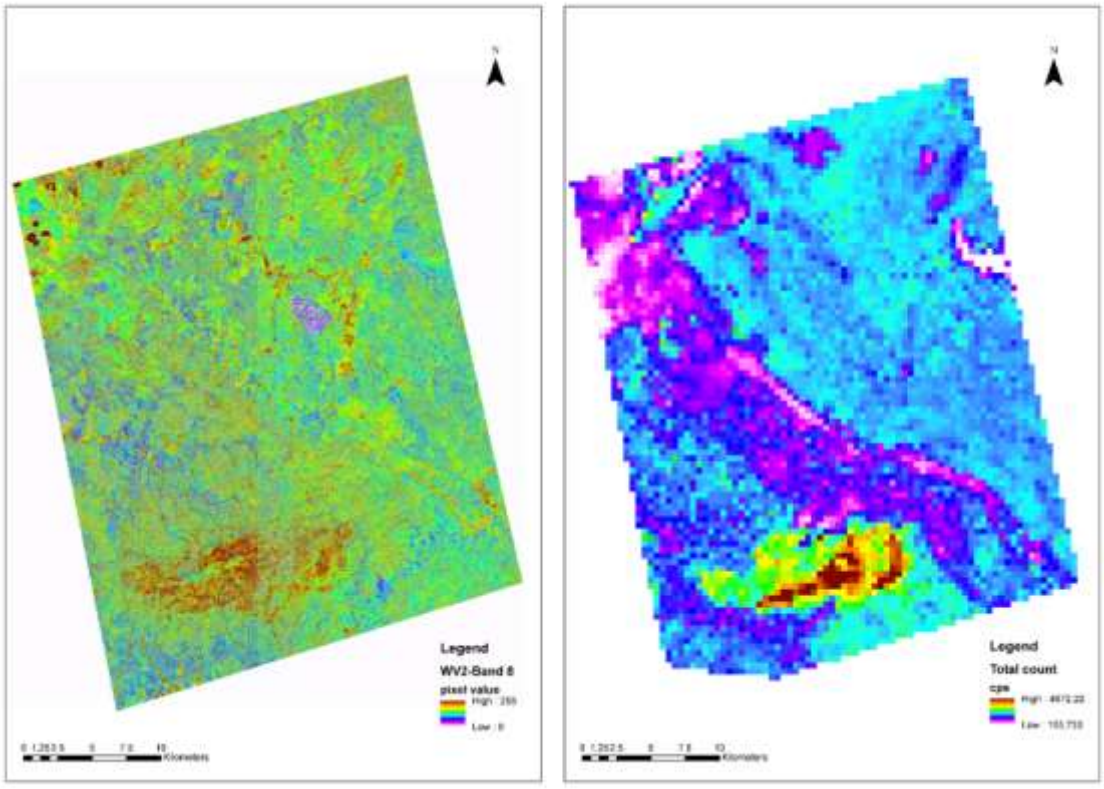

Figure 7.4: Band 8 (left image) mosaic interpolation compared with TC (cps-right image) interpolation. Satellite images courtesy of the DigitalGlobe Foundation and airborne gamma radiation courtesy of the LNEG.

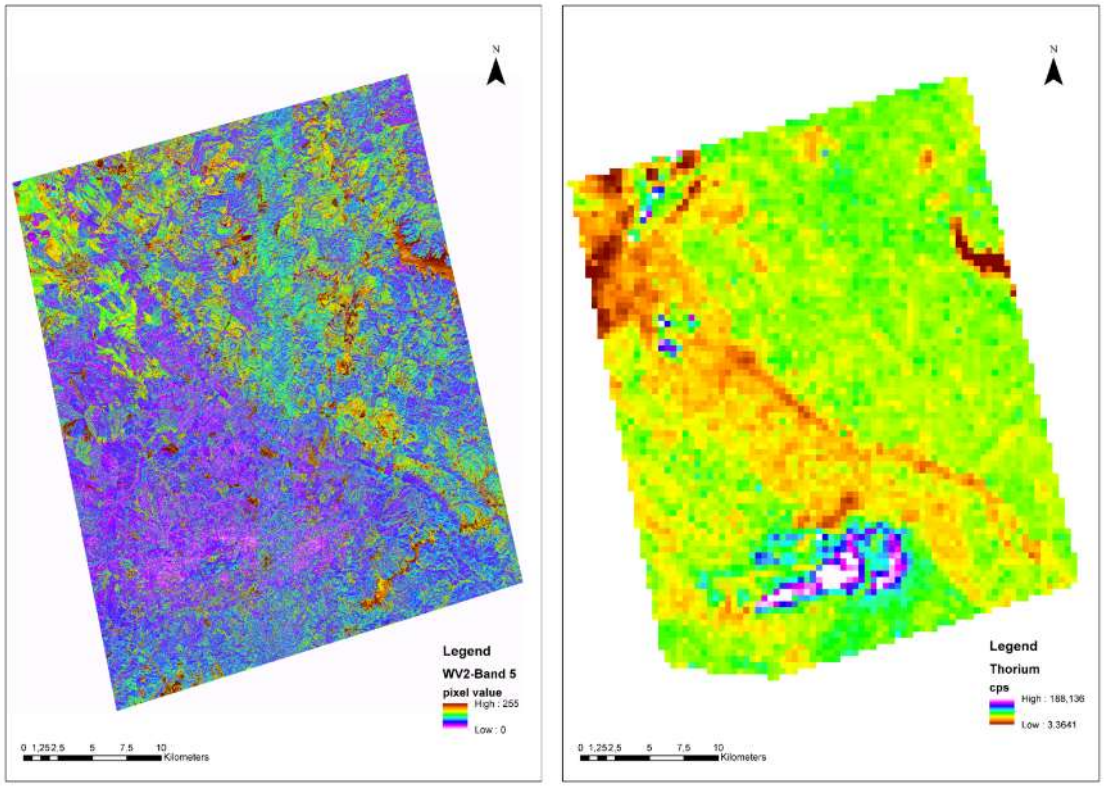

Figure 7.5: Band 5 (left image) mosaic interpolation compared with Th (cps-right image) interpolation. Satellite images courtesy of the DigitalGlobe Foundation and airborne gamma radiation courtesy of the LNEG.

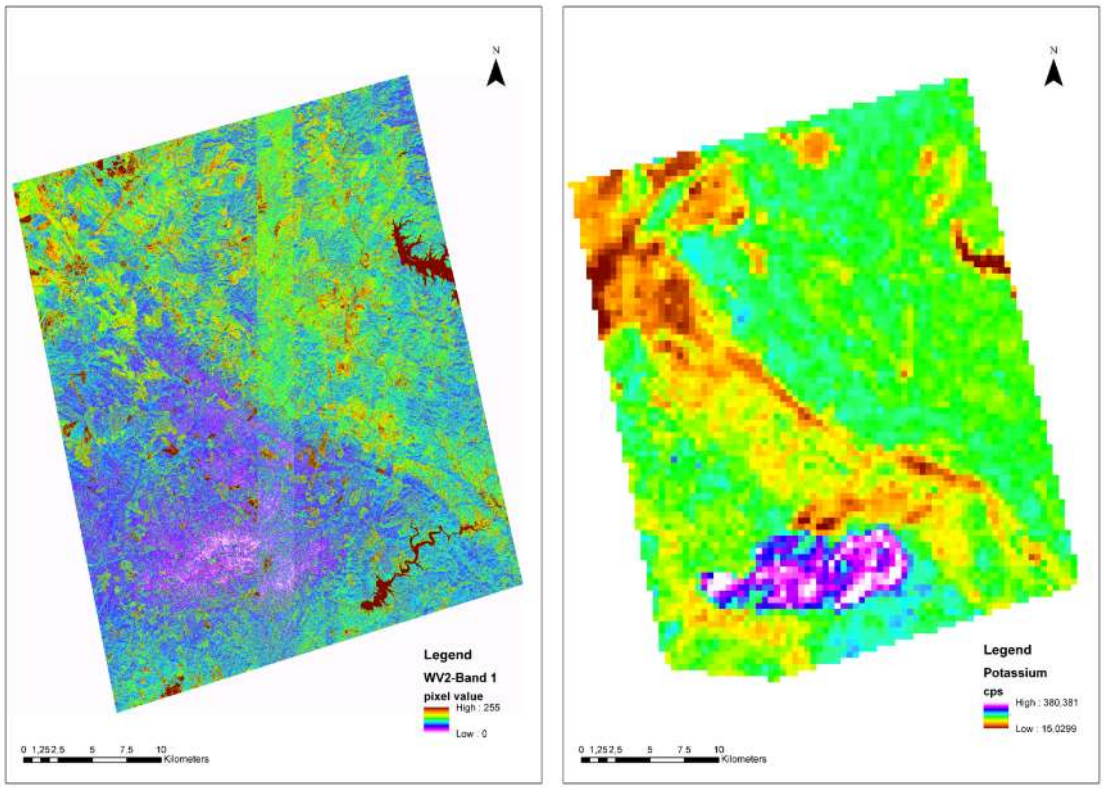

Figure 7.6: Band 1 (left image) mosaic interpolation compared with K (cps-right image) interpolation. Satellite images courtesy of the DigitalGlobe Foundation and airborne gamma radiation courtesy of the LNEG.

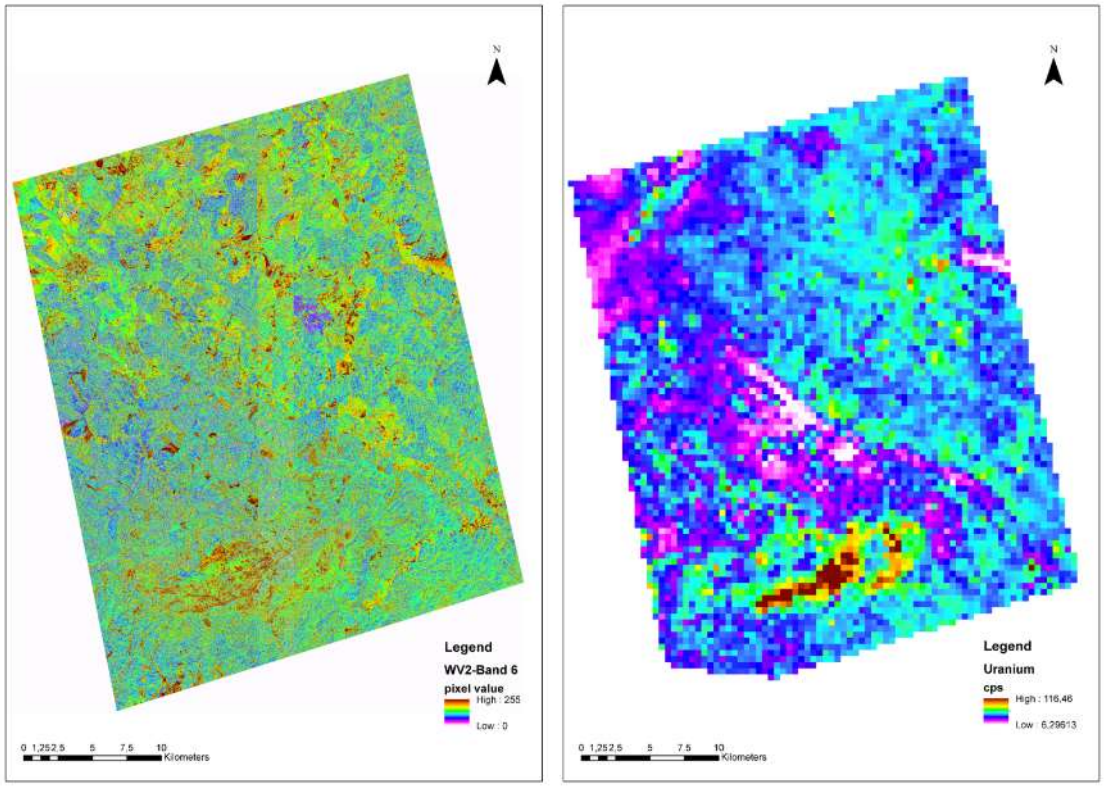

Figure 7.7: Band 6 (left image) mosaic interpolation compared with U (cps-right image) interpolation. Satellite images courtesy of the DigitalGlobe Foundation and airborne gamma radiation courtesy of the LNEG.

Pyrolysis Rock-Eval|7.4

All examined samples of the SPZ formations, presented in the appendix 10.65 and table 7.2, show a very high degree of similarity in terms of the kerogen type as well as its degree of thermal maturity. Hydrocarbon potential, based on Hydrogen Index (HI), of the examined samples, falls in the very narrow range of values between 0.36 and 44 mgHC/gTOC. The thermal maturity parameter (Tmax) is characterized by very wide range of values between 317 and 610°C. The average Tmax value oscillates around 490°C. Total Organic Carbon content (TOC) fluctuates between 0.20 and 3.21 wt%, and generation potential expressed as S2 parameter falls in the range between 0.01 and 0.23 mgHC/gRock. Major contribution of the TOC is unproductive residual carbon (average 98%) which, together with the values of the Tmax and HI might suggest to the conclusion that the examined samples went through the whole oil window, condensate and upper part of the gas window zones. The samples revealed their very high thermal maturation typical for lower part of the gas window zone suggesting that the rocks have probably expelled all hydrocarbons they were able to generate. The samples are predominated by gas-prone extremely hydrogen depleted type III/IV kerogen (Graphs 7.2 and 7.3), which is presently totally unproductive with respect to hydrocarbon generation.

Is important to note the harmony between rock-eval and VR (McCormack *et al.*, 2007, Fernandes *et al.*, 2012, Barberes *et al.*, 2014a) data, from the hydrocarbon potential point of view. From an exploratory point of view, these results mean that all the potential for hydrocarbons generation, in these formations, has already been exhausted, thus representing a senile petroleum system.

Formation	TOC (wt%)	RE S1 (mg Hc/g rock)	RE S2 (mg Hc/g rock)	RE S3 (mg CO2/g rock)	Tmax (°C)	HI (mg Hc/g TOC)	OI (mg CO2/g TOC)	S2/S3	S1/TOC *100	PI
Brejeira 1	0.26									
Brejeira 2	0.91	0.04	0.23	0.25	499	25	27	0.92	4.41	0.15
Brejeira 3	1.36	0.11	0.06	0.18	438	4	13	0.33	8.10	0.65
Brejeira 4	0.89	0.12	0.09	0.32	444	10	36	0.28	13.43	0.57
Brejeira 5	0.84	0.06	0.03	0.30	426	4	36	0.10	7.13	0.67
Brejeira 6	0.88	0.06	0.09	0.10	509	10	11	0.90	6.87	0.40
Brejeira 7	0.44									
Brejeira 8	0.72									
Brejeira 9	0.75									
Brejeira 10	0.32									
Brejeira 11	0.39									
Brejeira 12	0.68									
Brejeira 13	0.70									
Brejeira 14	1.37	0.04	0.01	0.44	424	1	32	0.02	2.92	0.80
Brejeira 15	0.75									
Brejeira 16	0.81									
Brejeira 17	0.79									
Brejeira 18	0.46									
Brejeira 19	0.67									
Brejeira 20	0.99	0.04	0.05	0.36	383	5	36	0.14	4.05	0.44
Brejeira 21	0.45									
Brejeira 22	0.90									
Brejeira 23	0.52									
Brejeira 24	0.58									
Brejeira 25	1.18	0.04	0.22	0.19	610	19	16	1.16	3.39	0.16
Brejeira 26	0.66	0.03	0.13	0.05	351	20	8	2.60	4.55	0.17
Brejeira 27	0.98	0.03	0.11	0.00	362	11	0		3.06	0.23
Brejeira 28	0.77	0.03	0.15	0.05	317	19	7	3.00	3.90	0.17
Brejeira 29	0.50	0.03	0.11	0.05	489	22	10	2.20	6.00	0.18
Brejeira 30	0.66	0.02	0.09	0.17	490	14	25	0.53	3.03	0.15
Brejeira 31	0.57	0.02	0.10	0.02	490	18	4	5.00	3.51	0.15
Brejeira 32	0.47	0.03	0.12	0.00	330	26	1		6.38	0.20
Brejeira 33	0.52	0.02	0.13	0.01	386	25	2	13.00	3.85	0.14
Brejeira 34	0.20	0.02	0.09	0.17	490	44	81	0.53	10.00	0.17
Brejeira 35	0.46	0.02	0.09	0.03	490	20	6	3.00	4.35	0.18
Brejeira 36	0.56	0.02	0.10	0.03	491	18	6	3.33	3.57	0.16
Brejeira 37	0.55	0.02	0.10	0.01	335	18	1	10.00	3.64	0.19
Brejeira 38	0.68	0.03	0.15	0.17	390	22	25	0.88	4.41	0.16
Brejeira 39	0.68	0.03	0.15	0.01	364	22	1	15.00	4.41	0.15
Mértola 1	0.66									
Mértola 2	0.73									
Mértola 3	1.50	0.08	0.04	0.28	347	3	19	0.14	5.41	0.67
Mértola 4	0.78									
Mira 1	0.23									
Mira 2	1.28	0.02	0.01	0.83	424	1	65	0.01	1.59	0.67
Mira 3	0.99	0.01	0.01	0.67	312	1	67	0.01	1.02	0.50
Mira 4	1.84	0.02	0.05	0.42	357	3	23	0.12	1.13	0.29
Mira 5	0.79									
Mira 6	0.95									
Mira 7	0.79									
Mira 8	0.52									
Mira 9	0.85									
Mira 10	0.90									

Table 7.2: Table with organic data (TOC and Rock-Eval pyrolysis), from Mértola, Mira and Brejeira Formations, analyzed by Weatherford and Polish Geological Institute.

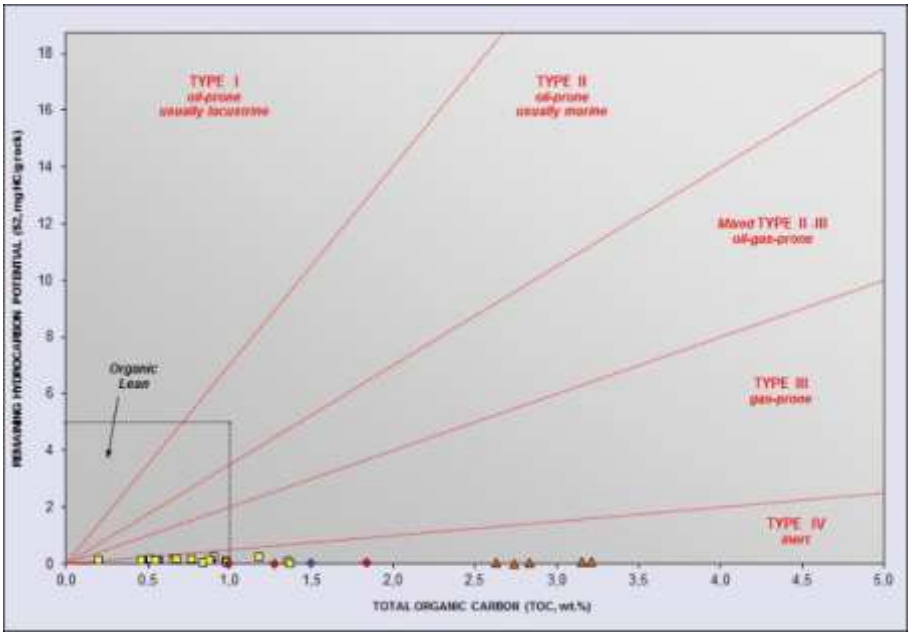

Graph 7.2: Graph representing the relationship between hydrocarbon potential and TOC. Yellow squares representing Brejeira Fm., red diamonds Mira Fm. and blue circle Mértola Fm.

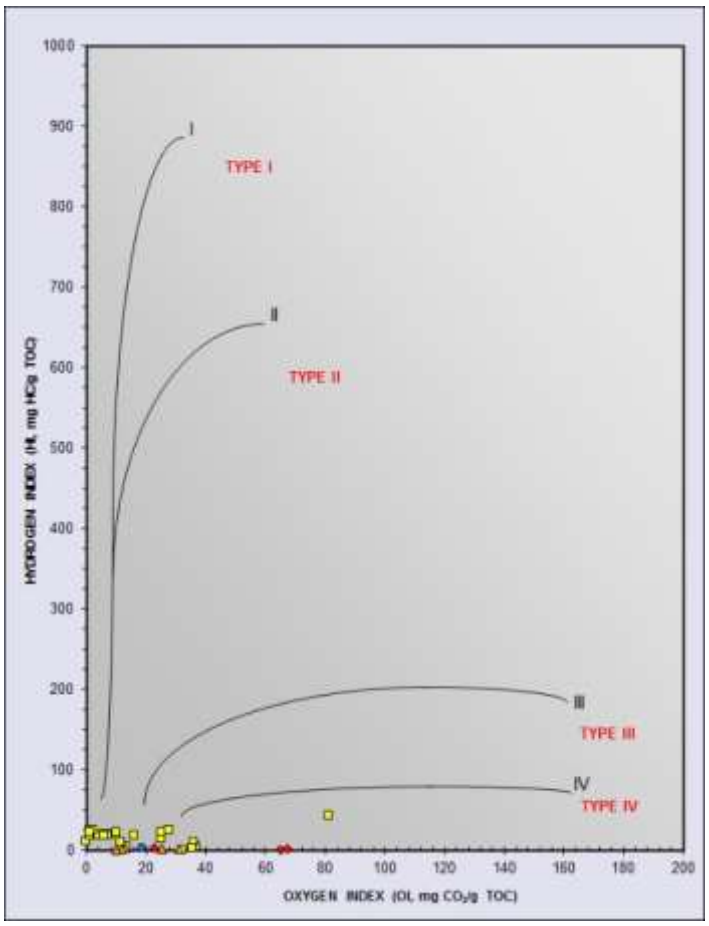

Graph 7.3: Graph representing the relationship between hydrogen index (HI) and oxygen index (OI). Yellow squares representing Brejeira Fm., red diamonds Mira Fm., and blue circle Mértola Fm.

Toluene | 7.5

7.5.1 | Soil-water System

In all the water samples analyzed for this work, high levels of toluene were detected, as shown in the graph (7.4 and 7.5), appendices of chromatograms (10.32 to 10.62 [as a courtesy, the Isolab b.v. sent to this project a chromatogram of pure toluene]), and the sheet results (Appendix 10.1). It is important to note that these amounts were obtained from gas (headspace) phase. This means that, following the partition coefficient of toluene in water-air systems at 20 °C (K = 4.39), the concentration of compound in the original sample (liquid phase), before analysis, is at least 4.39 times bigger (Restek, 2000; Kolb & Ettre, 2006; Tipler, 2013). The amounts of toluene in groundwater samples are significantly higher than the values in soil samples (Appendix 10.1), being less than 1 ppm in 81% of these samples.

There are two different points of view to be discussed about the presence of this compound in groundwater:

From exploratory point of view, Collins (1975) believe that natural concentrations of toluene and benzene in water are hydrochemical indexes which indicate the presence of oil and gas in subsurface. Accumulations of oil and gas can give rise to the presence of a number of low molecular weight hydrocarbons (oil and gas are the main source of benzene and toluene in oilfield waters) that have low odor thresholds in drinking-water (Collins, 1975; WHO, 2011). The ratio of toluene to benzene in 27 crude oils from various sources ranged from 2.0 to 11.3. Toluene is less soluble than benzene in distilled water, where the ratio is about 0.3 (McAuliffe, 1963). Gas chromatographic methods proved to be good for determining the amount of toluene and other hydrocarbons in the petroleum associated waters, according to Zarrella *et al.* (1967).

According to Burtell & Jones III (1996), extensive reservoir fluid compositional studies and research have shown that soluble aromatic hydrocarbons, such as, benzene, toluene, and xylenes make up a large proportion of the dissolved hydrocarbons found in brines associated with hydrocarbon reservoirs.

Light hydrocarbons (C1 to C4) originate from both thermogenic and biogenic processes very often, normally the hydrocarbons in the gasoline range originate thermogenically and are therefore associated with petroleum systems (Bandeira de Mello *et al.*, 2007).

A key objective of the Seneshen *et al.* (2010) study was to conduct low-cost demonstrations of new exploration technologies to identify surface geochemical anomalies that represent potential hydrocarbon-prone areas especially in the environmentally sensitive Paradox Basin (Utah, USA). According to the authors, there are strong toluene anomalies in soils over the northwest part of Lisbon field that are upwind of production. Isohexane (2-methylpentane) is also anomalous in two adjacent samples over a distance of 150 m and in one isolated sample over a gas field. In fracture-fill soils the most important variables for predicting gas and oil are methane and propane, respectively (Seneshen *et al.*, 2010).

No significant benzene levels were detected, above GC-IRMS detection capacity, but this absence can be explained by the biodegradation and oxidation in water, that maybe can be more active in benzene than in toluene. According to Prince & Walter (2016), it is reasonable to expect that the biodegradation of a broad range of compounds will be enhanced in the presence of toluene. Gülensoy & Alvarez (1999) reported enhanced aerobic biodegradation of benzene, p-xylene, and naphthalene by several pseudomonads when toluene was present, and a similar phenomenon occurred under anaerobic conditions (Prince & Sutlita, 2007).

As we can see, the toluene levels in the samples are much higher than is usually found in other places, being only comparable with values from

severe industrial contamination (Barberes *et al.*, 2018). Possible anthropogenic/industrial contamination is practically discarded because the sampling area is isolated, sparsely populated and with few gas stations (Map 1.1 and Appendix 10.63). 93.5% of the values range between 1,000 and 6,000 ppb and 55% are higher than 3,000 ppb (Table 7.4). Is also important to note that the samples W33 and W33-1 were collected from the same borehole, in different seasons (summer and winter), and presented the same amount of toluene.

In order to discard the possibility of this expressive amounts of toluene come from the bactericide, the Isotech lab runed a test and kindly shared the results with this project (Table 7.3) and, with the same purpose, the Isolab b.v. injected the used bactericide in the GC (Appendix 10.3).

According to the ARH Alentejo (2011), a measurement of the toluene levels was carried out in the industrial effluent from the Sines refinery (Map 1.1 and Appendix 10.63 - located 62 km from the nearest sampling point and 83 km from the farthest sampling point, on the NW of the sampling zone) dispatcher for treatment at Ribeira de Moinhos sewage treatment. The results show toluene levels below 1 ppb.

Isojar with DI water before adding bactericide		
Methane FID	0.00185	percent
Hexanes	0.00045	percent
Carbon Dioxide	0.12382	percent
Oxygen	21.43022	percent
Nitrogen	77.00959	percent
Isojar and Bacteriacide after sitting 24hours		
Methane FID	0.00844	percent
Hexanes	0.0005	percent
Carbon Dioxide	0.11597	percent
Oxygen	21.46837	percent
Nitrogen	77.16056	percent
Ambient Air		
Methane FID	0.00035	percent
Hexanes	0.00045	percent
Carbon Dioxide	0.13822	percent
Oxygen	21.53791	percent
Nitrogen	77.50446	percent

Table 7.3: Table with tests results (analyzed by Isotech) proven that the bactericide used in Isojar don't have any influence in the final results. The chromatogram from ambient air is on the appendix 10.2.

From the health impact point of view and following the health-based guideline suggested by the World Health Organization (WHO, 2011), toluene levels in SPZ drink-water are worrying. Following the 0.7 ppm recommended by WHO and considering that the measured lower values (<1 ppm) are inserted into this limit, we can say that the groundwater, in the sampling zone, is contaminated by toluene (Table 7.4). As said before, these levels are much higher than is usually found in drink-water, being only comparable with severe industrial contamination.

Concentration	# samples	% samples	% limit
<1 mg/L	2	6	-
1 mg/L	2	6	50%
2 mg/L	10	32	143%
3 mg/L	7	23	286%
4 mg/L	3	10	429%
5 mg/L	6	19	572%
6 mg/L	1	3	715%
Total	31	100	

Table 7.4: The toluene concentrations found in the analyzed samples with percentage above the limit established by World Health Organization (WHO, 2011).

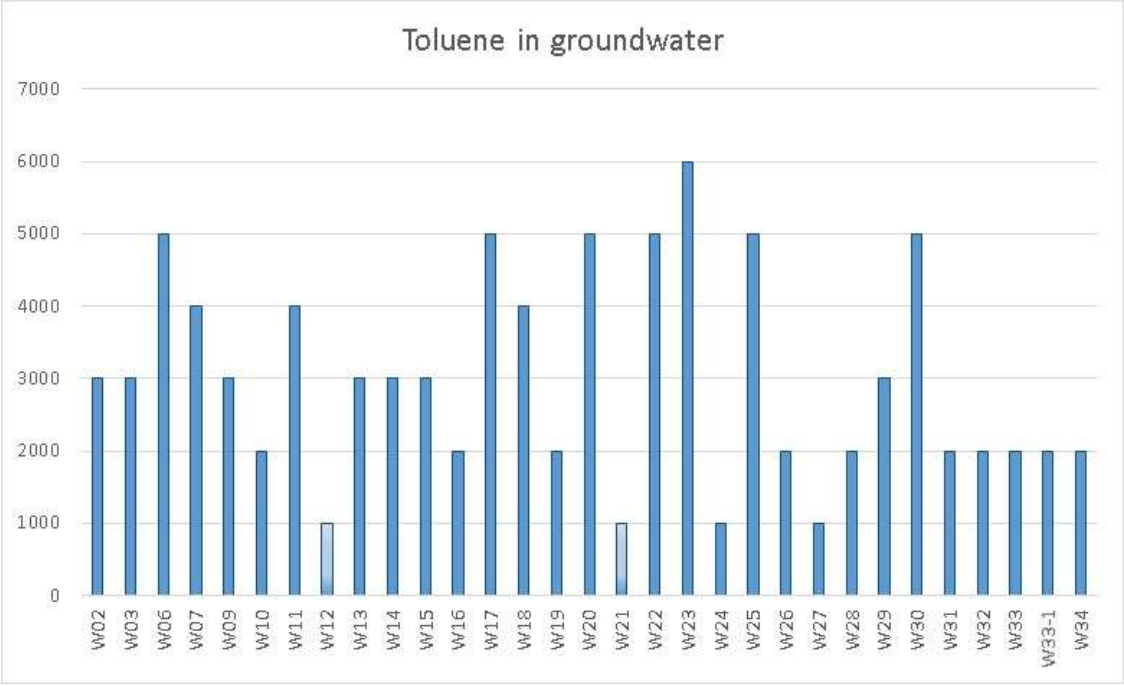

Graph 7.4: Values of toluene (µg/L) found in all water samples.

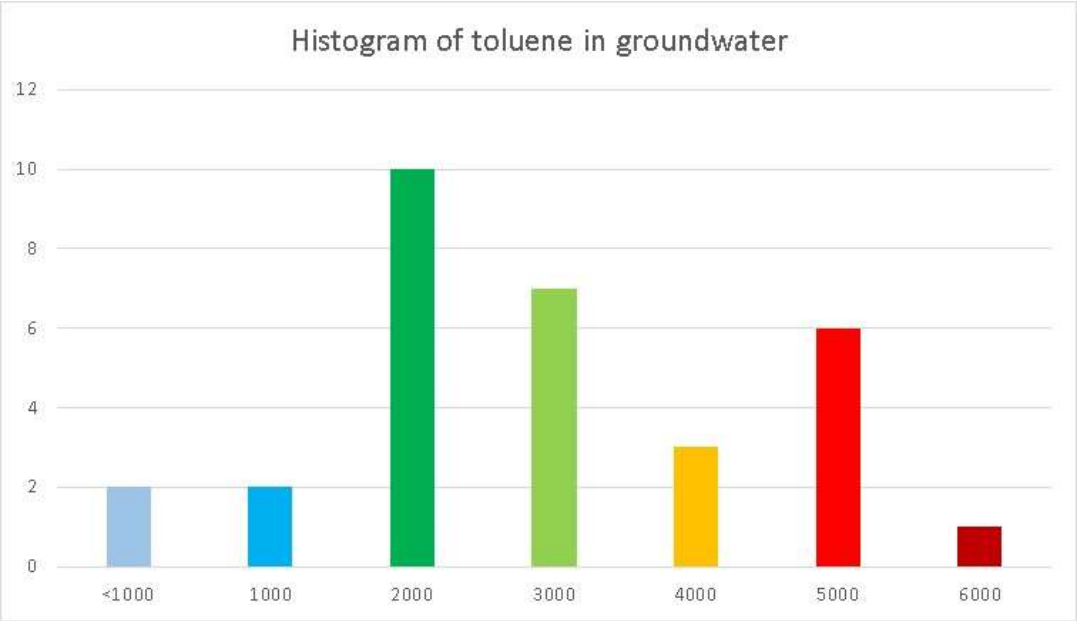

Graph 7.5: Histogram of toluene values (µg/L) in groundwater.

7.5.2 | Worldwide Occurrence of Toluene in Groundwater

According to Leusch & Bartkow (2010) toluene is occasionally detected in drinking water supplies (this hydrocarbon is one of the volatile organic compounds commonly detected in groundwater), but occurrence is not widespread and levels are generally below 3 ppb (but can go as high as 3,500 ppb in groundwater from industrially- polluted sites). The highest level reported, in USA groundwater, in 1983 was 1.4 ppb (WHO, 2004). Toluene has been reported in industrial effluents in Canada. Raw process effluent from petroleum refineries in Ontario contained an average concentration of toluene of 0.6 ppb (Government of Canada, 1992). The average daily concentration for the refinery with the greatest discharge of toluene was 2.1 ppb (maximum of 17.1 ppb); the average daily loading was 0.05 kg/d in the process effluent (Government of Canada, 1992). Still in Ontario, samples taken in a contaminated shallow aquifer at a depth of 6 m beside an existing industrial chemical waste disposal lagoon,

concentrations of toluene above 3,900 ppb were reported (Government of Canada, 1992). In Europe, groundwater contaminated by point emissions, maximum toluene levels of 1,100 ppb were reported (Loch *et al.*, 1989).

In a total of more than 800 water samples taken across Canada from 1985 to 1988, concentrations of toluene in only six samples were greater than 0.5 ppb. These included one surface water sample (0.9 ppb), one drinking water sample (0.6 ppb), two groundwater samples (0.6 and 3.9 ppb), and two samples of undiluted sewage treatment plant effluent (31 and 32 ppb) (Government of Canada, 1992).

Individual gasoline hydrocarbons were detected infrequently in aquifers in USA. Only one gasoline hydrocarbon, toluene, was detected in more than 1% of aquifer samples (Figure 7.8), according to Zogorski *et al.* (2006), and approximately 1% of all groundwater-derived public drinking-water systems in the USA, toluene levels are above 0.5 ppb (WHO, 2004).

Concentrations of 0.8 ppb and 1.9 ppb have been reported in the Rhine river in Germany and Switzerland, respectively (Merian & Zander, 1982). Concentrations in the Morava River in Slovakia range from a winter maximum of 0.58 ppb to a summer maximum of 3.49 ppb (WHO, 2004); in Spain, levels as high as 22 ppb have been detected at the mouth of the Besos River (Gomez-Belinchon & Grimalt, 1991). In coastal waters, maximum levels of 1 ppb have been found (WHO, 2004).

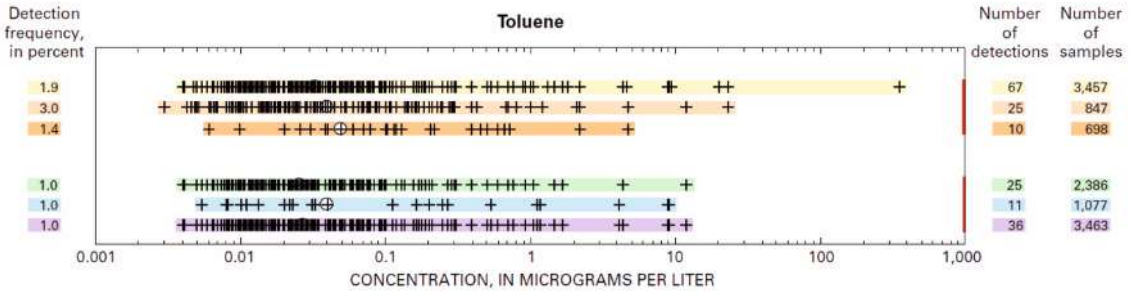

Figure 7.8: Concentration of selected volatile organic compounds (toluene) in samples of untreated groundwater. Adapted from Zogorski et al. (2006).

7.5.3|The Implication for Health

According to World Health Organization (WHO, 2011) the maximum contaminant level (MCL), the health-based guideline, for toluene is 700 ppb (in drink-water) (Table 7.5). It is readily absorbed completely from the gastrointestinal tract after ingestion and rapidly distributed in the body, with a preference for adipose tissue then the kidneys, liver and brain (ATSDR 2000; WHO, 2011). Toluene is rapidly metabolized and, following conjugation, excreted predominantly in urine (WHO, 2011). Therefore, potential health effects from long-term exposure above the toluene MCL are in nervous systems, brain, kidney and/or livers problems with fatigue and drowsiness being the most obvious symptoms (ATSDR, 2000; US EPA, 2009).

Guideline value	0.7 mg/L
Occurrence	Concentration of a few micrograms per litre have been found in surface water, groundwater and drinking-water;point emissions can lead to higher concentrations in groundwater (up to 1 mg/L);It may also penetrate plastic pipes from contaminated soil
TDI	223 µ/kg body weight based on a LOAEL of 312 mg/kg body weight per day for marginal hepatotoxic effects observed in a 13-week gavage study in mice, adjusting for daily dosing and using na uncertainty factor for 1000 (100 for interspecies and intraspecies variattion and 10 for the short suration of the study and use of a LOAEL instead of a NOAEL)
Limit of detection	0.13 µg/L by GC with FID;6 µg/L by GC-MS
Treatment perfomance	0.001 mg/L should be achievable using air stripping
Guideline value derivation · allocation to water · weight · consumption	 10% of TDI 60 kg adult 2 litres/day
Additional comments	The guideline value exceeds the lowest reported odour threshold for toluene in water
Assessment date	2003

Table 7.5: Guideline from World Health Organization about toluene with important information for health-care. Adapted from WHO (2011).

Light Hydrocarbons: Molar Composition and Isotopic Signature | 7.6

7.6.1 | Soil-water System

The background value, for CH_4, in the soil samples, was assumed as 2 ppm, given that this amount occurs in 80% of the SPZ samples (Graphs 7.6 and 7.7; Appendices 10.1 and 10.5 to 10.24). The background value, for CH_4, in the water samples is between 2-4 ppm, given that 75% of the sampled values are in this range (Graphs 7.6 and 7.8; Appendices 10.1 and 12.02 to 10.62).

Hydrocarbon microseeps anomaly were found on the border between Mira and Brejeira Formations (Map 7.3), and in a water sample located very close to the same border (~1 km distance). This contact, made by faults, folds and thrusts, works as a perfect pathway for hydrocarbons migration, up to the surface. The samples located in this area (F08, F09, F081, W34 and F10) presented values of 2101, 296, 196, 70 and 56.9 ppm, respectively, and represent interesting amounts of hydrocarbons when compared with the case studies presented by several authors (Appendices 10.1, 10.26, 10.27, 10.25, 10.62 and 10.28).

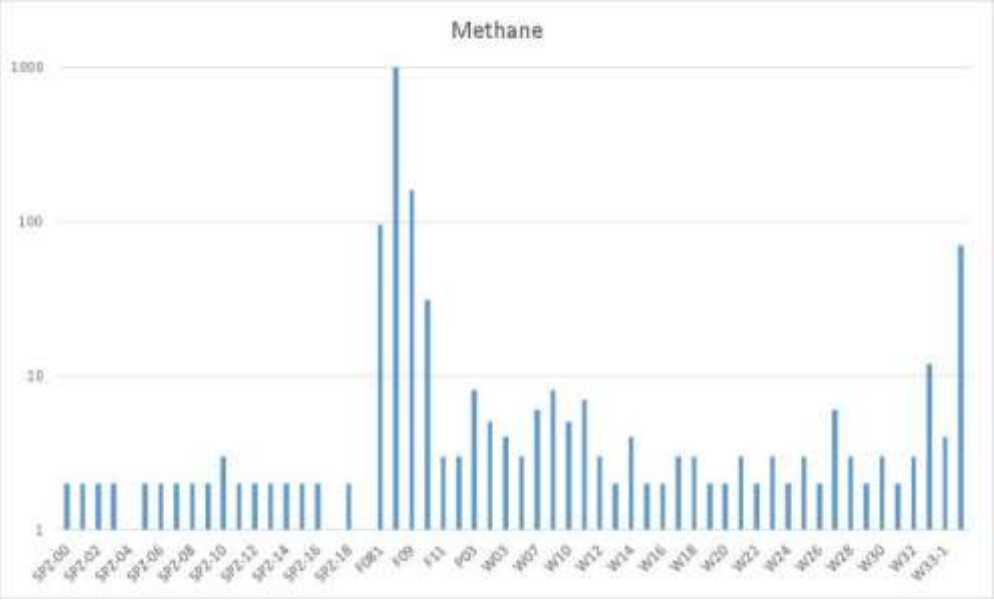

Graph 7.6: Values of methane measured in all samples.

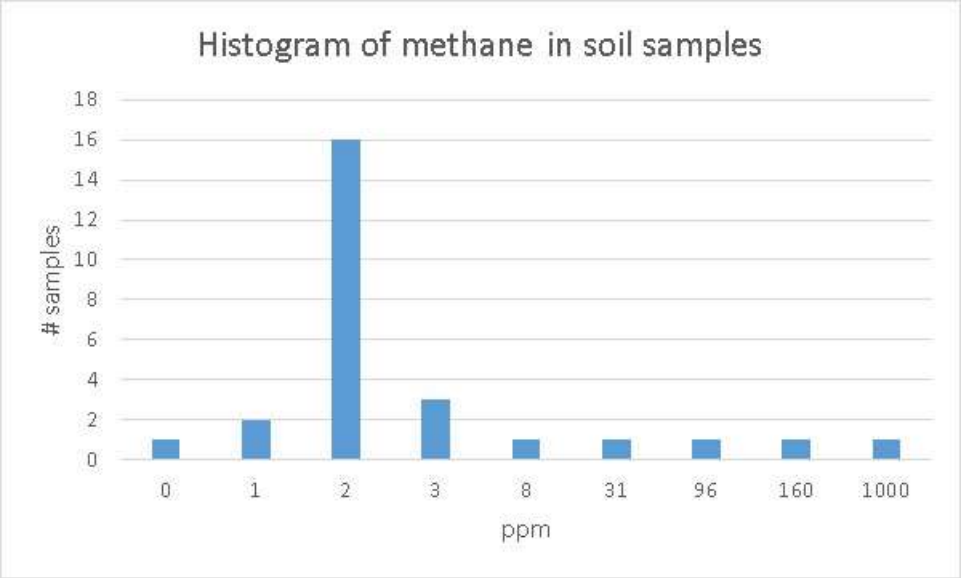

Graph 7.7: Values of methane measured in soil samples.

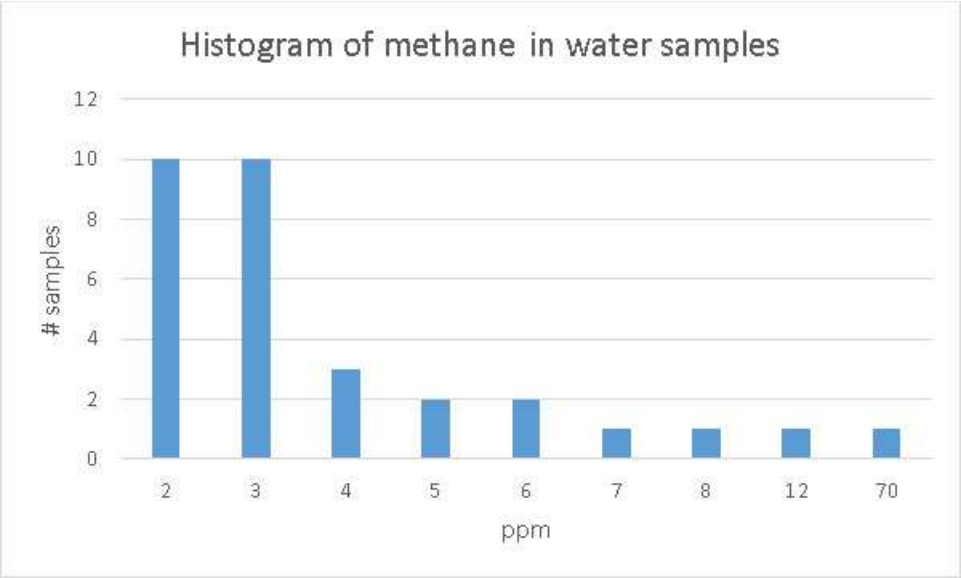

Graph 7.8: Values of methane measured in water.

There is a higher occurrence of C4 and C5 fractions in the analysed samples, e.g. the n-C5 were found in 57% of the samples, with a predominant occurrence in water samples. Moreover, these fractions are much more common in water than in soil samples, occurring in 93.5% of them.

All the samples classified as a hydrocarbon anomaly contain all analysed fractions (CH_4, C_2H_6, C_2H_4, C_3H_8, C_3H_6, *i*-C_4, *n*-C_4, *i*-C_5, *n*-C_5 and C_{6+})

emphasizing a potential mixed of different hydrocarbons sources (high mature thermogenic, low mature thermogenic and biogenic).

It is also important to note the significant presence of 2-methylpentane (isohexane) in all soil samples (Appendices 10.5 to 10.24). As said before, these hydrocarbons are also used to detect surface emanations from petroleum systems (Seneshen *et al.*, 2010).

The isotopic signature of the 5 analyzed samples are presented in the graph 7.9 and the appendix 10.1, and clearly represent two different sources of thermogenic hydrocarbons. The results were also compared with the $\delta^{13}C$ of the samples from Jesus Baraza mud volcano (Stadnitskaia *et al.*, 2006). The individual values are very similar and present the same trend with some levels (Graph 7.10). This is an important information, from the exploration point of view, because as we saw in the chapter 2, not only Jesus Baraza MV but all the other MV presented in the map 2.1 contain thermogenic hydrocarbons. Furthermore, as said before, the seismic lines (Figures 2.6, 2.7 and 2.8) presented by Maldonado *et al.* (1999) and Ramos *et al.* (2014) show that the same Paleozoic rocks of SPZ, are probably the basement under this MVs.

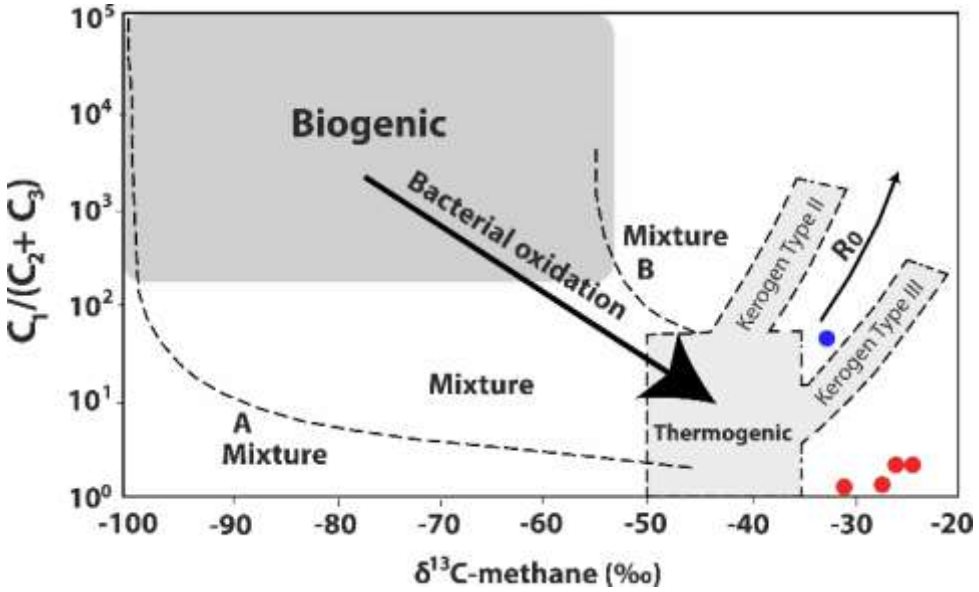

Graph 7.9: Genetic classification of methane given by the molecular ratio C1/(C2+C3) and the carbon isotopic composition of methane, $\delta^{13}C_1$ (Bernard et al. 1978). The blue dot represents W34 sample and the red dots represent F08, 081, 09 and 10 samples.

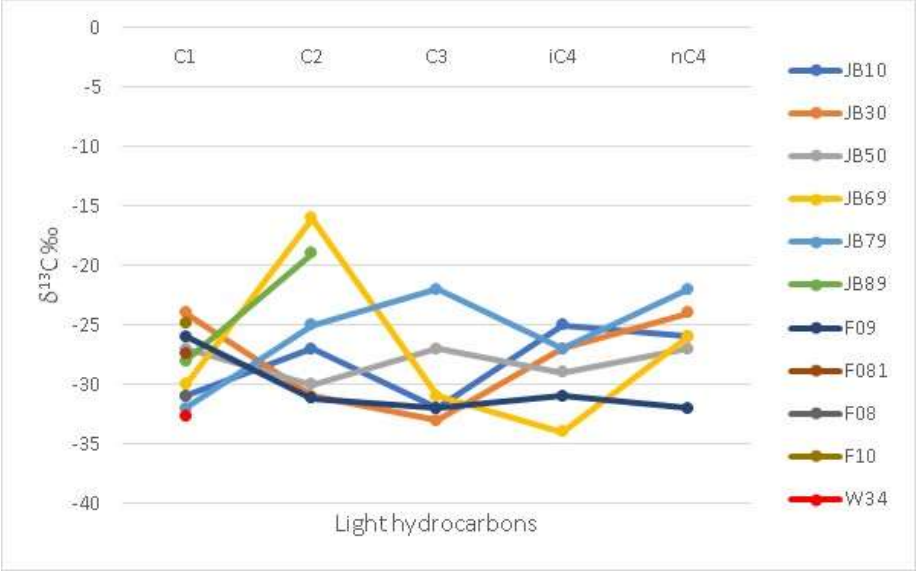

Graph 7.10: Comparative graph between isotopic values from Jesus Baraza mud volcano (different depths [Stadnitskaia et al., 2006]) and the measured values for this project (five samples). The numbers, in the JB samples, means the depth (cm) of the sampling.

Map 7.3: The highest methane levels.

7.6.2|Worldwide Occurrence of CH_4 in Soil-water Systems

Freitas *et al.* (2010) reports high concentrations of methane (>4.8 ppm) were found in contaminated sites by both gasoline and ethanol (samples from North America and Brazil), indicating biodegradation of both fuels were capable of generating methane in potentially dangerous concentrations (Table 7.6).

	Sample	Ethanol (mg/L)	Methane (mg/L)	Acetate (mg/L)	Butyrate (mg/L)	Methane $\delta^{13}C$ (‰)
Ontario, Canada	BH-2	10.6	18.1	428	86	-26.3
	BH-3	n/d	13.9	275	129	-35.4
	BH-5	n/d	14.9	10	n/d	-35.3
	BH-9	n/d	23	600	594	-27.9
	BH-9	n/d	13	608	525	-39.2
	BH-14	808	3.25	557	2170	-12
	BH-14	32.4	7.82	529	680	-16
Brazil	BR1	n/d	4.02	n/d	n/d	-78
	BR2	n/d	5.35	7.1	n/d	-42.6
	BR3-A	n/d	0.049	n/d	n/d	-37.2
	BR3-B	n/d	0.163	n/d	n/d	-53.5
	BR4-A	n/d	1.66	2.8	n/d	-62.7
	BR4-B	n/d	15.9	n/d	n/d	-65.3
	BR5-A	n/d	6.43	n/d	n/d	-60.4
	BR5-B	5020	14.4	934	2590	-26.6
	BR6-A	83100	17.1	3580	449	-11
	BR6-B	0.6	11.1	34.7	81.5	-25.7

Table 7.6: Ethanol and biodegradation product concentration. Adapted from Freitas et al. (2010).

In July 1990, the U.S. Geological Survey began a study of methane contamination of groundwater in the Animas River Valley between Durango, Colorado, and Aztec, New Mexico. The purpose of the study was to identify the possible sources of and migration pathways for methane in shallow groundwater in the study area (Chafin *et al.*, 1996).

According to the report the shallow groundwater, obtained from alluvium and Tertiary sedimentary rocks overlying Cretaceous gas-bearing formations, in the northwestern part of the San Juan Basin locally, is contaminated by methane (Chafin *et al.*, 1996).

The maximum soil-gas methane concentration registered was 1,200 ppm and the minimum (most part of the samples) was lower than 0.005 ppm, adjacent to gas-well casings (Chafin *et al.*, 1996).

The measurements and nearby soil-gas-methane concentrations for selected water wells and springs were divided in dissolved and soil-gas. In general, the dissolved values are higher than soil-gas values. The most part of the samples measurements, in both cases, are lower than 0.005 ppm. The higher values for dissolved CH_4 was 39 ppm and for soil-gas 0.5 ppm (Chafin *et al.*, 1996).

According to Naftz *et al.* (1998) since 1995, 121 samples of soil-gas (1 meter depth) have been analyzed for methane concentration at 96 sites in the vicinity of Price, Utah (USA). Soil-gas methane concentrations ranged from the minimum reporting limit of 0.005 ppm to 1,400 ppm at a pumping coal-bed methane well north of Price, Utah over a period of 18 months. Seventy-nine percent of the soil-gas samples had a methane concentration less than the reporting limit of 0.005 ppm. The soil-gas-methane reporting limit was equaled or exceeded in 21% of the samples. All sample sites with detectable methane concentrations were limited to either conventional natural gas or coal-bed methane development wells (Naftz *et al.*, 1998).

Fourteen groundwater samples from springs, wells, and drains were collected within the study area and analyzed for methane concentration. Only one water sample contained a detectable methane concentration (0.061 ppm) (Naftz *et al.*, 1998). This sample was collected in a pond downstream from the discharge from a spring. The detectable methane in this sample likely resulted from bacterial decomposition of organic

matter in the bottom of the pond. Methane concentrations in the remaining water samples did not exceed the minimum reporting limit of 0.005 ppm (Naftz *et al.*, 1998).

Soil-gas samples collected in the Animas River Valley registered 29 ppm. The reason(s) for the lower soil-gas-methane concentrations in the Price area is unknown, however, coalbed-methane development has occurred for a longer time period in the Animas River Valley, thereby increasing the time available for gas migration through natural and human-made pathways (Naftz *et al.*, 1998). Similar rock types (sandstone, shale, and coal beds) are found in both areas. Evaluation of the different characteristics of these rock types, such as bed thickness, amounts of clay and sand proportions within each rock type, and fracturing, could aid in determining the difference in methane concentrations found in samples collected from both areas (Naftz *et al.*, 1998).

Stolp *et al.* (2006) reported the monitoring of methane gas in soils and groundwater at selected locations in Carbon and Emery counties in Utah, between 1995 and lasted through 2003 (Stolp *et al.*, 2006). The program focused on established production-well sites and methane-gas production fields near residential areas. A total of 420 shallow (2- to 4-feet depth) soil-gas and groundwater samples were collected from 174 soil and 15 groundwater sites (Stolp *et al.*, 2006). The average measured methane concentration for the monitoring period (1995-2003) was 2,740 ppm; the median concentration was less than 10 ppm. For calculation of summary statistics, sample values below the minimum detection limit or greater than the maximum detection limit were assigned the value of the detection limit (Stolp *et al.*, 2006). Two hundred and ten samples (52 percent of the sample set) had concentrations that were less than the detection limit. Twenty samples (5 percent of the sample set) had concentrations greater than 10,000 ppmv (Table 7.7 [Stolp *et al.*, 2006]).

Area	Average concentration (ppmv)	Median concentration (ppmv)	Minimum concentration (ppmv)	Maximum concentration (ppmv)	Number of Samples
Willow Creek	800	<10	<10	6,390	15
Price/Helper	2,260	10	<1	>100,000	75
South of Price	1,750	<10	<1	>100,000	152
Huntington	15	4	<1	160	24
Orangeville/Ferron	4,920	<10	<1	>100,000	137

Table 7.7: Summary statistics of methane concentration for five areas of coal-bed production, Carbon and Emery Counties, Utah, 1995-2003. Adapted from Stolp et al. (2006).

Dissolved methane was detected in 78% of analyzed groundwater wells with an average concentration of 4.0 ppm and a range of 0−37.1 ppm, in Colorado, USA (Li & Carlson, 2014). Greater than 95% of the methane found in groundwater wells was classified as having a microbial origin, and there was minimal overlap between the C and H isotopic characterization of the produced gas and dissolved methane measured in the aquifer (Li & Carlson, 2014). Neither density of oil/gas wells nor distance to oil/gas wells had a significant impact on methane concentration suggesting other important factors were influencing methane generation and distribution (Li & Carlson, 2014). Thermogenic methane was detected in two aquifer wells indicating a potential contamination pathway from the producing formation, but microbial-origin gas was by far the predominant source of dissolved methane in the Wattenberg field (Li & Carlson, 2014).

In Northeastern Pennsylvania Molofsky *et al.* (2013) evaluated whether elevated methane concentrations in the data set exhibited a relationship to gas development activities, methane concentrations in water wells located in gas production areas were compared to those located in nonproduction areas (Molofsky *et al.*, 2013). According to the authors, water wells in gas production areas (322 wells), approximately 3.7% contained methane concentrations that exceeded 7000 µg/L, while 3.3% of water wells in nonproduction areas (1379 wells) contained methane concentrations above 7000 µg/L (Molofsky *et al.*, 2013). The authors suggest that this slight difference may be attributable to the fact that gas

production areas contain a greater percentage of valley water wells (61% of 322 water wells) than nonproduction areas (49% of 1379 water wells) (Molofsky *et al.*, 2013).

Molofsky *et al.* (2013) evaluation of site-specific isotopic and molecular data from water wells in the Dimock Township suggests that hydrocarbon gases present in these water wells are consistent with Middle and Upper Devonian gases above the Marcellus sampled in the annular spaces of local gas wells.

Alpers *et al.*, (1990) paper describes results of a preliminary attempt to determine the source of the CO2 in soil gases overlying massive sulfide mineralization at Crandon, Wisconsin (USA), using stable isotopes of carbon dioxide in soil gas (Alpers *et al.*, 1990). The variation of methane values in the 20 samples analyzed is between 1-7 ppm, in soil gas.

A total of 68 drinking-water samples were collected in Pennsylvania and New York from bedrock aquifers (Lockhaven, 8; Catskill, 47; and Genesee, 13) that overlie the Marcellus or Utica shale formations (Osborn *et al.*, 2011).

In active gas-extraction areas (one or more gas wells within 1 km), average and maximum methane concentrations in drinking-water wells increased with proximity to the nearest gas well and were 19.2 and 64 ppm of CH_4 (n ¼ 26), a potential explosion hazard; in contrast, dissolved methane samples in neighboring non-extraction sites (no gas wells within 1 km) within similar geologic formations and hydrogeologic regimes averaged only 1.1 ppm ($P < 0.05$; $n = 34$) (Figure 7.9 and Table 7.8 [Osborn *et al.*, 2011]).

Several models have been developed to explain the relatively common phenomenon of rapid vertical transport of gases (Rn, CH_4, and CO_2) from depth to the surface, including pressure-driven continuous gas-phase flow through dry or water-saturated fractures and density-driven

buoyancy of gas microbubbles in aquifers and water-filled fractures (Osborn *et al.*, 2011).

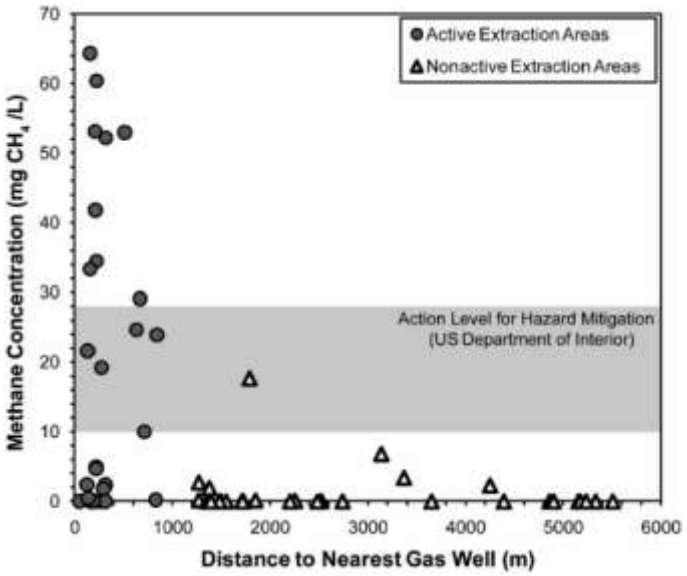

Figure 7.9: Methane concentrations (ppm of CH_4) as a function of distance to the nearest gas well from active (closed circles) and nonactive (open triangles) drilling areas. Note that the distance estimate is an upper limit and does not take into account the direction or extent of horizontal drilling underground, which would decrease the estimated distances to some extraction activities. Adapted from Osborn et al. (2011).

Water source, *n* (number of samples)	milligrams CH_4 L^{-1}	$\delta^{13}C$-CH_4 ‰
Nonactive Catskill, 5	1.9 ± 6.3	-52.5 ± 7.5
Active Catskill, 13	26.8 ± 30.3	-33.5 ± 3.5
Nonactive Genesee, 8	1.5 ± 3	-57.5 ± 9.5
Active Genesse, 1	0.3	-34.1
Active Lockhaven, 7	50.4 ± 36.1	-40.7 ± 6.7
Total active wells, 21	19.2	-37 ± 7
Total nonactive wells, 13	1.1	-54 ±11

Table 7.8: Mean values ± standard deviation of methane concentrations (ppm of CH_4) and carbon isotope composition in methane in shallow groundwater $\delta^{13}C$-CH_4 sorted by aquifers and proximity to gas wells (active vs. nonactive). Adapted from Osborn et al. (2011).

From 1997 to 2005, the USGS sampled groundwater using standard sampling protocols from 170 wells in West Virginia for dissolved gases, including CH_4 (USGS, 2006). Methane concentrations in groundwater for

these 170 wells ranged from not detected to 68.5 ppm (USGS, 2006). Methane was detected in 131 of 170 of these wells and was present in concentrations greater than 28 ppm in 13 of these wells (USGS, 2006). Another 13 wells had methane concentrations ranging from 11.9 to 24.3 ppm, 32 wells had concentrations ranging from 1.00 to 10.0 ppm, and 73 wells had detectable methane concentrations less than 1.00 ppm (USGS, 2006). Methane was detected in wells in 43 of the 47 counties sampled, but methane concentrations exceeding 10 ppm were found in wells in only 11 counties, with 22 of 26 of these samples from eight counties located in the southern coal fields of West Virginia (USGS, 2006).

Kappel & Nystrom (2012) paper reports about dissolved methane in New York groundwater. The samples collected through 2011 indicate that concentrations of methane in groundwater from most wells measured (91 percent of the wells) were at or below the Office of Surface Mining action level of 10 ppm (Kappel & Nystrom, 2012), and a large number of wells (47 percent) had no detectable methane. However, according to the authors, methane concentrations from several wells exceeded 10 ppm (9 percent); in five cases, the measured concentrations were greater than 28 ppm (2 percent).

Methane was detected in both unconsolidated and bedrock aquifers across New York (Kappel & Nystrom, 2012). In unconsolidated aquifers, 93 percent of the wells had non-detect to low-level methane concentrations (methane concentrations <1 ppm), and less than 1 percent of the wells (one well) was greater than the saturation value of 28 ppm (Kappel & Nystrom, 2012). The greater methane concentrations are most likely associated with confined glacial aquifers over black shale bedrock. In bedrock formation aquifers, 73 percent of the methane concentrations were less than 1 ppm, while nearly 4 percent had concentrations greater than 28 ppm across the State (Kappel & Nystrom, 2012). Three of the four highest methane values in bedrock wells were

associated with Devonian-aged black shale bedrock; in total, many of the greater methane concentrations were most likely associated with wells drilled into these shales (Kappel & Nystrom, 2012).

Emission of natural gas from the borewells of Vengannapally village in Anantapur district of Andhra Pradesh (India) was reported off late and surface geochemical survey was carried out to determine the concentration and establish the source of the leaking gas (Madhavi *et al.*, 2008). The light gaseous hydrocarbon concentration of 33 soil samples, collected from a depth of about 1 m were determined by acid desorption technique using Gas Chromatograph equipped with flame ionization detector (Madhavi *et al.*, 2008). The observed concentrations (in ppb) vary from: CH_4, = 12-223; C_2H_6 = 3-36; C_3H_8 = 2-24; i-C_4H_{10} = 18; and n-C_4H_{10} = 1-21, respectively. The isotopic signature of the methane $\delta^{13}C_1$ ranges between -25‰ and -35‰. The headspace gas analyses of the water samples collected from the borewells was also carried out (Madhavi *et al.*, 2008). The observed concentrations (in ppm) vary from: CH_4 = 18 - 237626; C_2H_6 =2-4. The isotopic signature of the methane $\delta^{13}C_1$ ranges from -50‰ to -63‰. The present study attempts to characterize the light gaseous hydrocarbons in the shallow soil samples and gas samples from Vengannapally village in terms of its concentration distribution and nature of origin (Madhavi *et al.*, 2008).

Fontana (2000) reported that the Public Service Company of Colorado (PSC), contracted ESN Rocky Mountain to install a soil gas monitoring system near the southeast boundary of the Leyden gas storage facility (Colorado, USA). Seventeen soil gas monitoring points were installed. Soil gas samples have since been collected three separate times about two weeks apart. The author interpreted the results (Table 7.9) as background levels.

The table 7.10 show the hydrocarbon content of gases in faults at 61–91 m depth in Dallas, Texas, according to Saunders *et al.* (1999). Also

according to the authors, the table 7.11 show the fault-related and hydrocarbon microseepage anomalies over a Michigan Basin prospect.

	methane	ethane	ethene	propane	propene	ibutane	nbutane	ipentane	npentane	ihexane	nhexane
Máx	5.58	0.49	0.13	0.19	0.09	0.04	0.07	0.01	0.02	0.04	0.01
Min	1.53	0	0	0	0	0	0	0	0	0	0

Table 7.9: Descriptive statistics on all sampling events. Values in ppm. Adapted from Fontana (2000).

Sample	Dist (ft.)	Methane (ppm)	Ethane (ppm)	Ethene (ppm)	Propane (ppm)	Propene (ppm)	Butanes (ppm)
1	8987	5.81	0.15	0.07	0.03	0.01	0.04
2	9392	7.5	0.17	0.03	0.07	0	0.13
3	9549	8.89	0.28	0.03	0.08	0.02	0.14
4	9027	14.68	1.4	0	0.31	0	0.26
5	8512	15.6	0.48	0.05	0.59	0.02	0.77
6	2950	19.79	0.84	0.05	0.39	0.05	0.31
7	1092	23.35	1.5	0.1	0.61	0.12	0.78
8	7467	26.42	0.62	0.08	0.02	0.06	0.02
9	8672	41.74	1.29	0.09	0.18	0.05	0.35
10	9327	92.46	2.69	0.08	0.96	0	1.4
11	5576	8.27	5.25	0.1	1.75	0.1	0.39
12	4767	133.73	9.72	0.1	3.08	0.13	1.89
13	5772	152.42	5.55	0.01	1.86	0.03	1.55
14	4280	263.78	16.13	0.1	8.99	0.15	7.94
15	9697	252.4	11.44	0.43	3.14	0.27	4.69
16	2354	267.7	15.06	0.1	5.78	0.25	4.8
17	6602	27.15	12.46	0.43	5.43	0.25	4.93
18	8032	338.49	8.61	0.05	2.44	0.01	2.06
19	582	64.18	14.09	0.15	2.29	0.3	2.84
20	9486	444.79	34.85	0	16.92	0	15.6
21	7312	59.09	14.23	0.04	6.85	0.14	5.86
22	3706	10268.7	111.55	0.1	29.76	1.2	41.81
23	5242	228.18	55.24	0.1	14.33	0.25	9.39
24	8807	1593.1	36.12	2.24	34.21	1.1	30.24
25	0	1865.49	116.18	2.3	23.17	1.54	9.58
26	9112	2967.15	72.86	0.36	30.1	0.84	22.78
27	5727	17,315.92	466.32	1	82.96	1.52	55.24

Table 7.10: Hydrocarbon content of gases in faults at 200-300 ft depth in Dallas, Texas. Adapted from Saunders et al. (1999).

Sample	Methane (ppm)	Ethane (ppm)	Ethene (ppm)	Propane (ppm)	Propene (ppm)	Ethane/ Ethene (ppm)	Propane/ Propene (ppm)
Background							
1	10.46	0.3	0.41	0.22	0.2	0.73	1.1
2	9.09	0.19	0.3	0.12	0.15	0.63	0.8
3	9.54	0.23	0.33	0.13	0.14	0.7	0.93
4	7.82	0.18	0.26	0.1	0.13	0.69	0.77
5	13.13	0.37	0.46	0.16	0.21	0.8	0.76
Minor Microseepage Anomaly							
6	17.01	0.65	0.92	0.27	0.51	0.71	0.53
7	22.45	0.41	0.35	0.21	0.23	1.17	0.91
8	30.12	0.69	0.54	0.22	0.29	1.28	0.76
9	30.36	0.56	0.61	0.17	0.3	0.92	0.57
10	20.05	0.39	0.41	0.14	0.22	0.95	0.64
11	18.37	0.41	0.32	0.19	0.17	1.28	0.12
12	19.32	0.36	0.42	0.14	0.21	0.86	0.67
13	30.81	0.61	0.41	0.16	0.23	0.149	0.7
Fault Related							
14	25.37	3.23	0.29	3.6	0.25	11.14	14.4
Minor Microseepage Anomaly Continued							
15	20.58	0.39	0.3	0.14	0.15	1.3	0.93
16	21.51	0.63	0.67	0.25	0.33	0.94	0.76

Table 7.11: Fault-related and microseepage hydrocarbon anomalies over a Michigan Basin prospect. Adapted from Saunders et al. (1999).

Hydrocarbon Generation by Igneous Intrusions | 7.7

According to Santos Neto (2004), under the influence of intrusive igneous rocks (high temperature), any organic-rich rock, with hydrocarbon potential, can generate thermogenic gases in a relatively short geological time. However, the isotopic carbon profile of this special type of gas is different from the thermogenic generation (conventional systems) by basin subsidence (Graph 7.11). Notice the relative enrichment of methane in ^{13}C compared to the other hydrocarbons (Graph 7.11 [Santos Neto, 2004]). The isotopic profile of F09 sample shows a similarity with other samples from Brazilian Paleozoic basins.

Taking into account the proximity of the sampling area with to the Monchique Igneous massif (Appendix 10.63), this could be a possible

explanation for the hydrocarbon origin in some parts of the SPZ, although according to McCormack *et al.* (2007), these Mesozoic igneous intrusions have not raised maturation levels in the Palaeozoic rocks, even in close proximity to dyke margins.

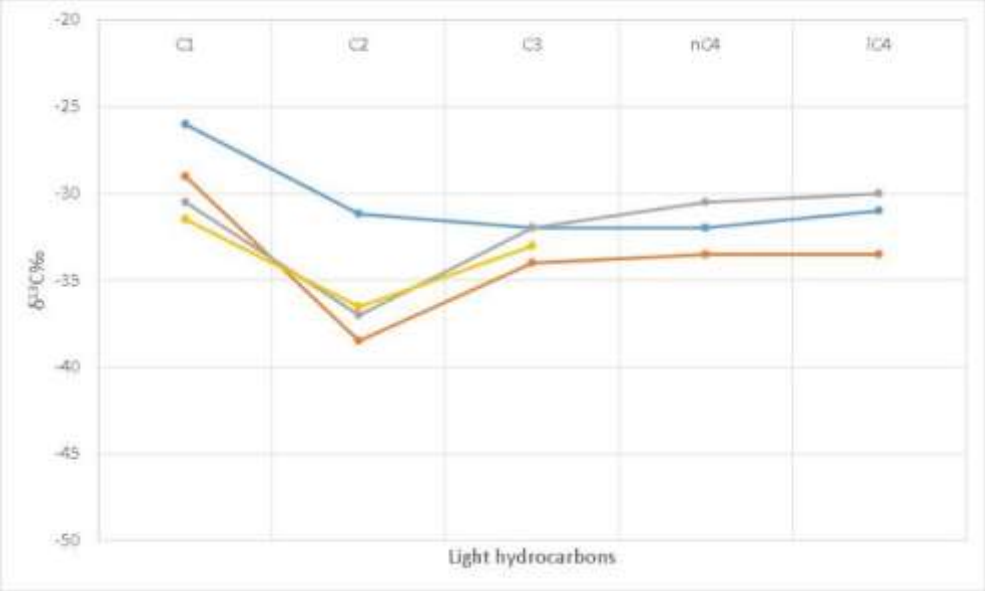

Graph 7.11: Carbon isotopic profile, C1-C4, characteristic of thermogenic gases generated under thermal influence of igneous intrusions (Cerqueira et al., 1999). The blue line represents F09 sample isotopic profile. The cases compared are found in the Paleozoic basins of Paraná, Solimões and Amazonas (Santos Neto, 2004).

Unsaturate Hydrocarbons and Bacterial Activity | 7.8

The action of the aerobic methylotrophs bacteria is evident on soil samples of the studied area. The graph (7.12) show a clear relationship between the increase of hydrocarbon gases on soil and the increase of carbon dioxide amount. As suggested by Conrad (1996), these bacteria are consuming the hydrocarbon gases and generating CO_2.

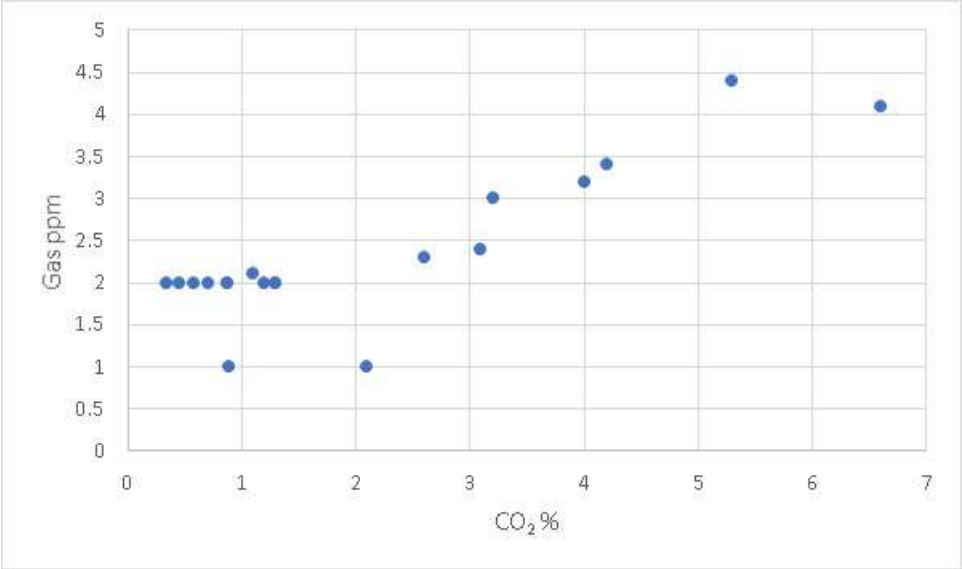

Graph 7.12: Comparison between CO_2 values and total gas (light hydrocarbons) values measured from SPZ samples.

Ethene and/or propene are present in 48% of the samples, but a few more concentrated in soil than water samples. The ethane is present in 10 samples and trend to concentrate with higher values of methane (<8 ppm). Propane is present in 16 samples and follow the same logical as ethane, concentrate with high amounts of methane. Both light hydrocarbons are much more present in soil than in water (Appendix 10.1).

As said before, the isotopic composition does not represent any biogenic signature of the hydrocarbons present in samples. However, the possibility of a mixed gases is still acceptable, given that this mixture can be made by more amount of thermogenic hydrocarbons than biogenic hydrocarbons. Therefore, the isotopic signature should be more influenced by heavy thermogenic signal than light biogenic signal. Saunders *et al.* (1999) argues that the anomalously high ethane/ethene and propane/propene ratios for sample 14 (Table 7.11 and highlighted sample in table 7.12) as compared to average background and minor anomaly microseepage values are typical of fault leakage. As can be noted

in the table 7.12, the same increase ratio is present in "sweet" samples from SPZ.

The unsaturated hydrocarbons ethene and propene are not usually found in natural gas reservoirs, but they are relatively common constituents of interstitial soil gases (Saunders *et al.*, 1999). Both the saturated and unsaturated hydrocarbons typically show anomalously higher concentrations over oil and gas fields compared to normal background values (Saunders *et al.*, 1999). According to Saunders *et al.* (1999), the ethene and propene result from either chemical or biological oxidation of part of the ethane and propane microseeping from reservoirs. Rapid leakage of ethane and propane upward through major faults does not allow adequate time for significant oxidation to occur, yielding higher ratios of saturated to unsaturated hydrocarbons in the soil gas (Saunders *et al.*, 1999).

Sample	Ethane/ Ethene (ppm)	Propane/ Propene (ppm)	Ethane/ Ethene (ppm) [Saunders *et al*. (1999)]	Propane/ Propene (ppm) [Saunders *et al*. (1999)]
F08	22.6	3.4	0.73	1.1
P03	1.0	0.8	0.63	0.8
F081	0.5	1.8	0.7	0.93
F09	5.2	1.0	0.69	0.77
F10	1.9	1.0	0.8	0.76
F11	1.7	1.0	0.71	0.53
F12	1.0	1.0	1.17	0.91
			1.28	0.76
			0.92	0.57
			0.95	0.64
			1.28	0.12
			0.86	0.67
			0.149	0.7
			11.14	14.4
			1.3	0.93
			0.94	0.76

Table 7.12: Ethane/ethene and propane/propene ratios from 7 "sweet" samples from SPZ. The anomalously high ethane/ethene and propane/propene ratios for sample highlighted as compared to average background and minor anomaly microseepage values are typical of fault leakage (Adapted from Saunders et al., 1999).

According to Whiticar *et al.* (1994), the presence of considerable amounts of ethene and propene (up to 7.1 [hydrocarbon percent]) together with the accelerated maturation of organic matter support the hypothesis, considering the geologic setting, that it is highly probable that the thermogenic gas was formed by hydrothermal processes.
Ullom (1988) and Saenz *et al.* (1991) advocated the use of ethene and propene for petroleum exploration in the form of ratios of ethane/ethene and propane/propene as a guide to determining the biogenic or thermogenic origin of the microseepage. Neither ethene or propene indicate a relationship between nonproducing or producing areas.

According to Ferreira (2002), the ratio between paraffins and olefins in soil gas analyses is probably the most effective tools for identifying thermogenic hydrocarbons in soil. The enrichment in paraffins is interpreted as an evidence of thermogenic gas seepage from underlying gas field. The author refers that when thermogenic gas microseeps are detected on the surface, the soil gas is enriched in saturated hydrocarbons, thus increasing the saturated/unsaturated ratio.

The possible origin of this biogenic hydrocarbon is part of Amils *et al* (2008) article. The work' selected study site was Peña de Hierro on the north flank of the Rio Tinto Anticline, which comprises a thick volcanosedimentary succession composed of dark shales, basaltic lavas, rhiolitic materials, fine ashes and tuffites, and green/purple shales. The hydrothermal activity is recorded as complex-massive sulfide lenses or stockwork veins of pyrite and quartz, which occur at the upper part of the IPB volcanic sequence (Leistel *et al.* 1998). As said before, on the geological framework, a clear geological relationship can be established between the IPB, the BAFG and the SW Portugal domains (Oliveira, 1990a). Stratigraphically, IPB is located under BAFG and the SW Portugal domains.

According to Amils *et al.* (2008), dissolved methane was detected in many samples, indicating that methanogenic activity occurred throughout the

ore body (Figure 7.10). Decreasing CH_4 and H_2 was accompanied by increasing SO_4^{2-} and CO_2. Although not stoichiometric, this relationship suggests that anaerobic methane oxidation may occur in this zone. The alteration of the sulfide ore has induced the production of different gases: CO_2, CH_4, and H_2, all of them participating in the biogeochemical cycles involved in the IPB decomposition (Amils *et al.*, 2008). The novel observations of H_2 and CH_4 production show that a variety of resources are available to support autotrophic microbial respiration in the subsurface both within and down-gradient from the ore body (Amils *et al.*, 2008).

Ethane and propane so far have never been generated in significant quantities by microbial processes (Oremland *et al.*, 1988).

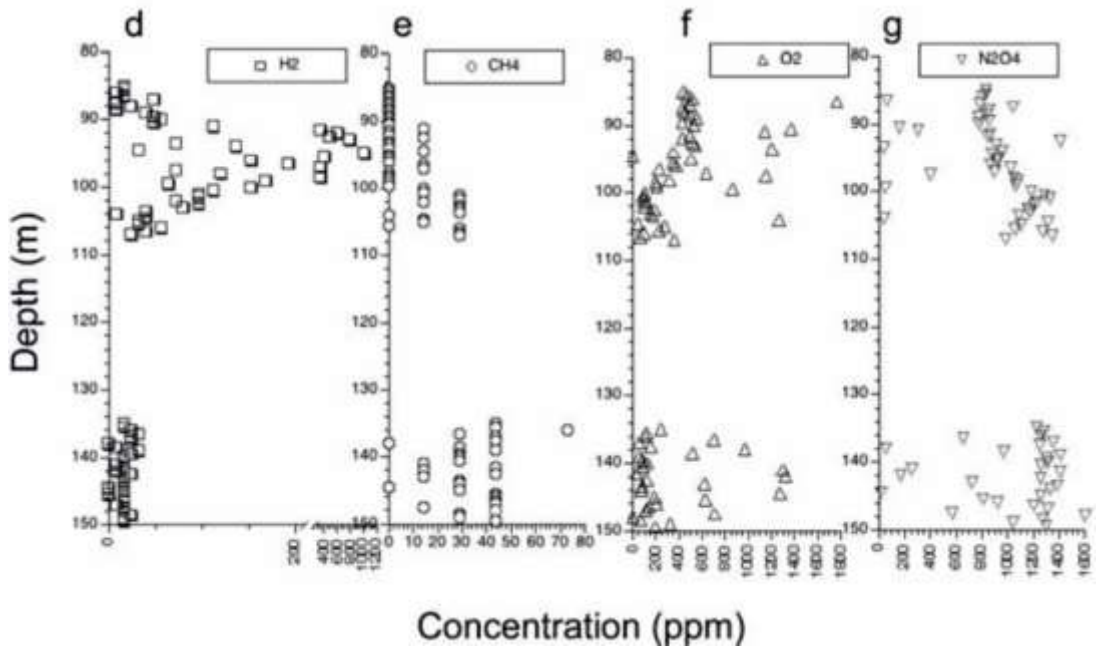

Figure 7.10: Concentration (in ppm) of dissolved gases in BH4 formation water sampled. Dissolved gases H_2 (d), CH_4 (e), O_2 (f) and NO_2 (g). Adapted from Amils et al. (2008).

The hypothesis, suggested by Whiticar *et al.* (1994), the presence of ethene and propene in considerable amounts as an indicative of thermogenic gas formed by hydrothermal processes, cannot be discarded, as well.

CONCLUSIONS, FINAL REMARKS, COST EVALUATION AND FUTURE PERSPECTIVES | 8.0

Conclusions | 8.1

The methodologies used to define the sampling areas (TN and HA) proved to be very efficient to show possible hydrocarbon emanations. However, the use of WV-2 images seems to be more economically viable solution for obtaining radiometric data, considering the high costs associated with the acquisition of airborne gamma-ray.

As verified in the map 2.1, the SPZ extends at least to the Spanish territory (onshore and offshore) and also to the Portuguese offshore, thus presenting a significant geographical extension. This information is extremely important for a possible assessment of the economic evaluation of hydrocarbon exploration in the region, not only for Portuguese, but also for Spanish and maybe for Moroccan government.

From the geological prospecting point of view the presence of hydrocarbon gases in SPZ formations is clear and evident. They are present in soil and water, with significantly high levels, and the integration with TOC,

vitrinite reflectance, rock-eval pyrolysis and GC-IRMS reveals the presence of a senile unconventional petroleum system, with possible interbedded of levels with different degrees of organic maturation (leading to a mixture of thermogenic gases). The possible presence of biogenic gases (ethene and propene) raises the hypothesis that Iberian Pyrite Belt is located under the South Portuguese Zone.

It's also important to note that, according to Skupio & Barberes (2017), in the Paleozoic shales from Pomerania region (Poland) the hydrocarbons are present above 3000 m depth. This information can provide an estimative, by analogy, of how much deep the emanations can come from, at SPZ.

The Mesozoic basins adjacent to the study area, the Algarve and the Alentejo Basins (onshore and offshore), are composed by lithologies with a porosity and permeability superior to those found in SPZ shales and greywackes. Thus, a migration of any hydrocarbons fluids, from these areas, is contrary to basic fluid dynamics. It's also important to mention that, according to the isotopic results present in this thesis and using the relation between isotopic results and vitrinite reflectance, suggested by Stahl *et al.* (1981) (figure 6.3), as a reference, the hydrocarbons found in the SPZ formations represent a high maturity system. However, according to Fernandes *et al.* (2013), the Mesozoic rocks of the Algarve Basin lie within the oil window. Vitrinite reflectance ranges from 0.52-0.7 $\%R_r$ in the Lower Cretaceous to 1-1.1 $\%R_r$ in the Upper Triassic-Hettangian. Miocene rocks that unconformably overlie the Mesozoic strata are immature (0.42-0.47 %Rr). Thus, it's difficult take these basins as a possible source of this gases.

Currently, the Algarve and Alentejo regions (where the samples are located) are very sensitive areas for the development of hydrocarbon exploration projects. Society in general has constructed a negative image of this activity based on misleading and sensationalist information, beginning with the politicians. The research of the exploratory potential

of a given region is not only an economic but also a political, social and environmental issue (natural contamination of groundwater by hydrocarbons, as seen in this project, is a good example). As previously seen, water contaminated by toluene represents a serious concern to the health of the locals (it is not yet known where the contamination is going from a geographical point of view) and wells with high methane levels represents a serious risk to the locals safety. The author and his advisers informed the Portuguese authorities (environmental and health agencies) about the contamination, once it was found.

Lastly, two water samples (W33 and W34) from two different boreholes (few meters distance) contains worrying levels of CH_4, from the safety point of view. As said before, in the chapter 6, recommended action levels for methane dissolved in water (Eltschlager *et al.*, 2001), suggested that when the level of methane gas is between 10 and 28 ppm monitoring is required (warning, investigate) and immediate action is needed above 28 ppm. The sample W33 has a concentration of 12 ppm of CH_4 and W34 contains 70 ppm, presenting a serious risk of borehole explosion (the water is fully saturated with methane and the air is now flammable). Considering the significant loss of methane (Parker & Britt, 2012; Molofsky *et al.*, 2016), as an inevitable consequence of the sampling method, these values are the minimum content of the boreholes.

Final Remarks | 8.2

The natural gas was introduced in Portugal in 1997 and between this year and 2001 “gas works gas” was gradually replaced by gas in the commercial/public service and residential sectors (Graph 8.1 and Table 8.2 [International Energy Agency, 2016a]).

According to International Energy Agency (2016b) report, in 2016 20% of the electricity was generated by natural gas (52% of total electricity

generation was made by fossil fuels) in this country (Graph 8.2). In the same year, and according to the same report, Portugal imported 51.15% of the gas from Algeria (Table 8.1 [International Energy Agency, 2016b]).

According to Eurostat (2015), in the year of 2013 Portuguese industry consumed 70% of total gas in Portugal (Table 8.2). In this value, consumed by the industry, just the non-metallic minerals industry (such as glass, ceramic, cement, etc.) consumed 40%. Still according to the same report, the industry consumed 35% of the electricity in Portugal, in 2013 (Table 8.2).

Eurostat (2016) highlights the development of electricity and natural gas prices for both industrial and household users in the European Union (EU); furthermore, price information for petroleum products is also provided (Graphs 8.3, 8.4, 8.5 and 8.6 [Eurostat 2016]).

The price and reliability of energy supplies, electricity in particular, are key elements in a country's energy supply strategy (Eurostat 2016). Electricity prices are of particular importance for international competitiveness, as electricity usually represents a significant proportion of total energy costs for industrial and service-providing businesses (Eurostat 2016). In contrast to the price of some fossil fuels, which are usually traded on global markets with relatively uniform prices, there is a wider range of prices within the EU Member States for electricity or natural gas (Eurostat, 2016). The price of electricity and natural gas is, to some degree, influenced by the price of primary fuels and, more recently, by the cost of carbon dioxide (CO_2) emission certificates (Eurostat, 2016).

In Portugal, the price of electricity and natural gas are among the highest in European Union. The cost of electricity, for household consumers (Graph 8.3), practiced in 2015 in Portugal was the 7º most expensive price in EU (0.229 EUR/kWh) and for industry (Graph 8.4) was the 8º most expensive (0.115 EUR/kWh) (Eurostat, 2016). The scenario is worse

when we analyze the cost of gas in this country. In the same year, Portugal practiced the 2º most expensive price in EU (0.098 EUR/kWh) for household consumers (Graph 8.5) and the 4º most expensive (0.038 EUR/kWh) for industry (Graph 8.6 [Eurostat, 2016]). The basic prices (without taxes and levies), for natural gas in Portugal, are the most expensive practiced in EU (Graphs 8.5 and 8.6 [Eurostat, 2016]).

Unlike other parts of the world, natural gas and electricity transmission networks in Europe are very well structured. As can be seen in the European high voltage transmission grid (*http://www.geni.org/globalenergy/library/national_energy_grid/europe/europeannationalelectricitygrid.shtml* [Global Energy Network Institute, 2017]) and the European natural gas network (Map 8.1 [European Network of Transmission System Operators for Gas, 2016]). These two maps demonstrate that the production of natural gas and electricity in European territory can be easily marketed across the whole continent.

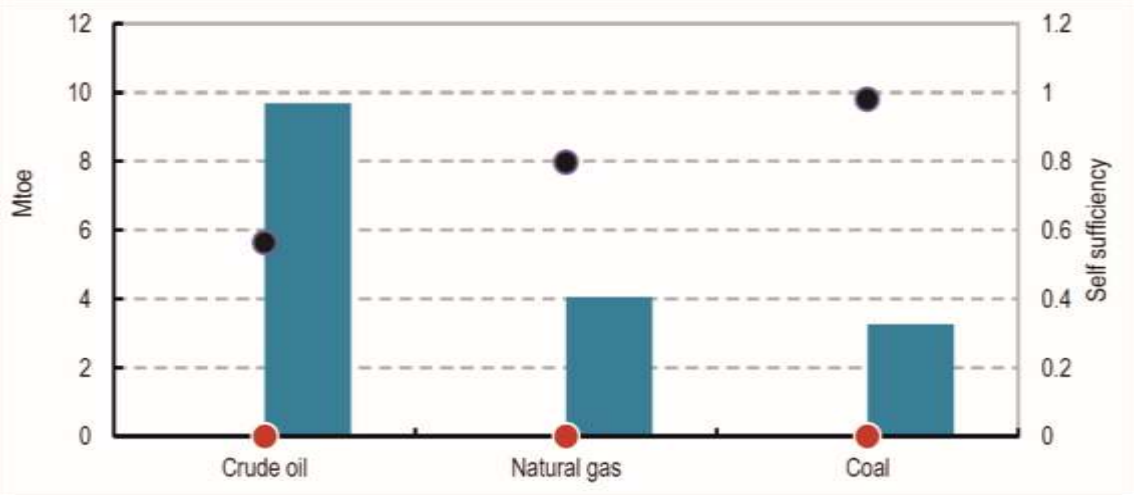

Graph 8.1: Production and self-sufficiency of Portugal 2015. The blue bars represent total primary energy supply (TPES- defined as energy production plus energy imports, minus energy exports, minus international bunkers, then plus or minus stock changes). Adapted from International Energy Agency (2016b).

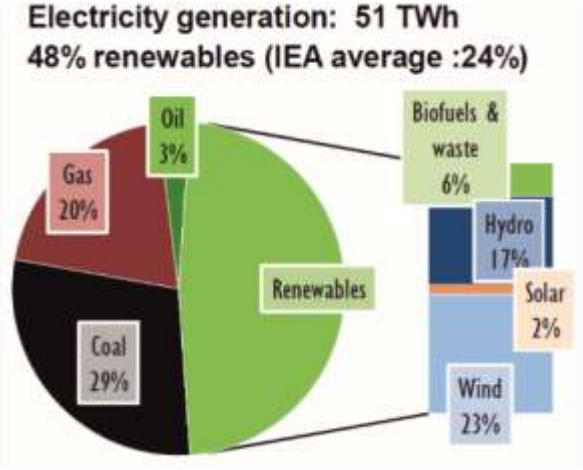

Graph 8.2: Energy system transformation. Adapted from International Energy Agency (2016b).

Portugal does not have significant proved reserves of natural gas. There is no gas production in the national territory and, therefore, the country depends on imports to supply all the domestic needs (International Energy Agency, 2011). Barberes (2013) suggests that the exploration of potential reserves of hydrocarbons in Portugal would mean a new stage of energy production in Portugal and organic-rich shales, which appear in various parts of the country, appear as hydrocarbon source/reservoirs rocks (unconventional petroleum system).

FUEL	IMPORT COUNTRY
Crude Oil	Angola (23.19%)
	Saudi Arabia (13.84%)
Oil Products	Spain (59.85%)
	United States (13.67%)
Natural gas	Algeria (51.15%)
	Non-specified/Other (20.82%)
Coal	Colombia (97.56%)
	United States (2.33%)
ELECTRICITY	
Imports	Spain (100%)
Exports	Spain (100%)

Table 8.1: Energy security, main importers of crude oil, oil products, natural gas and coal. Adapted from International Energy Agency (2016b).

1973	1980	1990	2000	2005	2010	2013	2014	2015p
Production of natural gas (Unit: TJ-gross)								
-	-	-	-	-	-	-	-	-
Production of electricity from fossil fuels (Unit: GWh)								
2267	6871	18503	30247	37623	25008	20764	20143	26641
Net imports of natural gas (Unit: TJ-gross)								
-	-	-	94864	181102	209571	177377	161638	188515
Industry consumption of natural gas (Unit: TJ-gross)								
-	-	-	30648	44478	48968	50404	49162	n/d
Final consumption of natural gas (Unit: TJ-gross)								
-	-	-	36773	60814	72775	72882	72000	n/d

Table 8.2: Production of natural gas, energy from fossil fuels, net imports of natural gas, industry consumptions of natural gas and final consumption of natural gas, between 1973-2015. Adapted from International Energy Agency (2016a).

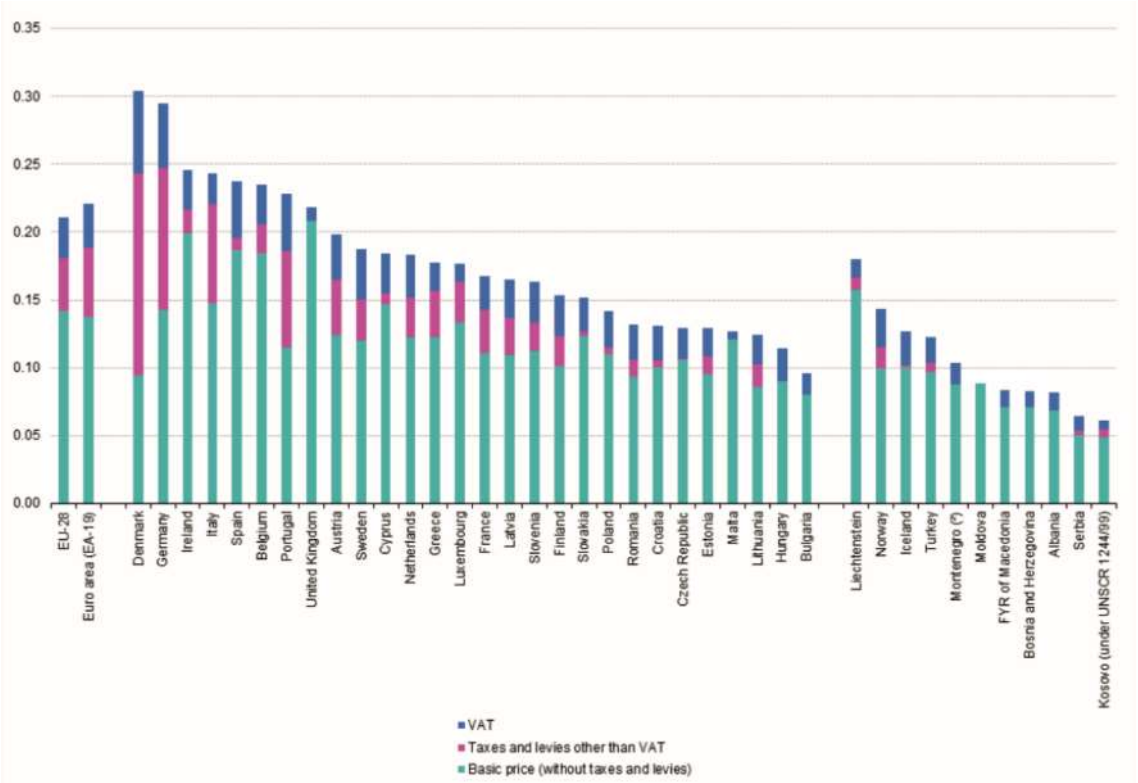

Graph 8.3: Electricity prices for household consumers, second half 2015 (1) (EUR/kWh). Adapted from Eurostat (2016).

Map 8.1: The European natural gas network (Portugal, Spain, France and Switzerland) – Capacities at cross-border points on the primary market. The pipelines are represented by grey lines. Adapted from European Network of Transmission System Operators for Gas (2016).

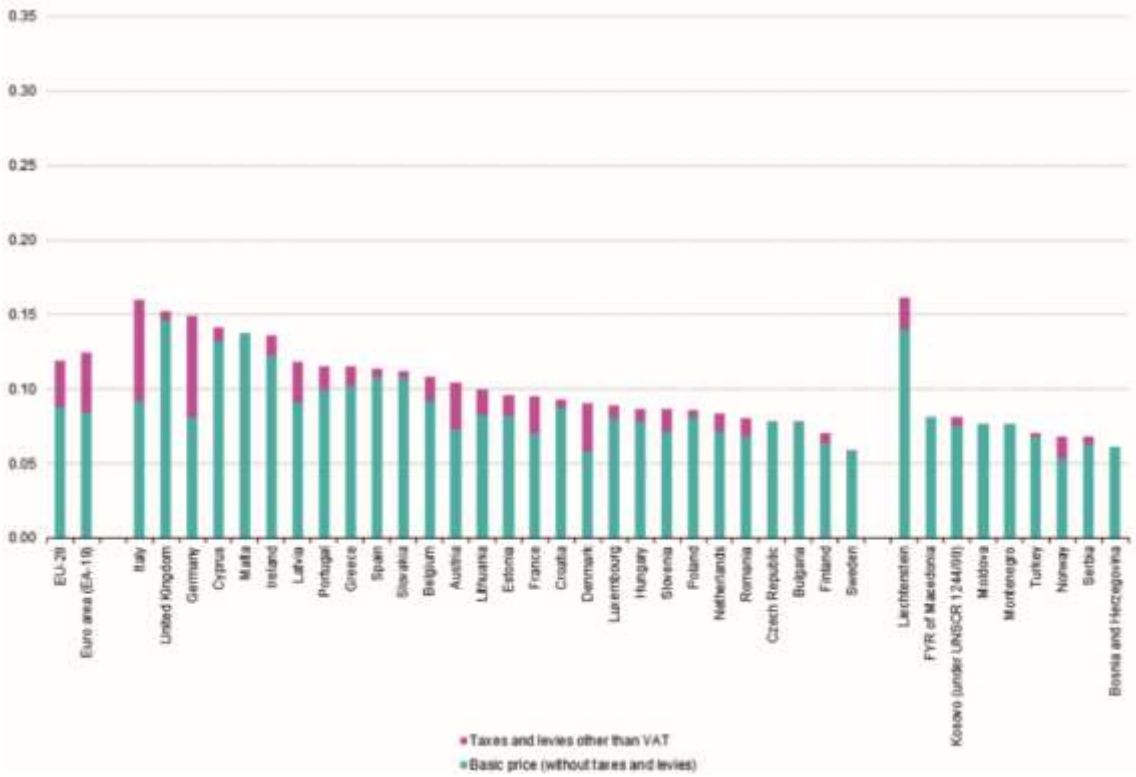

Graph 8.4: Electricity prices for industrial consumers, second half 2015 (1) (EUR/kWh). Adapted from Eurostat (2016).

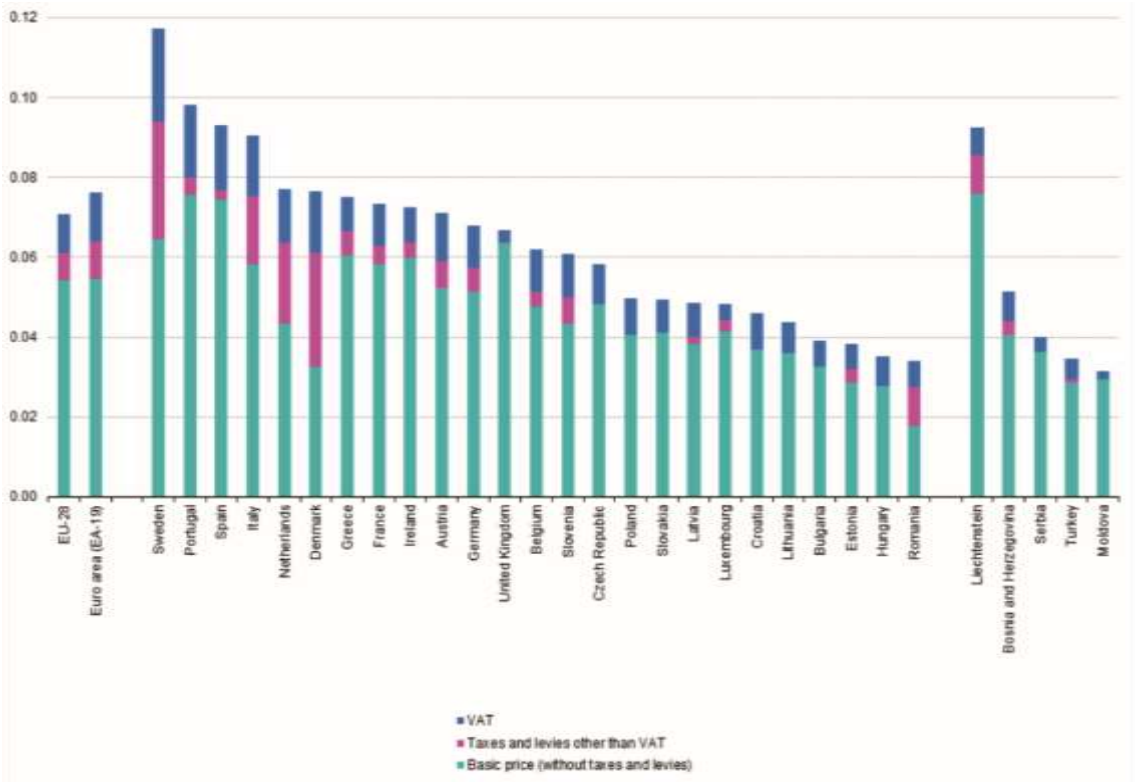

Graph 8.5: Natural gas prices for household consumers, second half 2015 (1) (EUR/kWh). Adapted from Eurostat (2016).

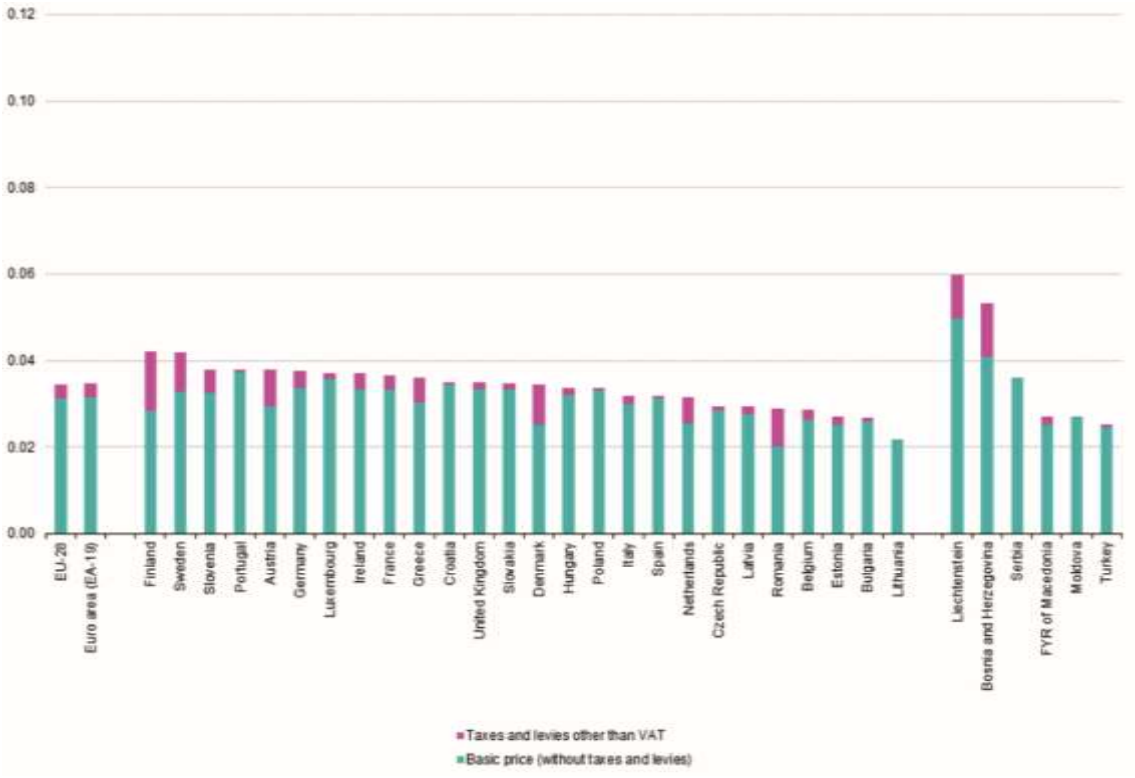

Graph 8.6: Natural gas prices for industrial consumers, second half 2015 (1) (EUR/kWh). Adapted from Eurostat (2016).

Cost Evaluation | 8.3

Research is the foundation and fundamental driver of the creation of new knowledge. Research requires investment, ongoing operational costs, continual strategic thinking, and a firm appreciation of its value (Stephens, 2013).

As said before, in the preface to this thesis, the values practiced in the petroleum industry (sales, profits, investments, etc.) are equivalent to the largest economies around the world. As one would expect, industrial interest research has a high associated cost.

The industrial costs of the laboratory analyze performed in this project are significantly high, ranging from US$ 40 per sample (TOC) to US$ 680 per sample (isotope). Therefore, the minimum industrial cost of the results obtained in this work (laboratory analysis, satellite imagery and airborne gamma ray) is around US$ 102,230 (taking into account the prices practiced in the current market), which adds a high value to the information contained herein.

The partnership with companies and laboratories made it possible to carry out analyzes and obtain data with significantly reduced costs, thus enabling the implementation of this project.

The results obtained using alternative (cheaper) methods appears as a possibility for the viabilization of projects with high associated costs. This becomes even more evident when we analyze the gamma radiation data presented in this thesis.

The cost of airborne GR survey (usually associated with magnetic survey) varies mainly depending on the country and the device (*personal communication*). By airplane it ranges between US$ 4 per flight line km (*e.g.*, South Africa and Australia) and US$ 20 per flight line km (*e.g.*, India and Brazil); by helicopter it ranges between US$ 40 per flight line km (*e.g.*, South Africa and Australia) and US$ 80 per flight line km (*e.g.*, India

and Brazil). Using the AOI as an example (1,000 km^2 with 75m of distance between flight lines), the final cost varies between US$ 52,800-US$ 264,000 (by airplane) and US$ 528,000-US$ 1,056,000 (by helicopter).

As mentioned earlier, the satellite images used in this study provide one of the best resolutions among those available today. The average cost, per square kilometer, of the WV2 images varies mainly if the product is "archive" (8-Band Panchromatic + Multispectral: US$ 19 per sq. km) or "new tasking" (8-Band Multispectral + Panchromatic: US$ 29 per sq. km) (LANDinfo, 2016). For example, to cover all the AOI, the cost ranges between US$ 19,000 and US$ 29,000 (1,000 km^2).

The results presented in this thesis show that it is possible, at least partially, to extract radiometric information from WV2 images. This could imply a significant cost reduction, between 45% and 98.2% in radiometric data acquisition, as it happened with the project to which this thesis refers. Moreover, a satellite image can be acquired in a few hours and the data processing can be done in a few days.

Future Perspectives | 8.4

Economic development, when well managed by the political class, has the natural consequence of social development, through the job creation, development of infrastructure, etc. The knowledge (mapping) of the natural resources is fundamental for the development of a solid geostrategic policy, since Portugal, as said in the introduction of this thesis, depends entirely on imports to supply its domestic demand for hydrocarbons.

An interesting example of natural resources capitalization is the Parnaíba complex of thermoelectric power plants (Brazil), administered by the ENEVA company. Taking advantage of the privileged location, near the

producing wells of natural gas, the plant has a high capacity of electric generation at a low cost. In addition, 3,700 direct jobs are generated.

The next steps, after the publication of this project, demand greater financial investments, mainly to increase the sampling grid (collection and analysis of more samples) and to perform a seismic acquisition campaigns. It is extremely important to evaluate the possible "paths" used by hydrocarbons to the surface, and also to verify the potential source levels of these hydrocarbons.

BIBLIOGRAPHY | 9.0

Abad, I., Mata, M.P., Nieto, F., Velilla, N. 2001. The Phyllosilicates in diagenetic-metamorphic rocks of the South Portuguese Zone, southwestern Portugal. The Canadian Mineralogist, 39, pp. 1571-1589, doi: 10.2113/gscanmin.39.6.1571.

Abad, I., Nieto, F., Velilla, N. 2002. Chemical and textural characterization of diagenetic to low-grade metamorphic phyllosilicates in turbidite sandstones of the South Portuguese Zone: a comparison between metapelites and sandstones. Schweiz. Mineral. Petrogr. Mitt., 82, pp. 303-324, doi: 10.5169/seals-62367.

Abrams, M.A. 2005. Significance of hydrocarbon seepage relative to petroleum generation and entrapment. Marine and Petroleum Geology, 22, pp. 457-477, doi: 10.1016/j.marpetgeo.2004.08.003.

Abrams, M.A. 2013. Best practices for the collection, analysis, and interpretation of seabed geochemical samples to evaluate subsurface hydrocarbon generation and entrapment. Offshore Technology Conference, 24219, 21p., doi: 10.4043/24219-MS.

Abrams, M. A., Dahdah, N. 2011. Surface sediment hydrocarbons as indicators of subsurface hydrocarbons – field calibration of existing and new surface geochemistry methods in the Marco Polo Area Gulf of Mexico. American Association Petroleum Geology Bulletin, 95 (11), pp. 1907-1935, doi: 10.1306/03211110130.

Abrams, M. A., Segall, M. P., Burtell, S. G. 2001. Best practices for detecting, identifying, and characterizing near-surface migration of

hydrocarbons within marine sediments. Offshore Technology Conference, 13039, 14p., doi: 10.4043/13039-MS.

Al-Alfy, I.M., Nabih, M.A., Eysa, E.A. 2013. Gamma ray spectrometry logs as a hydrocarbon indicator for clastic reservoir rocks in Egypt. Applied Radiation and Isotopes, 73, pp. 90-95, doi: 10.1016/j.apradiso.2012.11.016.

Almeida-Filho, R., Miranda, F.P., Yamakawa, T. 1998. Remote detection of a tonal anomaly in an area of hydrocarbon microseepage, Tucano basin, north-eastern Brazil. International Journal of Remote Sensing, 20 (13), pp. 2683-2688, doi: 10.1080/014311699212029.

Alpers, C.N., Dettman, D.L., Lohmann, K.C., Brabec, D. 1990. Stable Isotopes of Carbon Dioxide in Soil Gas Over Massive Sulfide Mineralization at Crandon, Wisconsin. Journal of Geochemical Exploration, 38 (1-2), pp. 69-86, doi: 10.1016/0375-6742(90)90093-p.

Amils, R., Fernández-Remolar, D., Gómez, F., González-Toril, E., Rodríguez, N., Briones, C., Prieto-Ballesteros, O., Sanz, J.L., Díaz, E., Stevens, T.O., Stoker, C.R. 2008. Subsurface Geomicrobiology of the Iberian Pyritic Belt. In: Dion, P. & Nautiyal, C.S. (eds.), Microbiology of Extreme Soils. Soil Biology 13. Springer-Verlag Berlin Heidelberg, pp. 205-223, doi: 10.1007/978-3-540-74231-9.

Aminzadeh F, Berge T, Connolly D, O'Brien G (eds.) 2013. Hydrocarbon Seepage: from source to surface. AAPG/SEG Special Publication - Geophysical Developments, 16, 256p, doi: 10.1190/1.9781560803119.

ARH Alentejo. 2011. Planos de Gestão das Bacias Hidrográficas Integradas nas Regiões Hidrográficas 6 e 7 – Região Hidrográfica 6, Volume I (Relatório), Parte 2 (Caracterização e Diagnóstico). Ministério da Agricultura, Mar, Ambiente e Ordenamento do Território, Portugal, 336p.

Ashcroft, A.E. 1997. Ionization methods in organic mass spectrometry. The Royal Society of Chemistry, UK, 176p, doi: 10.1039/9781847551191.

ATSDR. 2000. Toxicological profile for toluene. US Department of Health and Human Services, Agency for Toxic Substances and Disease Registry, USA.

B'Hymer, C. 2010. Headspace Sampling in GC. In: Cazes, J. (ed.), Encyclopedia of Chromatography. CRC Press, USA, pp. 1050-1058, doi: 10.1108/09504121011067166.

Bandeira de Mello, C.S., Françolin, J.B.L., Miller, D.J., Gonçalves, R.C.S., Capilla, R., Lopes, J.P., Jesuíno, L.S., Silva Freitas, L.C., Soares Filho, J.R.S., Fontes, R.A. 2007. Principais metodologias de prospecção geoquímica de hidrocarbonetos em superfície. In: Licht, O.A.B., Bandeira de Mello, C.S. & Silva C.R. (eds.), Prospecção Geoquímica de Depósitos Minerais Metálicos, Não-Metálicos, Óleo e Gás. Rio de Janeiro, SBGq, CPRM, 788p.

Barberes, G.A. 2013. A utilização da espectrometria de raios gama na exploração de shale gas - Caso do carbonífero da Zona Sul Portuguesa. M.Sc. Thesis, University of Coimbra, 110p. (unpublished).

Barberes, G.A., Fonseca, P.E., Pena dos Reis, R., Pimentel, N., Azevedo, M. 2014a. Preliminary assessment of potential for Shale Gas in South Portuguese Zone carboniferous units. Comunicações Geológicas, 101 (II), pp. 737-741.

Barberes, G.A., Karcz, P., Pena dos Reis, R., Pimentel, N., Fonseca, P.E., Azevedo, M. 2015. Organic geochemical results from the shales of the South Portuguese Zone, southern Portugal. AAPG Datapages/Search and Discovery, Article #90226, Lisbon, Portugal, Book of Abstracts.

Barberes, G.A., Pena dos Reis, R., Pimentel, N., Fonseca, P.E., Azevedo, M. 2014b. Application of Thorium-Normalized method to identify any hydrocarbons anomalies in South Portuguese Zone Carboniferous units. Comunicações Geológicas, 101 (II), pp. 743-746.

Barberes, G.A., Pena dos Reis, R., Spigolon, A.L.D., Fonseca, P.E., Bandeira de Mello, C., Barata, M.T. 2018. Groundwater Natural Contamination by Toluene in Beja and Faro Districts, Portugal. Geosciences, 8 (1), 9, doi:10.3390/geosciences8010009.

Bernard, B.B., Brooks, J.M., Sacket, W.M. 1978. Light hydrocarbons in recent Texas continental shelf and slope sediments. Journal of Geophysical Research, 83, pp. 4053-4061, doi: 10.1029/jc083ic08p04053.

Berge, T.B. 2011. Recognition and Meaning of Hydrocarbon Seeps. AAPG Search and Discovery, Article #40759.

B.F. Environmental Consultants Inc. 2012. Methane Gas Migration and Your Water Well – A Pennsylvania Perspective. B.F. Environmental Consultants Inc., 2p.

Boyer, C., Clark, B. 2011. Shale Gas: A Global Resource. OilField Review, 23 (3), pp. 28-39.

Boyle, R.W. 1982. Geochemical prospecting for thorium and uranium deposits. Elsevier Publishing Company, 498p.

Brandon Weil, A., Gutiérrez-Alonso, G., Johnston, S.T., Pastor-Galán, D. 2013. Kinematic constraints on buckling a lithospheric-scale orocline along the northern margin of Gondwana: A geologic synthesis. Tectonophysics, 582, pp. 25-49, doi: 10.1016/j.tecto.2012.10.006.

Brown, A. 2000. Evaluation of possible gas microseepage mechanisms. AAPG Bulletin, 84 (11), pp. 1775-1789, doi: 10.1306/8626C389-173B-11D7-8645000102C1865D.

Burtell, S.G., Jones III, V.T. 1996. Exploration benzene content of subsurface brines can indicate proximity of oil, gas. Oil & Gas Journal Newsletter (http://www.ogj.com/articles/print/volume-94/issue-23/in-this-issue/exploration/exploration-benzene-content-of-subsurface-brines-can-indicate-proximity-of-oil-gas.html).

Cerqueira, J.R., Santos Neto, E.V.; Takaki, T, Prinzhofer, A. 1999. Ocorrência de hidrocarbonetos de diferentes origens num mesmo sistema de reservatórios na parte centro-sul da Bacia do Paraná. Congresso de Geoquímica dos países de língua portuguesa, Congresso Brasileiro de Geoquímica, Anais da Sociedade Brasileira de Geoquímica, pp. 383-388.

Chafin, D.T., Swanson, D.M., Grey, D.W. 1996. Methane-Concentration and Methane-Isotope Data for Ground Water and Soil Gas in the Animas River Valley, Colorado and New Mexico, 1990-91. U.S. Geological Survey. Water Resources Investigation Report 93-4007, 49p.

Clarke, R.H., Cleverly, R.W. 1991. Leakage and post-accumulation migration. In: England, W.A. & Fleet, A.J. (eds.), Petroleum migration. Geological Society Special Publication, London, 59, pp. 265-271.

Clark, P.E., Rilee, M.L. 2010. Remote sensing tools for exploration-Observing and interpreting the electromagnetic spectrum. Springer, 343p., doi 10.1007/978-1-4419-6830-2.

Cline, J.D., Holmes, M.L. 1977. Submarine seepage of natural gas in Norton Sound, Alaska. Science, 198, pp. 1149-1153, doi: 10.1126/science.198.4322.1149.

Collins, A.G. 1975. Geochemistry of OilField Waters. Elsevier, Amsterdam, 496p, doi: 10.1016/s0376-7361(08)x7011-6.

Collins, W., Raines, G.L., Canney, F.C. 1978. Airborne spectroradiometer detection of heavy-metal stress in vegetation canopies; Prog, and Abstracts 5th Internat. Assoc. Genesis Ore Deposits, Snowbird, Utah, 74p.

Conrad, R. 1996. Soil microorganisms as controllers of atmospheric trace gases (H_2, CO, CH_4, OCS, N_2O, and NO). Microbiological Reviews, American Society for Microbiology, pp. 609–640.

Czaja, W., Manning, B., McLean, L., Murphy, J.M. 2015. Fusion of aerial gamma ray survey and remote sensing data for a deeper understanding of radionuclide fate after radiological incidents: examples from the fukushima dai-ichi response. Journal of Radioanalytical and Nuclear Chemistry, 307 (3), pp. 2397-2401, doi: 10.1007/s10967-015-4650-z.

Deines, P. 1980. The isotopic composition of reduced organic carbon. In: Fritz, P. & Fontes, J.Ch. (eds.), Handbook of Environmental Isotope Geochemistry. The Terrestrial Environment, 1, Elsevier, Amsterdam, pp. 329-406.

Días-del-Río, V., Somoza, L., Martínez-Frias, J., Mata, M.P., Delgado, A., Hernandez-Molina, F.J., Lunar, R., Martín.Rubi, J.A., Maestro, A., Fernández-Puga, M.C., León, R., Llave, E., Medialdea, T., Vázquez, J.T. 2003. Vast fields of hydrocarbon-derived carbonate chimneys related to the accretionary wedge/olistostrome of the Gulf of Cádiz. Marine Geology, 195, pp. 177-200, doi: 10.1016/s0025-3227(02)00687-4.

Dias, R., Ribeiro, A., 1993. Porto-Tomar Shear Zone, a major structure since the beginning of the Hercynian Orogeny. Terra Abstracts supplement number 6 to Terra Nova 5, 11.

Dias, R., Ribeiro, A. 1995. The Ibero-Armorican Arc: A collision effect against an irregular continent? Tectonophysics, 246, pp. 113-128, doi: 10.1016/0040-1951(94)00253-6.

Dias, R., Ribeiro, A., Romão, J., Coke, C., Moreira, N. 2016. A review of the arcuate structures in the Iberian Variscides; constraints and genetic models. Tectonophysics, 681, pp. 170-194, doi: 10.1016/j.tecto.2016.04.011.

DigitalGlobe 2016. WorldView-2 data sheet, http://global.digitalglobe.com/sites/default/files/DG_WorldView2_DS_PROD.pdf (accessed May, 2016).

El-Sadek, M.A. 2002. Application of thorium-normalized airborne radio-spectrometric survey data of Wadi Araba area, North-eastern Desert, Egypt, as a guide to the recognition of probable subsurface petroleum accumulations. Applied Radiation and Isotopes, 57, pp. 121-130, doi: 10.1016/s0969-8043(02)00082-9.

Eltschlager, K.K., Hawkins, J.W., Ehler, W.C., Baldassare, F. 2001. Technical measures for the investigation and mitigation of fugitive methane hazards in areas of coal mining. U.S. Department of the Interior – Office of Surface Mining. Pittsburgh, PA, 124p.

Etiope, G. 1998. Transport of radioactive and toxic matter by gas microbubbles in the ground. J. Environ. Radioactivity, 40 (1), pp. 11-13, doi: 10.1016/s0265-931x(97)00068-4.

Etiope, G. 2004. New Directions: GEM—Geologic Emissions of Methane, the missing source in the atmospheric methane budget. Atmospheric Environment, 38, pp. 3099-3100, doi: 10.1016/j.atmosenv.2004.04.002.

Etiope, G. 2005. Mud volcanoes and microseepage: the forgotten geophysical components of atmospheric methane budget. Ann Geophys, 48, pp. 1-7, doi: 10.4401/ag-3175.

Etiope, G. 2009a. A global dataset of onshore gas and oil seeps: a new tool for hydrocarbon exploration. Oil and Gas Business, 10p.

Etiope, G. 2009b. GLOGOS, A New Global Onshore Gas-Oil Seeps Dataset. AAPG Search and Discovery, Article #70071.

Etiope, G. 2009c. Natural emissions of methane from geological seepage in Europe. Atmospheric Environment, 43, pp. 1430-1443, doi: 10.1016/j.atmosenv.2008.03.014.

Etiope, G. 2015. Natural gas seepage-The earth's hydrocarbon degassing. Springer, Switzerland. 199p, doi: 10.1007/978-3-319-14601-0.

Etiope, G., Klusman, R.W. 2002. Geologic emissions of methane to the atmosphere. Chemosphere, 49, pp. 777-789, doi: 10.1016/s0045-6535(02)00380-6.

Etiope, G, Klusman, R.W. 2010. Microseepage in drylands: flux and implications in the global atmospheric source/sink budget of methane. Glob. Plan. Change, 72, pp. 265-274, doi: 10.1016/j.gloplacha.2010.01.002.

Etiope, G., Lombardi, S. 1996. Laboratory simulation of geogas microbubble flow. Environ. Geol, 27, pp. 226-232, doi: 10.1007/bf00770436.

European Network of Transmission System Operators for Gas. 2016. The European Natural Gas Network 2016 – Capacities at Cross-Border Points on the Primary Market. http://www.entsog.eu/public/uploads/files/maps/transmissioncapacity/2016/ENTSOG_CAP_MAY2016_A0FORMAT.pdf (accessed January, 2017)

Eurostat. 2015. Energy balance sheets - 2013 data. Eurostat Statistical books. ISSN 1830-7558, 84p.

Eurostat. 2016. Energy price statistics - Statistics Explained. http://epp.eurostat.ec.europa.eu/statisticsexplained/ (accessed January, 2017).

Fernandes, P., Rodrigues, B., Borges, M., Matos, V., Clayton, G. 2013. Organic maturation of the Algarve Basin (southern Portugal) and its bearing on thermal history and hydrocarbon exploration. Marine and Petroleum Geology, 46, pp. 210-233, doi: 10.1016/j.marpetgeo.2013.06.015.

Fernandes, P., Musgrave, J.A., Clayton, G., Pereira, Z., Oliveira, J.T., Goodhue, R., Rodrigues, B. 2012. New evidence concerning the thermal history of Devonian and Carboniferous rocks in the South Portuguese Zone. Journal of the Geological Society of London, 169, pp. 647-654, doi: 10.1144/jgs2011-156.

Ferreira, J.C. 2002. Light Hydrocarbons in Soil Underlain by Exclusively Crystalline Rocks and in Sedimentary Basins: Exploratory Implications. Revista Latino Americana de Geochímica Orgânica, 6, pp. 31-39.

Fertl, W.H. 1979. Gamma ray spectral data assists in complex formation evaluation. Society of Petrophysicists and Well-Log Analysts, 20, pp. 3-37.

Figueiras, J., Mateus, A., Gonçalves, M.A., Waerenborgh, J., Fonseca, P. 2002. Geodynamic evolution of the South Variscan Iberian Suture as recorded by mineral transformations. Geodinamica Acta, 15 (2002), pp. 45-61, doi: 10.1080/09853111.2002.10510738.

Fonseca, P., Ribeiro, A. 1993. Tectonics of Beja-Acebuches Ophiolite: a major suture in the Iberian Variscan Foldbelt. Geol. Rundsch. Springer, 82, pp. 440-447, doi: 10.1007/bf00212408.

Fonseca, P., Munhá, J., Pedro, J., Rosas, F., Moita, P., Araújo, A., Leal, N. 1999. Variscan Ophiolites and high-pressure metamorphism in southern Iberia. Ofioliti, 24 (2), pp. 259-268.

Fonseca, P.E., Pimentel, N., Pena dos Reis, R., Barberes, G.A. 2015. Carboniferous Black-Sahles and Shale-Gas Potential in Southwestern Portugal. Post-Conference Field-trip. 20th-21st May 2015, 1st ed., AAPG – Europe Region Annual Conference & Exhibition, Lisbon, Portugal.

Fontana, J.V. 2000. Soil Gas Monitoring Activities near the Southeastern Boundary of the Leyden Gas Storage Facility, Leyden Colorado. ESN Rocky Mountain – Environmental Services Network. ESN Project, 0126, 28p.

Freitas, J.G., Fletcher, B., Aravena, R., Barker, J.F. 2010. Methane Production and Isotopic Fingerprinting in Ethanol Fuel Contaminated Sites. Ground Water, 48 (6), pp. 844-857, doi: 10.1111/j.1745-6584.2009.00665.x.

Friedman, G.M., Sanders, J.E. 1978. Principles of Sedimentology. John Wiley & Sons, Inc., New York, 792p.

Geosoft 2005. Montaj 256-Channel Radiometrics Processing. Radiometric processing extension for Oasis Montaj v6.1. User Guide and Tutotial. Geosoft Knowlodge from Data, 43p.

Gilbert, D., Woodruff, C., Preston, A., Thomas, R., Wood, M. 1983. Exposure and Risk Assessment for Toluene. PB8S-221505. National Technical Information Service, Springfield, VA, 182p.

Global Energy Network Institute. 2017. European high voltage transmission grid. http://www.geni.org/globalenergy/library/national_energy_grid/europe/europeannationalelectricitygrid.shtml (accessed April, 2017).

Gomez-Belinchon, J.I., Grimalt, J.O. 1991. Volatile organic compounds in two polluted rivers in Barcelona (Catalonia, Spain). Water Research, 25, pp. 577-589, doi: 10.1016/0043-1354(91)90130-i.

Government of Canada. 1992. Toluene - Priority Substances List Assessment Report Nº 4. Canadian Environmental Protection Act. Canada Communication Group, Publishing, 26p.

Grob, R.L. 2004. Theory of Gas Chromatography. In: Grob, R.L. & Barry, E.F. (eds.) Modern practice of gas chromatography. John Wiley & Sons, USA, pp. 25-64, doi: 10.1002/0471651141.

Ground Water Protection Council and All Consulting. 2009. Modern Shale Gas Development in the United States: A Primer. Washington, DC, US Department of Energy Office and Fossil Energy and National Energy Technology Laboratory.

Gülensoy, N.; Alvarez, P.J.J. 1999. Diversity and correlation of specific aromatic hydrocarbon biodegradation capabilities. Biodegradation, 10, 331–340.

Hale, M. 2000. Genesis, behaviour and detection of gases in the crust. In: Govett, G.J.S. (ed.) Handbook of exploration geochemistry volume 7 - Geochemical Remote Sensing of the Sub-Surface. Elsevier, The Netherlands, pp. 3-16.

Hemphill, W.R., Watson, R.D., Bigelow, R.C., Hessen, T.D. 1977. Measurement of luminescence of geochemically stressed trees and other materials. U.S. Geol. Surv. Prof. Paper, 1015, pp. 93-112.

Holmes, A.J., Roslev, P., Mcdonald, I.R., Iversen, N., Henriksen, K., Murrell, J.C. 1999. Characterization of methanotrophic bacterial populations in soils showing atmospheric methane uptake. Applied and Environmental Microbiology, American Society for Microbiology, 65 (8), pp. 3312-331, pmid: 10427012.

Horsfield, B., Rullkotter, J. 1994. Diagenesis, Catagenesis and Metagenesis of Organic Matter. In: Magoon, L.B. & Dow, W.G. (eds.), The Petroleum System - from Source to Trap. AAPG Memoir, United States of America, pp. 189-200, doi: 10.1306/M60585C10.

Hovland, M., Jensen, S., Fichler, C. 2012. Methane and minor oil macro-seep system - their complexity and environmental significance. Mar. Geol., pp. 332-334 and 163-173, doi: 10.1016/j.margeo.2012.02.014.

Hunt, J.M. 1996. Petroleum geochemistry and geology. W.H. Freeman and Co, New York, 743p.

International Energy Agency. 2016a. World Energy Statistics. OECD/IEA, 789p.

International Energy Agency. 2016b. Portugal - Energy System Overview. IEA-Energy Balance, 1p.

International Energy Agency. 2011. Oil & Gas Security Emergency Response of IEA Countries, Portugal. OECD/IEA, http://www.iea.org/publications/freepublications/publication/portugal_20 11.pdf. (accessed April, 2013).

Isotech. 2014. Procedure for taking cuttings samples in IsoJars®. Isotech Laboratories Inc., USA, 1p. (available in: http://www.isotechlabs.com/products/other/isojars.html).

James, A.T. 1983. Correlation of natural gas by use of carbon isotopic distribution between hydrocarbon components. AAPG Bulletin, 67, pp. 1176-1191, doi: 10.1306/03B5B722-16D1-11D7-8645000102C1865D.

Jones, V.T., Drozd, R.J. 1983. Prediction of oil or gas potential by near-surface geochemistry. AAPG Bulletin, 67, pp. 932-952, doi: 10.1306/03B59AA8-16D1-11D7-8645000102C1865D.

Jorge, R.C.G.S., Fernandes, P., Rodrigues, B., Pereira, Z., Oliveira, J.T. 2013. Geochemistry and provenance of the Carboniferous Baixo Alentejo Flysch Group, South Portuguese Zone. Sedimentary Geology, 284-285, pp. 133-148, doi: 10.1016/j.sedgeo.2012.12.005.

Kappel, W.M., Nystrom, E.A. 2012. Dissolved Methane in New York Groundwater. U.S. Geological Survey, Open-file Report 2012-1162, 6p.

Kisch, H.J. 1987. Correlation between indicators of very low-grade metamorphism. In: Frey, M. (ed.), Low-Temperature Metamorphism. Blackie and Son, London, pp. 227-300.

Khan, S.D., Jacobson, S. 2008. Remote sensing and geochemistry for detecting hydrocarbon microseepages. GSA Bull., 120, 96-105, doi: 10.1130/0016-7606(2008)120[96:RSAGFD]2.0.CO;2.

Kirk, R.E., Othmer, D.F., Grayson, M., Eckroth, D. 2004. Kirk-Othmer Encyclopedia of Chemical Technology. John Wiley, New York, 5th Edition, 22950p, doi: 10.1002/0471238961.

Klusman, R.W. 2003. Rate measurements and detection of gas microseepage to the atmosphere from an enhanced oil recovery/sequestration project, Rangely, Colorado, USA. Applied Geochemistry, 18, pp. 1825–1838, doi: 10.1016/s0883-2927(03)00108-2.

Klusman, R.W., Saeed, M.A. 1996. Comparison of light hydrocarbon microseepage mechanisms. In: Schumacher, D. & Abrams, M.A. (eds.), Hydrocarbon Migration and Its Near-Surface Expression Amer. Assoc. Petrol. Geol. Memoir 66, Tulsa, OK, pp. 157-168, doi: 10.1306/M66606C12.

Kolb, B, Ettre, L.S. 2006. Static headspace-gas chromatography – theory and practice. Wiley-Interscience, USA, 349p.

Korn, D. 1997. The Palaeozoic ammonoids of the South Portuguese Zone. Memórias do Instituto Geológico e Mineiro, 33, 131p.

Kostakis, K., Harrison, J.P. 1999. Numerical analysis of gasbubble flow in water-filled natural fractures. Comput. Geosci., 24, pp. 3-28, doi: 10.1016/S0266-352X(98)00027-5.

Kristiansson, K. Malmqvist, L. 1982. Evidence for non-diffusive transport of 222Rn in the ground and a new geophysical model for the transport. Geophysics, 47, pp. 1444-1452, doi: 10.1190/1.1441293.

Kübler, B. 1967. La cristallinité de l'illite et les zones tout à fait supérieures de métamorphisme. In: Schaer J.P. (ed.), Étages tectoniques: colloque Neuchâtel 1966. A La Baconniere, Neuchâtel, pp. 105-122.

LANDinfo Worldwide Mapping LLC 2016. Buying Satellite Imagery: Pricing Information for High Resolution Satellite Imagery, http://www.landinfo.com/satellite-imagery-pricing.html (accessed May, 2016).

Law, B.E., Curtis, J.B. 2002. Introduction to Unconventional Petroleum Systems. AAPG Bulletin, 86 (11), pp. 1851–1852, doi: 10.1306/61eedda0-173e-11d7-8645000102c1865d.

Lawrence, S.J. 2006. Description, Properties, and Degradation of Selected Volatile Organic Compounds Detected in Ground Water - A Review of Selected Literature. Department of the Interior, U.S. Geological Survey, USA. 54p.

Lefort, J.P. 1989. Basement Correlation Across the North Atlantic. Springer-Verlag, Berlin, 148p, doi: 10.1007/978-3-642-73350-5.

Leistel, J.M., Marcoux, E., Theiblemont, D., Quesada, C., Sanchez, A., Almodovar, G.R., Pascual, E., Saez, R. 1998. The volcanic-hosted massive sulphide deposits of the Iberian Pyrite Belt. Mineralium Deposita, 33, pp. 2-30, doi: 10.1007/s001260050130.

Leusch, F., Bartkow, M. 2010. A short primer on benzene, toluene, ethylbenzene and xylenes (BTEX) in the environment and in hydraulic fracturing fluids. Griffity University Press. 8p.

Levine, J.R., Davis, A. 1989. The relationship of coal optical fabrics to the Alleghanian tectonic deformation in the central Appalachian foldand- thrust belt, Pennsylvania. Geological Society of America Bulletin, 101 (10), pp. 1333-1347, doi: 10.1130/0016-7606(1989)101<1333:TROCOF>2.3.CO;2.

Li, H., Carlson, K.H. 2014. Distribution and Origin of Groundwater Methane in the Wattenberg Oil and Gas Field of Northern Colorado. Environ. Sci. Technol., 48, pp. 1484−1491, doi: dx.doi.org/10.1021/es404668b.

Link, W.K. 1952. Significance of oil and gas seeps in world oil exploration. AAPG Bulletin, 36, pp. 1505-1540.

Loch, J.P.G., van Dijk-Looyaard, A., Zoeteman, B.C.J. 1989. Organics in groundwater. In: Wheeler, D., Richardson, M. L. & Bridges, J. (eds.), The Future for Water Quality in Europe. Pergamon Press, UK. pp: 39-55.

Lowrie, A., Hamiter, R., Mo¡ett, S., Somoza, L., Maestro, A., Lerche, I. 1999. Potential pressure compartments sub-salt in the Gulf of Mexico and beneath massive debris £ows in the Gulf of Cadiz. Final Proc. 19th Conf. GCSSEPM Advanced Reservoir Characterization, Houston, TX, USA, pp. 271-280.

Macgregor, D.S. 1993. Relationships between seepage, tectonics and subsurface petroleum reserves. Marine and Petroleum Geology, 10, pp. 606-619, doi: 10.1016/0264-8172(93)90063-X.

Madhavi, T., Mani, D., Lakshmi, M., Kalpana, G., Patil, D.J., Dayal, A.M. 2008. Surface Geochemical Studies for Light Gaseous Hydrocarbons: Findings from Recent Gas Seepages in Anantapur, Andhra Pradesh. 7th International Conference & Exposition on Petroleum Geophysics, P-285, 3p.

Maier, U., Mayer, U., Crathwohl, P. 2005. Natural Attenuation of Volatile Hydrocarbons in the Unsaturated Zone – modeling for the Vaerlose

field site. In: Thomson, N.R. (ed.), Bringing Groundwater Quality Research to the Watershed Scale. Proceedings of CG2004, the 4th International Groundwater Quality Conference, Canada, IAHS Publi., 297p.

Magoon, L.B., Dow, W.G. 1994, The Petroleum System. In: Magoon, L.B. & Dow, W.G. (eds.), The petroleum system: From source to trap: AAPG Memoir 60, 34p.

Magoon L.B., Schmoker, J.W. 2000. The total petroleum system - the natural fluid network that constraints the assessment units. U.S. Geological Survey World Petroleum Assessment 2000, description and results: USGS digital data series 60. World Energy Assessment team, 31p.

Malmqvist, L., Kristiansson, K. 1984. Experimental evidence for an ascending microflow of geogas in the ground. Earth and Planetary Science Letters, 70, pp. 407-416, doi: 10.1016/0012-821X(84)90024-4.

Malmqvist, L., Kristiansson, K. 1985. A physical mechanism for the release of free gases in the lithosphere. Geoexploration, 23, pp. 447-453, doi: 10.1016/0016-7142(85)90072-9.

Maldonado, A., Somoza, L., Pallarés, L. 1999. The Betic orogen and the Iberian–African boundary in the Gulf of Cadiz: geological evolution (central North Atlantic). Marine Geology, 155, pp. 9-43, doi: 10.1016/S0025-3227(98)00139-X.

Mantero, E.M., Alonso-Chaves, F.M., García-Navarro, E., Azor, A. 2011. Tectonic style and structural analysis of the Puebla de Guzmán Antiform (Iberian Pyrite Belt, South Portuguese Zone, SW Spain). In: Poblet, J. & Lisle R.J. (eds.), Kinematic Evolution and Structural Styles of Fold-and-Thrust Belts. The Geological Society of London, Geological Society Special Publication, 349, pp. 203-222, doi: 10.1144/SP349.11.

Mateus, A., Figueiras, J., Gonçalves, M., Fonseca, P. 1999. Evolving fluid circulation within the variscan Beja-Acebuches Ophiolite complex (SE, Portugal). Ofioliti, 24 (2), pp. 269-282.

Matte, P. 1986. Tectonics and plate tectonic model for the variscan belt of Europe. Tectonophysics, 126, pp. 329-374, doi: 10.1016/0040-1951(86)90237-4.

Matthews, M.D. 1996. Migration - A view from the top. In: Schumacher, D. & Abrams, M.A. (eds.), Hydrocarbon Migration and Its Near-Surface Expression. Amer. Assoc. Petrol. Geol. Memoir 66, Tulsa, OK, pp. 139–155, doi: 10.1306/M66606C11.

McAuliffe, C. 1963. Solubility in water of Cl-C9 hydrocarbons. Nature, 200, pp. 1092-1093, doi: 10.1038/2001092a0.

McCormack, N., Clayton, G., Fernandes, P. 2007. The thermal history of the Upper Palaeozoic rocks of southern Portugal. Marine and Petroleum Geology, 24, pp. 145-150, doi: 10.1016/j.marpetgeo.2007.01.002.

McGraw-Hill (ed.) 2003. Dictionary of Chemistry, 2nd edition. McGraw-Hill, USA, 431p, doi: 10.1036/0071417974.

McNair, H.M, Miller, J.M. 2009. Basic gas chromatography. John Wiley & Sons, USA, 239p.

Mendez, A., Bruzual, J. 2003. Molecular characterization of petroleum and its fractions by mass spectrometry. In: Hsu, C.S. (ed.), Analytical advances for hydrocarbon research. Springer, USA, pp. 73-94, doi: 10.1007/978-1-4419-9212-3.

Merian, E., Zander, M. 1982. Volatile aromatics. In: Hutzinger O, (ed.), Handbook of environmental chemistry. 3 (B), Anthropogenic compounds, Berlin, Springer, pp. 117-161.

Merriman, R.J., Peacor, D.R. 1999. Very low-grade metapelites: mineralogy, microfabrics and measuring reaction progress. In:

Frey, M. & Robinson, D. (eds.), Low Grade-Metamorphism. Blackwell Science, Oxford, pp. 10-60.

Miller, J.M. 2005. Chromatography: concepts and contrasts. John Wiley & Sons, USA. 490p.

Moldoveanu, S.C., David, V. 2002. Sample preparation in chromatography. Elsevier, The Netherlands, 930p.

Molofsky, L.J., Connor, J.A., Wylie, A.S., Wagner, T., Farhat, S.K. 2013. Evaluation of Methane Sources in Groundwater in Northeastern Pennsylvania. Groundwater, 51 (3), pp. 333-349, doi: 10.1111/gwat.12056.

Molofsky, L.J., Richardson, S.D., Gorody, A.W., Baldassare, F., Black, J.A., McHugh, T.E., Connor, J.A. 2016. Effect of Different Sampling Methodologies on Measured Methane Concentrations in Groundwater Samples. Groundwater, 54 (5), pp. 669-680, doi: 10.1111/gwat.12415.

Moreno, C., González, F. 2004. Estatigrafía - Zona Sudportuguesa. In: J.A. Vera (ed.), Geología de España. SGE-IGME, Spain, pp. 201-204.

Mudelsee, M. 2003. Estimating Pearson's correlation coefficient with bootstrap confidence interval from serially dependent time series. Mathematical Geology, 35 (6), doi: 10.1023/b:matg.0000002982.52104.02.

Munhá, J. 1990. Metamorphic Evolution of the South Portuguese/Pulo Do Lobo Zone. In: Dallmeyer, R.D. & Martínez García, E. (eds.), Pre-Mesozoic Geology of Iberia. Springer-Verlag, Berlin, pp. 363-368, doi: 10.1007/978-3-642-83980-1.

Naftz, D.L., Hadley, H.K., Hunt, G.L. 1998. Determination of Methane Concentrations in Shallow Ground Water and Soil Gas near Price, Utah. U.S. Geological Survey. ES-191-97, 4p.

Oliveira, J.T. 1983. The marine Carboniferous of South Portugal: a stratigraphic and sedimentological approach. In: Lemos de Sousa, M.J. & Oliveira, J.T. (eds.). The Carboniferous of Portugal. Mem. Serv. Geol. Portugal, 29, pp. 3-37.

Oliveira, J.T. 1990a. Metamorphic Evolution of the South Portuguese/Pulo Do Lobo Zone. In: Dallmeyer, R.D. & Martínez García, E. (eds.), Pre-Mesozoic Geology of Iberia. Springer-Verlag, Berlin, pp. 363-368, doi: 10.1007/978-3-642-83980-1.

Oliveira, J.T. 1990b. Stratigraphy and syn-sedimentary tectonism in the South Portuguese Zone. In: Dallmeyer, R. D. & Martinez Garcia, E. (eds.), Pre-Mesozoic Geology of Iberia. Springer-Verlag, pp. 334-347, doi: 10.1007/978-3-642-83980-1.

Oliveira, J.T., Pereira, Z., Fernandes, P., Matos, J. 2007. Palynostratigraphic contributions to the understanding Ossa Morena and south portuguese zone geology, Portugal. Post meeting Field-trip 27-28 September 2007. CIMP Lisbon'07 Joint Meeting of Spores/Pollen and acritarch Subcommissions, 39p.

Oliveira, J.T., Relvas, J., Pereira, Z., Matos, J.X., Rosa, C., Rosa, D., Munhá, J.M., Fernandes, P., Jorge, R. & Pinto, A. 2013. Geologia da Zona Sul Portuguesa, com ênfase na estratigrafia e na vulcanologia física, geoquímica e mineralizações da Faixa Piritosa. In: Dias, R., Araújo, A., Terrinha, P. & Kullberg, J.C. (eds.), Geologia de Portugal Volume I, Escolar Editora, pp. 673–767.

Oliveira, J.T., Silva, J.B. 1988. Carta Geologica de Portugal a escala 1/50000. Noticia Explicativa da folha 46-D Mertola. Serv. Geol. Port.\

Oliveira, J.T., Wagner Genthis, C. 1983. The Mértola and Mira formations boundary between Doguedo and Almada do Ouro, marine Carboniferous of South Portugal. In: Lemos de Sousa, M.J. (ed.)

Contributions to the Carboniferous Geology and Palaeontology of the Iberian Peninsula. Universidade do Porto, Porto, pp. 1-39.

Onézime, J., Charvet, J., Faure, M., Bourdier, J., Chauvet, A. 2003. A new geodynamic interpretation for the South Portuguese Zone (SW Iberia) and the Iberian Pyrite Belt genesis. Tectonics, 22 (4), 1027p., doi:10.1029/2002TC001387.

Oremland, R.S., Whiticar, M.J., Strohmaier, F.E., Keine, R.P. 1988. Bacterial ethane formation from reduced, ethylated sulfur compounds in anoxic sediments. Geochimica et Cosmochimica Acta, 52, pp. 1895-1904, doi: 10.1016/0016-7037(88)90013-0.

Osborn, S.G., Vengosh, A., Warner, N.R., Jackson, R.B. 2011. Methane contamination of drinking water accompanying gas-well drilling and hydraulic fracturing. PNAS, 108 (20), pp. 8172–8176.

Oxford (ed.) 2005. Dictionary of Science, 15th edition. Oxford University Press, Oxford, UK, 888p.

Parker, L., Britt, S. 2012. The Effect of Bottle Fill Rate and Pour Technique on the Recovery of Volatile Organics. Groundwater Monitoring & Remediation, 32 (4), pp. 78-86, doi: 10.1111/j1745–6592.2012.01401.x.

Pena dos Reis, R., Pimentel, N., Garcia, A. 2011. The Lusitanian Basin (Portugal): stratigraphic analysis and geodynamic evolution. Boletim de Geociências da Petrobras, 19 (1/2), pp. 23-52.

Pereira, M.F., Chichorro, M., Williams, I.S., Silva, J.B. 2008. Zircon U–Pb geochronology of paragneisses and biotite granites from the SW Iberian Massif (Portugal): evidence for a paleogeographic link between the Ossa-Morena Ediacaran basins and the West African craton. In: J.P. Liégeois, E. Nasser (eds.) The Boundaries of the West African Craton, Geological Society of London Special Publication, 297, pp 385–408, doi: 10.1144/SP297.18.

Pereira, M.F., Ribeiro, C., Vilallonga, F., Chichorro, M., Drost, K., Silva, J.B., Albardeiro, L., Hofmann, M., Linnemann, U. 2013. Variability over time in the sources of South Portuguese Zone turbidites: evidence of denudation of different crustal blocks during the assembly of Pangaea. Int. J. Earth Sci. (Geol. Rundsch), Springer-Verlag, 103 (5), pp. 1453-1470, doi: 10.1007/s00531-013-0902-8.

Pereira, Z., Matos, J., Fernandes, P., Oliveira, J.T. 2007. Devonian and Carboniferous palynostratigraphy of the South Portuguese Zone, Portugal – An overview. Comunicações Geológicas, 2007 (94), pp. 53-79.

Pérez-Estaún, A., Bea, F., Bastida, F., Marcos, A., Martínez Catalán, J.R., Martínez Poyatos, D., Arenas, R., Díaz García, F., Azor, A., Simancas, J.F., González Lodeiro, F. 2004. La Cordillera Varisca Europea: El Macizo Ibérico. In: J.A. Vera (ed.) Geología de España. SGE-IGME, Spain, pp. 21-25.

Peters, K.E. 1999. Rock-Eval Pyrolysis. In: Marshall, C.P. & Fairbridge, R.W. (eds.), Encyclopedia of Geochemistry. Kluwer Academic Publishers, The Netherlands, pp. 551-554, doi: 10.1007/1-4020-4496-8.

Peters, K.E., Cassa, M.R. 1994. Applied Source Rock Geochemistry. In: Magoon, L.B. & Dow, W.G. (eds.), The Petroleum System - from Source to Trap. AAPG Memoir, United States of America, pp. 93-120, doi: 10.1306/M60585C5.

Peters, K.E., Walters, C.C., Moldowan, J.M. 2005. The Biomarker Guide, Volume 1 - Biomarkers and Isotopes in the Environment and Human History. Cambrigde University Press, UK, 471p.

Philp, R.P., Crisp, P.T. 1982. Surface geochemical methods used for oil and gas prospecting – a review. J. Geochem. Explor., 17, pp. 1-34, doi: 10.1016/0375-6742(82)90017-6.

Prince, R.C., Suflita, J.M. 2007. Anaerobic biodegradation of natural gas condensate can be stimulated by the addition of gasoline. Biodegradation, 18, 515–523.

Prince, R.C., Walters, C.C. 2016. Biodegradation of oil hydrocarbons and its implications for source identification. In Standard Handbook Oil Spill Environmental Forensics; Stout, S.A., Wang, Z., Eds.; Elsevier: Amsterdam, The Netherlands, pp. 869–916. ISBN 9780128096598.

Prost, G.L. 2014. Remote sensing for geoscientists - Image analysis and integration. CRC Press, Boca Raton/London/New York, 622p.

Quay, P., Stutsman, J., Wilbur, D., Snover, A., Dlugokencky, E., Brown, T. 1999. The isotopic composition of isotopic methane. Global Biogeochemical Cycles, American Geophysical Union, 13(2), pp. 445-461, doi: 10.1029/1998GB900006.

Quesada, C. 1991. Geolgical constraints on the Paleozoic tectonic evolution of tectonostratigraphic terranes in the Iberian Massif. Tectonophysics, 185 (1991), pp. 225-245, doi: 10.1016/0040-1951(91)90446-Y.

Quesada, C., Fonseca, P.E., Munhá, J., Oliveira, J.T., Ribeiro, A. 1994. The Beja-Acebuches Ophiolite (Southern iberia Variscan Fold Belt): geological characterization and geodynamic significance. Boletín Geológico y Minero, 105 (1), pp. 3-49.

Ramos, A., Fernández, O., Terrinha, P. Muñoz, J.A., Arnaiz, A. 2014. Mesozoic Tectonic and Paleogeographic Evolution of the Gulf of Cadiz and Algarve Basins, and Implications for Hydrocarbon Exploration. AAPG Search and Discovery, Article #10621.

Rechsteiner Jr., C.E., Crandall, J., Roques, N. 2015. Advances in Gas Chromatography for Petroleum Upstream, Refining, Petrochemical, and Related Environmental Applications. In: Ovalles, C. &

Rechsteiner Jr., C.E. (eds.), Analytical methods in petroleum upstream applications. CRC Press, USA, pp. 113-124.

Restek. 2000. A technical guide for static headspace analysis using GC. Lit. Cat.# 59895B. Restek Technical Guide, USA, 19p.

Ribeiro, A., Munhá, J., Dias, R., Mateus, A., Pereira, E., Ribeiro, L., Fonseca, P., Araújo, A., Oliveira, T., Romão, J., Chaminé, H., Coke, C., Pedro, J. 2007. Geodynamic evolution of the SW Europe Variscides. Tectonics, 26 (TC6009), 24p., doi:10.1029/2006TC002058.

Rice, D.D. 1992. Controls, habitat, and resources potential of ancient bacterial gas. In: Vially, R. (ed.), Bacterial Gas. Editions Technip, pp. 91-118.

Rice, D.D., Claypool, G.E. 1981. Generation, accumulation, and resource potential of biogenic gas. AAPG Bulletin, 65, pp. 5-25.

Roberts, H. H., Aharon, P., Carney, R., Larkin, J., Sassen, R. 1990. Sea floor response to hydrocarbon seeps, Louisiana continental slope. Geo-Marine Letters, 10, pp. 232-243, doi: 10.1007/BF02431070.

Rodrigues, B., Chew, D.M., Jorge, R.C.G.S., Fernandes, P., Veiga-Pires, C., Oliveira, J.T. 2015. Detrital zircon geochronology of the Carboniferous Baixo Alentejo Flysch Group (South Portugal); constraints on the provenance and geodynamic evolution of the South Portuguese Zone. Journal of the Geological Society, 172, pp. 294-308, doi: 10.1144/jgs2013-084.

Rostron, B.J., Toth, J. 1996. Ascending fluid plumes above Devonian pinnacle reefs: Numerical modeling and field example from west-central Alberta, Canada. In: Schumacher, D.S. & Abrams, M.A. (eds.), Hydrocarbon Migration and its Near-Surface Expression. Amer. Assoc. Petrol. Geol., Memoir 66, Tulsa, OK, pp. 185-201, doi: 10.1306/M66606C15.

Sackett, W.M. 1978. Carbon and hydrogen isotope effects during the thermocatalic production of hydrocarbons in laboratory simulation experiments. Geochimica et Cosmochimica Acta, 42, pp. 571-580, doi: 10.1016/0016-7037(78)90002-9.

Saenz, G., Pannell, H., Pingitore, N.E. 1991. Recent advances in near-surface organic geochemical prospecting for oil and gas. In: Foster, N.H. & Beaumont, E.A. (eds.), Source and Migration Processes and Evaluation Techniques, American Association of Petroleum Geologists, Tulsa, OK, pp. 135-140, doi: 10.1306/TrHbk543C14.

Sakhaee-Pour, A., Bryant, S.L. 2011. Gas Permeability of Shales. SPE Annual Technical Conference and Exhibition, Society of Petroleum Engineers, SPE 146944, 14p.

Sandstrom, M.W., Meredith, D., Kaplan, I.R., Isaac, R. 1983. Hydrocarbon geochemistry in surface sediments of Alaskan outer continental shelf; Part 2, Distribution of hydrocarbon gases. AAPG Bulletin, 67, pp. 2047-2052.

Santos Neto, E.V. 2004. Gas geochemistry: a new technology to evaluate petroleum systems. B. Geoci. Petrobras, Rio de Janeiro, 12, (2), pp. 357-383.

Saunders, D.F., Burson, K.R., Branch, J.F., Thompson, C.K. 1993. Relation of thorium-normalized surface and aerial radiometric data to subsurface petroleum accumulations. Geophysics, 58, pp. 1417-1427, doi: 10.1190/1.1443357.

Saunders, D.F., Burson, K.R., Thompson, C.K. 1999. Model for Hydrocarbon Microseepage and Related Near-Surface Alterations. AAPG Bulletin, 83 (1), 170-184, doi: 10.1306/00AA9A34-1730-11D7-8645000102C1865D.

Schermerhorn, L.J.G. 1970. The Deposition of Volcanics and Pyritite in the Iberian Pyrite Belt. Mineralium Deposita, 5, pp. 273-279, doi: 10.1007/BF00201992.

Schoell, M. 1983. Genetic Characterization of Natural Gases. AAPG Bulletin, 67 (12), pp. 2225-2238.

Schoenherr, J., Littke, R., Urai, J.L., Kukla, P.A., Rawahi, Z. 2007. Polyphase thermal evolution in the infra-Cambrian Ara Graoup (South Oman Salt Basin) as deduced by maturity of solid reservoir bitumen. Organic Geochemistry, 38(8), pp. 1293-1318, doi: 10.1016/j.orggeochem.2007.03.010.

Schumacher, D. 2012. Hydrocarbon Microseepage - A Significant but Underutilized Geologic Principle with Broad Applications for Oil/Gas Exploration and Production. AAPG Search and Discovery, Article #40943.

Schumacher, D., Abrams, M.A. 1996. Hydrocarbon migration and its near surface expression. AAPG Memoir, 66, 446p.

Sechman, H. 2012. Detailed compositional analysis of hydrocarbons in soil gases above multihorizon petroleum deposits - a case study from western Poland. App. Geochem., 27, pp. 2130-2147, doi: 10.1016/j.apgeochem.2012.06.004.

Seneshen, D.M., Chidsey, T.C., Morgan, C.D., Vanden Berg, M.D. 2010. New Techniques for new Hydrocarbon Discoveries - Surface Geochemical Surveys in the Lisbon and Lightning Draw Southeast Field Areas, San Juan County, Utah. Miscellaneous Publication, Utah Geological Survey,10 (2), 68p.

Sevastyanov, V.S. 2015. Isotope ratio mass spectrometry: Devices, methods, Applications. In: Sevastyanov, V.S. (ed.), Isotope ratio mass spectrometry of light gas-forming elements. CRC Press, USA, pp. 1-118.

Shelley, D., Bossière, G. 2000. A new model for the Hercynian Orogen of Gondwanan France and Iberia. Journal of Structural Geology, 22, pp. 757-776, doi: 10.1016/S0191-8141(00)00007-9.

Silva, J.B., Oliveira, J.T., Ribeiro, A. 1990. Structural Outline – South Portuguese Zone. In: Dallmeyer, R. D. & Martinez Garcia, E. (eds.), Pre-Mesozoic Geology of Iberia. Springer Verlag. pp. 348-362, doi: 10.1007/978-3-642-83980-1.

Silverman, S.R. 1971. Influence of petroleum origin and transformation on its distribution and redistribution in sedimentary rocks. 8th World Petroleum Congress Proceedings, 2, pp. 47-54.

Simancas, J.F., Carbonell, R., González Lodeiro, F., Pérez-Estaún, A., Juhlin, C., Ayarza, P., Azor, A., Martínez Poyatos, D., Almodóvar, G.R., Pascual, E., Sáez, R., Kashubin, A., Alonso, F., Álvarez Marrón, J., Bohoyo, F., Castillo, S., Donaire, T., Expósito, I., Flecha, I., Galadí, E., Galindo Zaldívar, J., González, F., González Cuadra, P., Macías, I., Martí, D., Martín, A., Martín Parra, L.M., Nieto, J.M., Palm, H., Ruano, P., Ruiz, M., Toscano, M. 2004. The Seismic Crustal Structure of the Ossa-Morena Zone and its geological interpretation. Journal of Iberian Geology, 30, pp. 133-142.

Simancas, J.F. 2004. Zona Sudportuguesa. In: J.A. Vera (ed.), Geología de España. SGE-IGME, Spain, pp: 201-204.

Skupio, R., Barberes, G.A. 2017. Spectrometric gamma radiation of the shale cores applied to determining sweet spots. Acta Gephysica, 65 (6), pp. 1219-1227, doi: http://sci-hub.tw/10.1007/s11600-017-0089-7.

Sparkman, O.D., Penton, Z.E., Kitson, F.G. 2011. Gas chromatography and mass spectrometry: a practical guide. Elsevier, USA, 610p, doi: 10.1016/B978-0-12-373628-4.00001-0.

Speight, J.G. 2001. Handbook of petroleum analysis. John Wiley & Sons, USA. 519p.

Stadnitskaia, A., Ivanov, M.K., Blinova, V., Kreulen, R., van Weering, T.C.E. 2006. Molecular and carbon isotopic variability of

hydrocarbon gases from mud volcanoes in the Gulf of Cadiz, NE Atlantic. Marine and Petroleum Geology, 23, pp. 281-296, doi: 10.1016/j.marpetgeo.2005.11.001.

Stahl, W.J. 1977. Carbon and nitrogen isotopes in hydrocarbon research and exploration. Chemical Geology, 20, pp. 121-149, 10.1016/0009-2541(77)90041-9.

Stahl, W.J. 1979. Carbon isotopes in petroleum geochemistry. In: Jäger, E. & Hunziker, J.C. (eds.), Lectures in Isotope Geology, Springer, pp. 274-282, doi: 10.1007/978-3-642-67161-6.

Stahl, W.J., Faber, E. Carey, B.D., Kirksey, D.L. 1981. Near-Surface Evidence of Migration of Natural Gas from Deep Reservoirs and Source Rocks. AAPG Bulletin, 65 (9), pp. 1543-1550.

Stephens, D.S. 2013. The Cost and Value of Research - Direct and indirect returns for the university and society, http://www.emory.edu/ACAD_EXCHANGE/issues/2013/spring/stories/stephens/index.html (accessed February, 2018).

Stolp, B.J., Burr, A.L., Johnson, K.K. 2006. Methane Gas Concentration in Soils and Ground Water, Carbon and Emery Counties, Utah, 1995-2003. USGS Scientific Investigations Report, 2006-5227, 20p.

Tang, J., Yin, H., Wang, G., Chen, Y. 2010. Methane microseepage from different sectors of the Yakela condensed gas field in Tarim Basin, Xinjiang, China. App. Geochem., 25, pp. 1257-1264, doi: 10.1016/j.apgeochem.2010.05.011.

Taylor, G.H., Teichmuller, M., Davis, A., Diessel, C.F.K., Littke, R., Robert, P. 1998. Organic Petrology. Gebruder Borntraeger, Berlin, Germany, 704p.

Tedesco, S.A. 1995. Surface Geochemistry in Petroleum Exploration, Chapman and Hall. 229p.

Thermo SCIENTIFIC. 2014. Thermo Scientific GC-IRMS. Discover more using the next generation of GC-IRMS. Thermo Fisher Scientific Inc., 8p.

Thrasher, J.A., Fleet, A.J., Hay, S.J., Hovland, M., Duppenbecker, S. 1996. Understanding geology as the key to using seepage in exploration: The spectrum of seepage styles. In: Schumacher, D. & Abrams, M.A. (eds.), Hydrocarbon Migration and its Near-Surface Expression. Amer. Assoc. Petrol. Geol. Memoir 66, Tulsa, OK, pp. 223-241, doi: 10.1306/M66606C17.

Tipler, A. 2013. An Introduction to Headspace Sampling in Gas Chromatography – Fundamentals and Theory. PerkinHelmer, Inc., USA, 34p.

Tissot, B.P, Welte, D.H. 1978. Petroleum Formation and Occurrence: a new approach to oil and gas exploration. Springer, Berlin, 538 p.

Tornos, F., Casquet, C., Relvas, J.M.R.S., Barriga, F.J.A.S., Sáez, R. 2002. The relationship between ore deposits and oblique tectonics: the SW Iberian Variscan Belt. In: Blundell, D.J., Neubauer, F. & von Quadt, A. (eds.), The Timing and Location of Major Ore Deposits in an Evolving Orogen. The Geological Society of London, Geological Society Special Publication, 204, pp. 179-198, doi: 10.1144/GSL.SP.2002.204.01.11.

Ullom, W.L. 1988. Ethylene and propylene in soil gas: Occurrence, sources and impact on interpretation of exploration geochemical data, Association of Petroleum Geochemical Explorationists Bulletin, 4(I), pp. 62-81.

US EPA (U.S. Environmental Protection Agency). 1987. Occurrence of Synthetic Organic Chemicals in Drinking Water, Food, and Air. PB89-192520. Office of Drinking Water. Washington, D.C., 175p.

US EPA (U.S. Environmental Protection Agency). 2009. National Primary Drinking Water Regulation. EPA 816-F-09-004. EPA's Safe Drinking Water. USA, 6p.

US National Petroleum Council. 2007. Unconventional Gas Reservoirs – Tight Gas, Coal Seams, and Shales. Washington, DC, working document of the NPC Global Oil and Gas Study, topic paper nº 29.

USGS. 2006. Methane in West Virginia ground Water. Fact Sheet 2006-3011, United State Geological Survey, 2p.

USGS World Energy Assessment Team. 2000. US Geological Survey World Petroleum Assessment 2000. Description and Results. Digital Data Series-DDS-60. US Department of the Interior, USGS.

Van der Meer, F., Yang, H., Kroonenberg, S., Lang, H., Van Gijk, P., Scholte, K., Van der Werff, H., 2002. Imaging Spectrometry and Petroleum Geology. In: F.D. Van der Meer, S.M. Jong (eds.), Imaging Spectrometry Basic Principles and Prospective Application, Springer, pp. 219-241.

Varhegyi, A., Hakl, J., Monnin, M., Morin, J.P., Seidel, J.L. 1992. Experimental study of radon transport in water as test for transportation microbubble model. J. Appl. Geophys, 29, pp. 37-46, doi: 10.1016/0926-9851(92)90011-9.

Verweij, J.M. 1993. Developments in Petroleum Science 35: Hydrocarbon migration system analysis, 1st ed., Elsevier, Amsterdam, The Netherlands.

Wagner, M., Piske, J., Smit, R. 2002. Case histories of microbial prospection for oil and gas, onshore and offshore northwest Europe. In: Schumacher, D. & LeSchack, L.A. (eds.), Surface exploration case histories: applications of geochemistry, magnetics and remote sensing. AAPG studies in geology nº 48 and SEG Geophys Ref Series nº 11, pp. 453-479.

Walters, C.C., Isaksen, G.H., Peters, K.E. 2003. Applications of light hydrocarbon molecular and isotopic compositions in oil and gas exploration. In: Hsu, C.S. (ed.), Analytical advances for hydrocarbon research. Springer, USA, pp. 247-266.

Weatherford. 2013. Shale Plays in Portugal. Report from Project BH-60993. Weatherford Laboratories.

Whiticar, M.J. 1994. Correlation of natural gases with their sources. In: Magoon, L.B. & Dow, W.G. (eds.), The Petroleum System - from Source to Trap. AAPG, pp. 261-283, doi: 10.1306/M60585C16.

Whiticar, M.J., Faber, E., Whelan, J.K., Simoneit, B.R.T. 1994. Thermogenic and bacterial hydrocarbon gases (free and sorbed) in Middle Valley, Juan de Fuca Ridge, Leg 1391. In: Mottl, M.J., Davis, E.E., Fisher, A.T., & Slack, J.F. (eds.), Proceedings of the Ocean Drilling Program, Scientific Results, 139.

WHO (World Health Organization). 2004. Toluene in Drinking-water. Background document for development of WHO Guidelines for Drinking-water Quality, 9p.

WHO (World Health Organization). 2011. Guidelines for Drinking-water Quality. WHO Graphics, Switzerland, 541p.

Wolfe, R.S. 1971. Microbial formation of methane. Advances in Microbial Physiology, 6, pp. 107-146, PMID: 4950179.

Xie, G.Z., Zhang, Y.H. 1997. The relation between gamma-ray and near-infrared radiation in gamma-ray loud blazars. The Astrophysical Journal, 477, pp. 114-117, doi: 10.1086/303673.

Yang, H., Van der Meer, F.D., Zhang, J. 2000. Aerospace Detection of Hydrocarbon-Induced Alteration. In: M. Hale (ed.), Geochemical Remote Sensing of the Sub-surface, Elsevier, pp. 233-245.

Yonetoku, D., Murakami, T., Nakamura, T., Yamazaki, R., Inoue, A. K., Ioka, K. 2004. Gamma-ray burst formation rate inferred from the

spectral peak energy–peak luminosity relation. The Astrophysical Journal, 609, pp. 935-951, doi: 10.1086/421285.

Zarrella, W.M., Mousseau, R.J., Coggeshall, N.D., Norris, M.S., Schrayer, G.J. 1967. Analysis and significance of hydrocarbons in subsurface brines. Geochim. Cosmochim. Acta, 31, pp. 1155-1166, doi: 10.1016/S0016-7037(67)80054-1.

Zhang, G., Zheng, Z., Shen, X., Zou, L., Huang, K. 2011. Remote sensing interpretation of areas with hydrocarbon microseepage in northeast China using Landsat-7/ETM+ data processing techniques. International Journal of Remote Sensing, 32 (21), pp. 6695-6711, doi: 10.1080/01431161.2010.512940.

Zogorski, J.S., Carter, J.M., Ivahnenko, T., Lapham, W.W., Moran, M.J., Rowe, B.L., Squillace, P.J., Toccalino, P.L. 2006. The Quality of Our Nation's Waters - Volatile Organic Compounds in the Nation's Ground Water and Drinking-Water Supply Wells. U.S. Department of the Interior, U.S. Geological Survey, USA.

Zou, C., Zhu, Rukai, Tao, S., Hou, L., Yuan, X., Song, Y., Niu, J., Dong, D., Liu, S., Jiang, L., Wang, S., Zhang, G. 2013. Unconventional Petroleum Geology. Elsevier, USA, 373p.

Result sheet																														
Sample	mole% in total gas		Gas composition [mole%] (Total hydrocarbons = 100%)									Wetness	Carbon isotope ratios ($d^{13}C$ vs. vPDB)									Gas composition [mole PPM]									
Number	CO2	C1	Methane	Ethane	Ethene	Propane	Propene	$i\text{-}C_4$	$n\text{-}C_4$	$i\text{-}C_5$	$n\text{-}C_5$	C_1/C_2	Methane	Ethane	Ethene	Propane	Propene	$i\text{-}C_4$	$n\text{-}C_4$	$i\text{-}C_5$	$n\text{-}C_5$	Methane	Ethane	Ethene	Propane	Propene	$i\text{-}C_4$	$n\text{-}C_4$	$i\text{-}C_5$	$n\text{-}C_5$	C6+	Toluene
SPZ-00	4.2	0.0002	57.8		29.6	4	3		1.5		4.1											2		1	0.1	0.1		0.1		0.1	2	<1ppm
SPZ-01	1.1	0.0002	95.9		4.1																	2		0.1							2	<1ppm
SPZ-02	1.2	0.0002	100																			2									1	<1ppm
SPZ-03	1.3	0.0002	100																			2									2	<1ppm
SPZ-04	3.1	0	75.3		19.3						5.4											0		0						0	<1 ppm	<1ppm
SPZ-05	0.34	0.0002	100																			2									2	<1ppm
SPZ-06	6.6	0.0002	48.7		26	8.7	11.4				5.1											2		1	0.4	0.5				0.2	3	<1ppm
SPZ-07	1.3	0.0002	100																			2									5	<1ppm
SPZ-08	4	0.0002	65.2		28.3	2.5	1.7				2.4											2		0.9	0.1	0.1				0.1	17	<1ppm
SPZ-09	2.6	0.0002	86.7		8.3	1.8					3.1											2		0.2	0					0.1	<1 ppm	<1ppm
SPZ-10	5.3	0.0003	61.7		30.5	2.2	2.2				3.4											3		1	0.1	0.1				0.2	2	<1ppm
SPZ-11	0.87	0.0002	100																			2									6	<1ppm
SPZ-12	3.1	0.0002	82.1		14	3.9																2		0.3	0.1						<1 ppm	<1ppm
SPZ-13	0.58	0.0002	100																			2									2	<1ppm
SPZ-14	0.71	0.0002	100																			2									<1 ppm	<1ppm
SPZ-15	3.2	0.0002	67.6		21.3	3.4	1.7		1.9		4											2		0.6	0.1	0.1		0.1		0.1	4	<1ppm
SPZ-16	0.87	0.0002	100																			2									5	<1ppm
SPZ-17	2.1	0.0001	100																			1									2	<1ppm
SPZ-18	0.46	0.0002	100																			2									1	<1ppm
SPZ-19	0.89	0.0001	100																			1									<1 ppm	<1ppm
F081	4.2	0.0096	49	23.8	4.5	10.2	5.8	0.58	3.9	0.66	1.6	2.1	-27.4									96	47	9	20	11	1	8	1	3	10	2
F08	3.1	0.1	47.6	26.9	1.2	12.8	3.7	0.63	4.7	0.78	1.7	1.77	-31									1000	565	25	269	78	13	99	16	36	117	5
F09	3.2	0.016	54	17.3	9.1	7.5	7.1	0.55	2.7	0.6	1.1	3.12	-26.0	-31.2	-28	-32	-31	-31	-32	-31	-33	160	51	27	22	21	2	8	2	3	17	5
F10	0.62	0.0031	53.6	17.4	10.2	7.2	7.7	0.51	2.4	0.55	0.52	3.08	-24.8									31	10	6	4	4	0.3	1	0.3	0.3	2	<1 ppm
F11	0.7	0.0003	80.8	6.9	6.9	2.7	2.7					11.71	Too small									3	0.3	0.3	0.1	0.1					<1 ppm	<1 ppm
F12	0.56	0.0003	62.5	11	11	6.5	6.5		2.4			5.68	Too small									3	0.5	0.5	0.3	0.3		0.1			<1 ppm	<1 ppm
P03	1.1	0.0008	63	10.1	10.5	5.3	7	0.36	1.8	1.1	0.83	6.24										8	1	1	0.7	0.9	0	0.2	0.1	0.1	<1 ppm	<1 ppm
W02	0.85	0.0005	94.5						2.9	1.9	0.75											5						0.2	0.1	0	4	3
W03	2.1	0.0004	82.7		7.4				1.3	5.1	3.4											4		0.4				0.1	0.2	0.2	3	3
W06	3.2	0.0003	82.3						3.7	8.2	5.8											3						0.1	0.3	0.2	6	5
W07	1.4	0.0006	92.5						1.8	3.3	2.5											6						0.1	0.2	0.2	5	4
W09	0.094	0.0008	83.9	0.98	2.4	1.3			3	4.4	4	85.61										8	0.1	0.2	0.1			0.3	0.4	0.4	4	3
W10	2.9	0.0005	89.5						1.5	5.1	4											5						0.1	0.3	0.2	3	2
W11	0.02	0.0007	95.7						0.67	1.8	1.8											7						0	0.1	0.1	5	4
W12	2.8	0.0003	87.7						3	4.7	4.7											3						0.1	0.2	0.2	<1 ppm	<1 ppm
W13	0.59	0.0002	86.4						1.7	6	6											2						0	0.1	0.1	3	3
W14	1.1	0.0004	89.9						1.3	5.2	3.5											4						0.1	0.2	0.2	4	3
W15	0.47	0.0002	79		5.3				2.5	5.9	7.2											2		0.1				0.1	0.1	0.2	4	3
W16	2.4	0.0002	78.9						3.6	10.5	7											2						0.1	0.3	0.2	3	2
W17	3.8	0.0003	82.4		3.1				2.2	5.8	6.4											3		0.1				0.1	0.2	0.2	6	5
W18	4.1	0.0003	80.3		7.2				2.8	5.7	4											3		0.3				0.1	0.2	0.1	4	4
W19	3.9	0.0002	86.8						0.92	6.5	5.8											2						0	0.1	0.1	3	2
W20	3.7	0.0002	86.4						6.9	4.7	2											2						0.2	0.1	0	5	5
W21	2.7	0.0003	80.3		11.2				4.8	2.3	1.4											3		0.4				0.2	0.1	0.1	<1 ppm	<1 ppm
W22	1.1	0.0002	86.7						6.2	4.2	3											2						0.1	0.1	0.1	5	5
W23	0.19	0.0003	85.3		2.8	3.6			4	2.1	2.1											3		0.1	0.1			0.1	0.1	0.1	7	6
W24	0.16	0.0002	83.5		7.4				3.6	3.5	2.1											2		0.2				0.1	0.1	0.1	2	1
W25	1.8	0.0003	88.1		4.9				2.9	2.7	1.4											3		0.2				0.1	0.1	0	5	5
W26	1.8	0.0002	87.2						4	5.6	3.1											2						0.1	0.1	0.1	2	2
W27	2.5	0.0006	93.8		2.1				0.68	1.8	1.6											6		0.1				0	0.1	0.1	2	1
W28	1.3	0.0003	93.7						2.9	3.4												3						0.1	0.1		2	2
W29	0.25	0.0002	88.1						3.1	5.6	3.2											2						0.1	0.1	0.1	3	3
W30	0.54	0.0003	95.2						4.8													3						0.2			5	5
W31	2	0.0002	95.3		1.9				2.8													2		0				0.1			2	2
W32	0.21	0.0003	100																			3									2	2
W33	2.7	0.0012	96		2.7				0.56	0.43	0.29											12		0.3				0.1	0.1	0	2	2
W33-1	1.4	0.0004	63.3	5.5	23		8.2					11.5	Too small									4	0.3	1		0.5					2	2
W34	3	0.007	97.1	1.3		0.99			0.42		0.2	74.7	-32.7									70	0.9		0.7			0.3		0.1	2	2

Appendix 10.1. Result sheet from all samples.

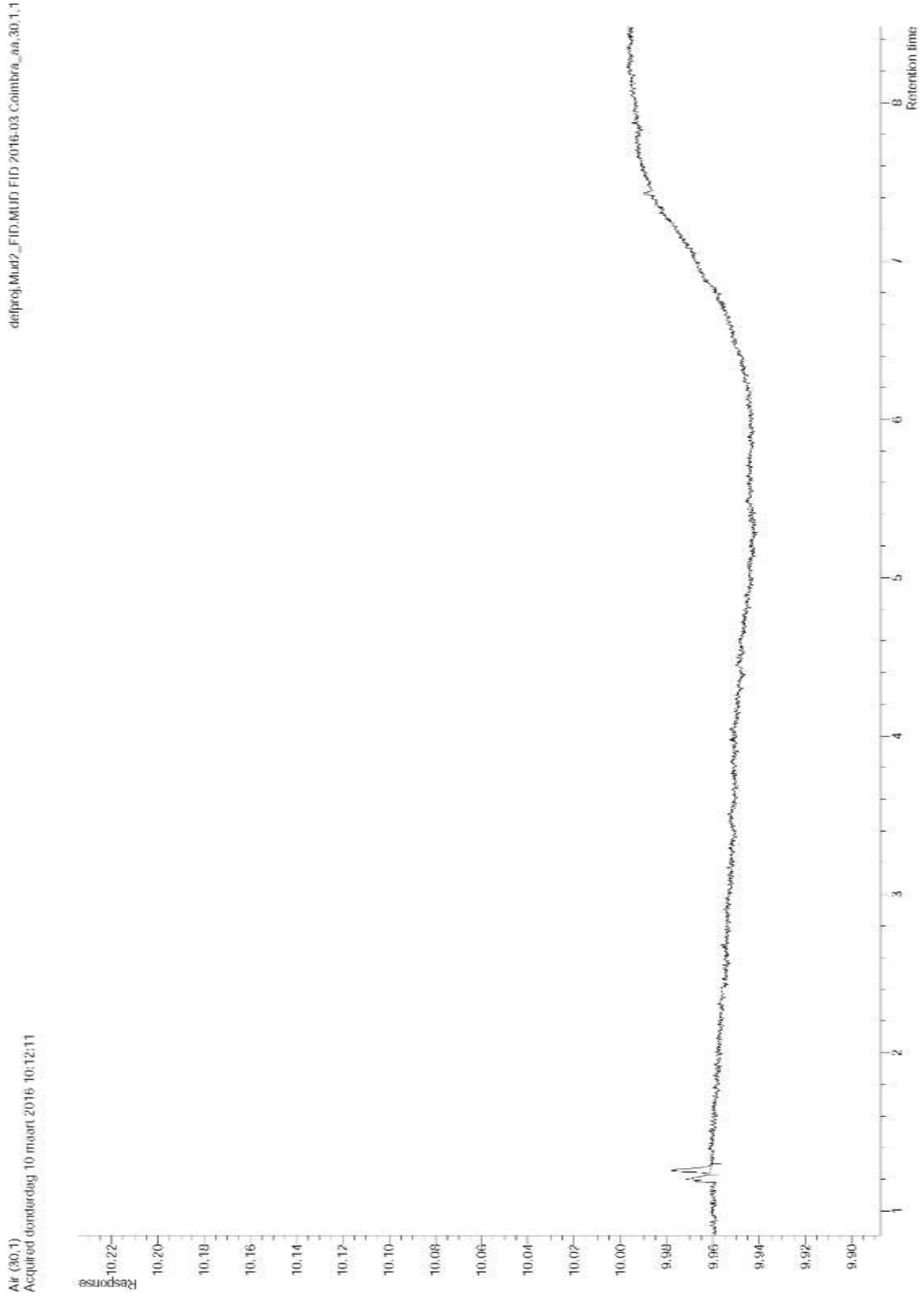

Appendix 10.2: Air chromatogram. Retention time (min) x Response (pA).

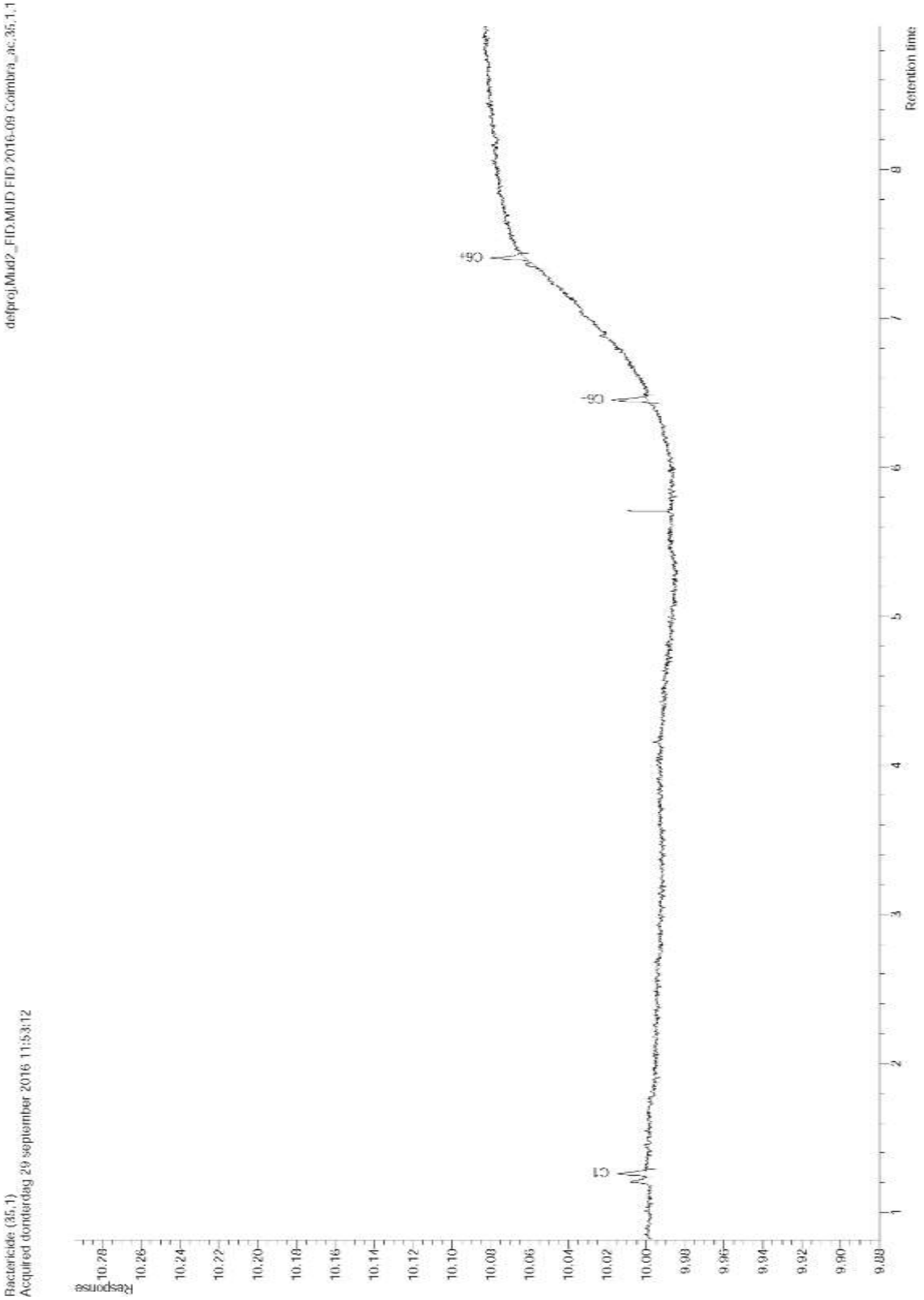

Appendix 10.3: Bactericide chromatogram. Retention time (min) x Response (pA).

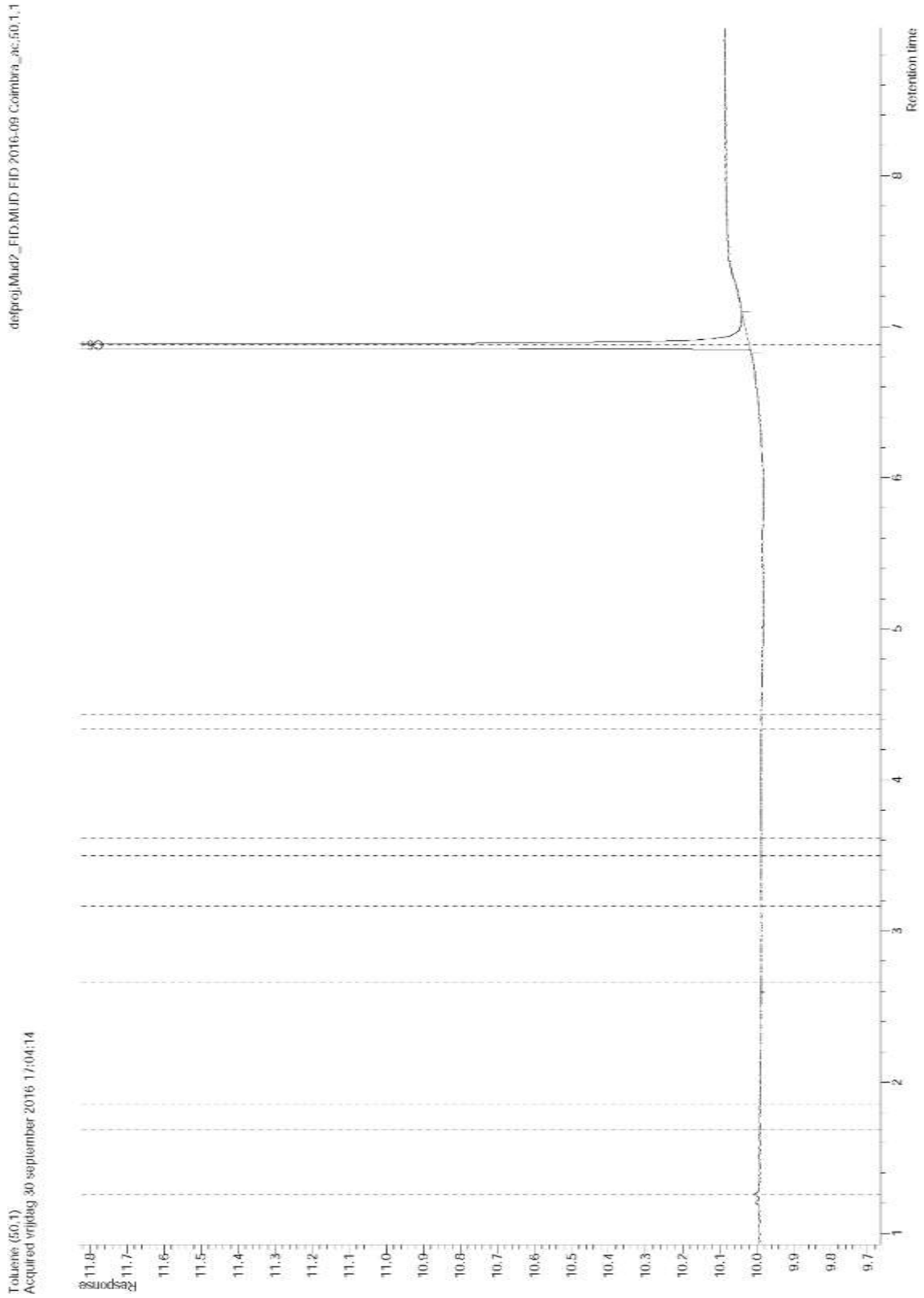

Appendix 10.4: Pure toluene chromatogram. Retention time (min) x Response (pA).

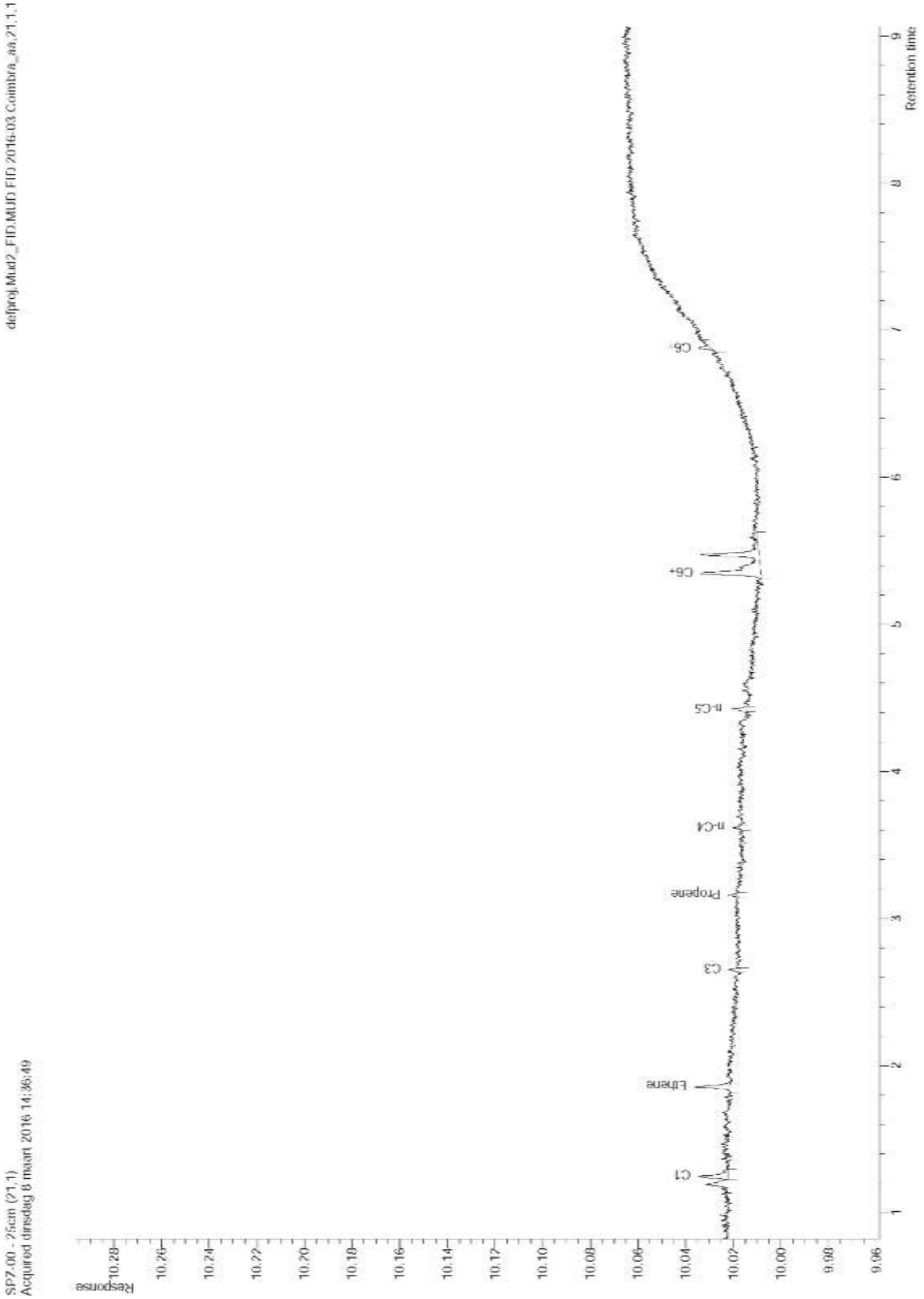

Appendix 10.5: SPZ-00 chromatogram. Retention time (min) x Response (pA).

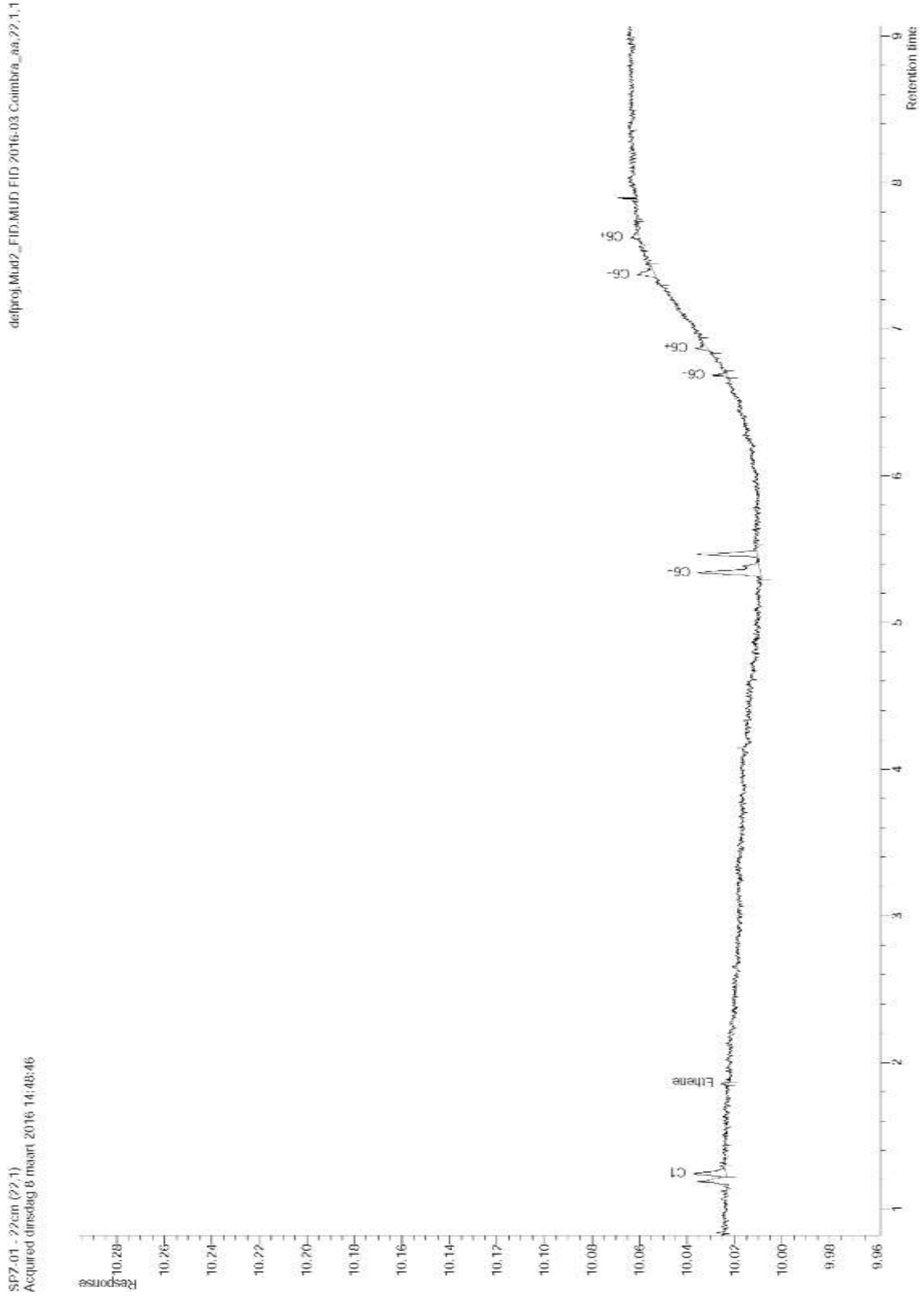

Appendix 10.6: SPZ-01 chromatogram. Retention time (min) x Response (pA).

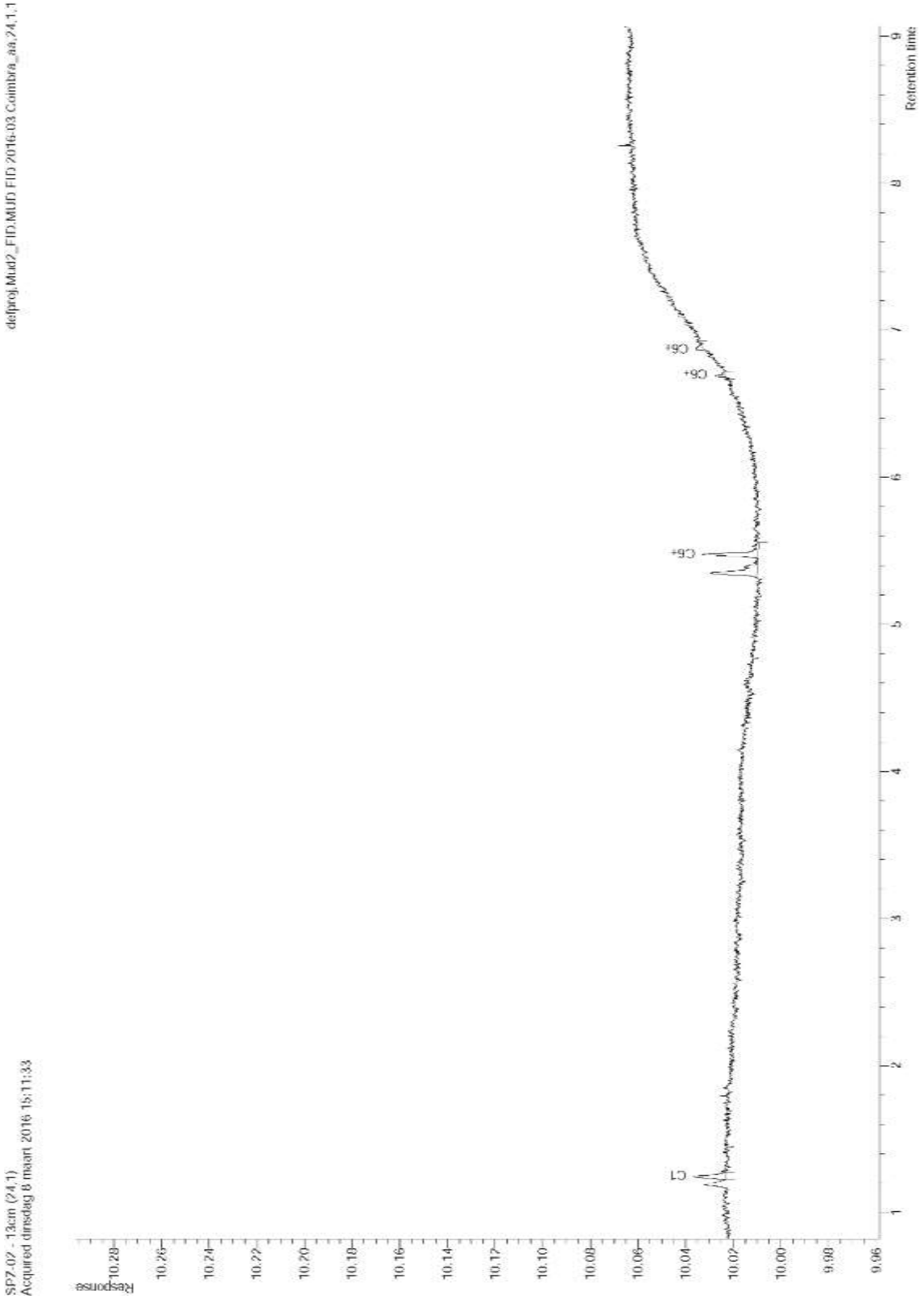

Appendix 10.7: SPZ-02 chromatogram. Retention time (min) x Response (pA).

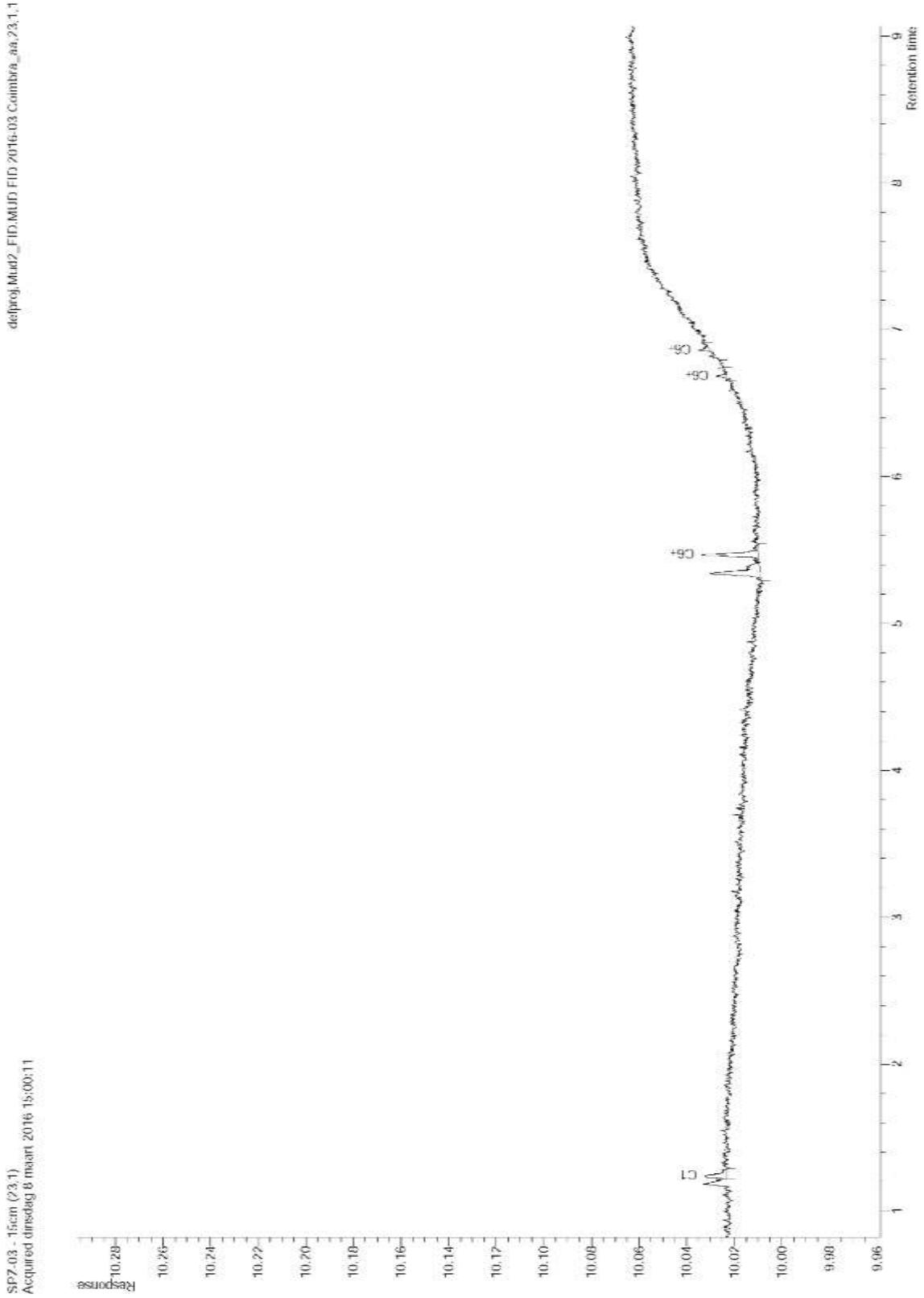

Appendix 10.8: SPZ-03 chromatogram. Retention time (min) x Response (pA).

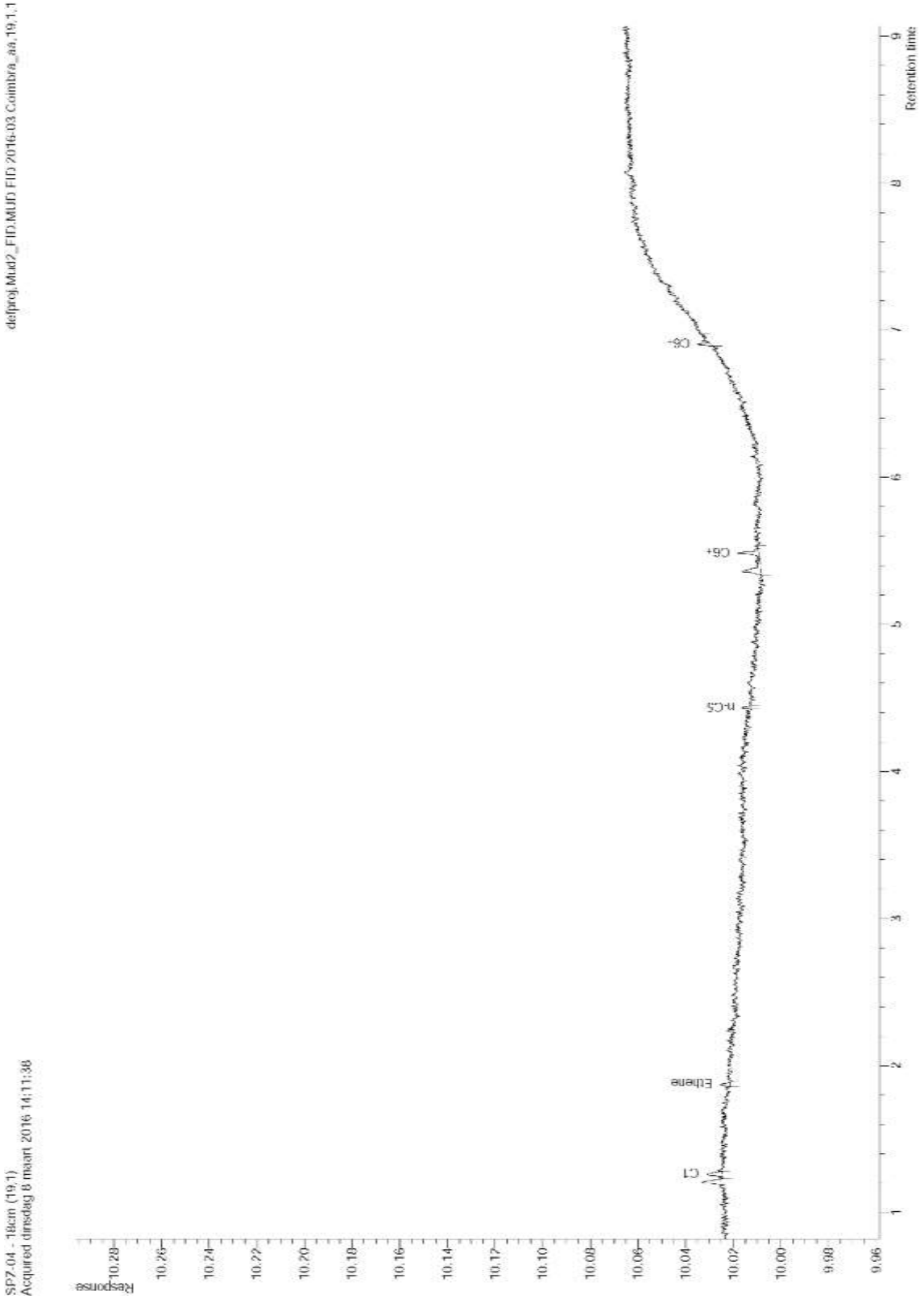

Appendix 10.9: SPZ-04 chromatogram. Retention time (min) x Response (pA).

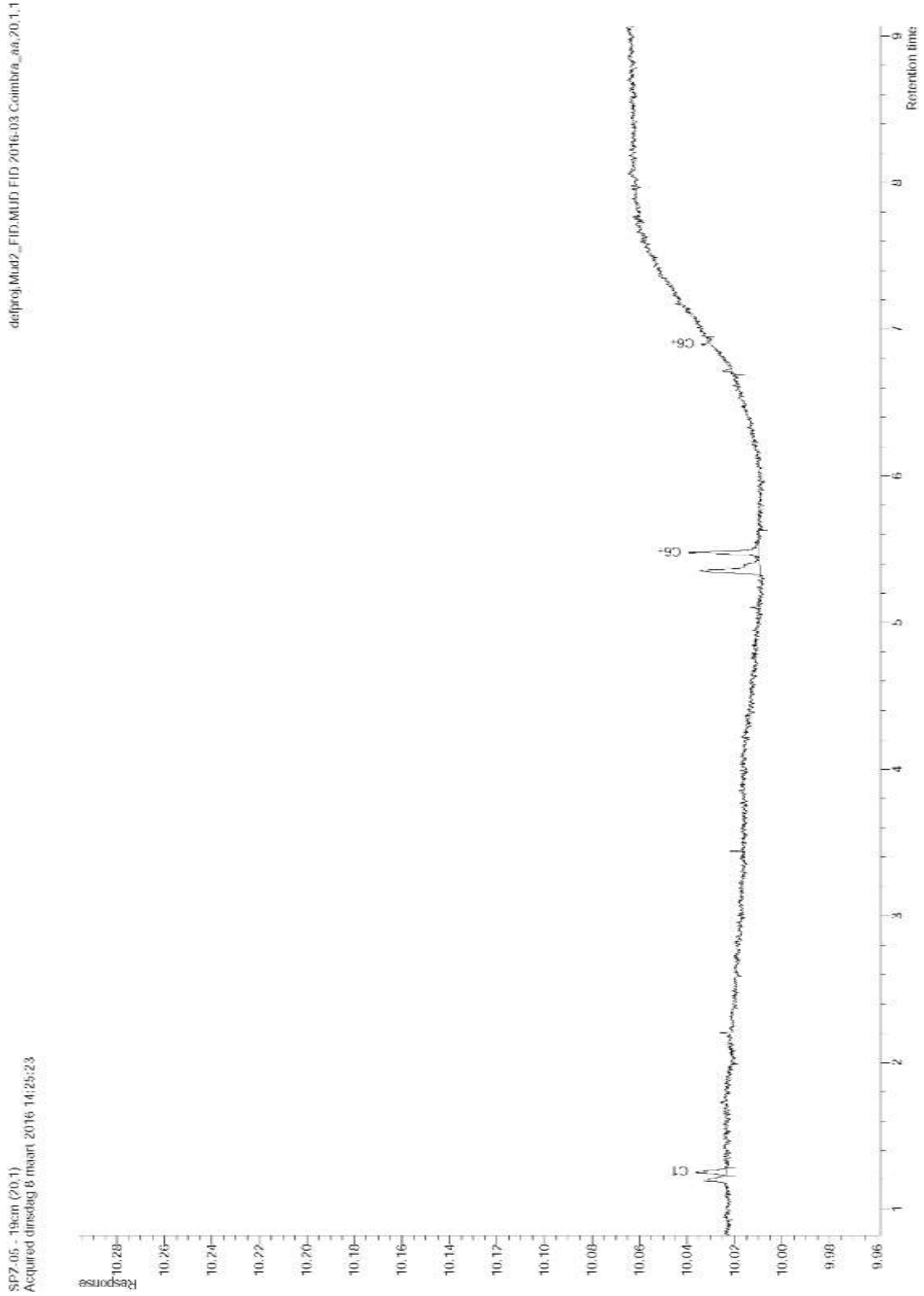

Appendix 10.10: SPZ-05 chromatogram. Retention time (min) x Response (pA).

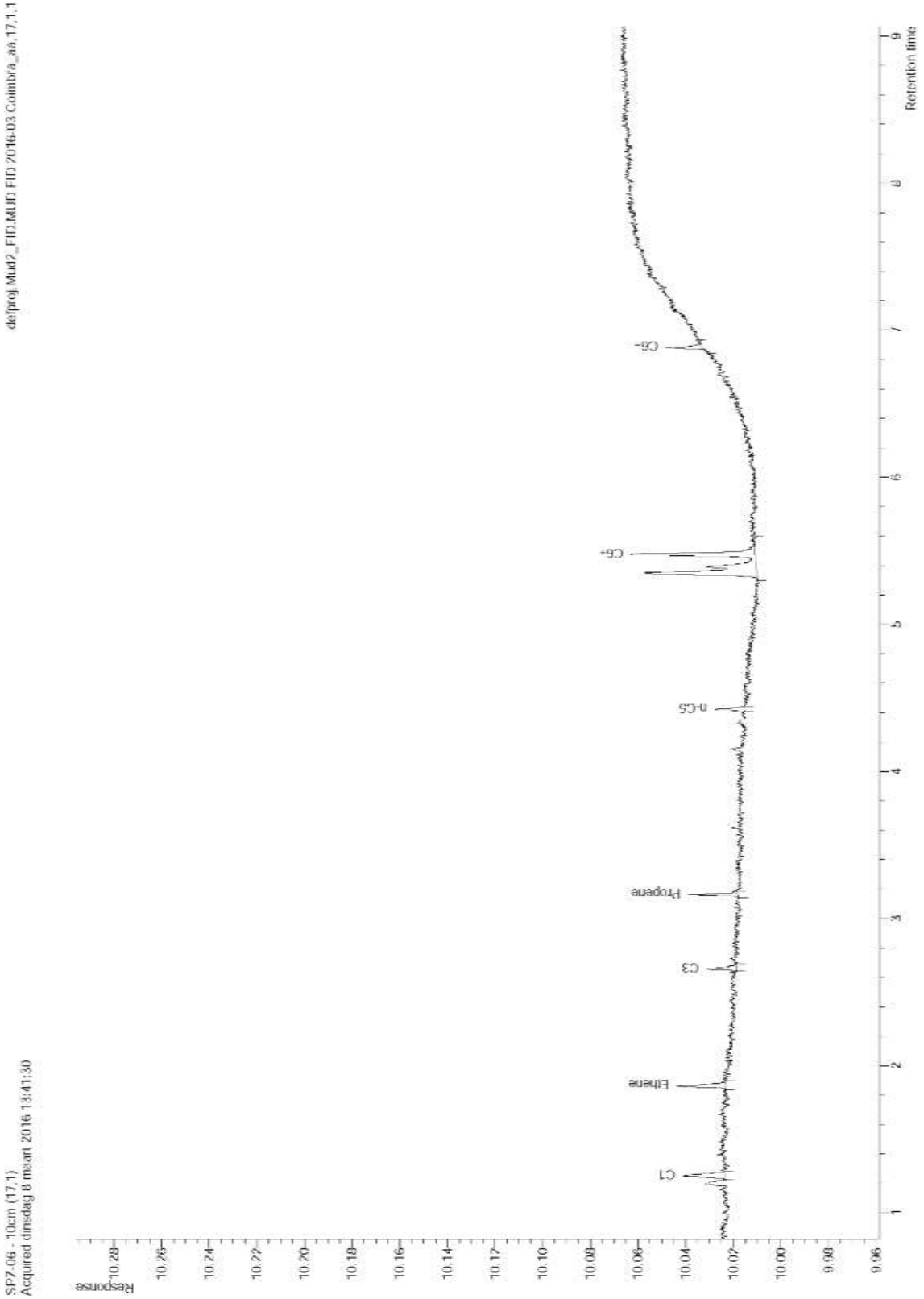

Appendix 10.11: SPZ-06 chromatogram. Retention time (min) x Response (pA).

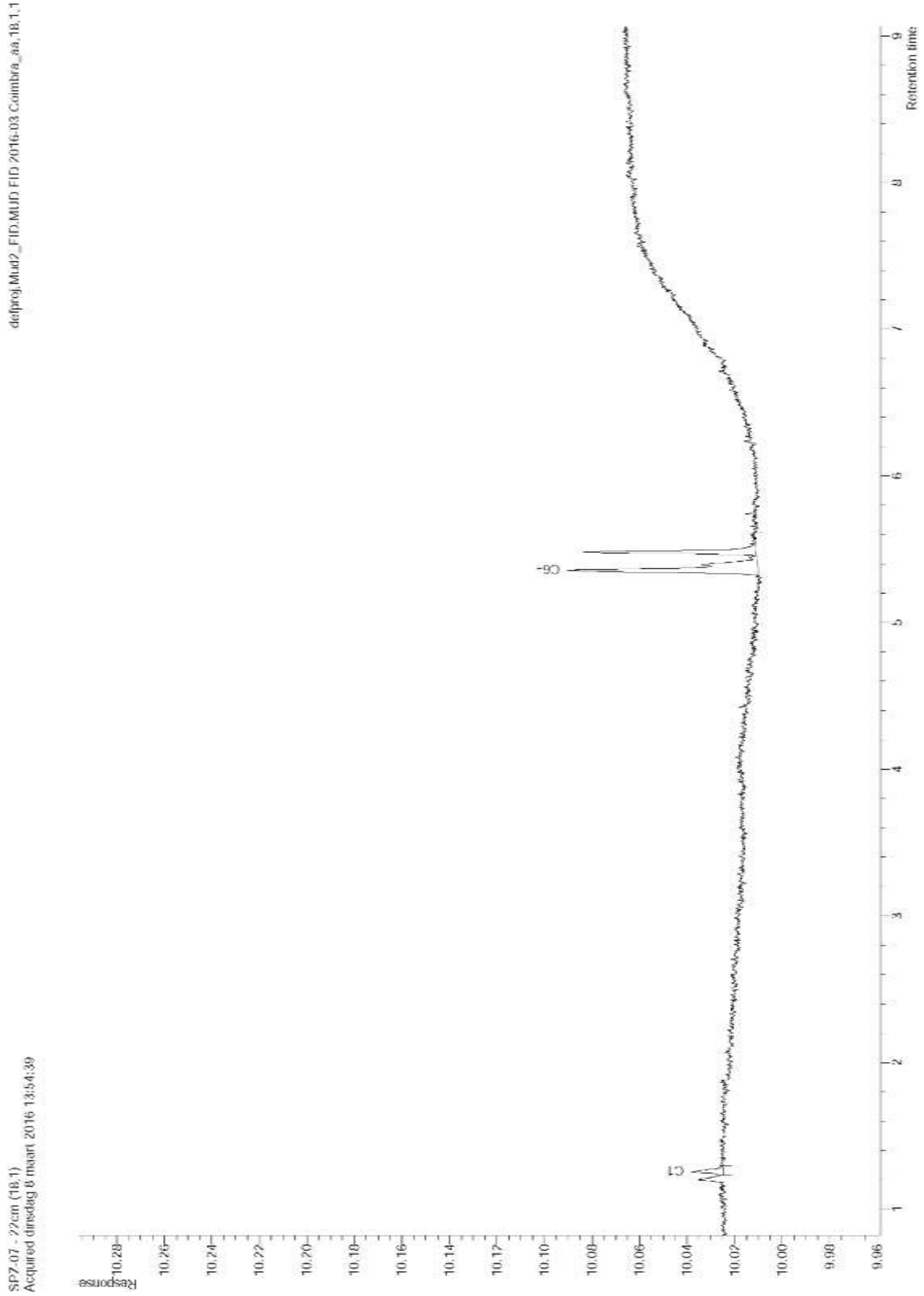

Appendix 10.12: SPZ-07 chromatogram. Retention time (min) x Response (pA).

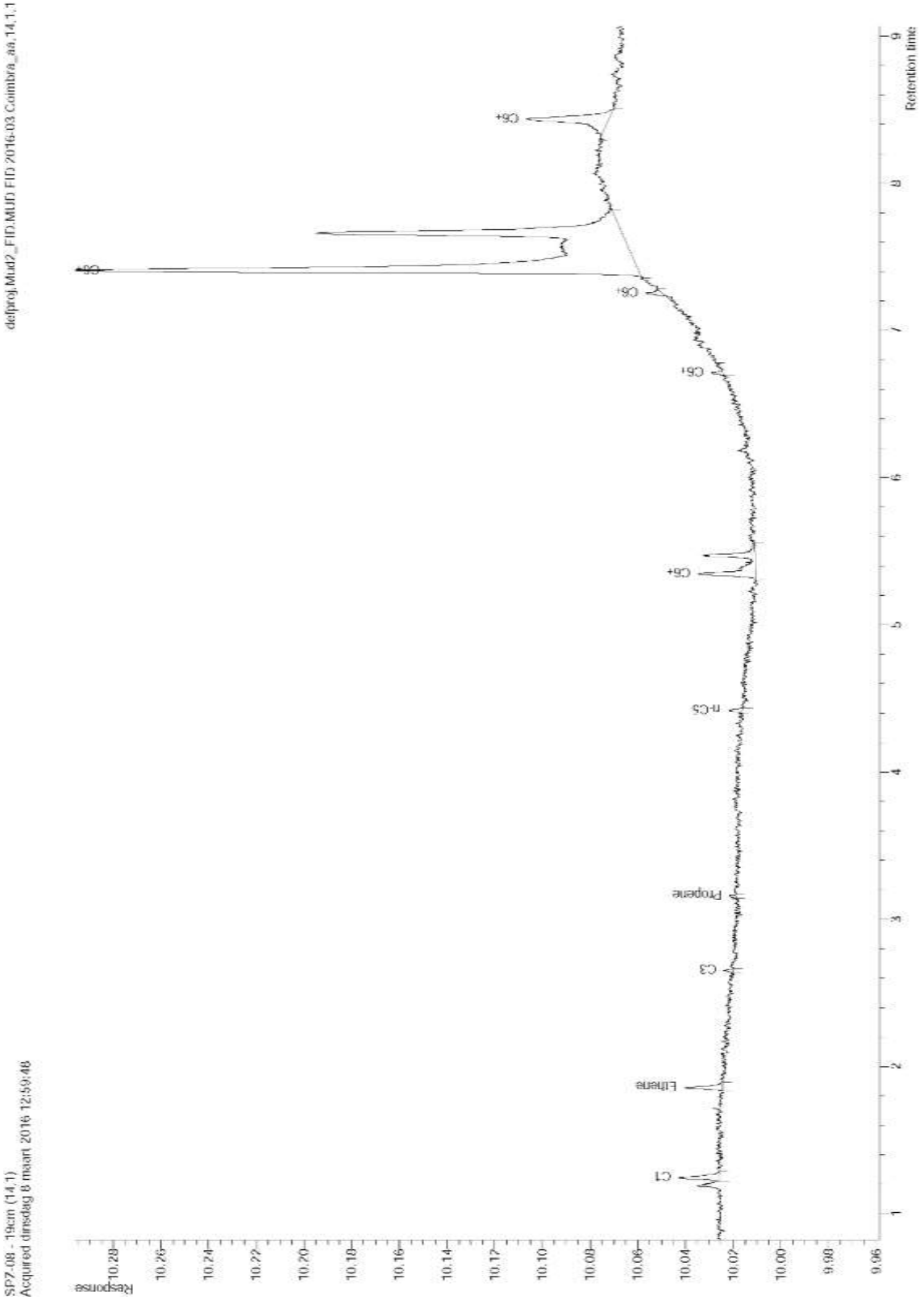

Appendix 10.13: SPZ-08 chromatogram. Retention time (min) x Response (pA).

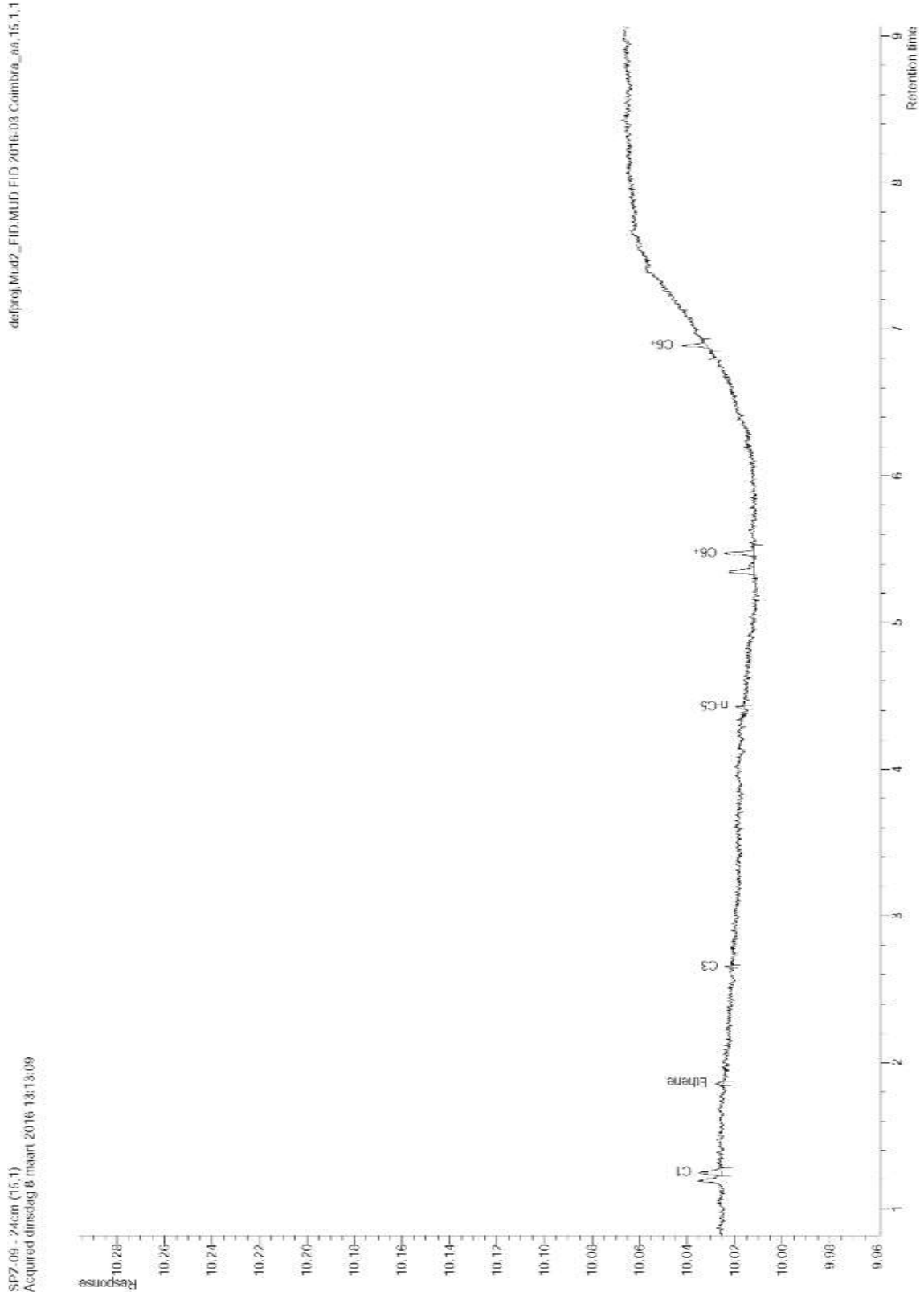

Appendix 10.14: SPZ-09 chromatogram. Retention time (min) x Response (pA).

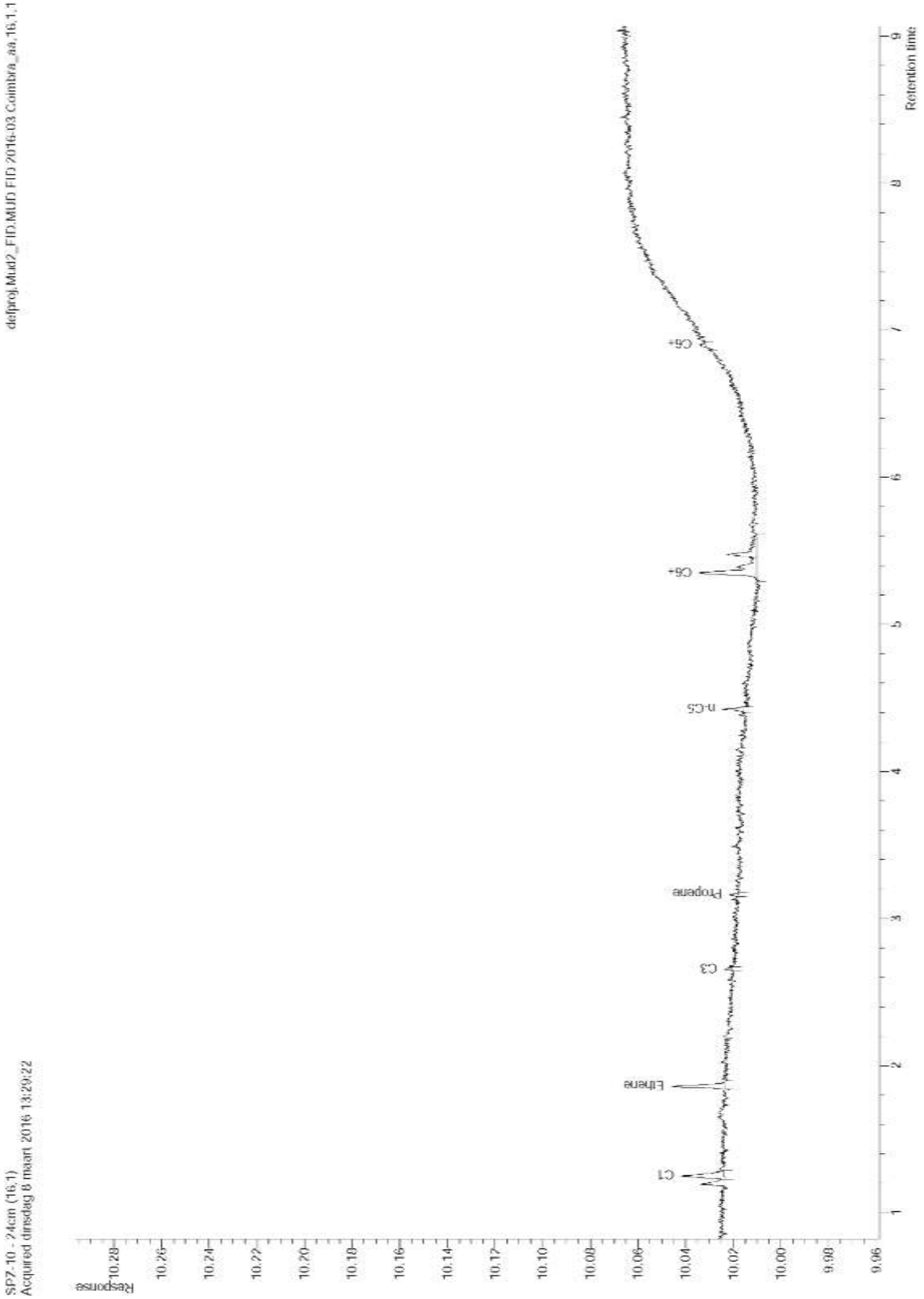

Appendix 10.15: SPZ-10 chromatogram. Retention time (min) x Response (pA).

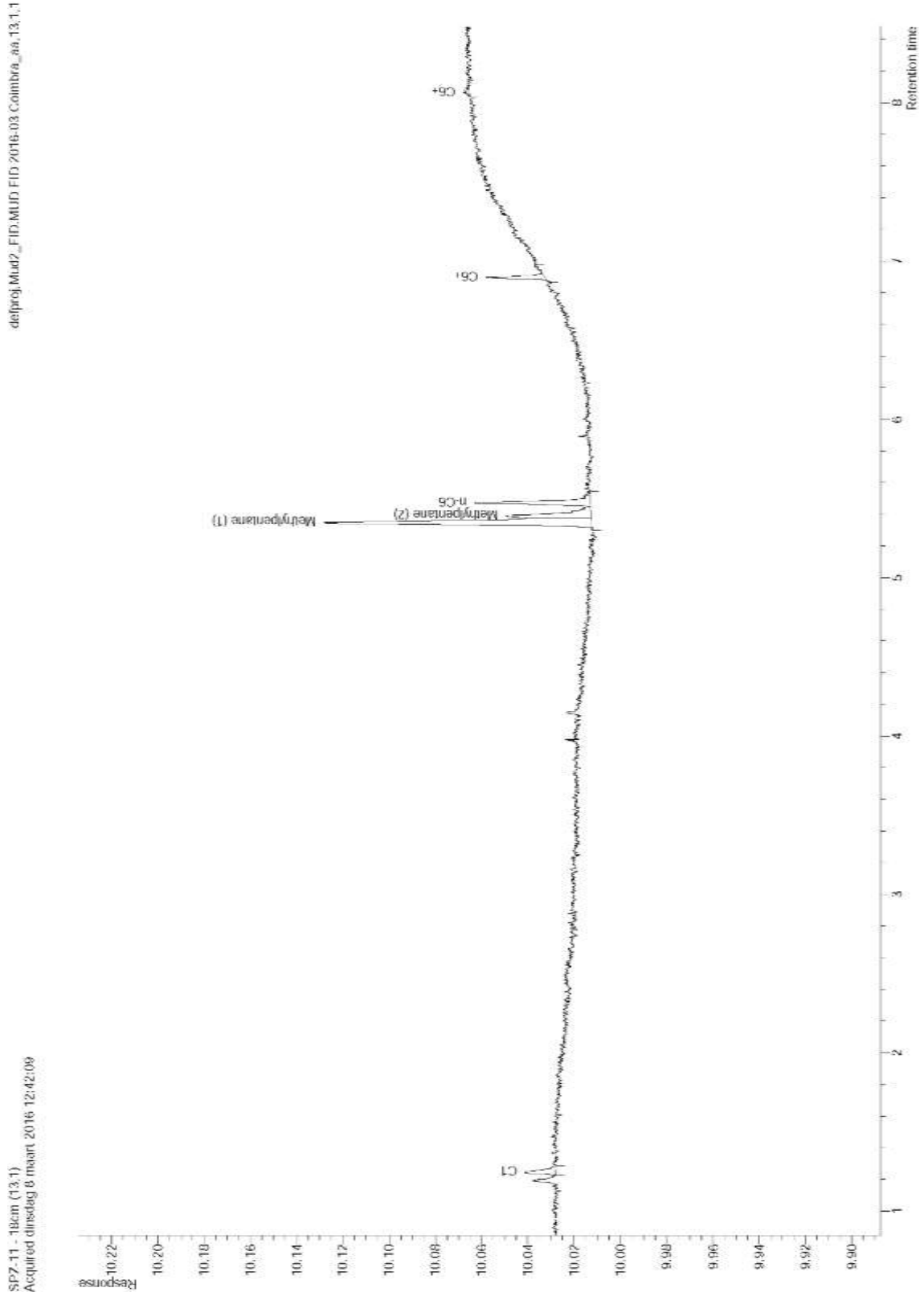

Appendix 10.16: SPZ-11 chromatogram. Retention time (min) x Response (pA).

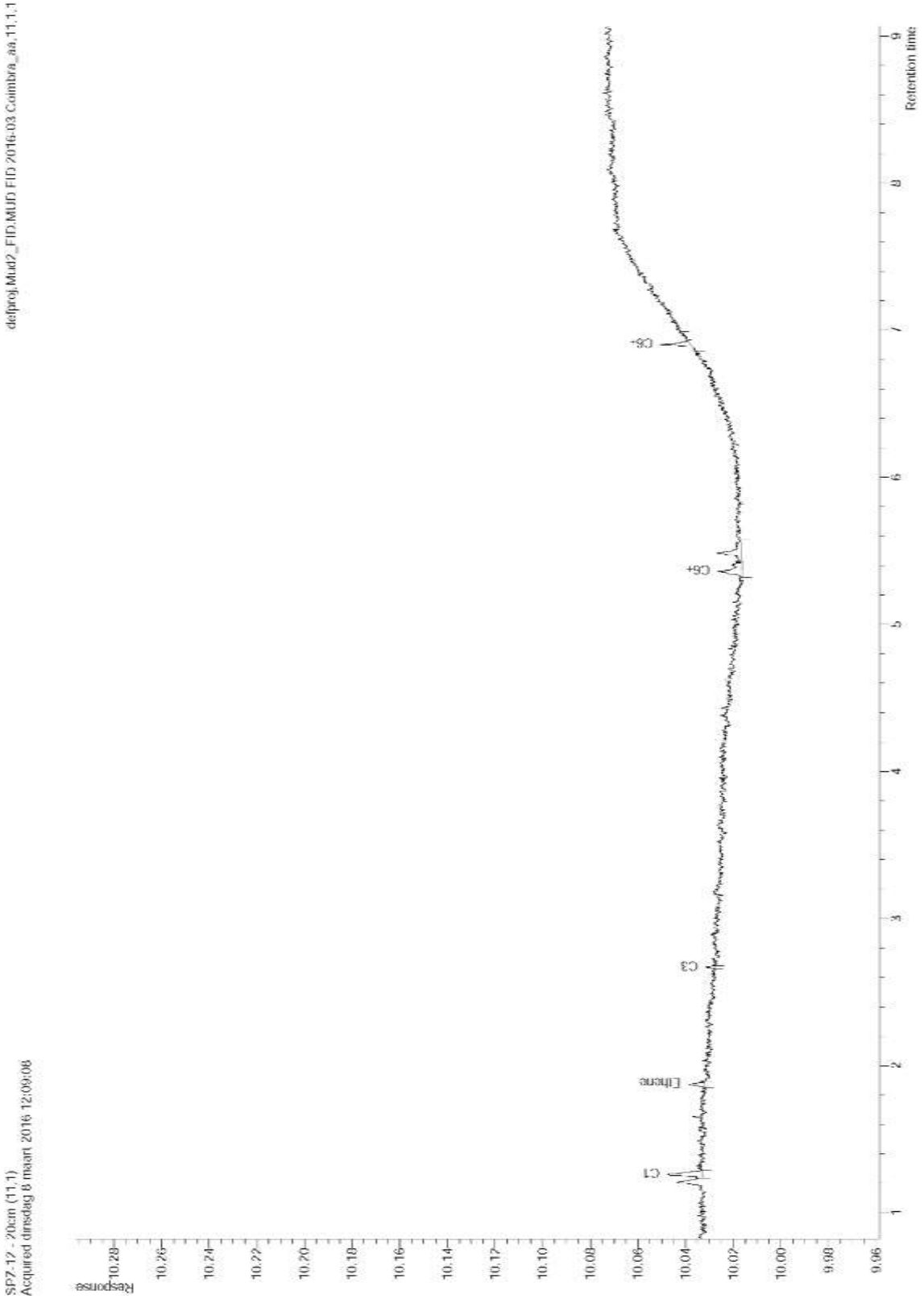

Appendix 10.17: SPZ-12 chromatogram. Retention time (min) x Response (pA).

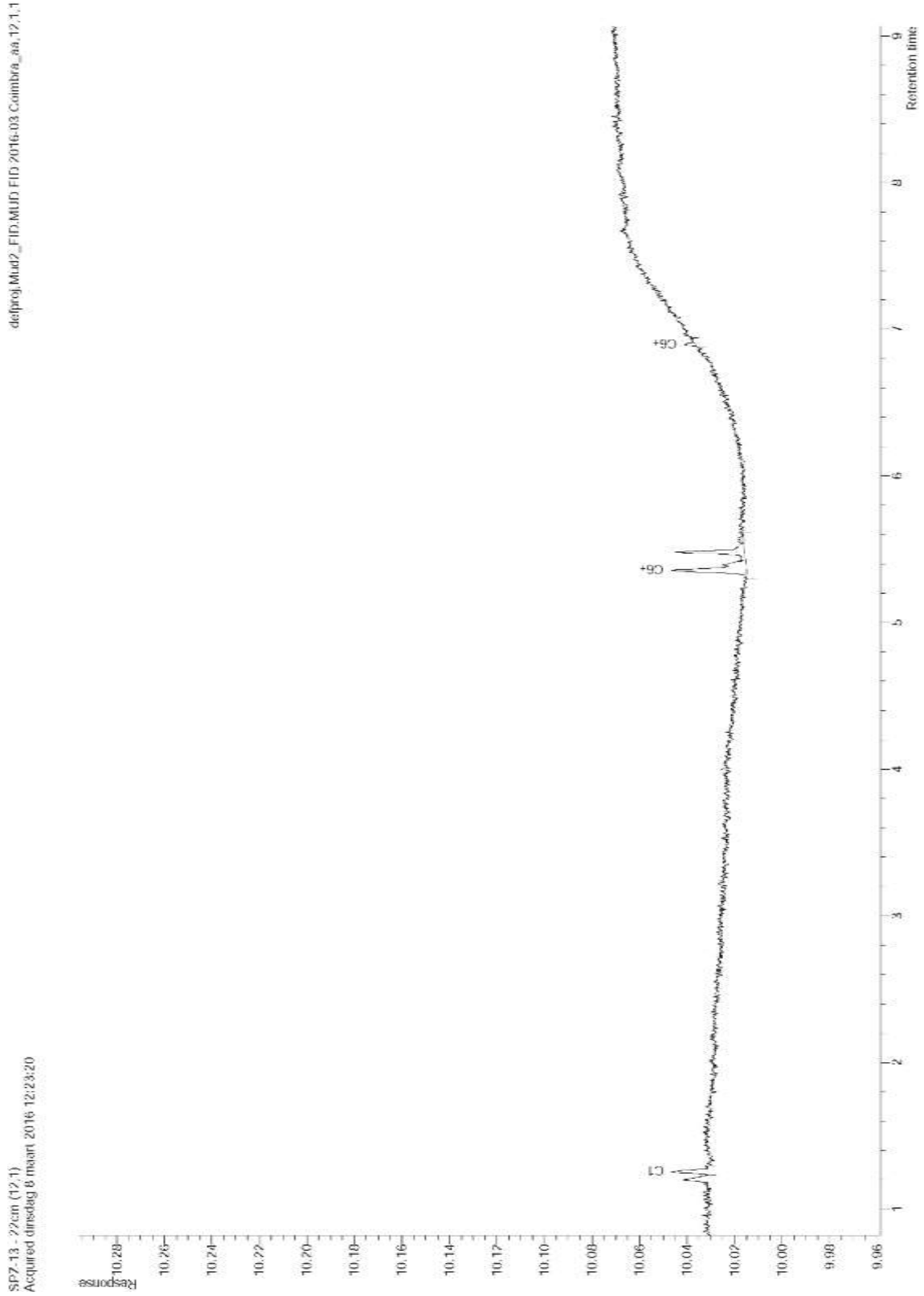

Appendix 10.18: SPZ-13 chromatogram. Retention time (min) x Response (pA).

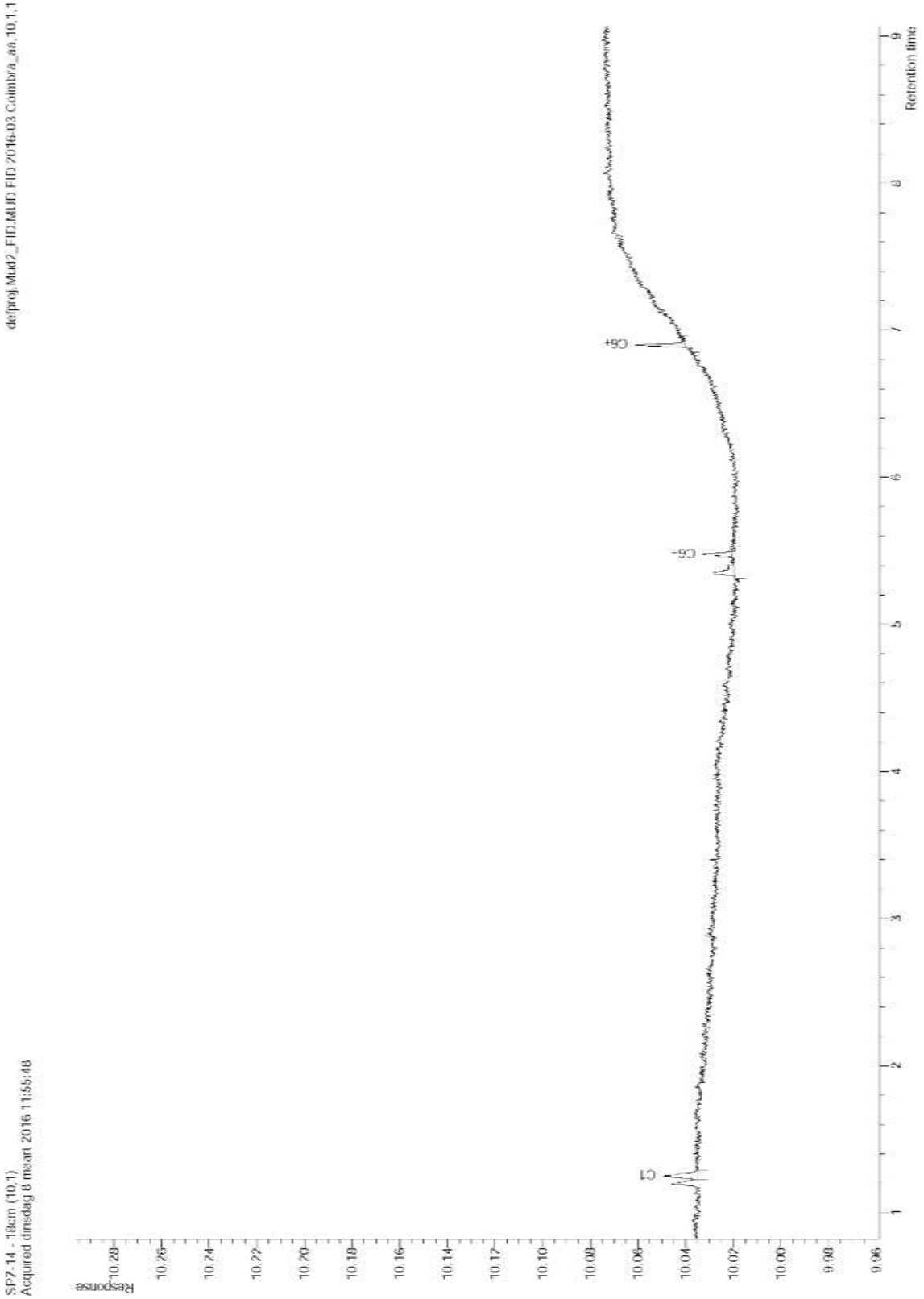

Appendix 10.19: SPZ-14 chromatogram. Retention time (min) x Response (pA).

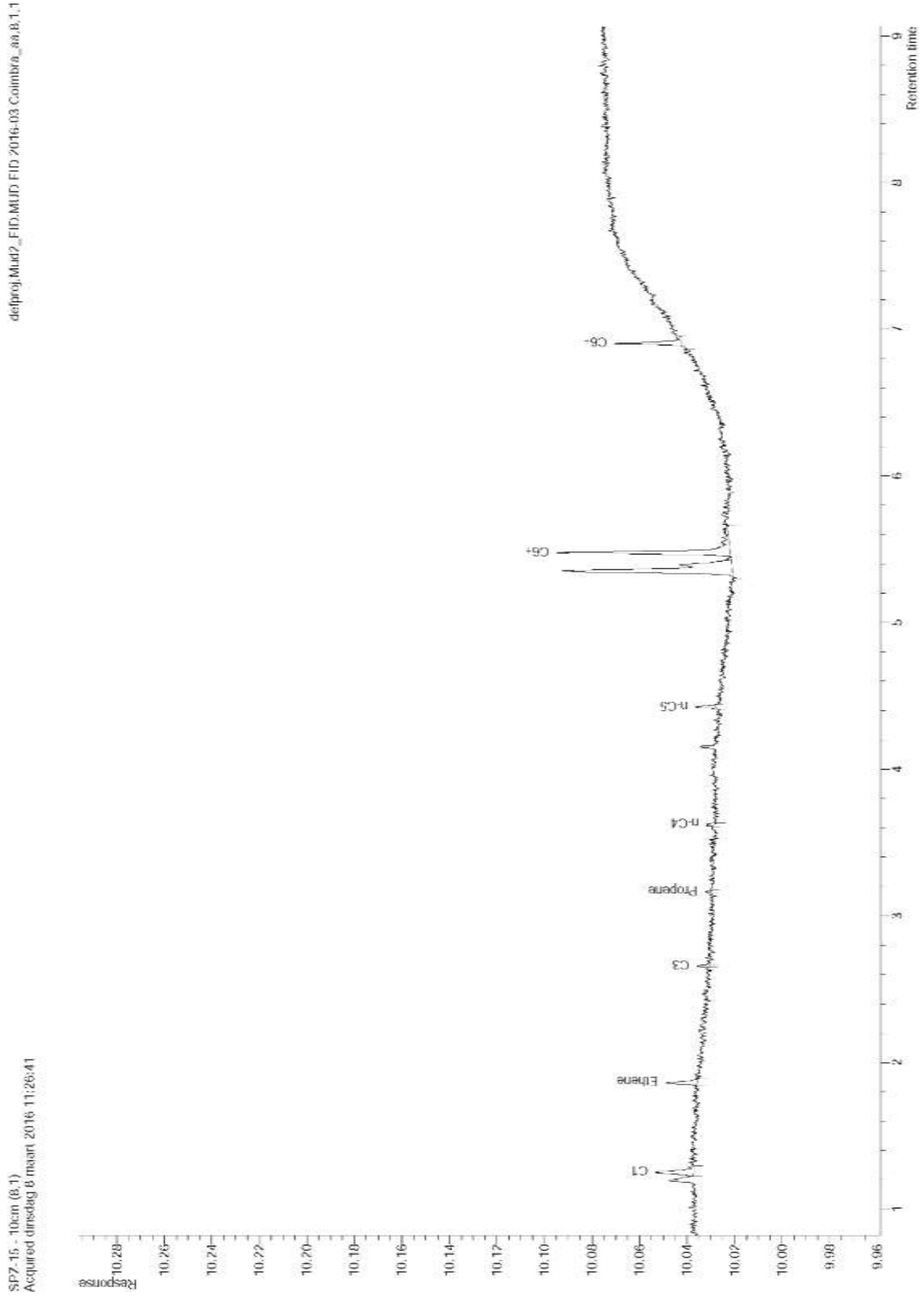

Appendix 10.20: SPZ-15 chromatogram. Retention time (min) x Response (pA).

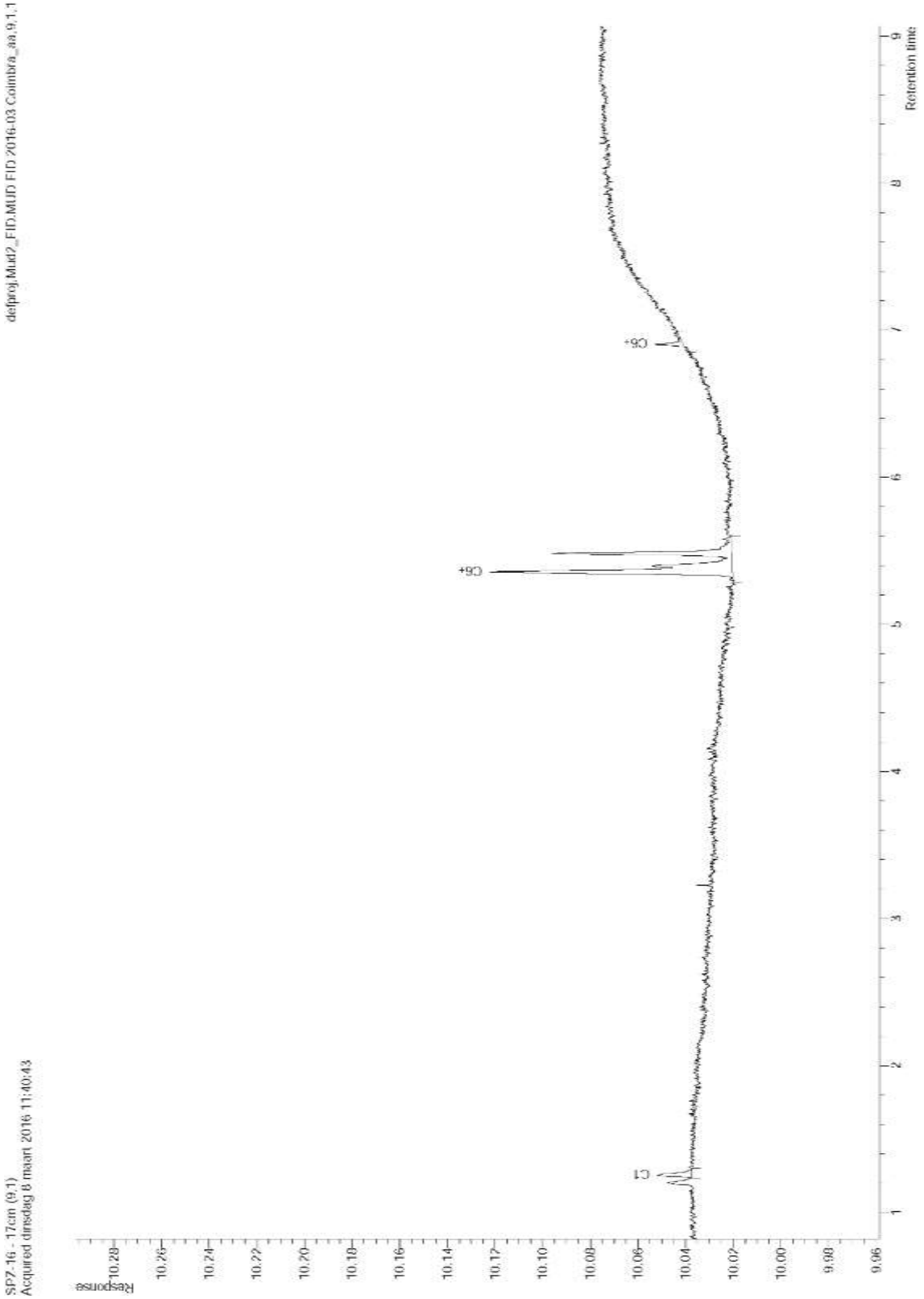

Appendix 10.21: SPZ-16 chromatogram. Retention time (min) x Response (pA).

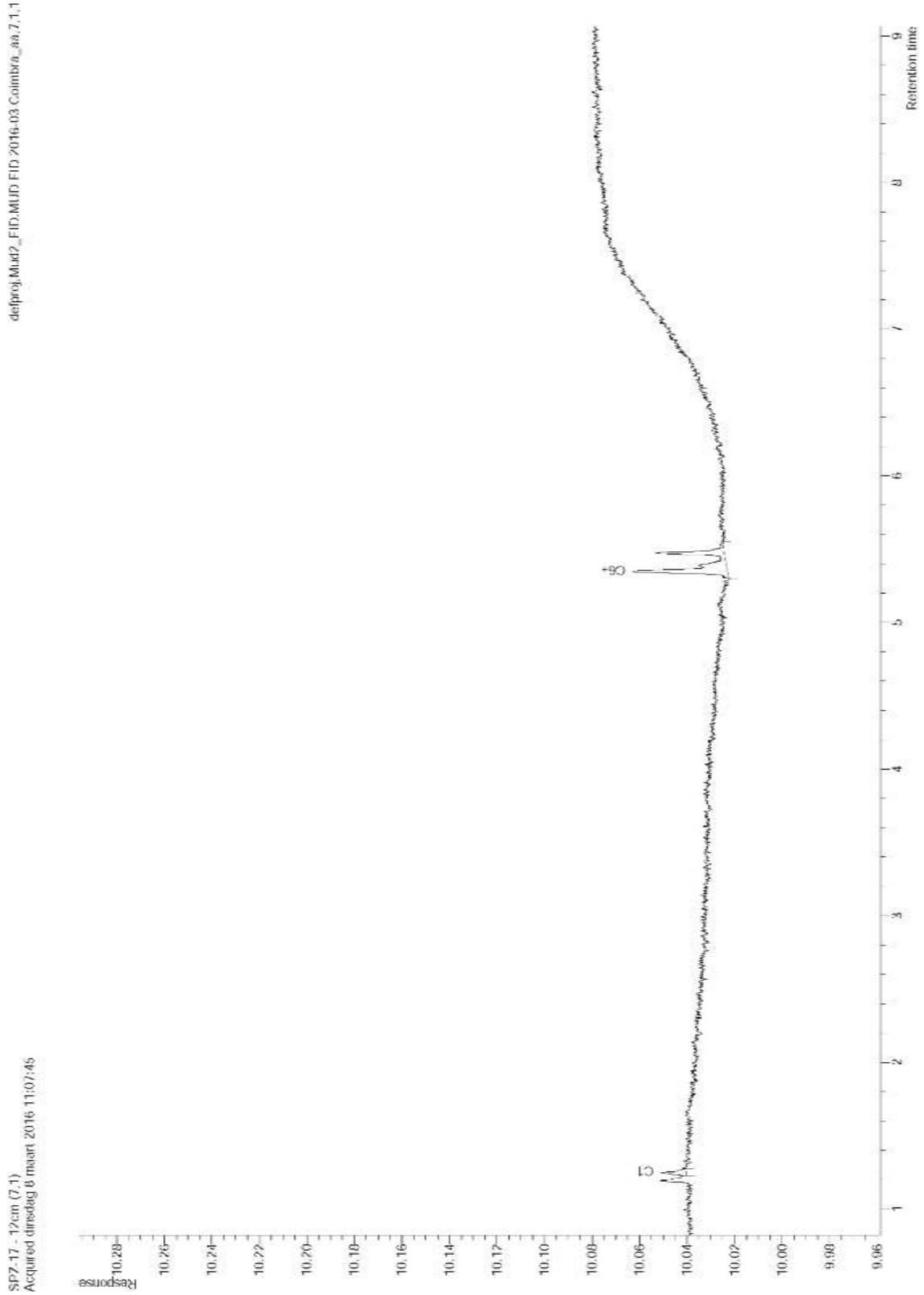

Appendix 10.22: SPZ-17 chromatogram. Retention time (min) x Response (pA).

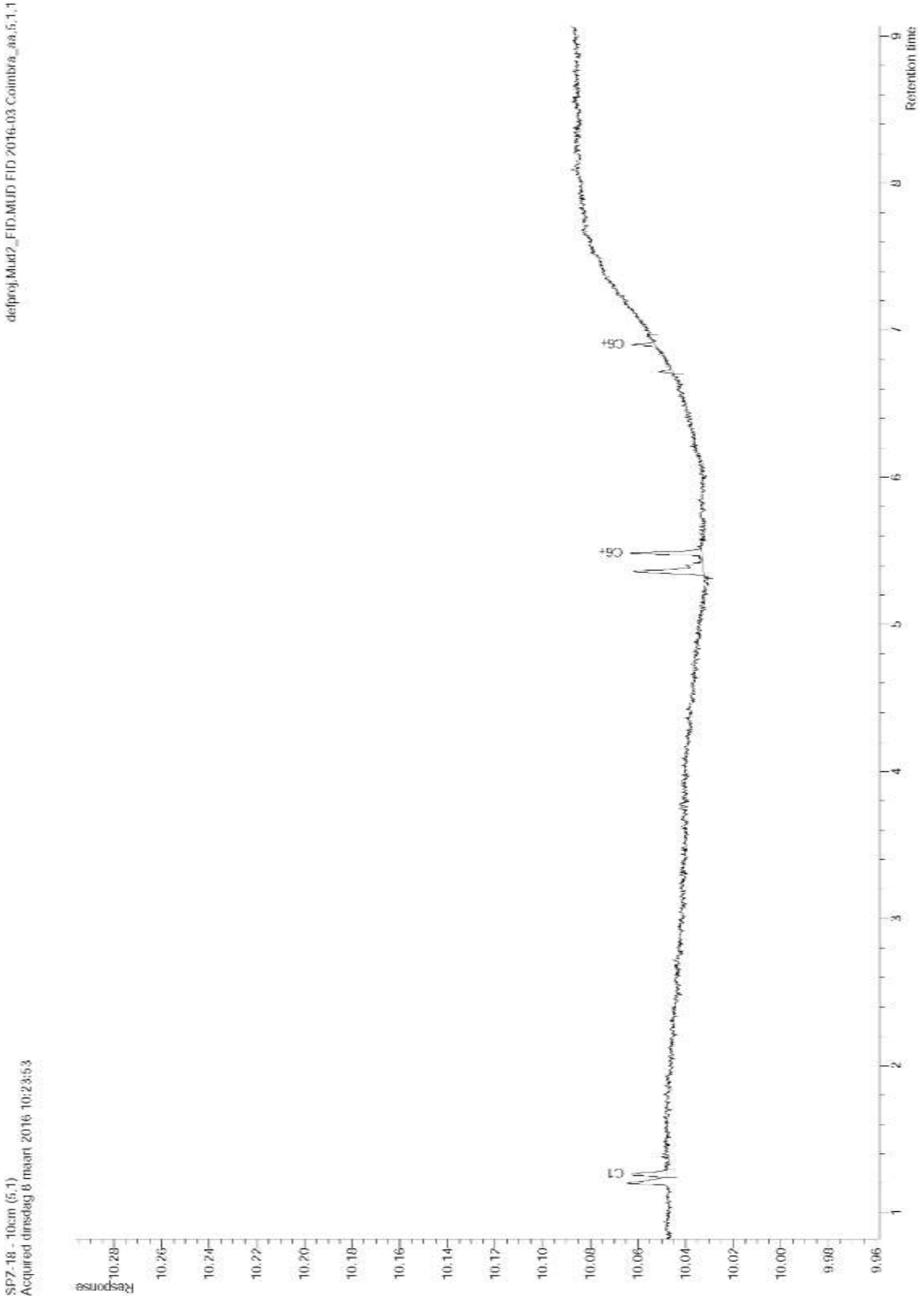

Appendix 10.23: SPZ-18 chromatogram. Retention time (min) x Response (pA).

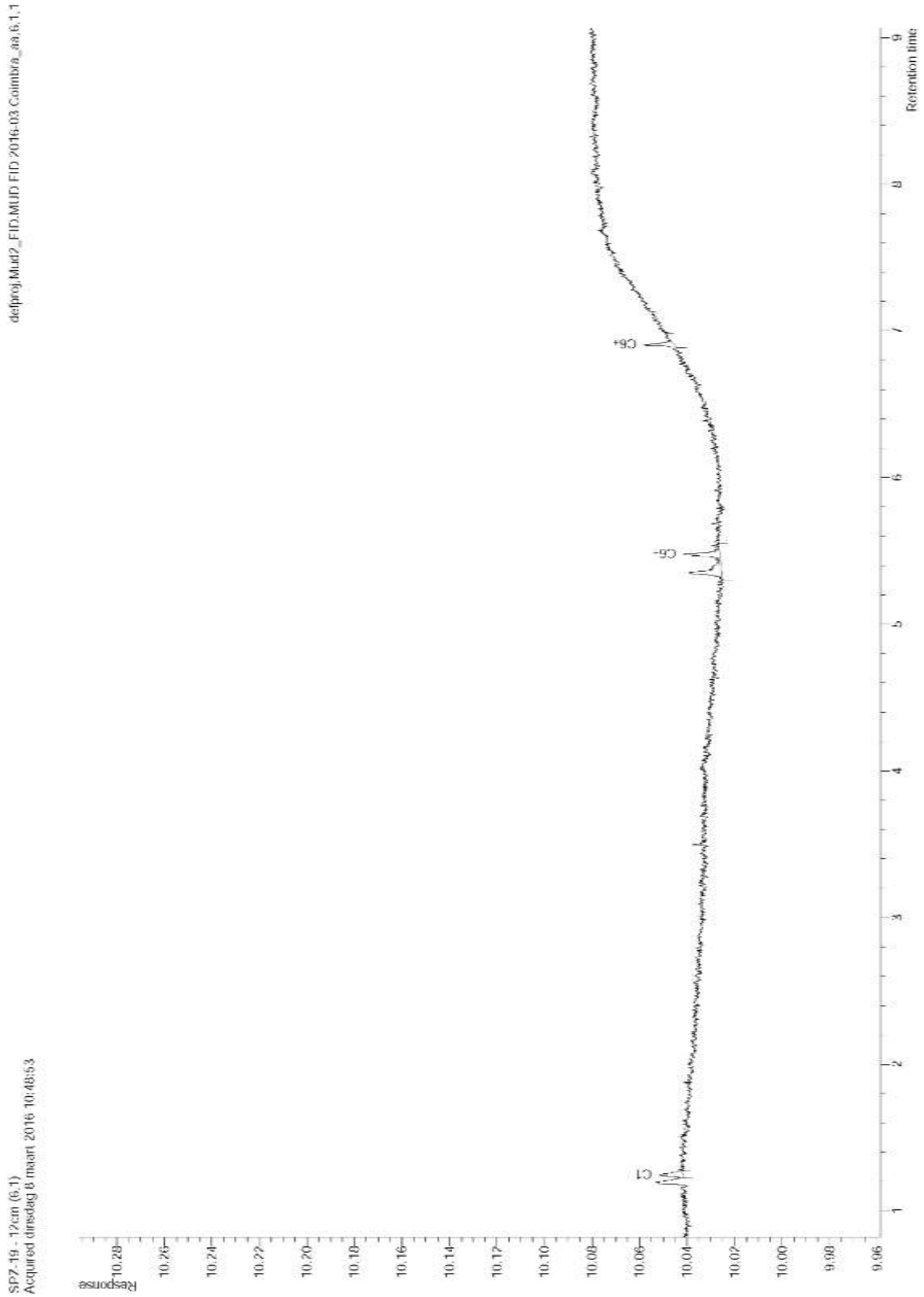

Appendix 10.24: SPZ-19 chromatogram. Retention time (min) x Response (pA).

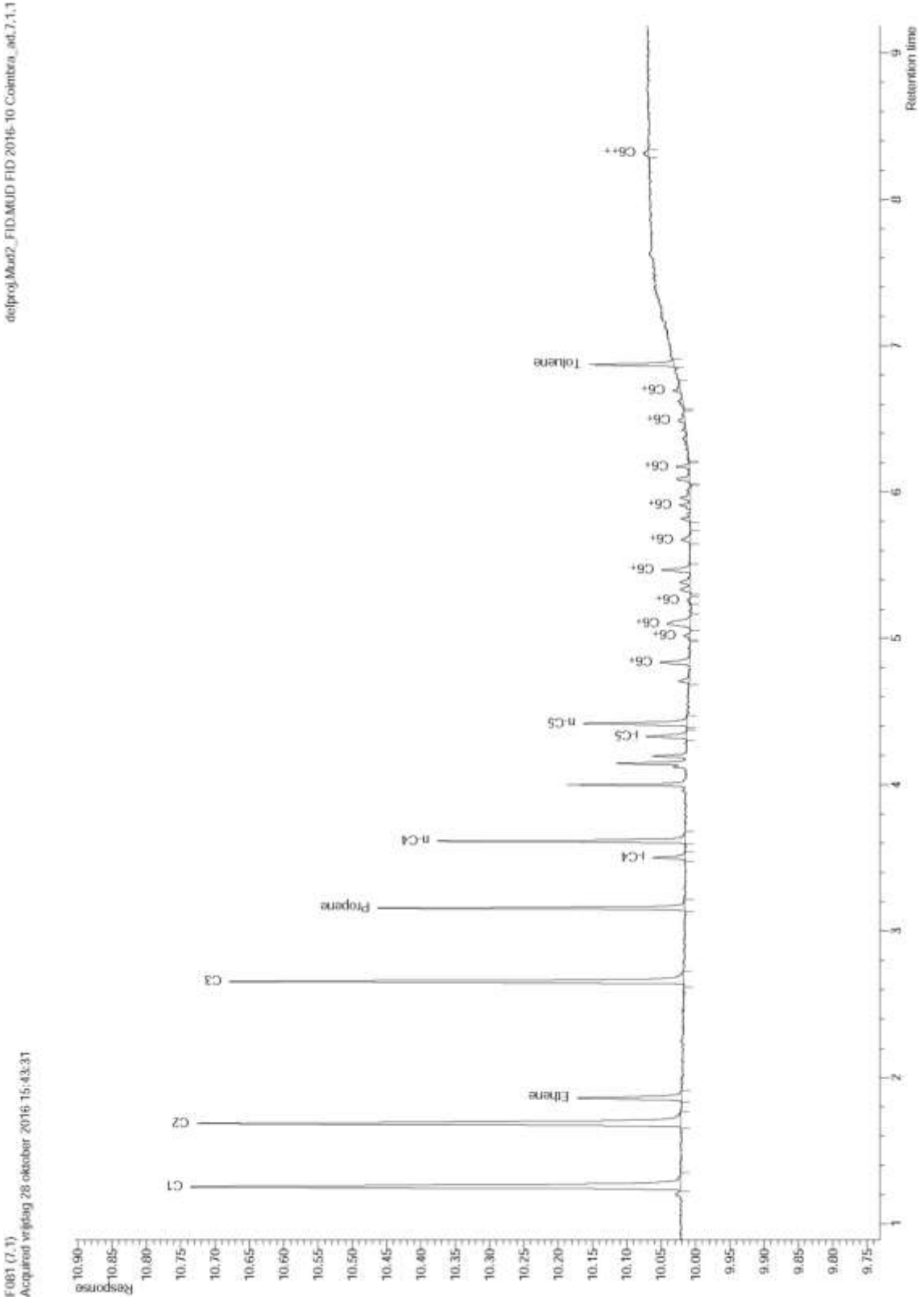

Appendix 10.25: F081 chromatogram. Retention time (min) x Response (pA).

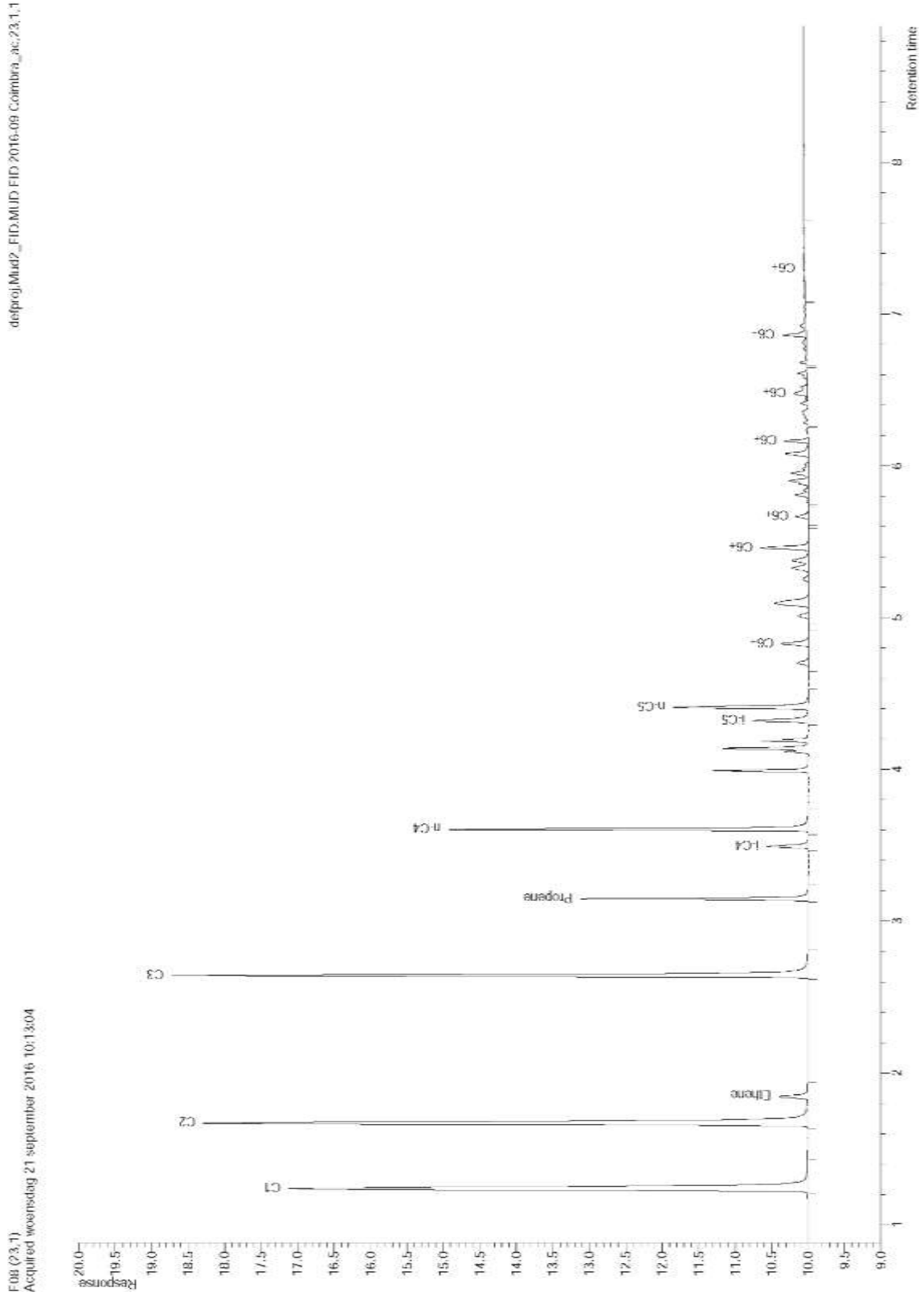

Appendix 10.26: F08 chromatogram. Retention time (min) x Response (pA).

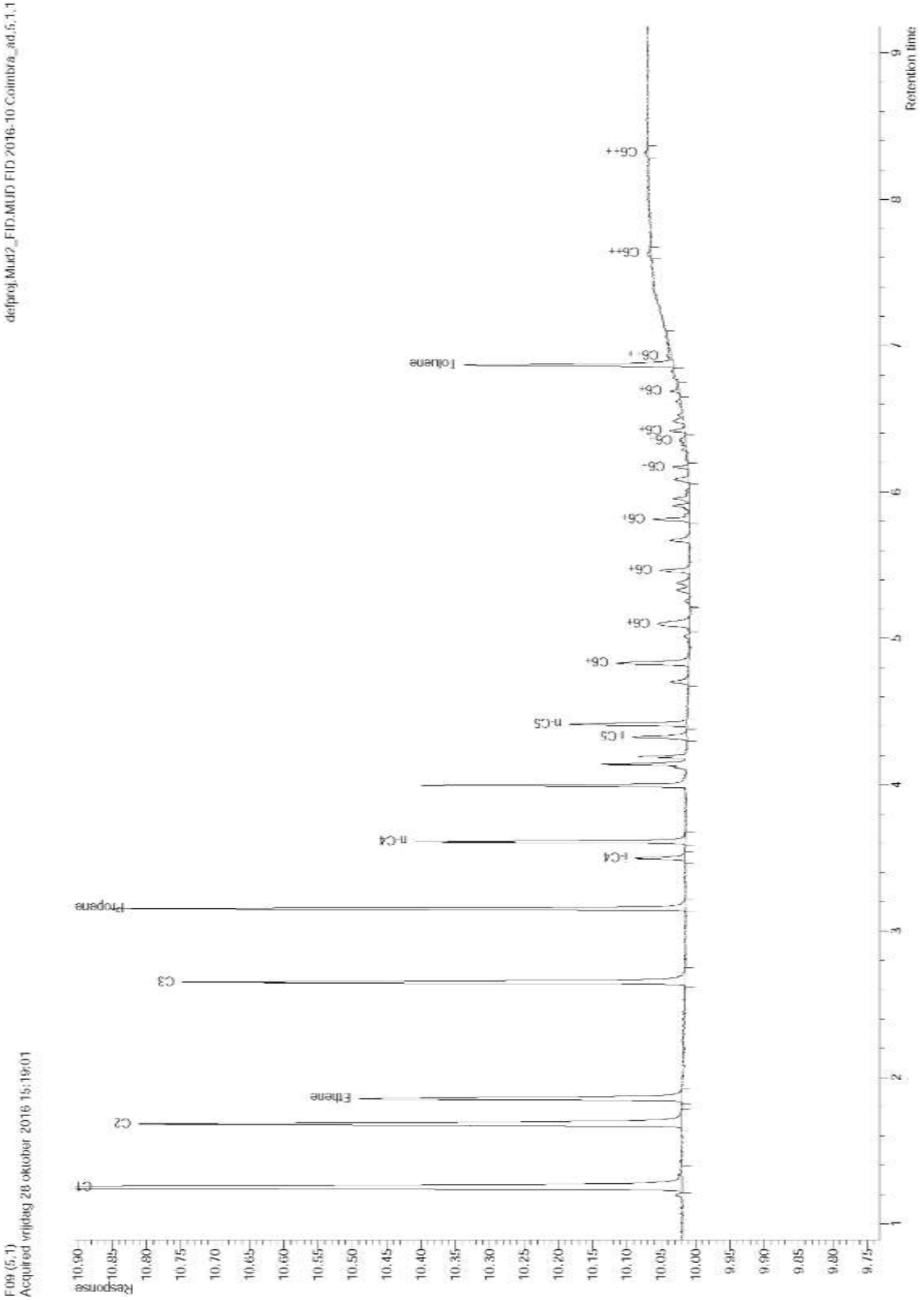

Appendix 10.27: F09 chromatogram. Retention time (min) x Response (pA).

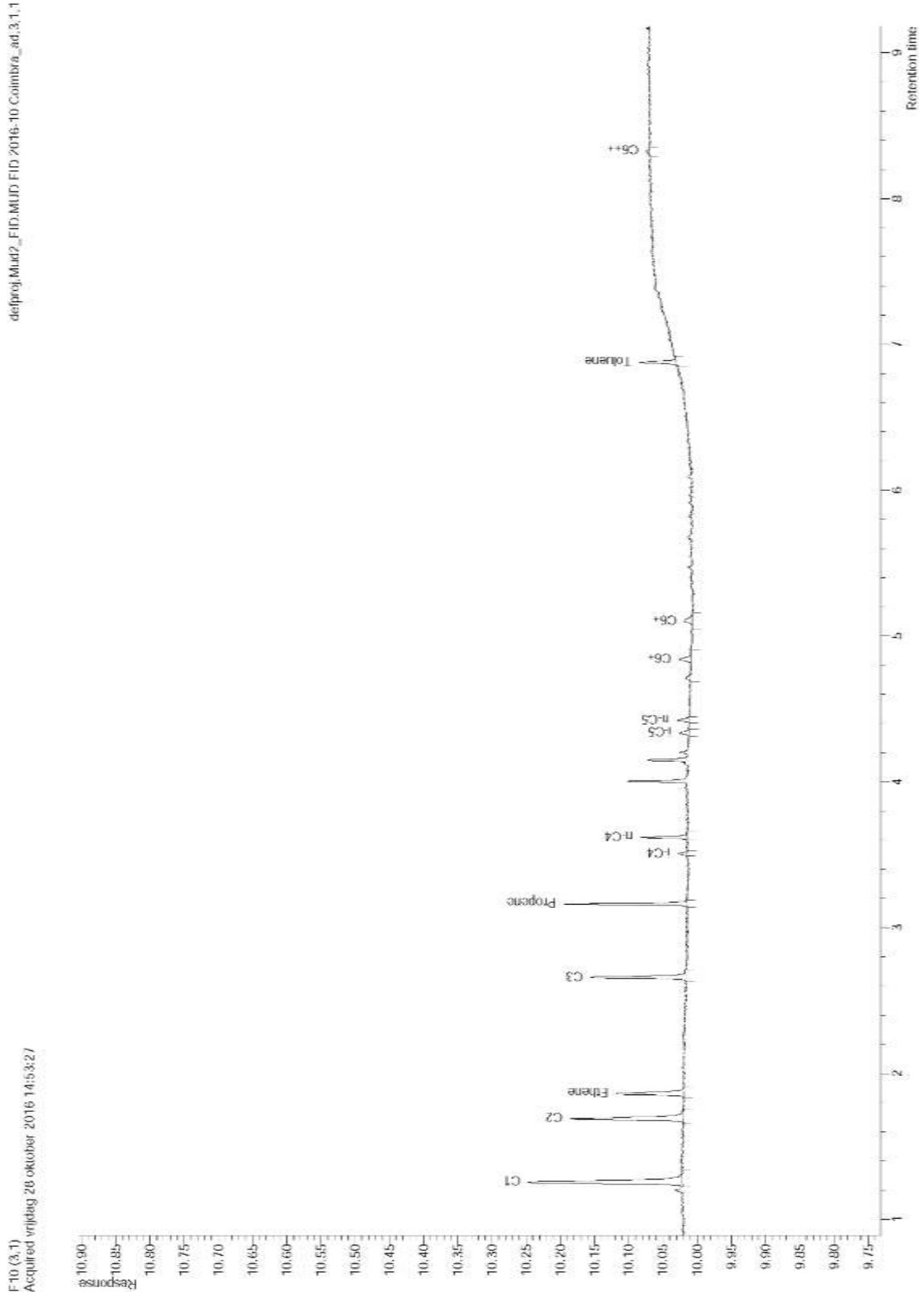

Appendix 10.28: F10 chromatogram. Retention time (min) x Response (pA).

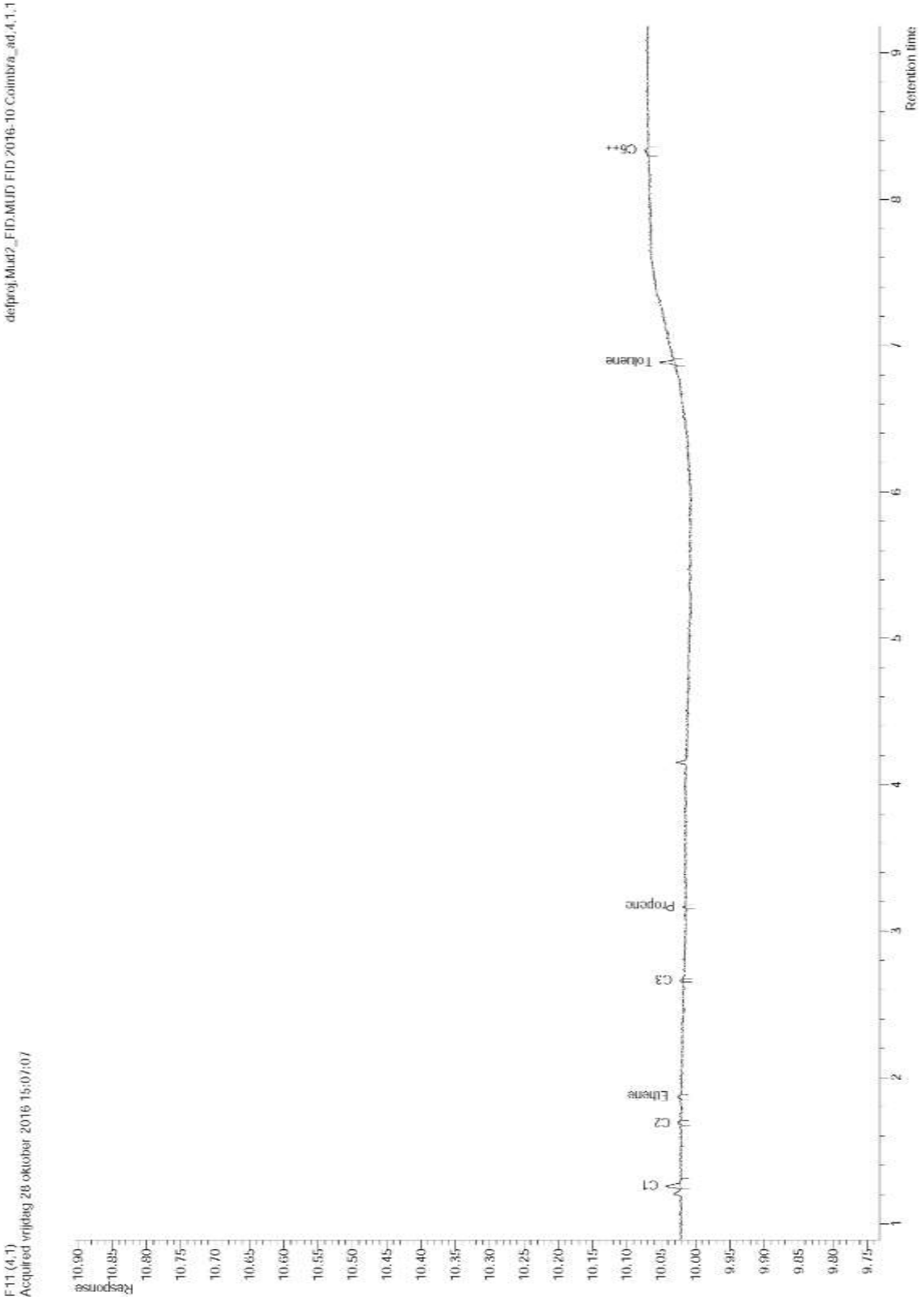

Appendix 10.29: F11 chromatogram. Retention time (min) x Response (pA).

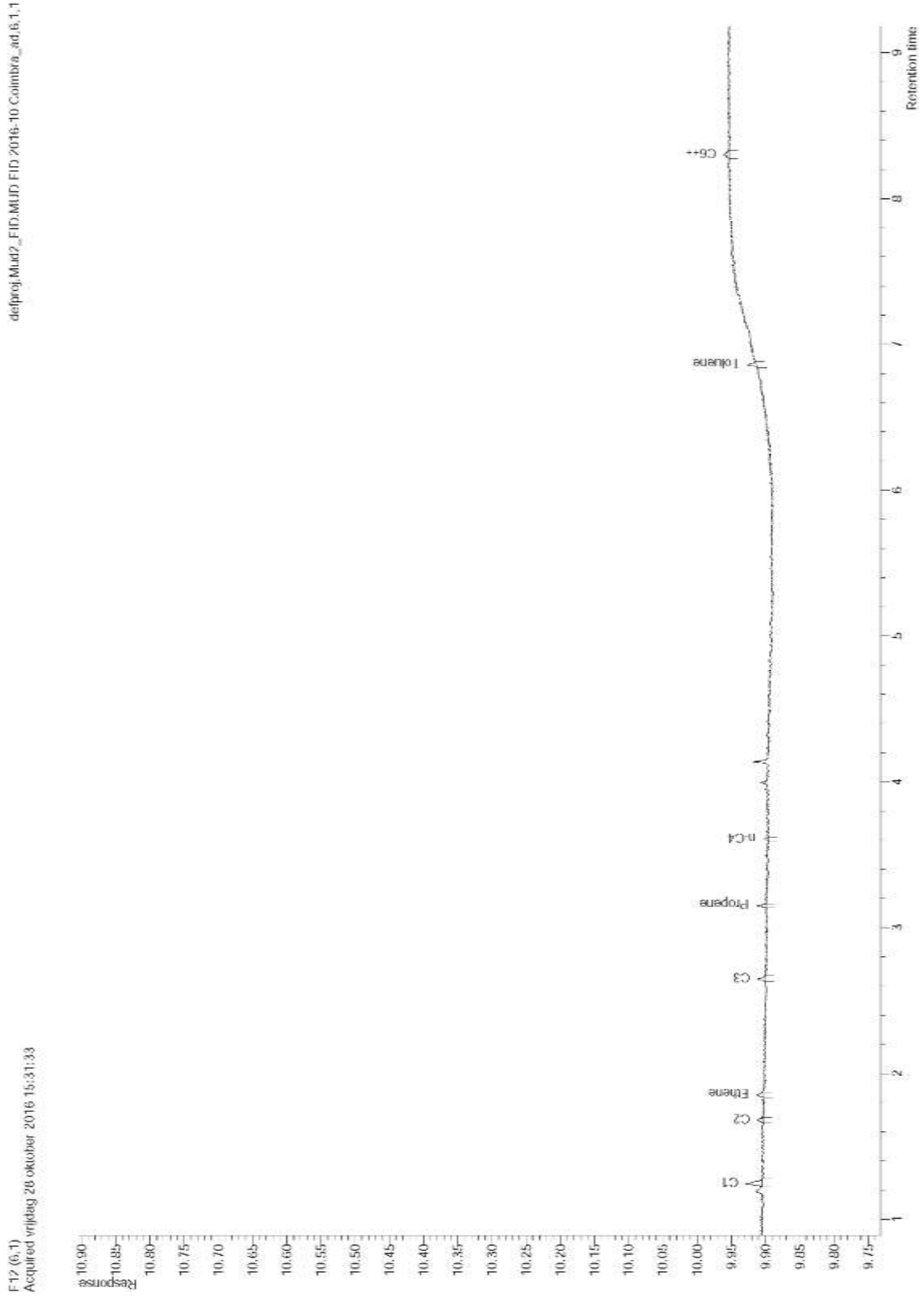

Appendix 10.30: F12 chromatogram. Retention time (min) x Response (pA).

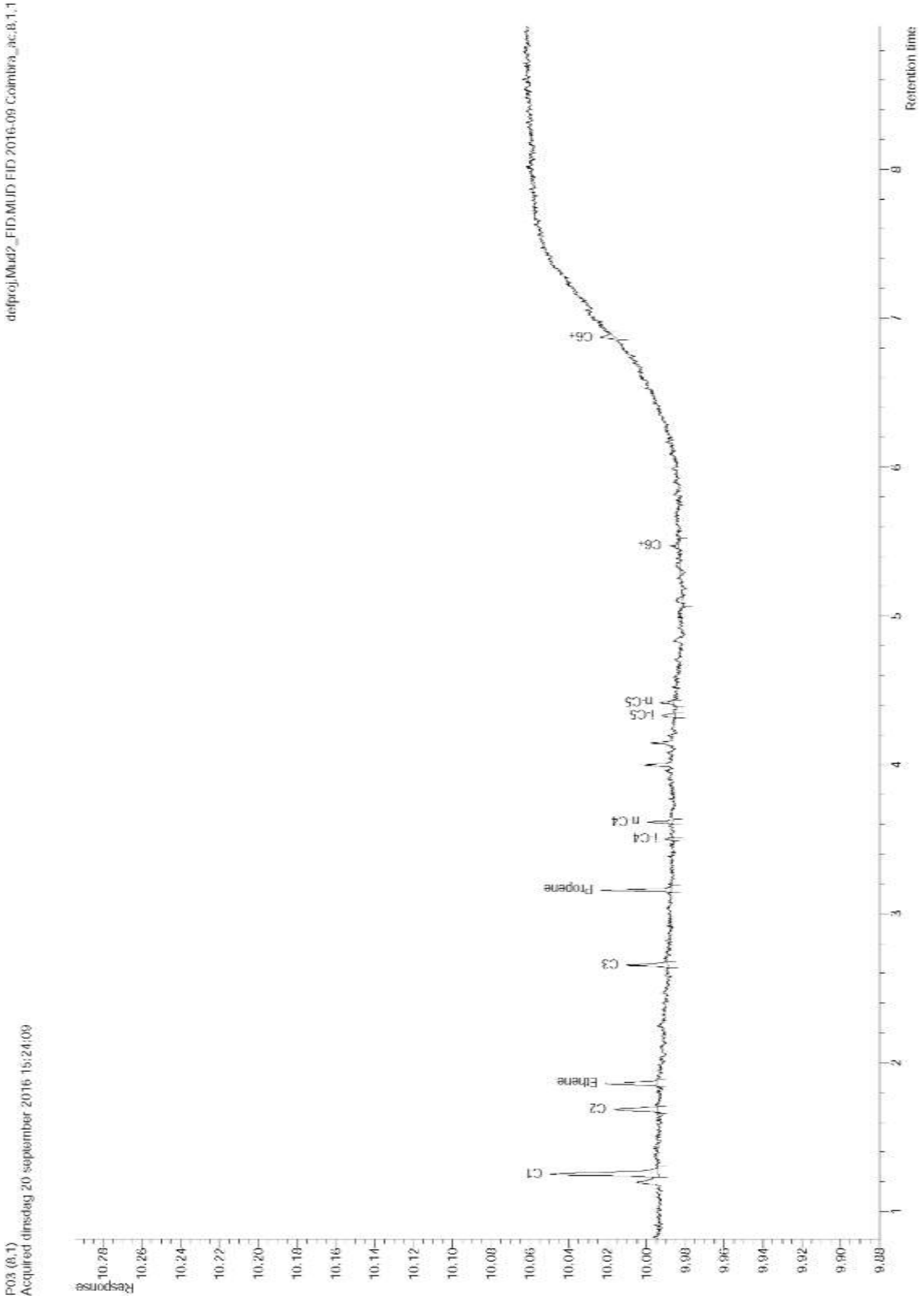

Appendix 10.31: P03 chromatogram. Retention time (min) x Response (pA).

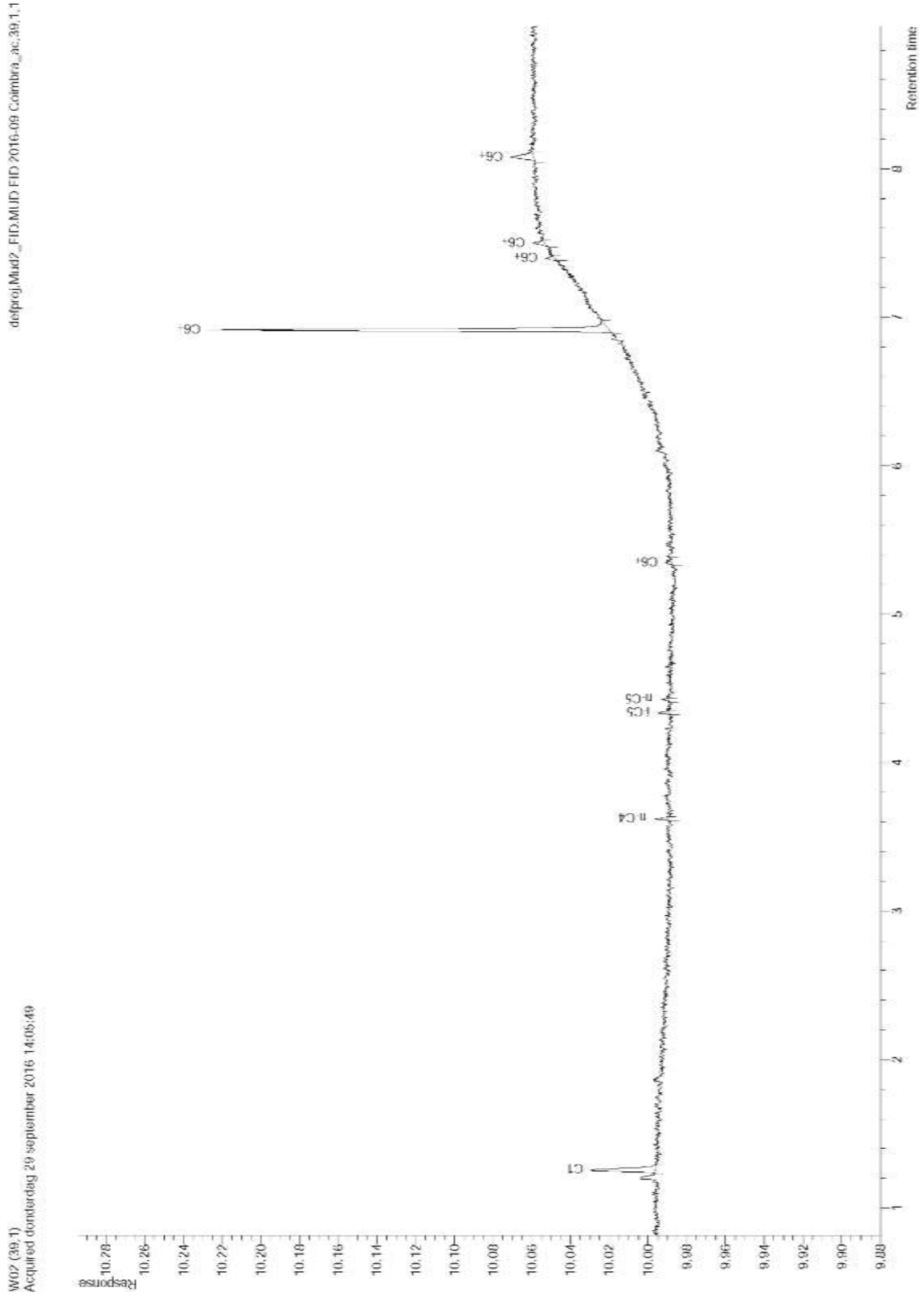

Appendix 10.32: W02 chromatogram. Retention time (min) x Response (pA).

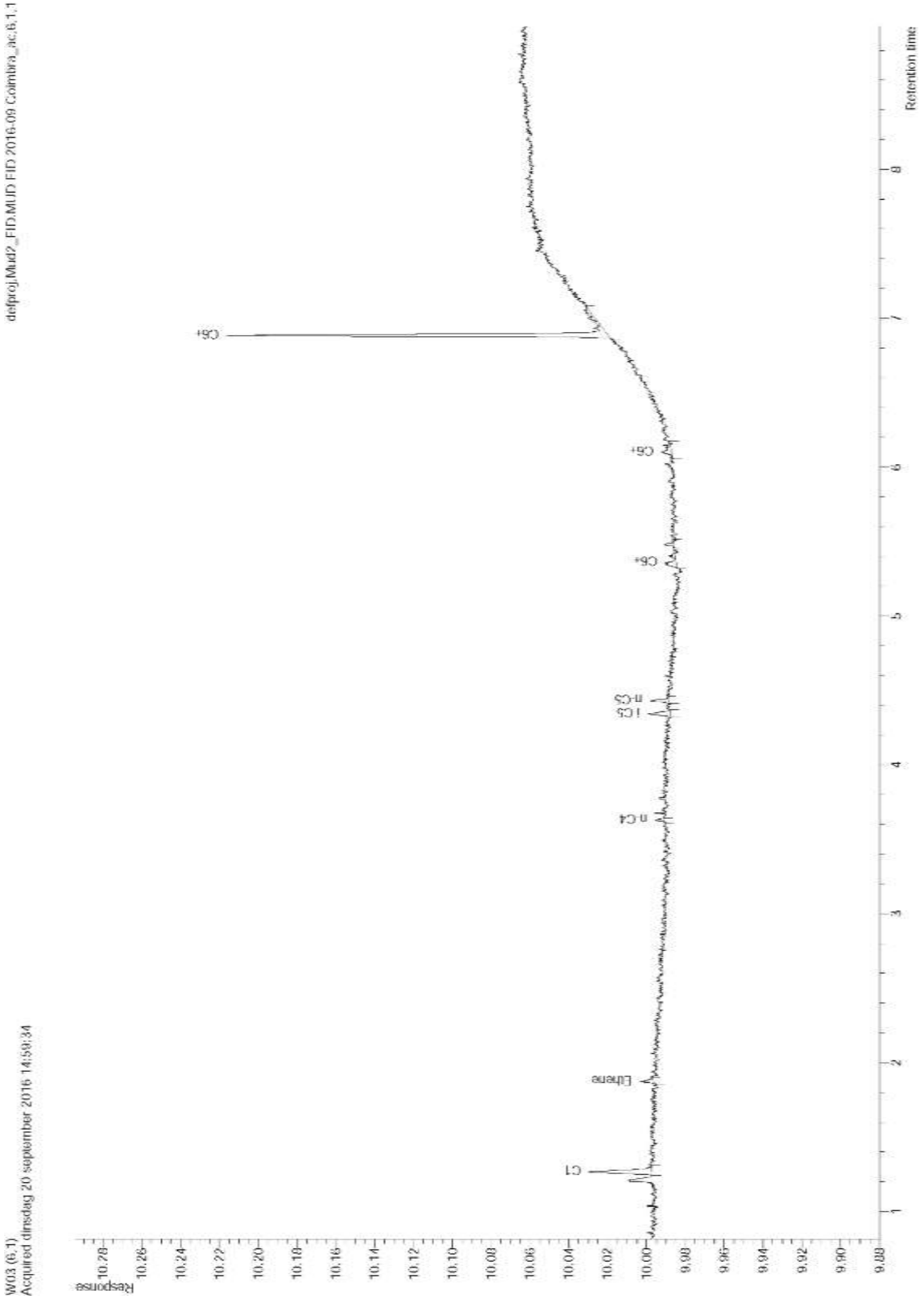

Appendix 10.33: W03 chromatogram. Retention time (min) x Response (pA).

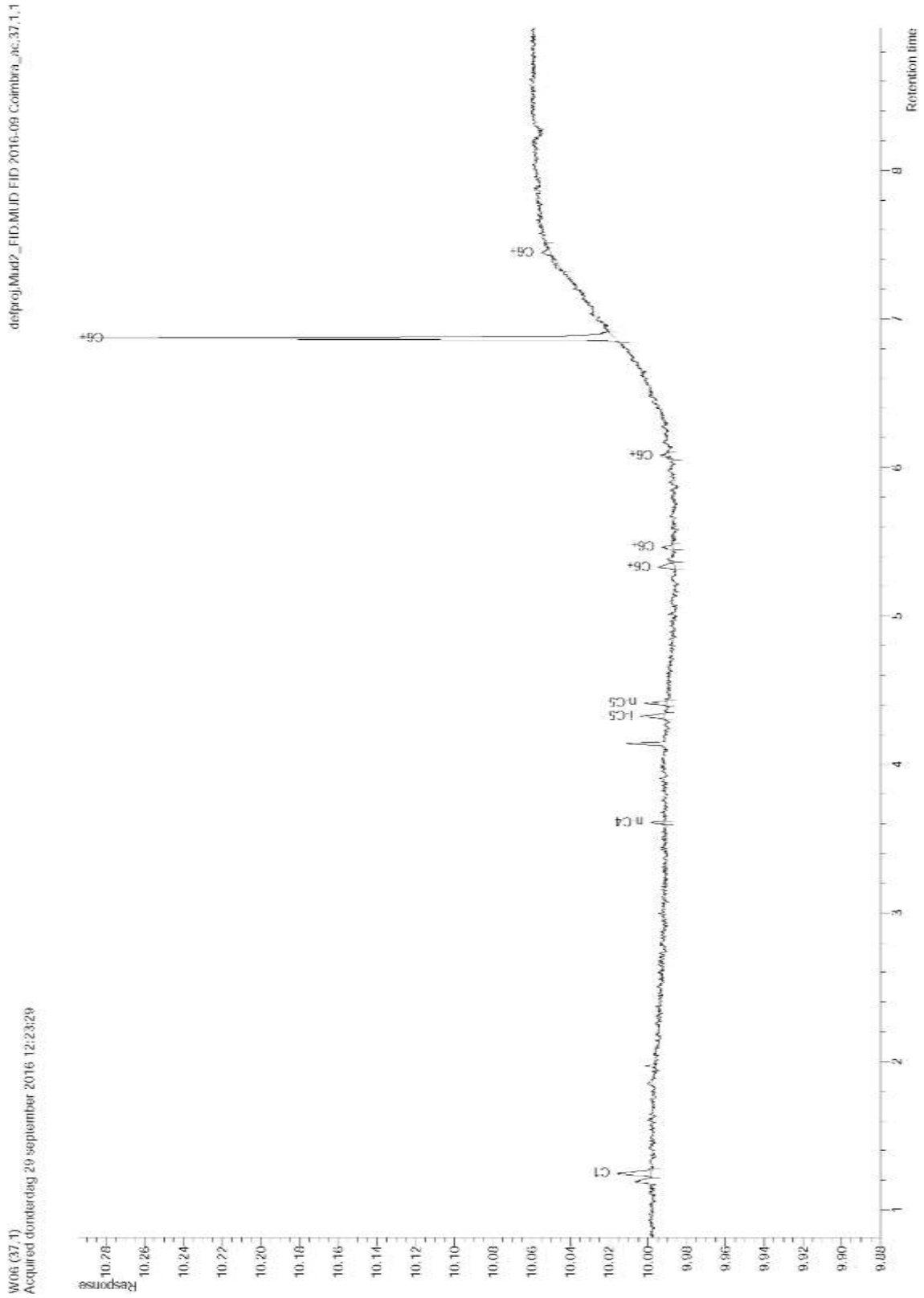

Appendix 10.34: W06 chromatogram. Retention time (min) x Response (pA).

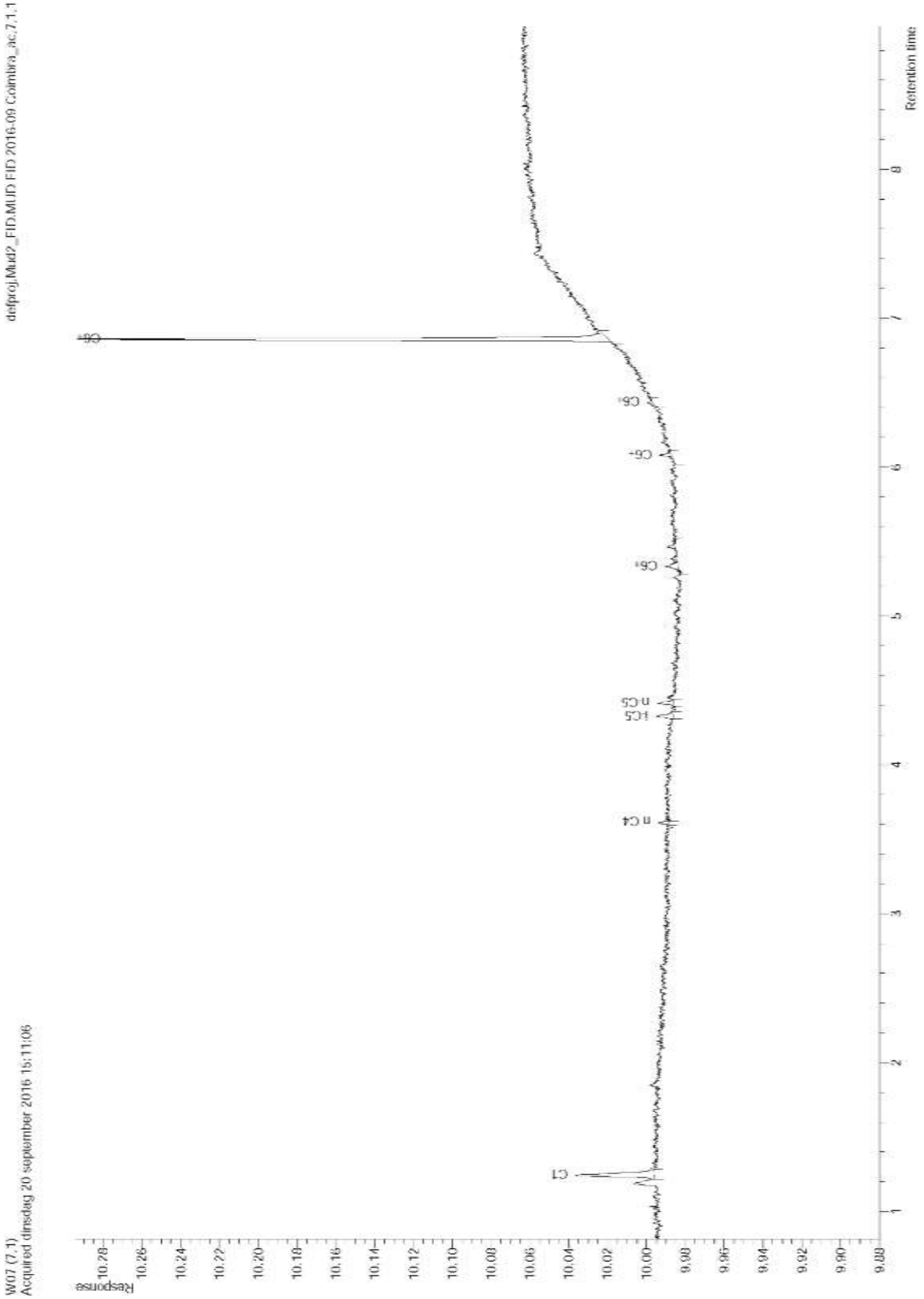

Appendix 10.35: W07 chromatogram. Retention time (min) x Response (pA).

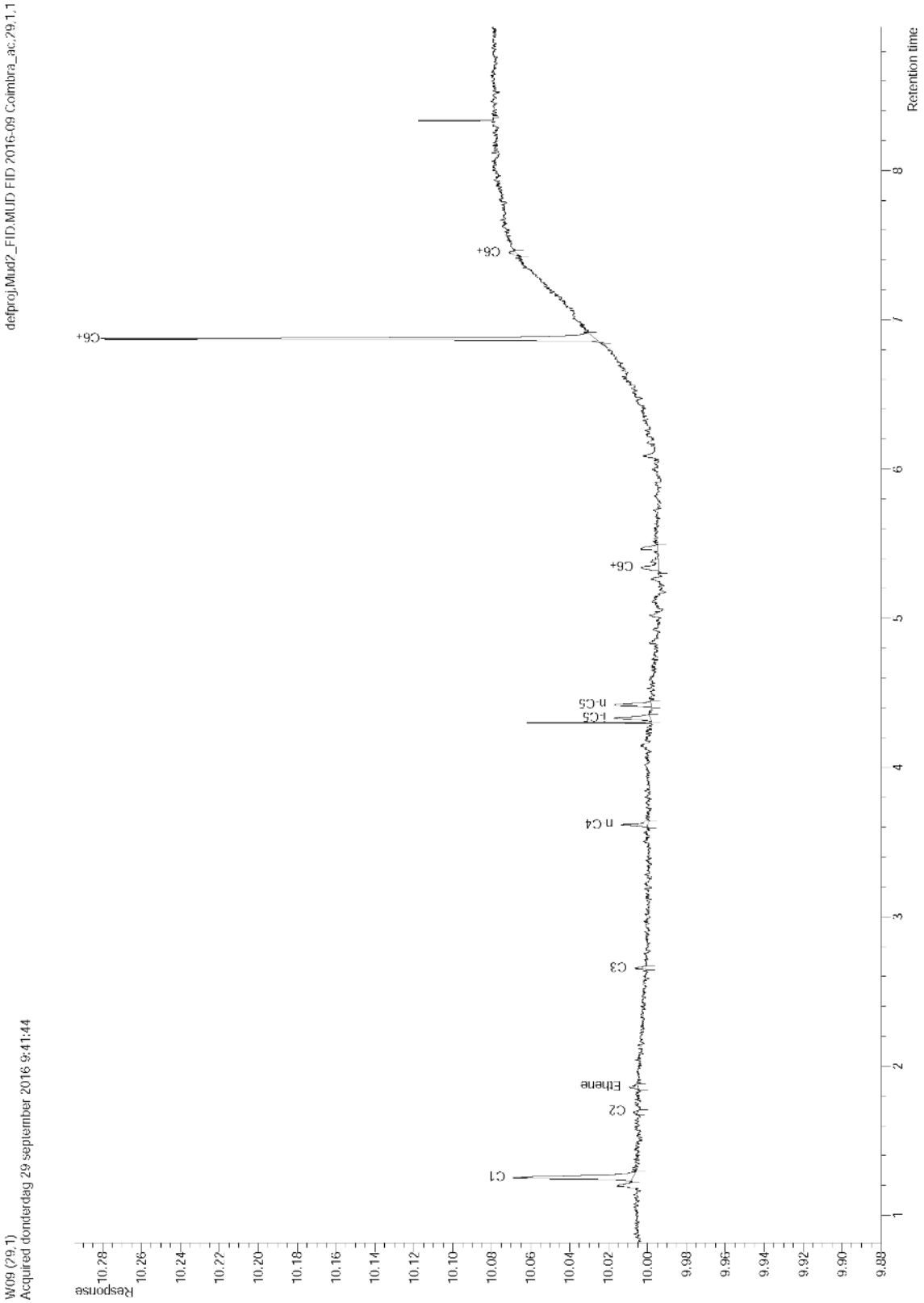

Appendix 10.36: W09 chromatogram. Retention time (min) x Response (pA).

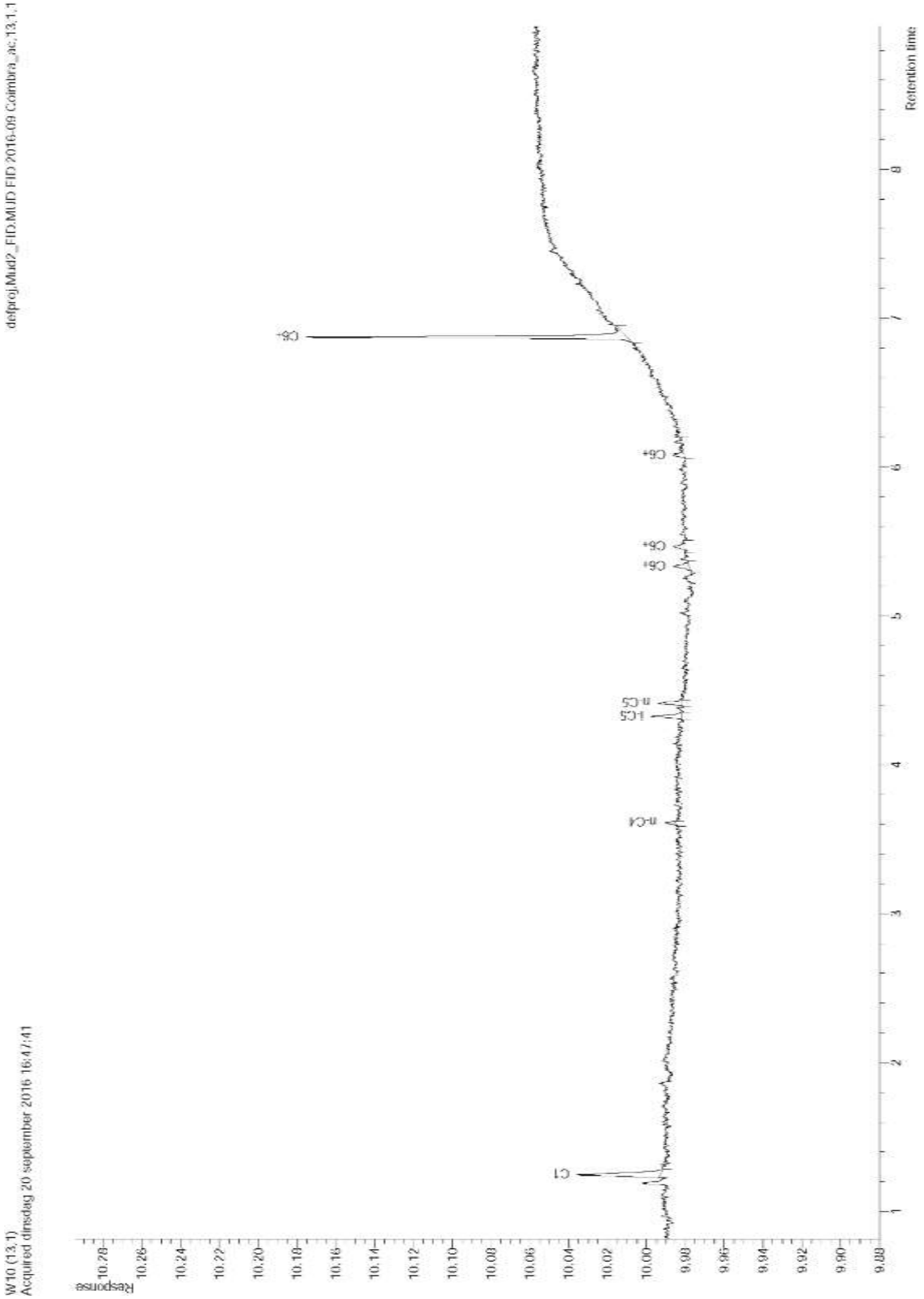

Appendix 10.37: W10 chromatogram. Retention time (min) x Response (pA).

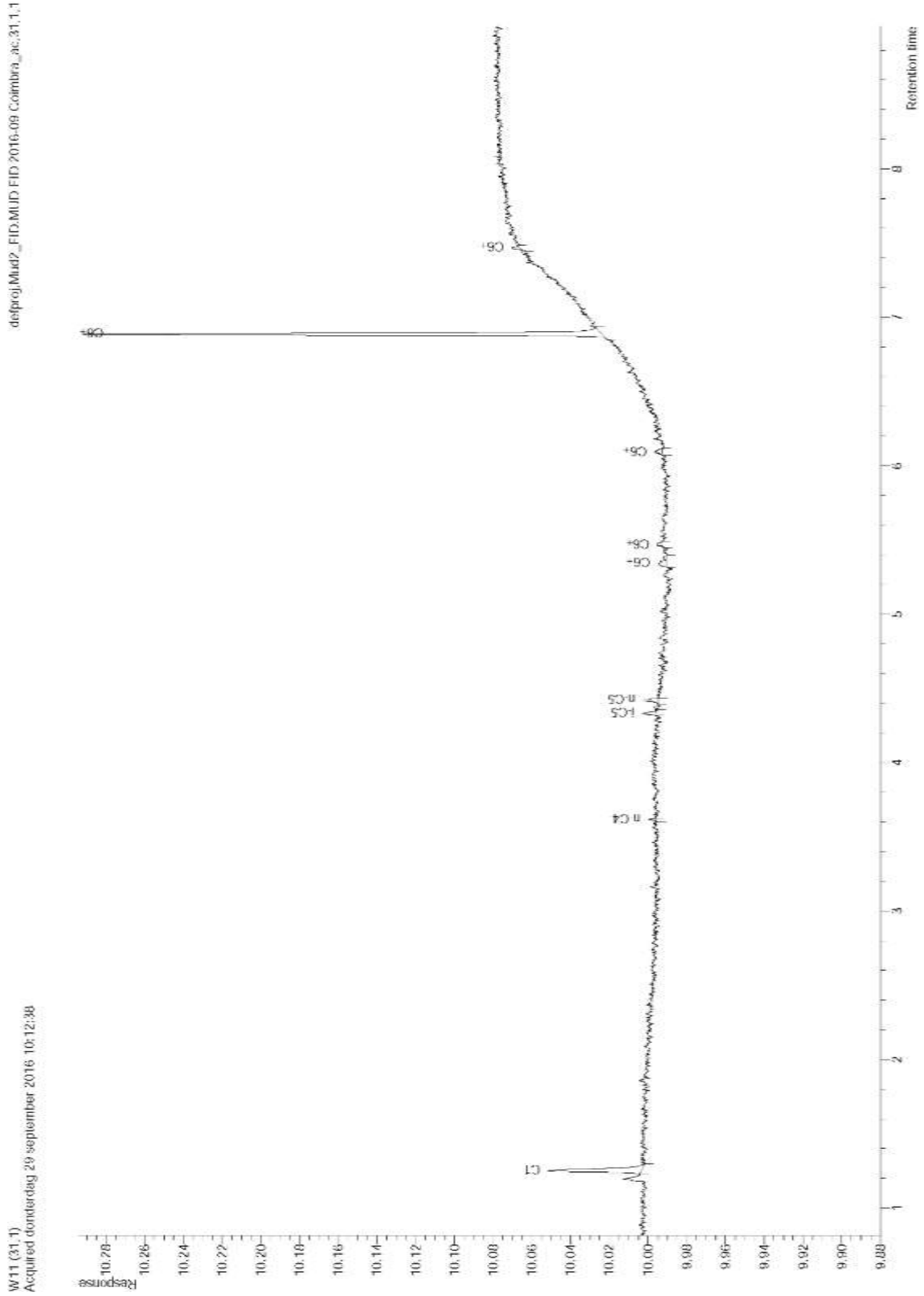

Appendix 10.38: W11 chromatogram. Retention time (min) x Response (pA).

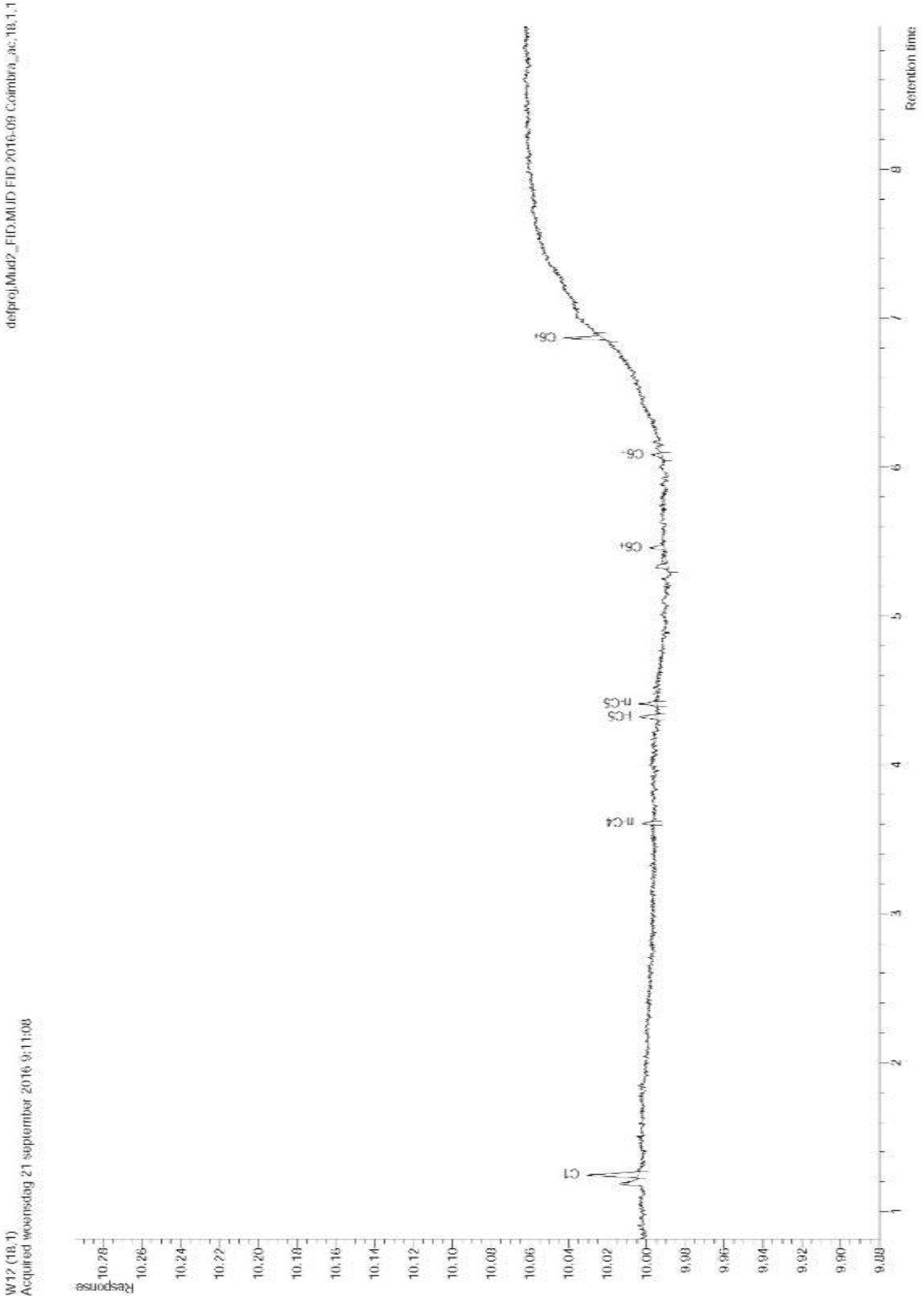

Appendix 10.39: W12 chromatogram. Retention time (min) x Response (pA).

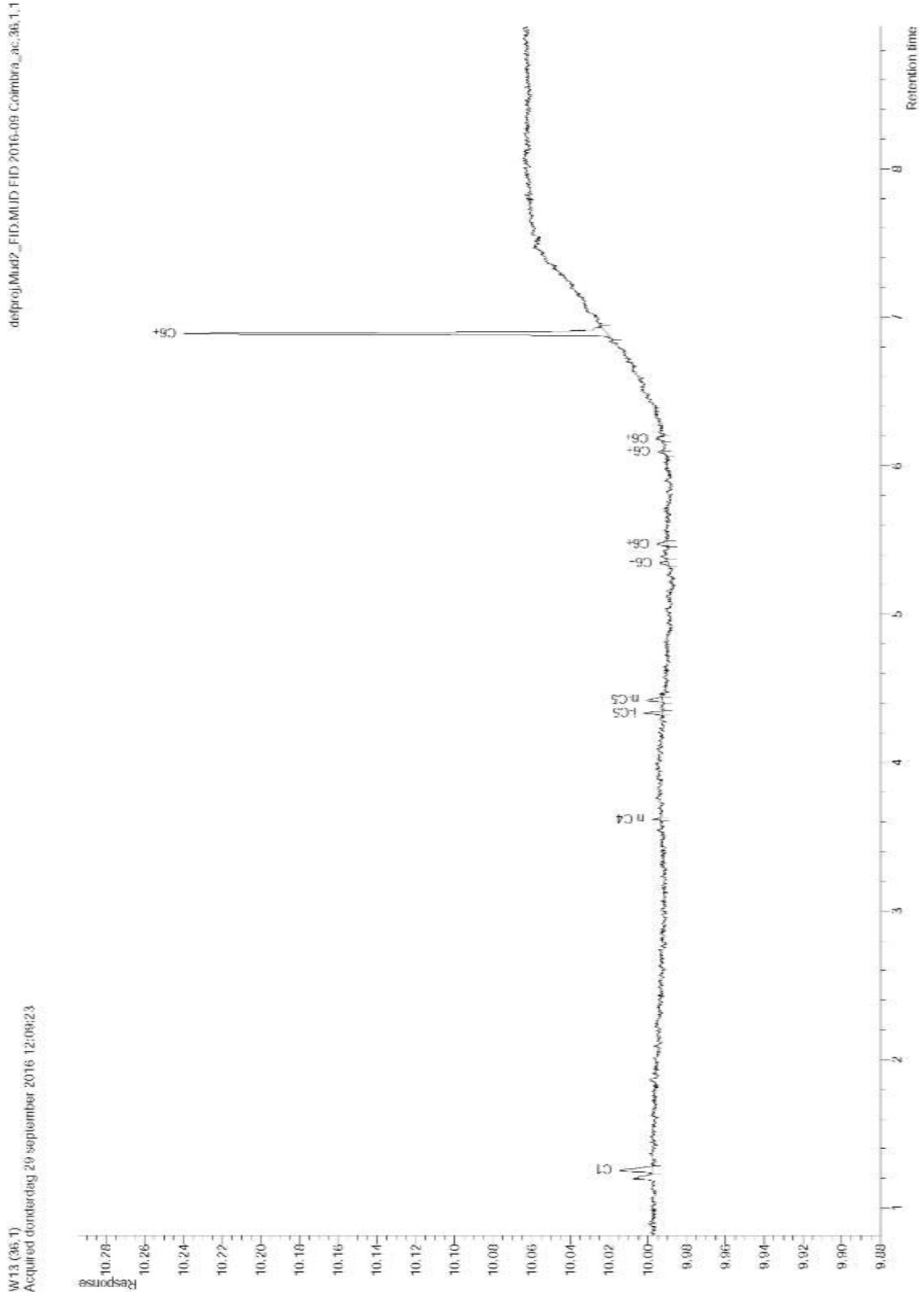

Appendix 10.40: W13 chromatogram. Retention time (min) x Response (pA).

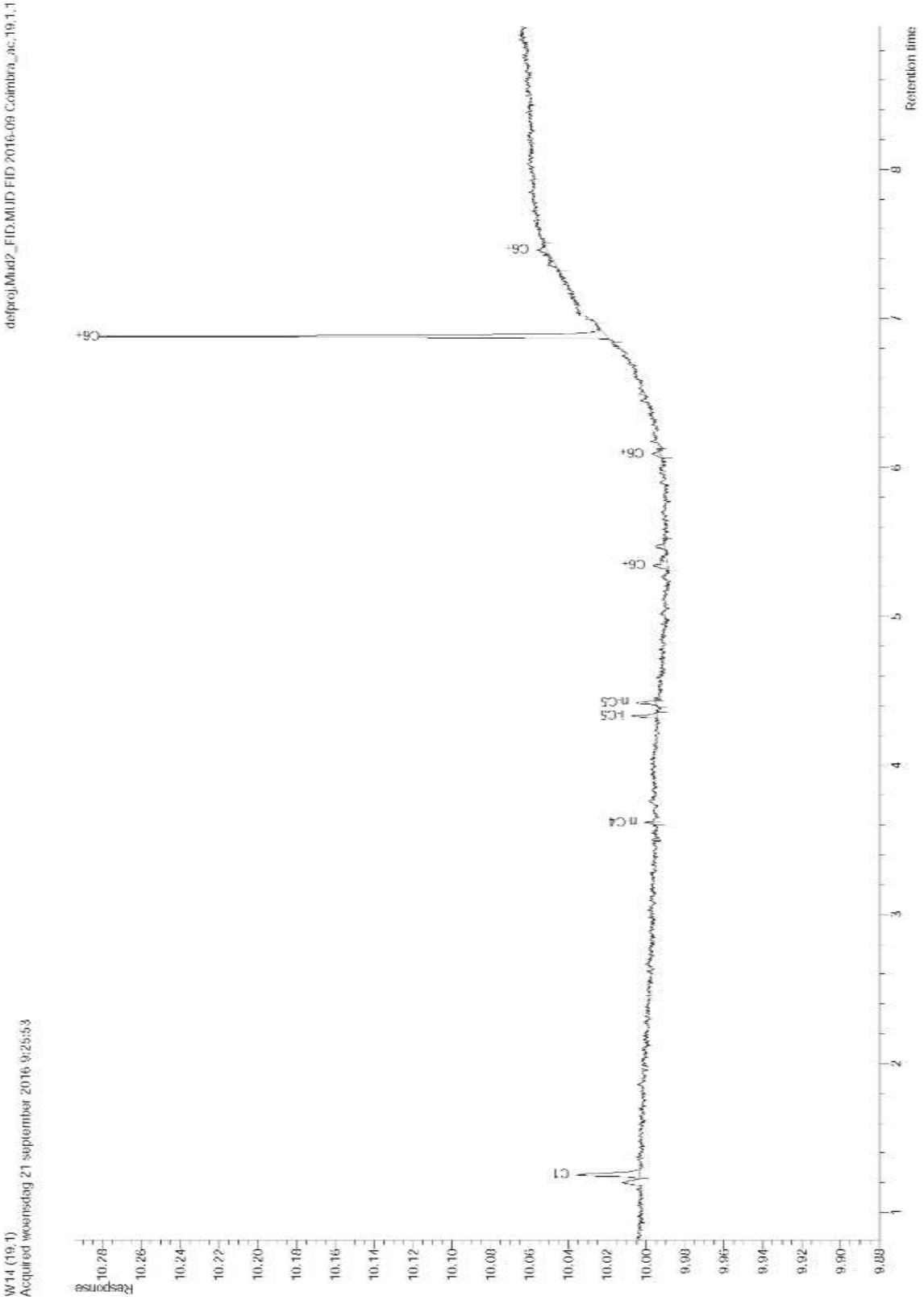

Appendix 10.41: W14 chromatogram. Retention time (min) x Response (pA).

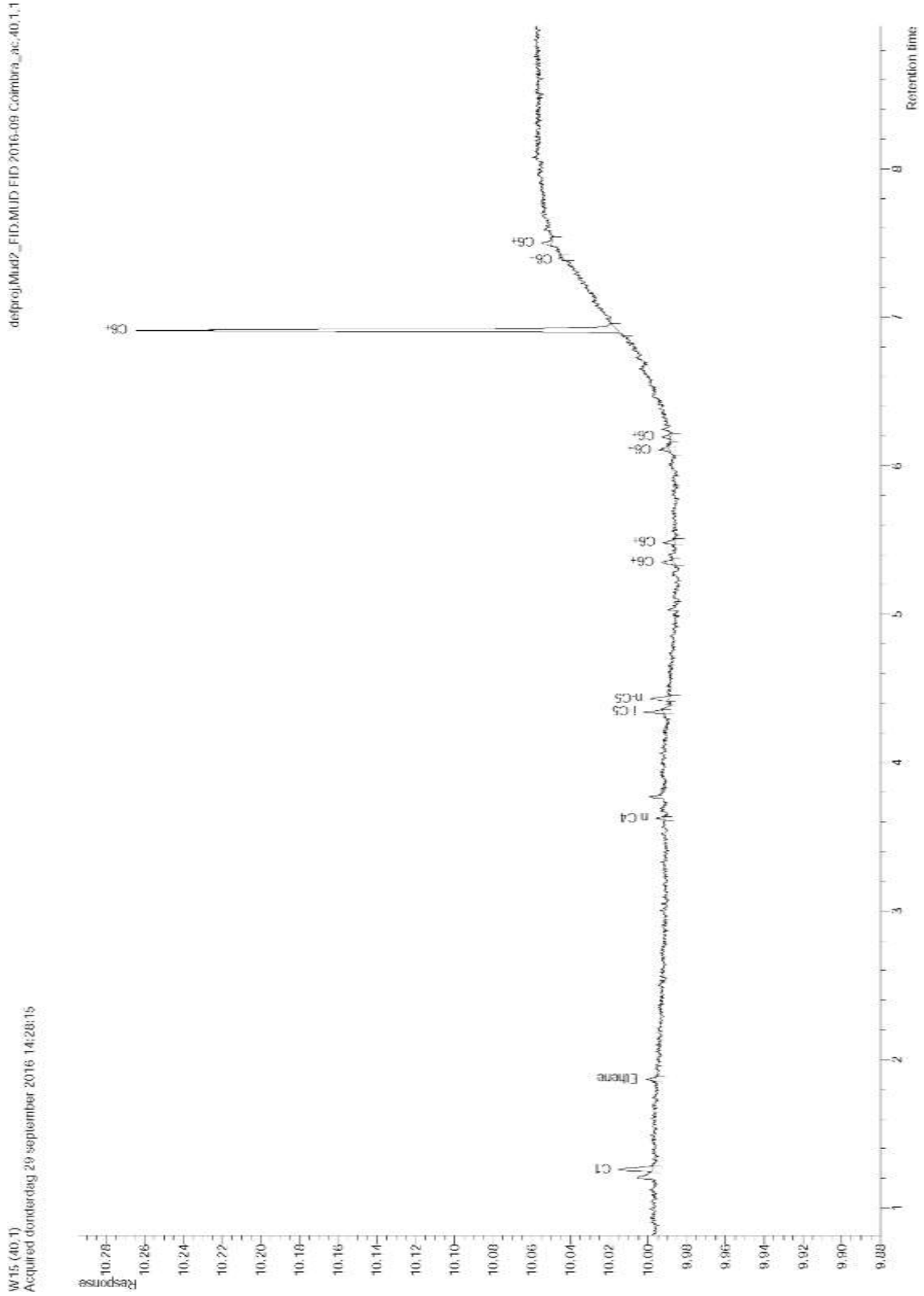

Appendix 10.42: W15 chromatogram. Retention time (min) x Response (pA).

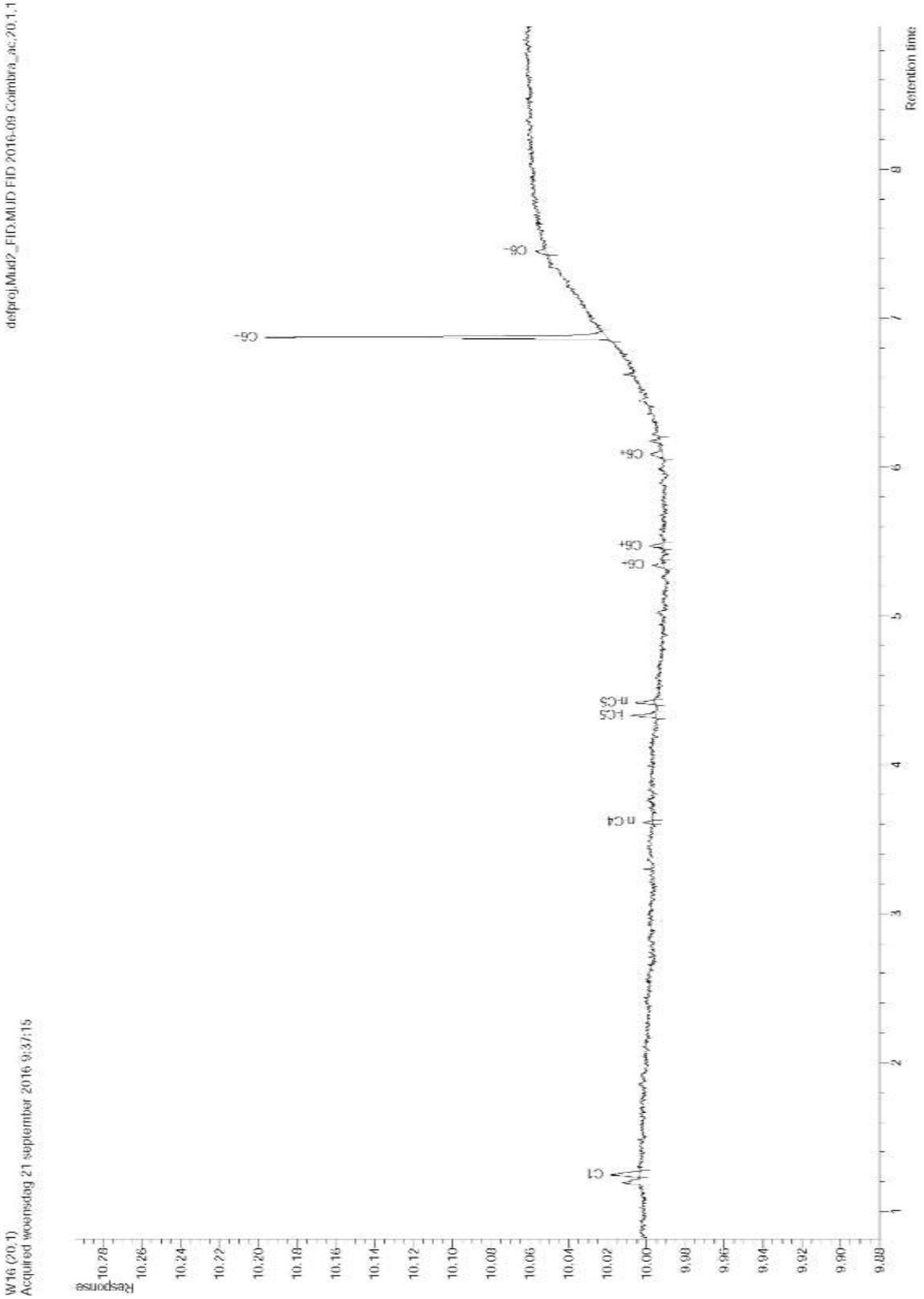

Appendix 10.43: W16 chromatogram. Retention time (min) x Response (pA).

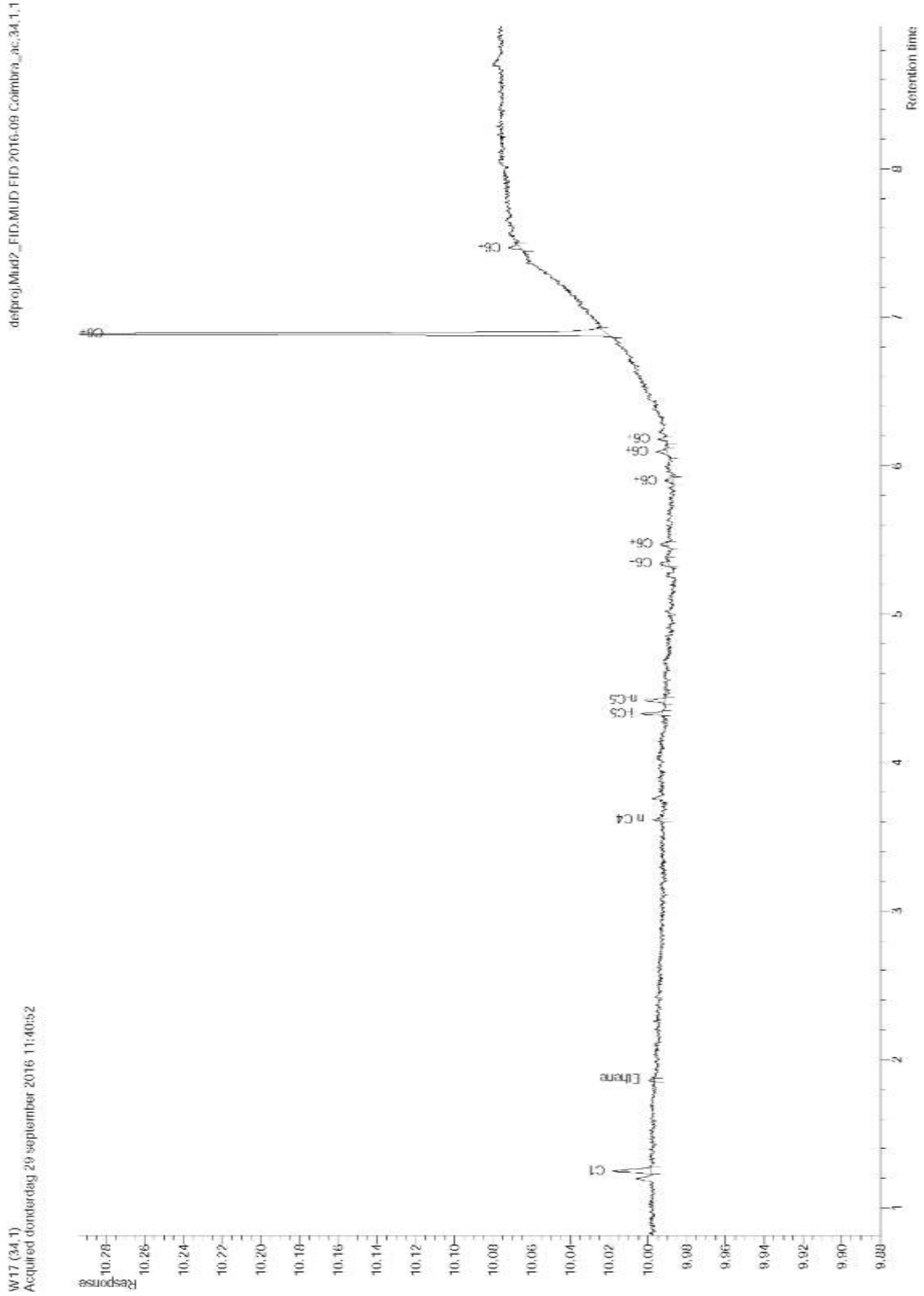

Appendix 10.44: W17 chromatogram. Retention time (min) x Response (pA).

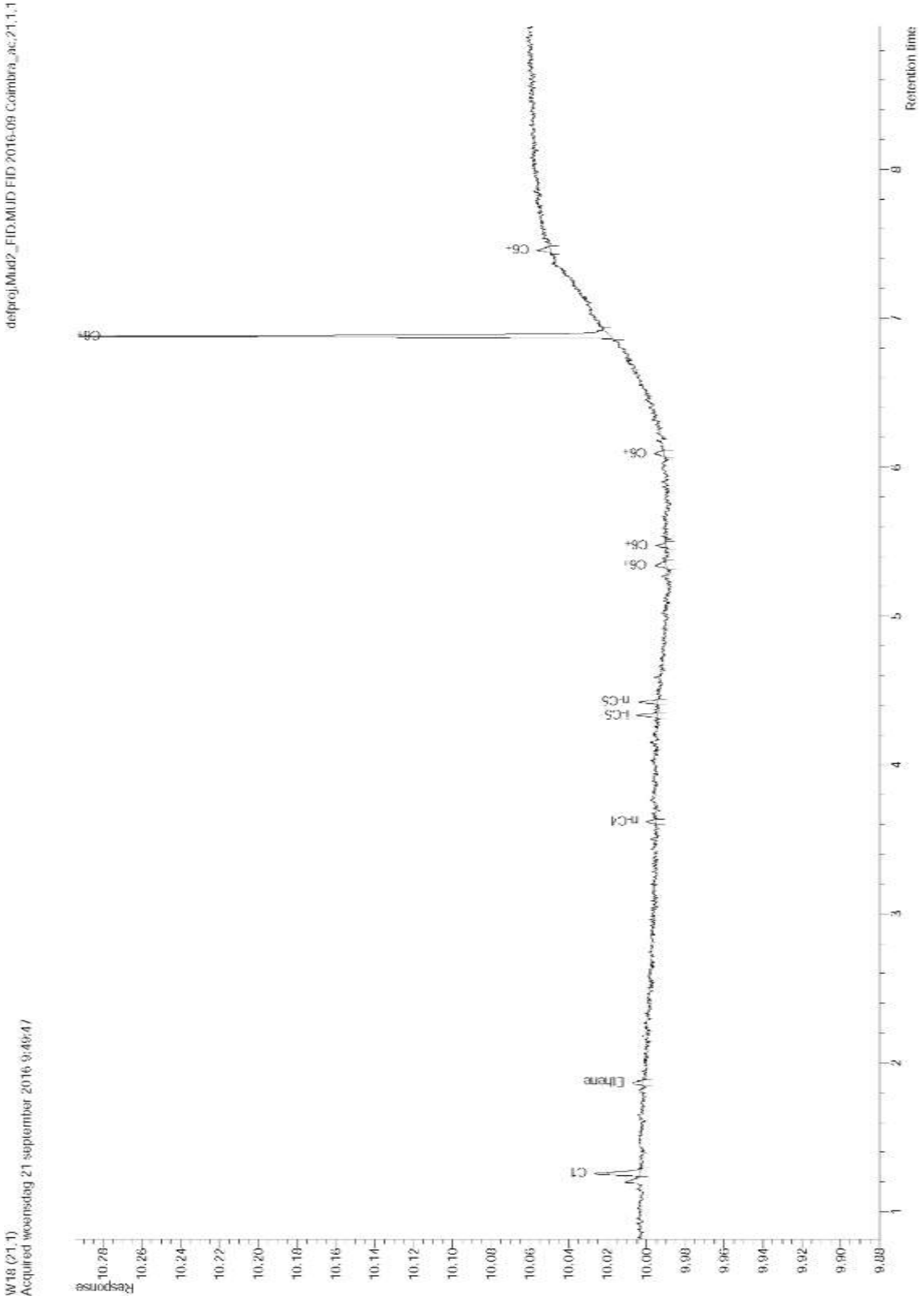

Appendix 10.45: W18 chromatogram. Retention time (min) x Response (pA).

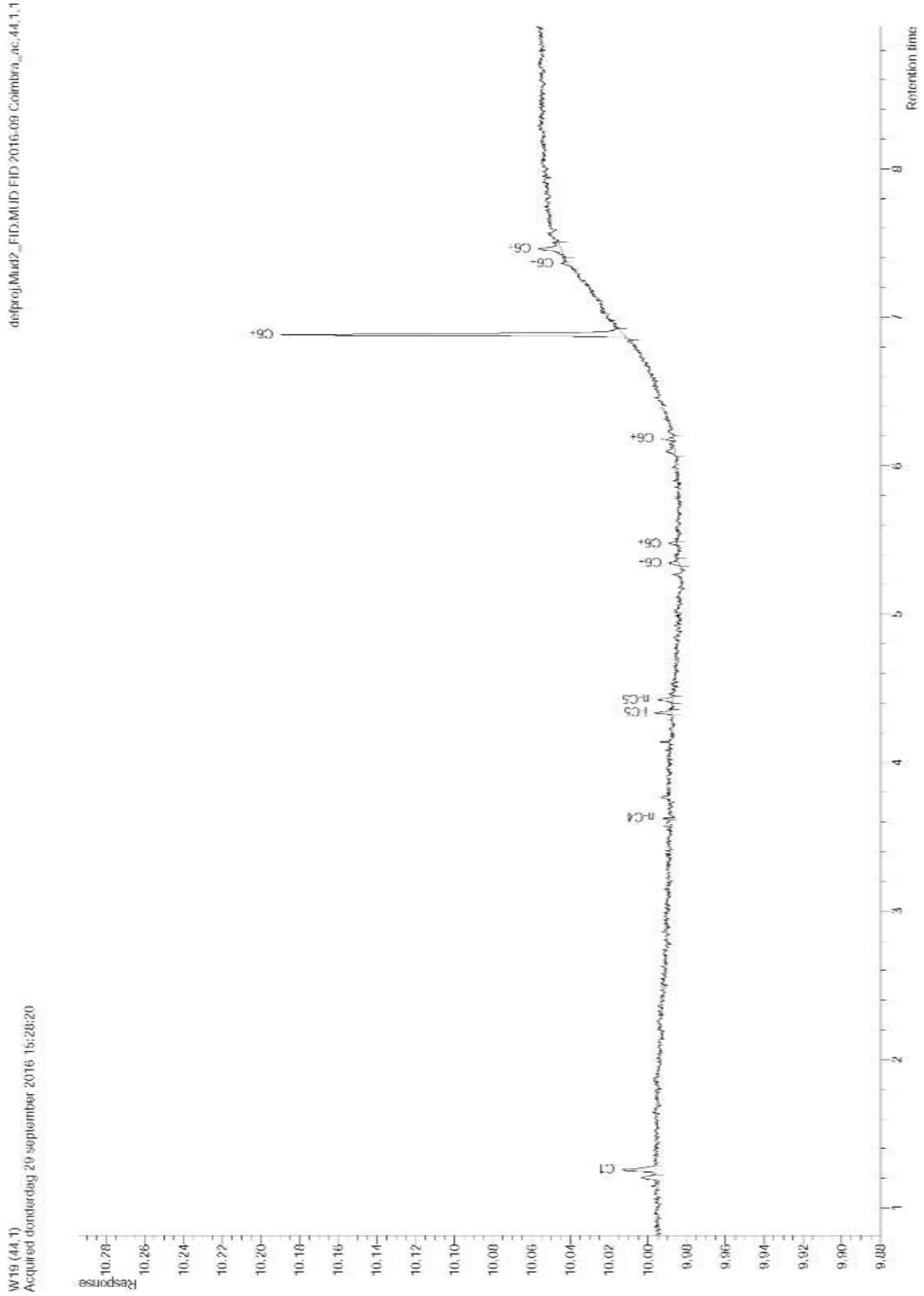

Appendix 10.46: W19 chromatogram. Retention time (min) x Response (pA).

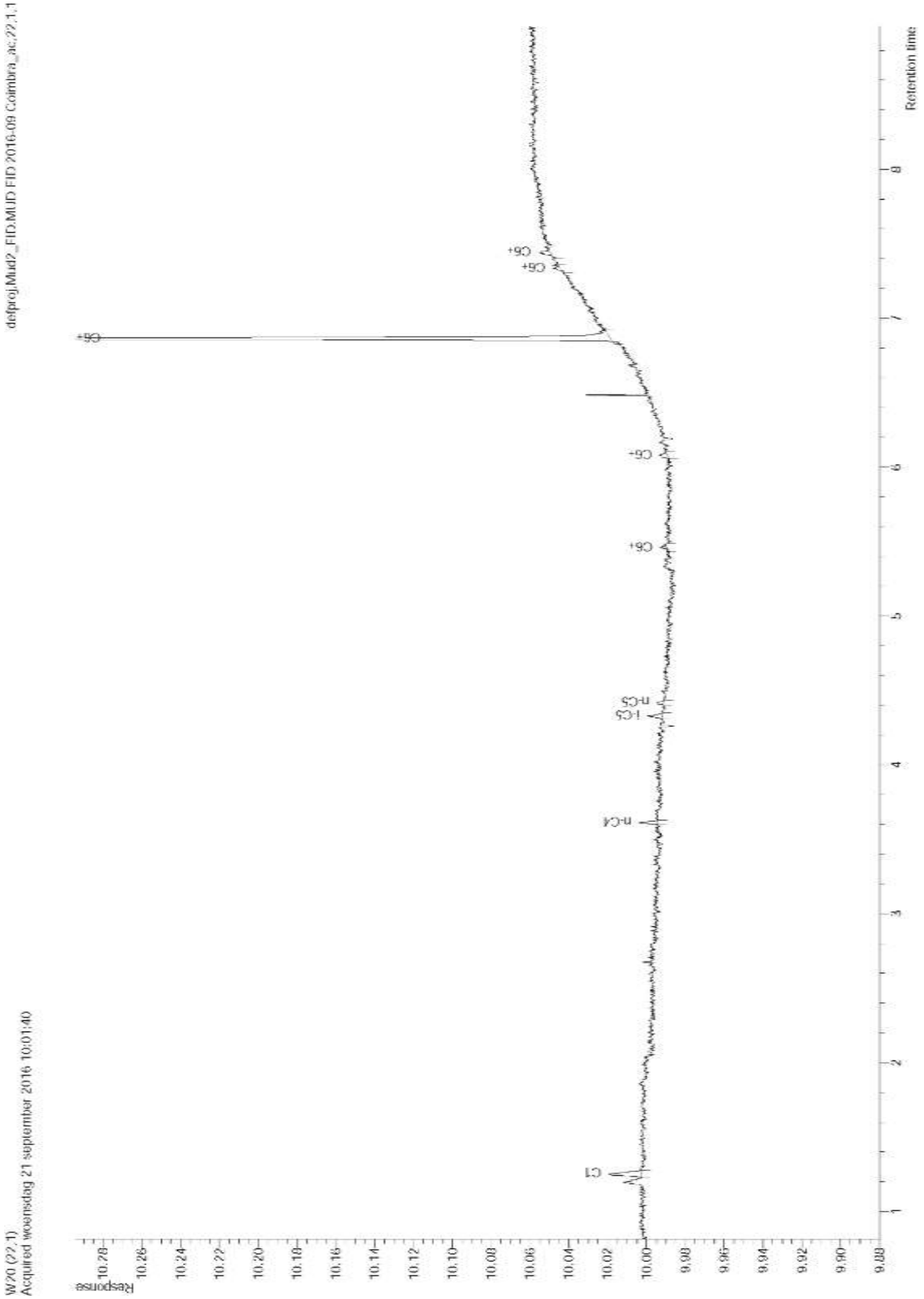

Appendix 10.47: W20 chromatogram. Retention time (min) x Response (pA).

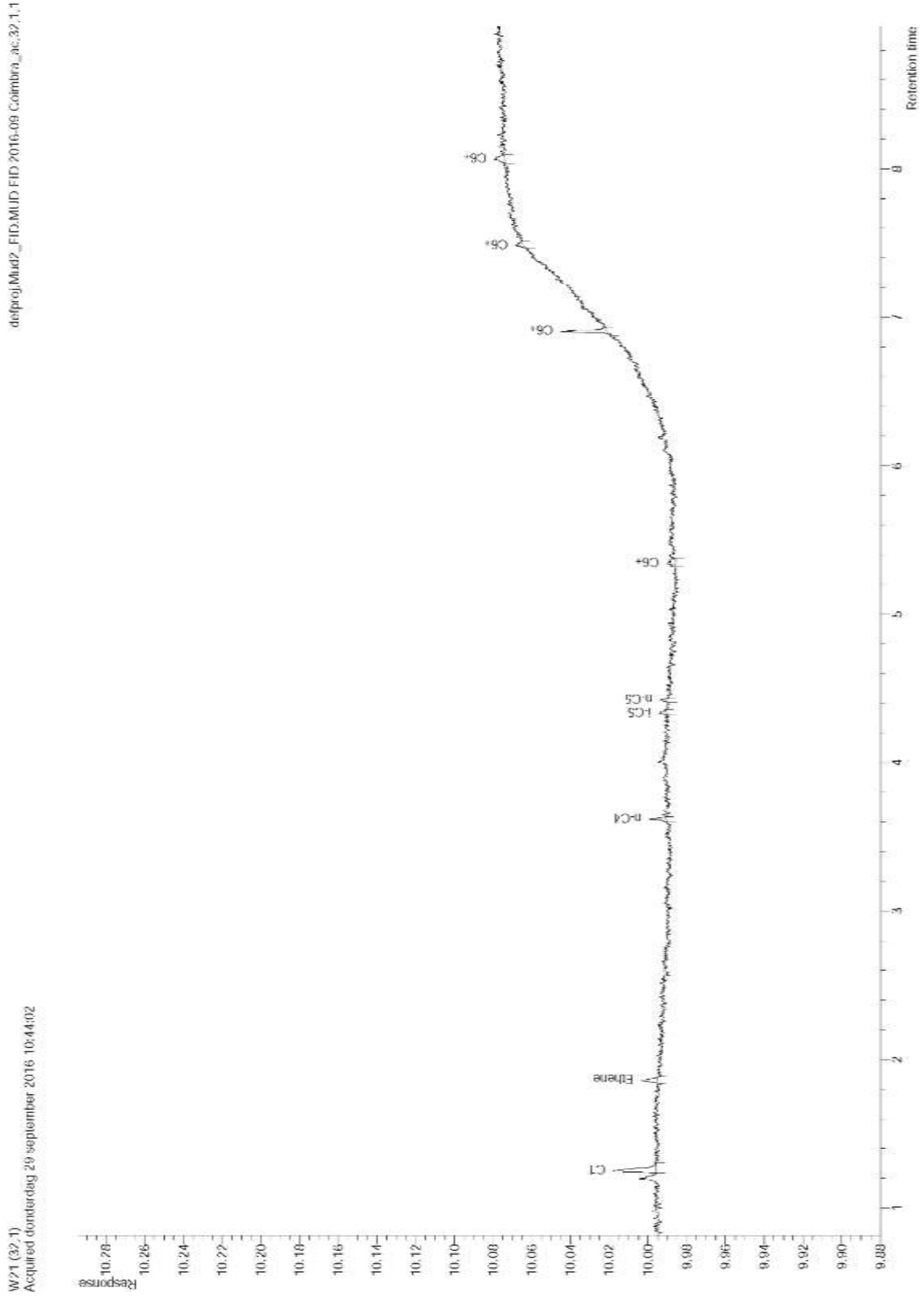

Appendix 10.48: W21 chromatogram. Retention time (min) x Response (pA).

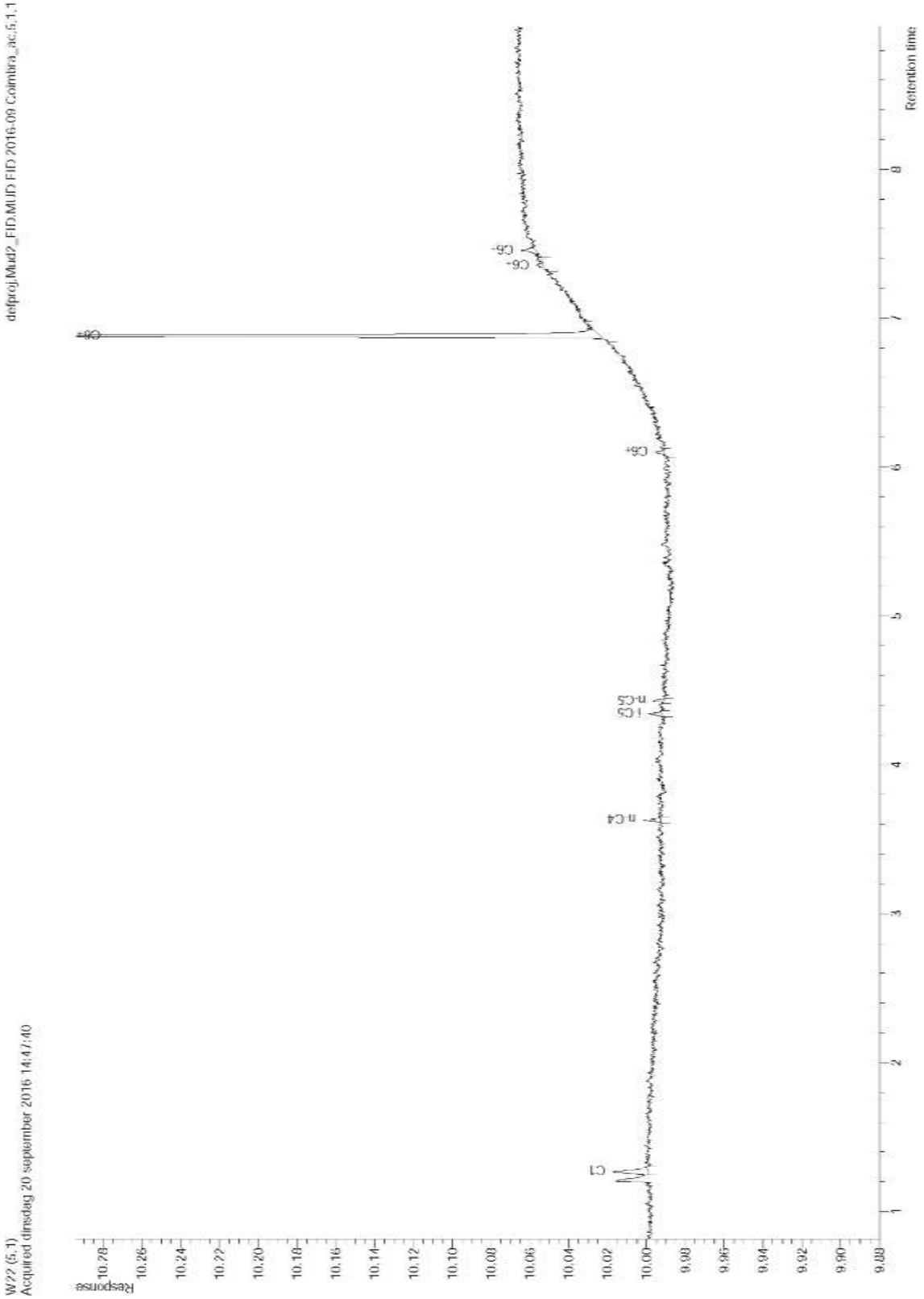

Appendix 10.49: W22 chromatogram. Retention time (min) x Response (pA).

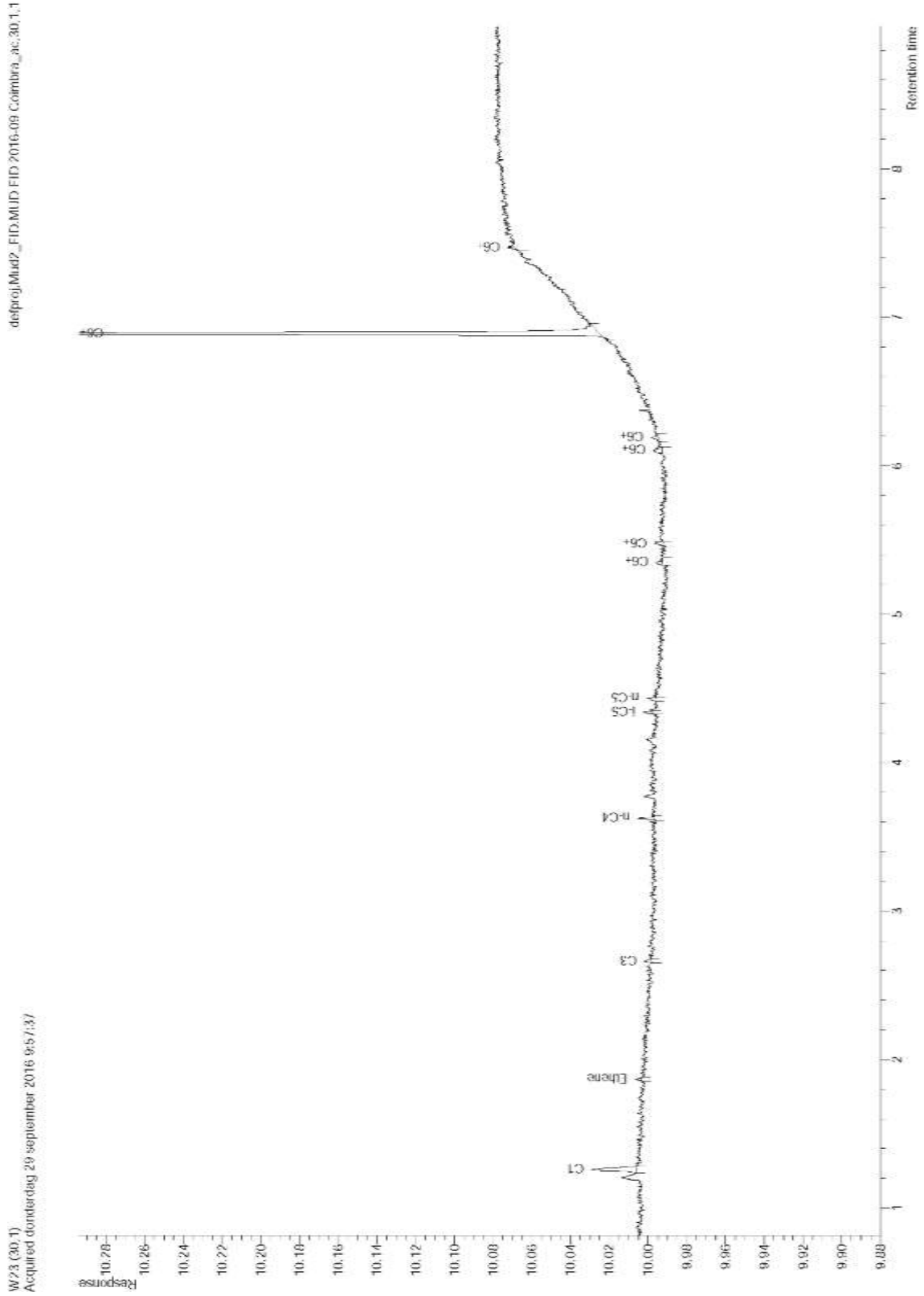

Appendix 10.50: W23 chromatogram. Retention time (min) x Response (pA).

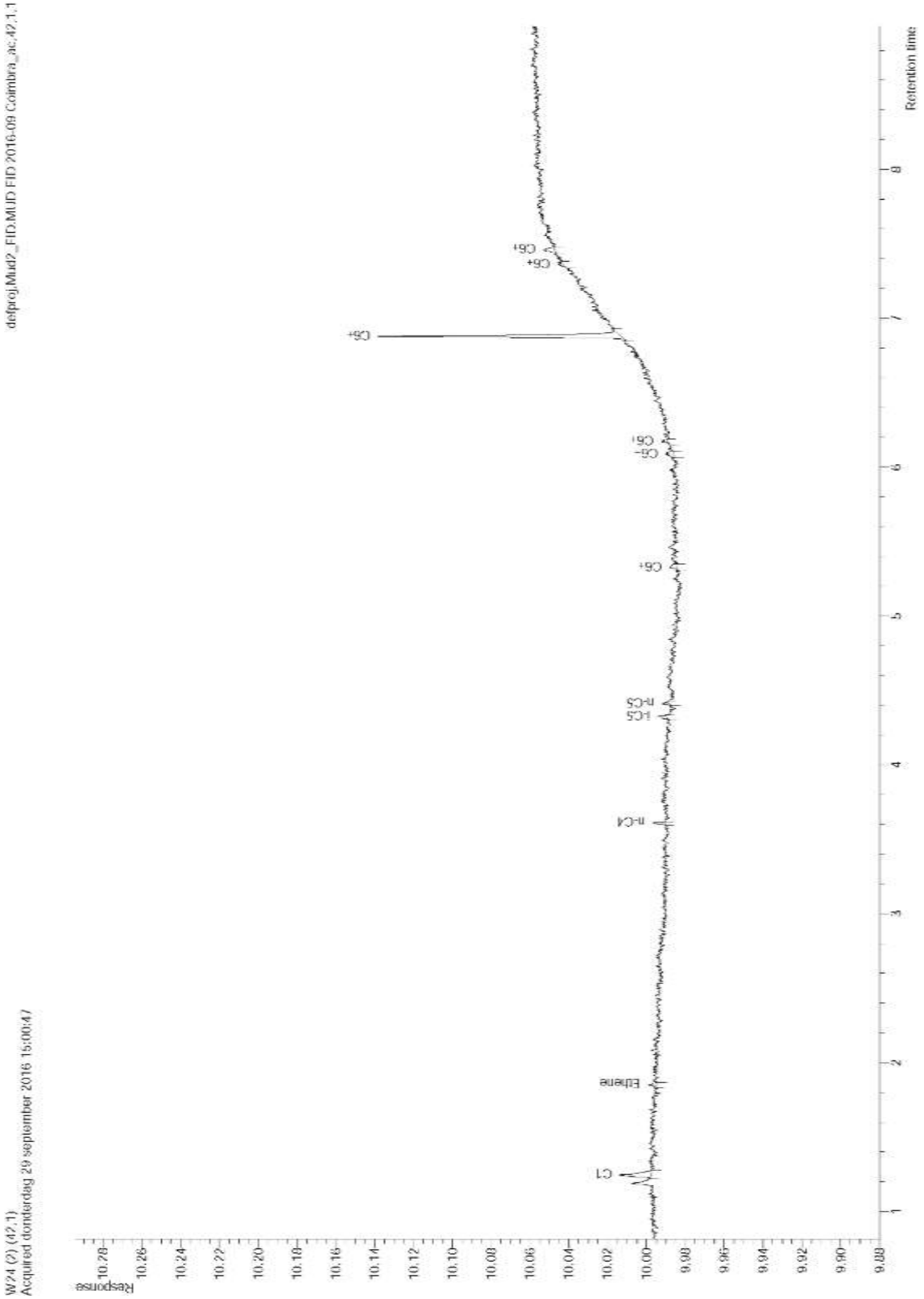

Appendix 10.51: W24 chromatogram. Retention time (min) x Response (pA).

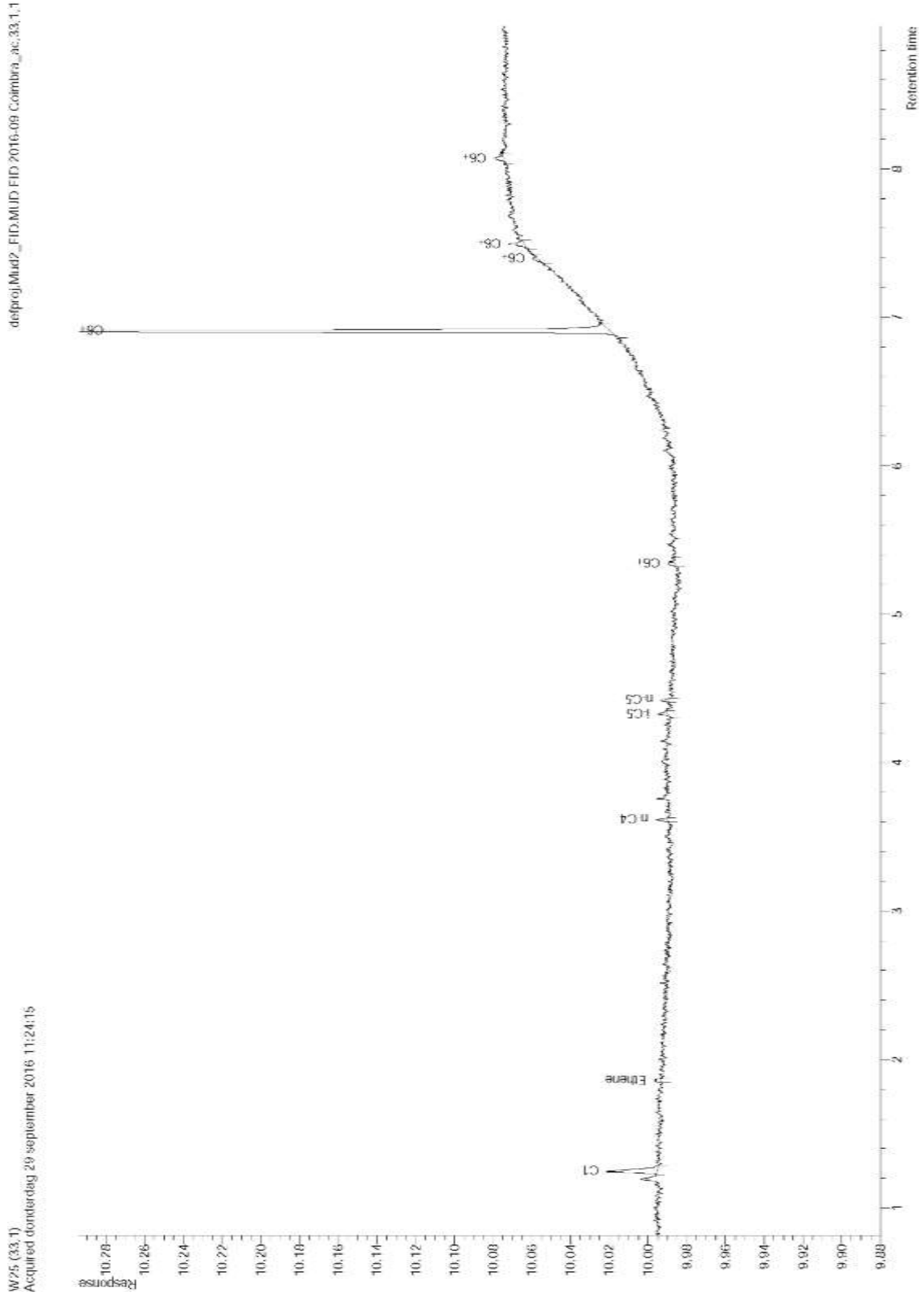

Appendix 10.52: W25 chromatogram. Retention time (min) x Response (pA).

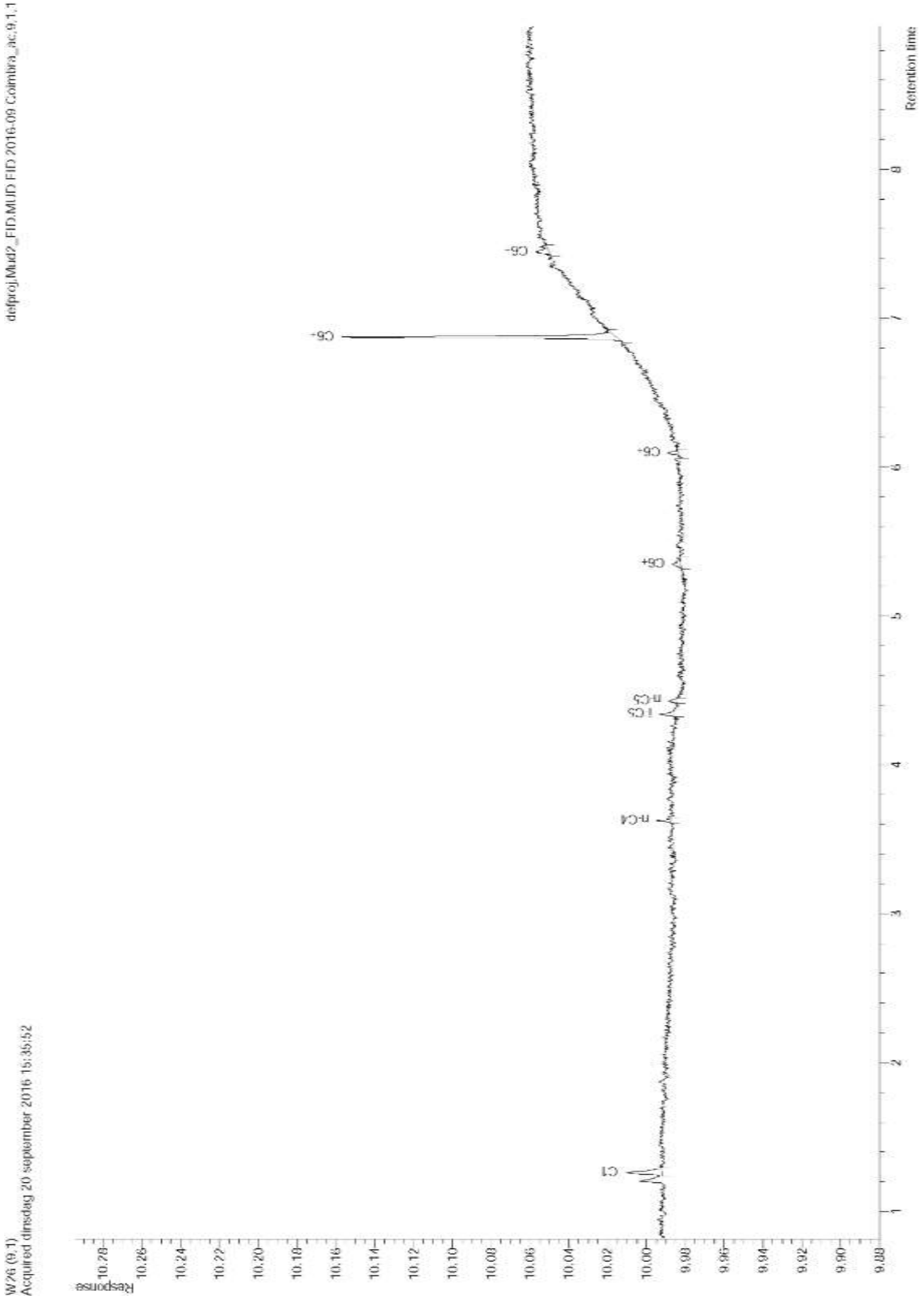

Appendix 10.53: W26 chromatogram. Retention time (min) x Response (pA).

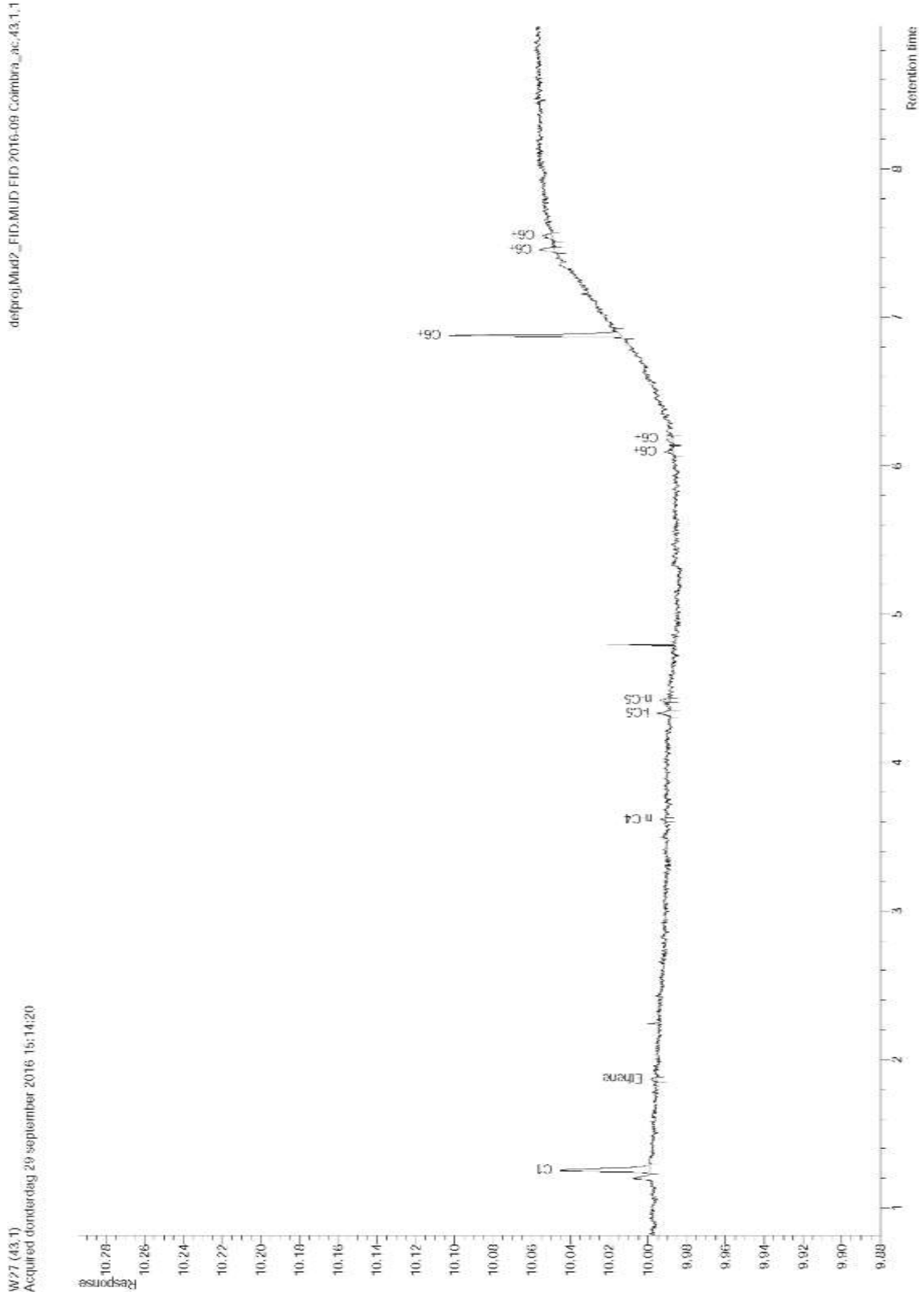

Appendix 10.54: W27 chromatogram. Retention time (min) x Response (pA).

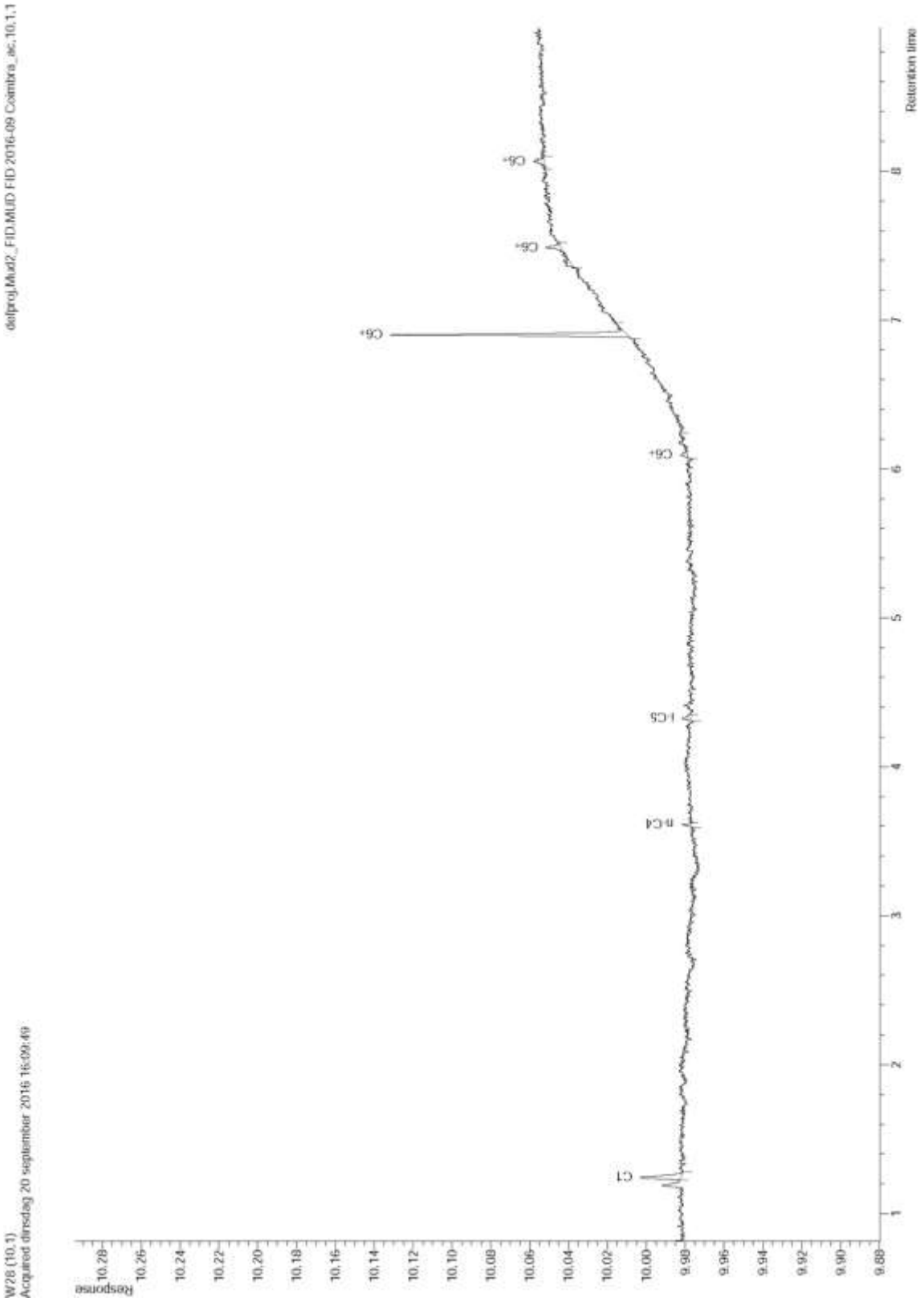

Appendix 10.55: W28 chromatogram. Retention time (min) x Response (pA).

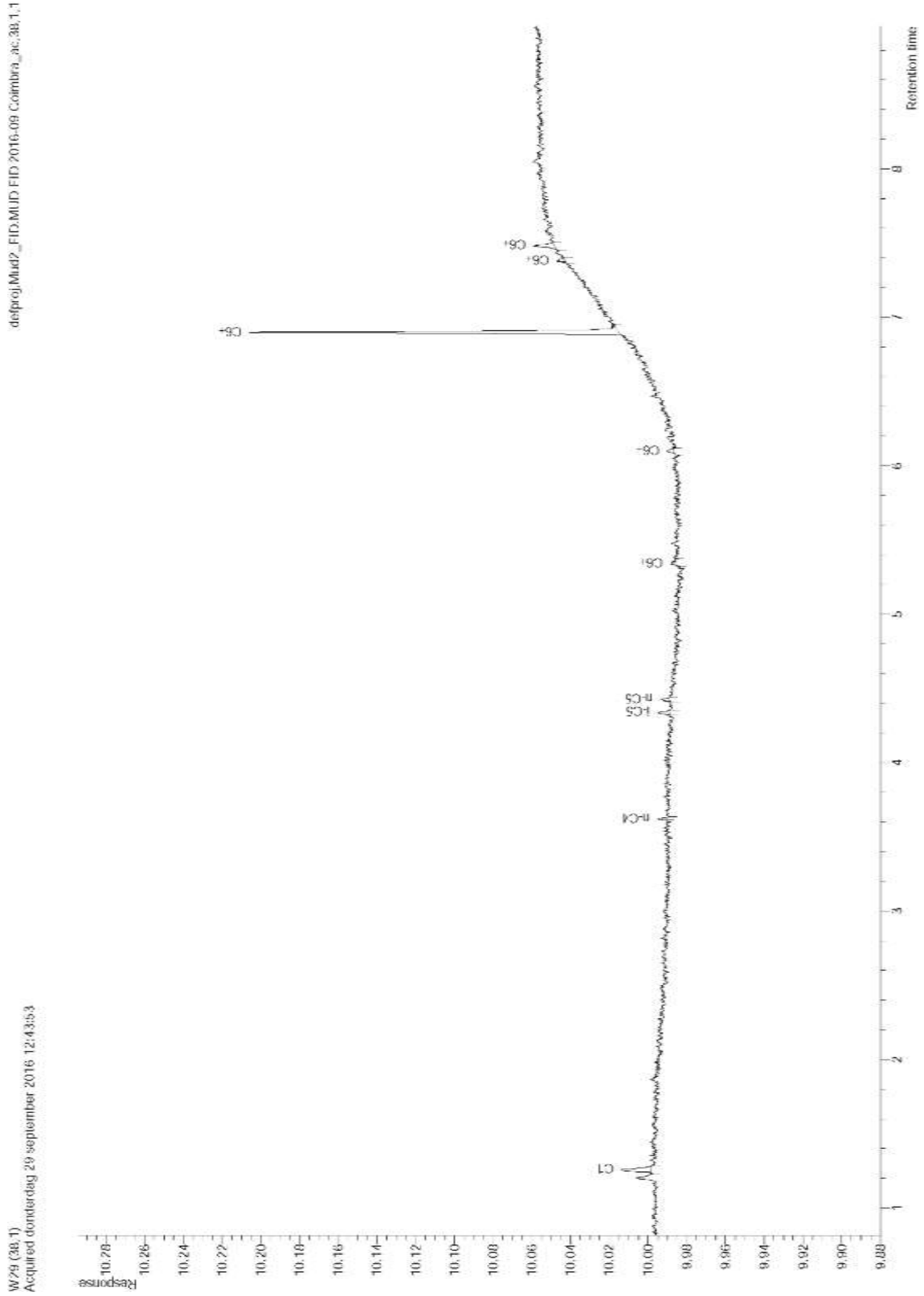

Appendix 10.56: W29 chromatogram. Retention time (min) x Response (pA).

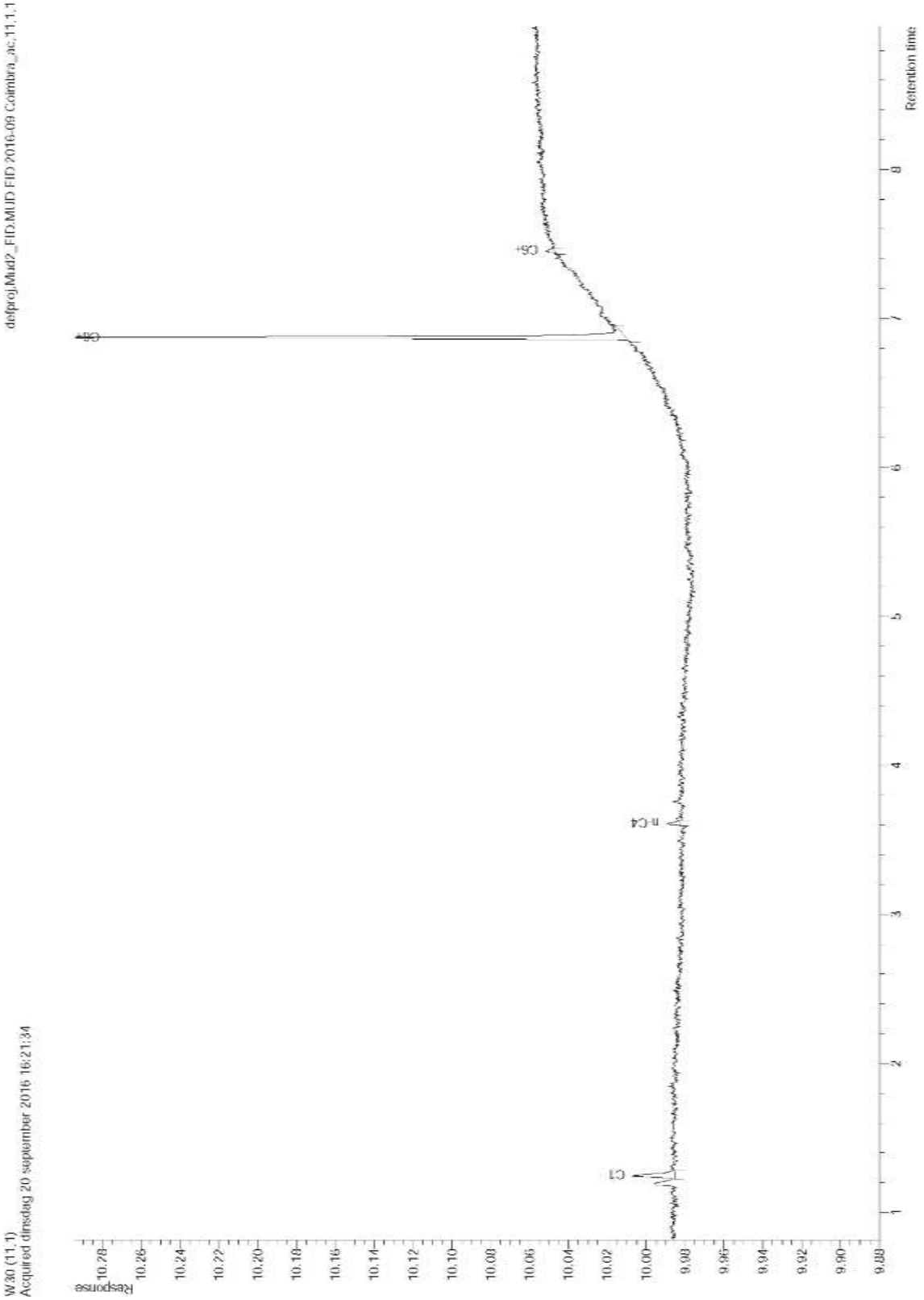

Appendix 10.57: W30 chromatogram. Retention time (min) x Response (pA).

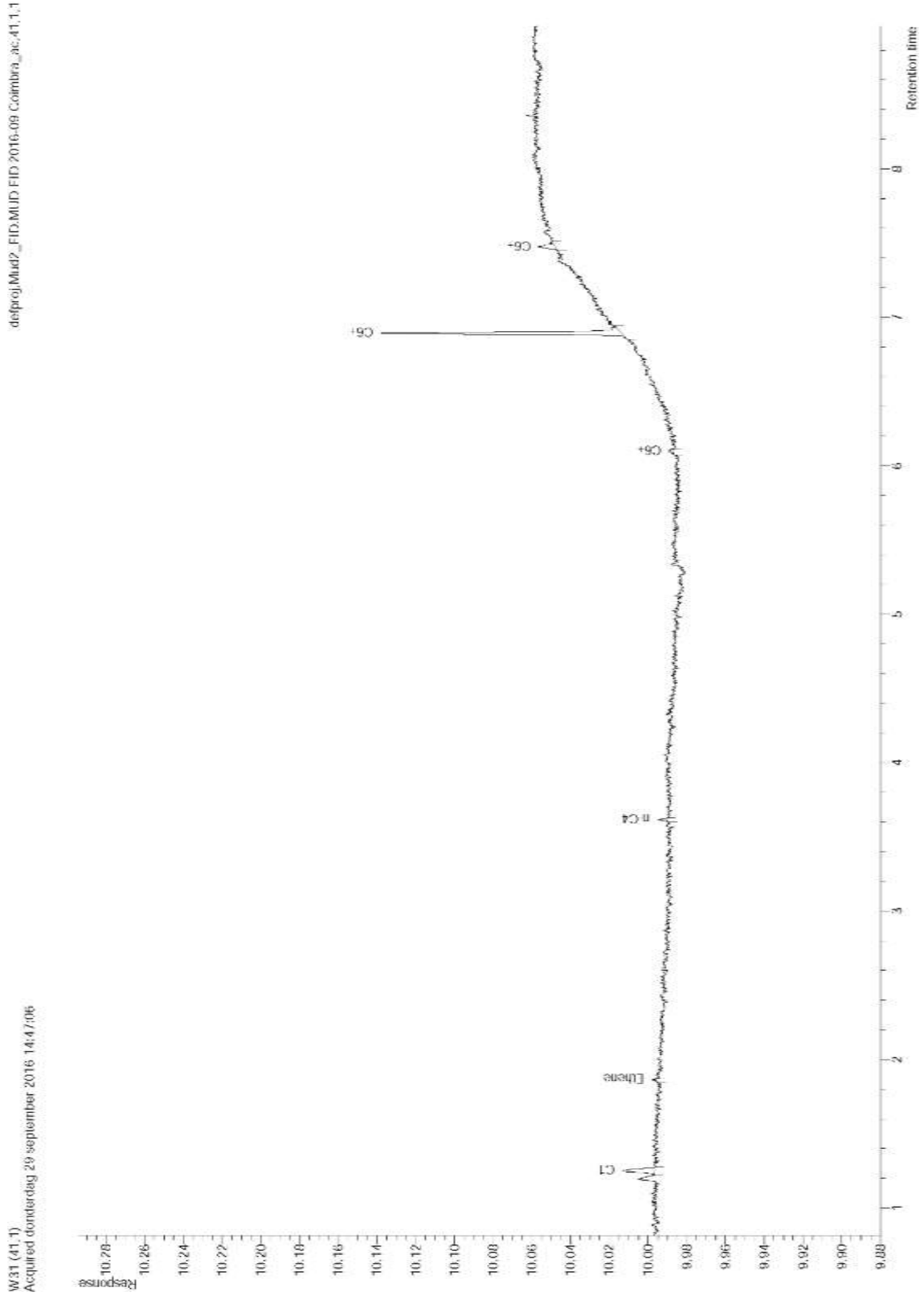

Appendix 10.58: W31 chromatogram. Retention time (min) x Response (pA).

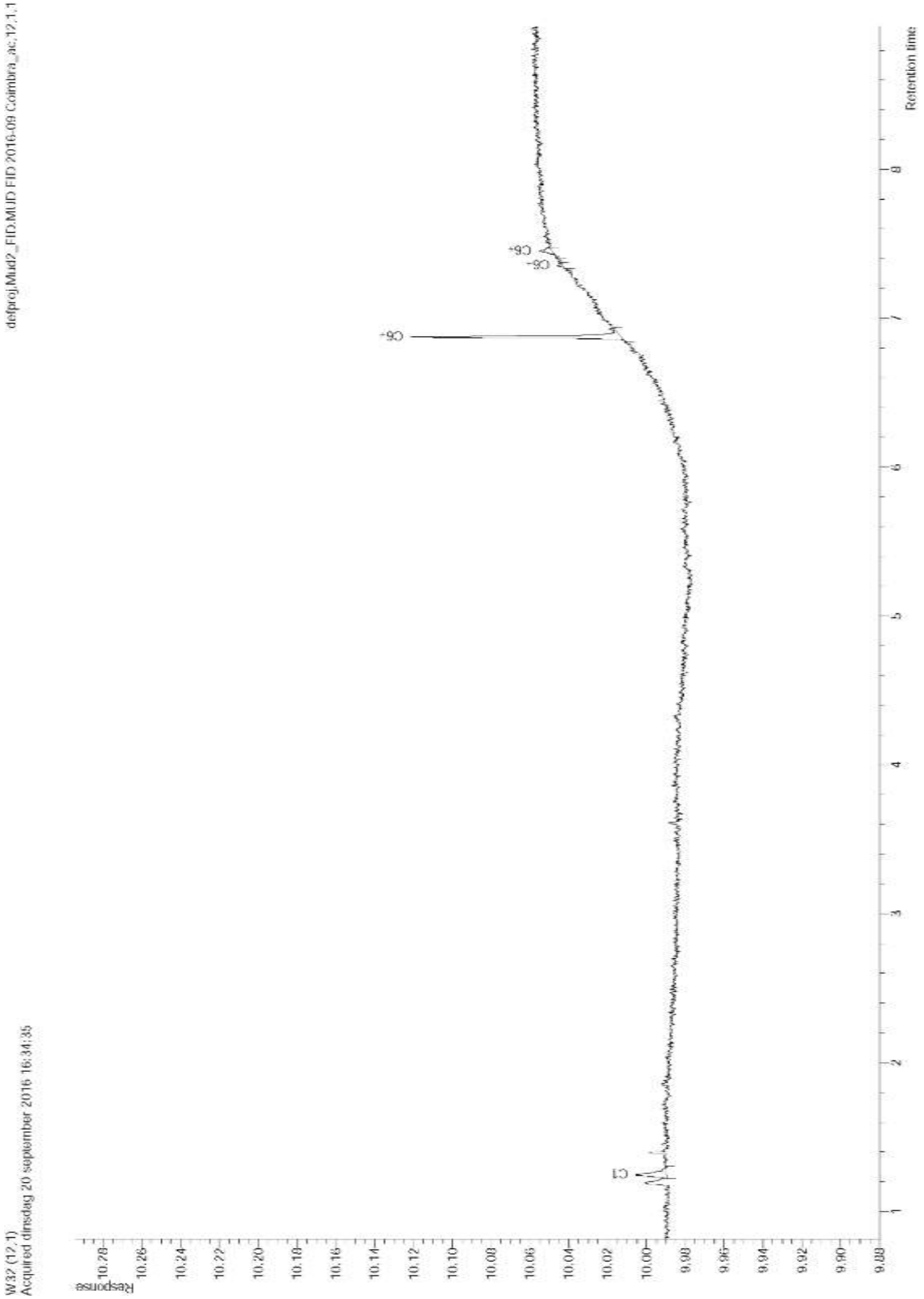

Appendix 10.59: W32 chromatogram. Retention time (min) x Response (pA).

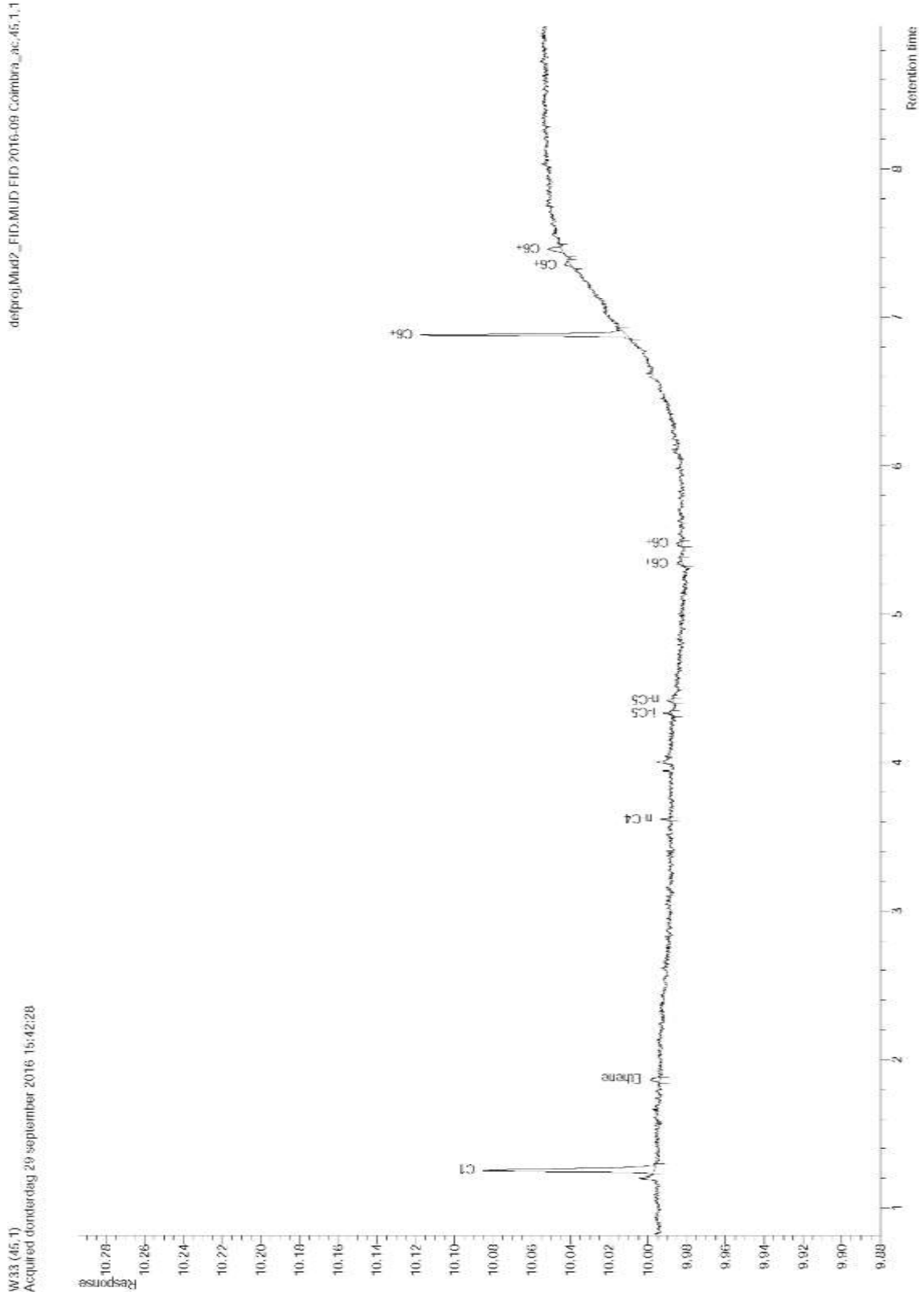

Appendix 10.60: W33 chromatogram. Retention time (min) x Response (pA).

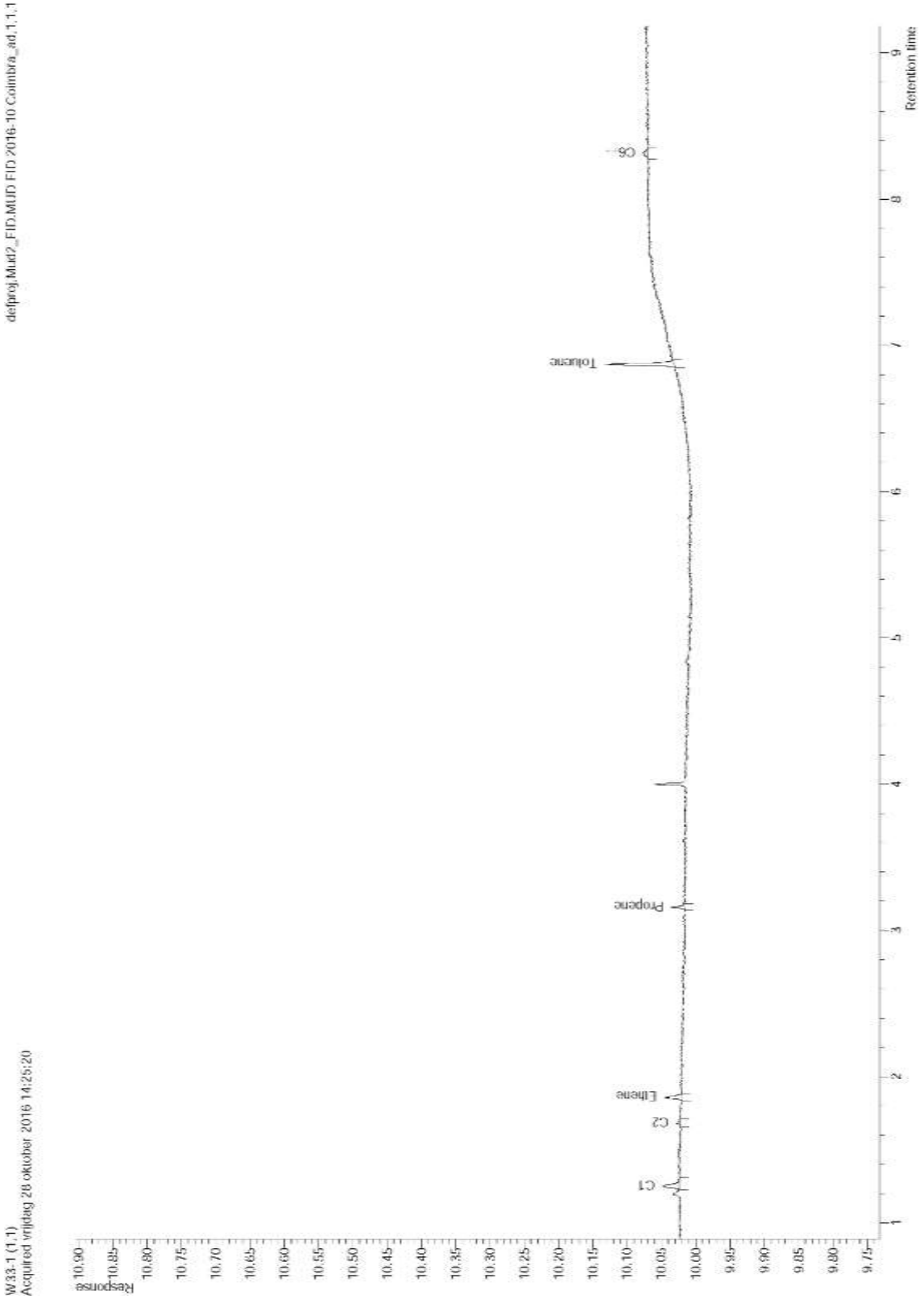

Appendix 10.61: W331 chromatogram. Retention time (min) x Response (pA).

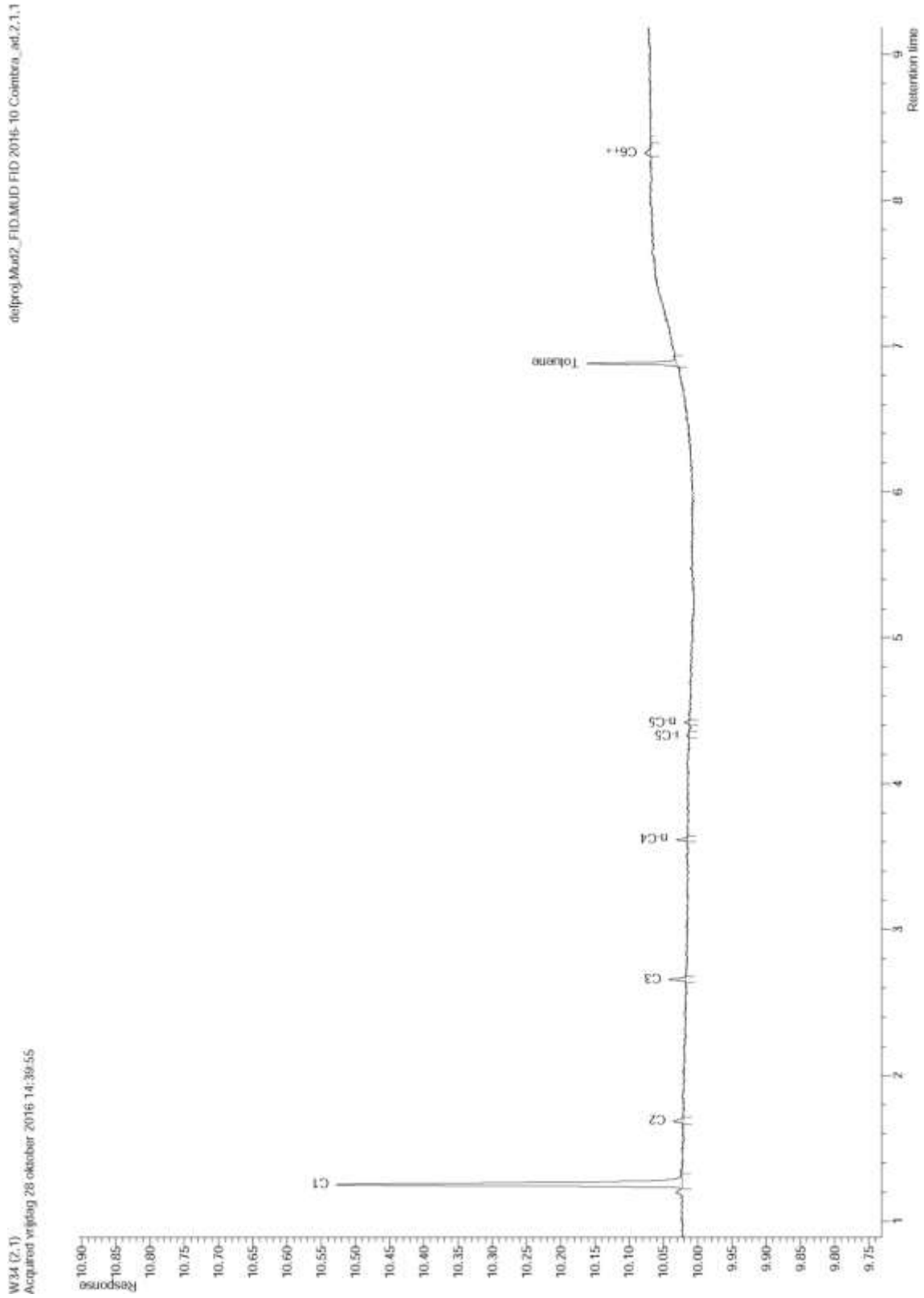

Appendix 10.62: W34 chromatogram. Retention time (min) x Response (pA).

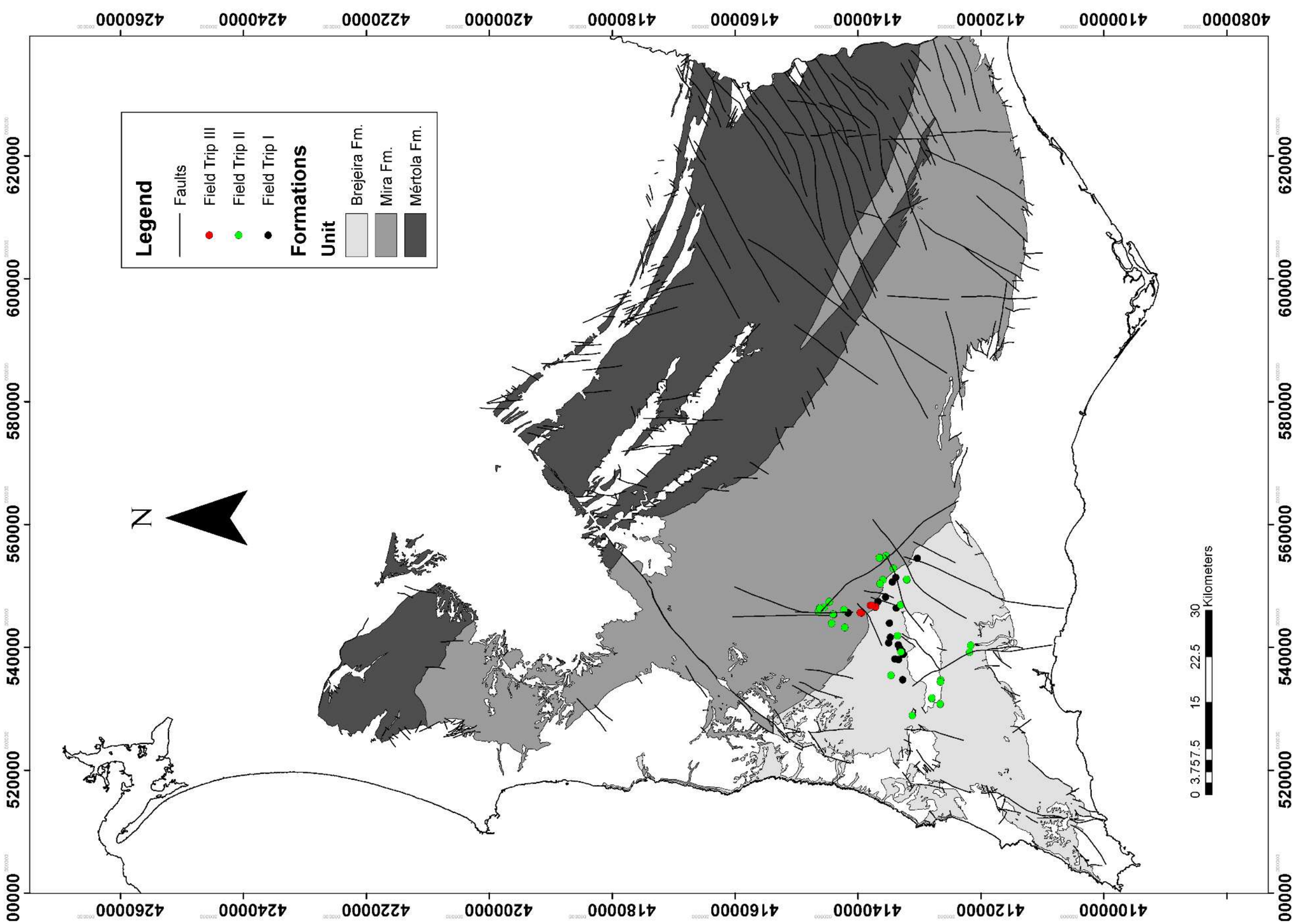

Appendix 10.63: Sample locations. and BAFG geological framework.

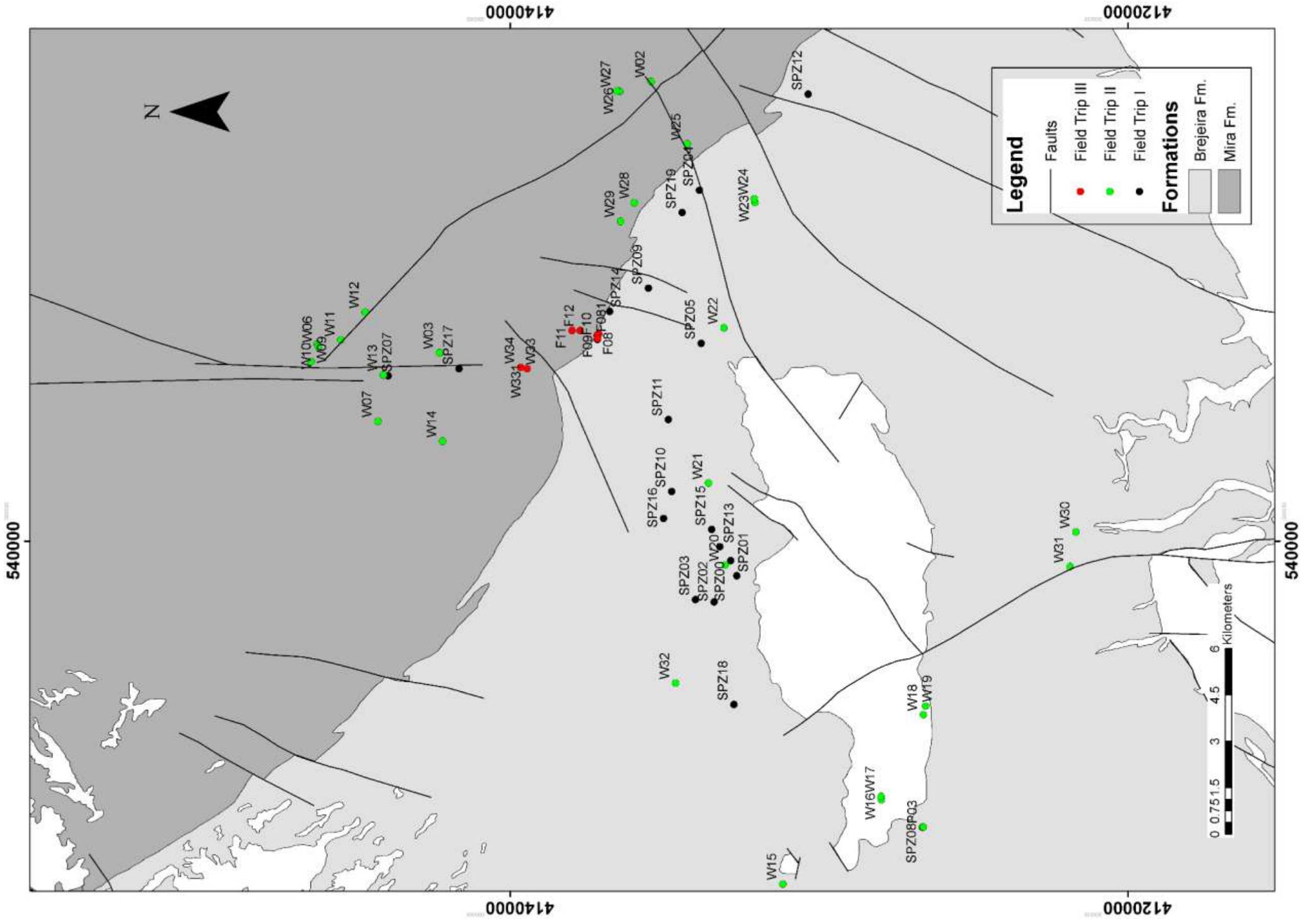

Appendix 10.64: Water and soil sample locations.

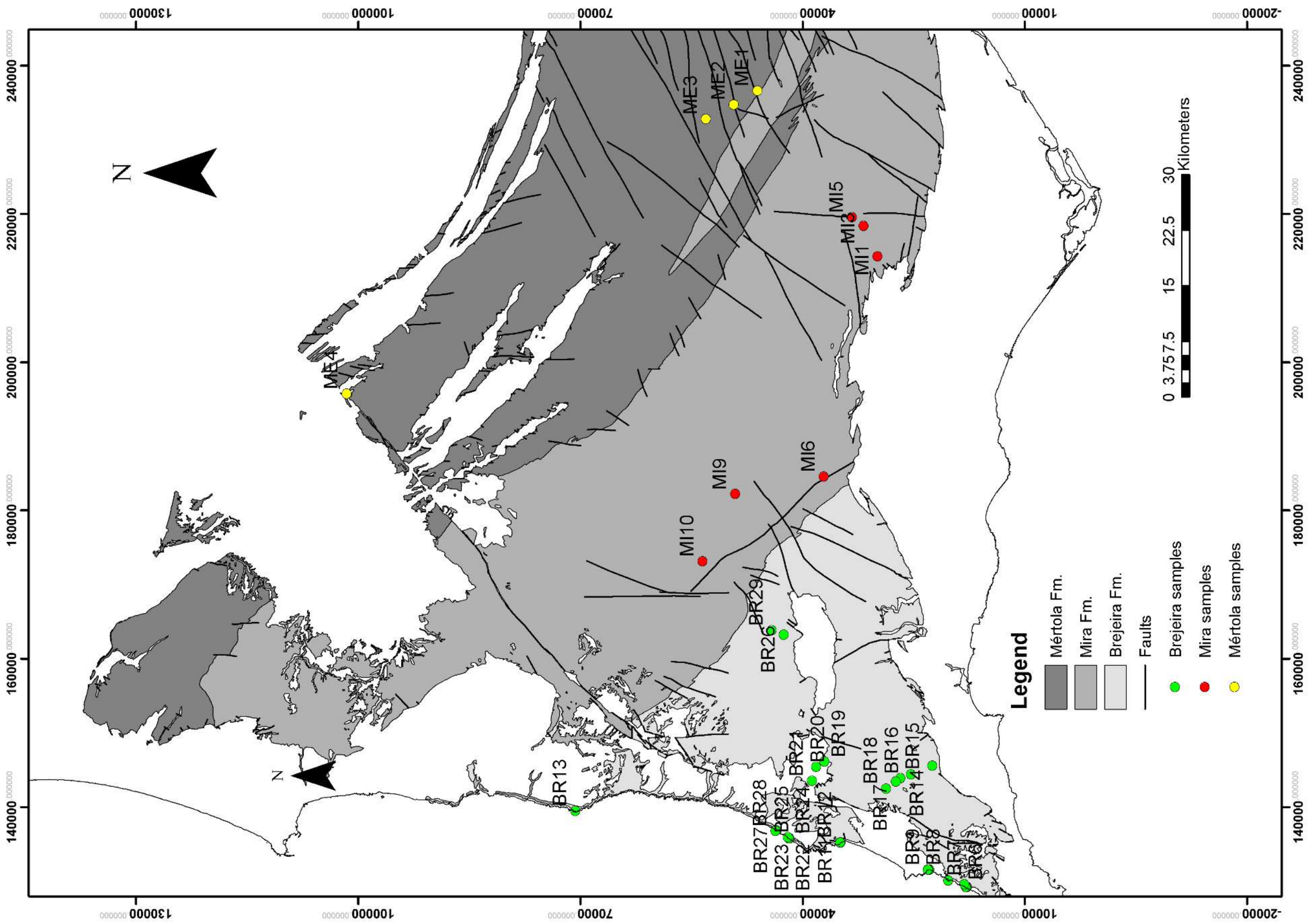

Appendix 12.65: Rock-eval samples locations.